

**Preparation and Characterization of Organic Silver Based Conductive  
Inks for Flexible Electronics**

**Wendong Yang**

Submitted for the degree of Doctor of Philosophy

Heriot-Watt University

School of Engineering and Physical Sciences

March 2019

The copyright in this thesis is owned by the author. Any quotation from the thesis or use of any of the information contained in it must acknowledge this thesis as the source of the quotation or information

## Abstract

Flexible electronics is of considerable interest for many applications due to the distinctive features of low-cost, flexibility and light weight capabilities. However, in translating the technology from research to practical applications there are several challenges. One of them is to formulate suitable ink materials. Organic silver ink, also known as particle free ink, has attracted great interest due to their flexibility in preparation, excellent stability and a relatively low sintering temperature (150~200°C) in comparison with nano silver ink. Although various kinds of organic silver inks have been created, they are still not ideal due to the low throughput, the complex synthetic process, and high temperatures for conductivity near bulk silver (generally >150°C). Therefore, it has been necessary to develop new types of low-temperature sintering organic silver conductive inks using simple procedures for practical applications on flexible substrates such as polymer films.

The aim of this thesis was to develop novel, low-temperature sintering ( $\leq 150^\circ\text{C}$ ) and highly conductive (near bulk silver) organic silver based inks using simple procedures for flexible electronics and study their properties and application. Three strategies were adopted to develop such inks. The first was to synthesize an organic silver/rGO hybrid ink. The second was to develop novel organic silver precursors with desirable electronic and thermal properties to formulate such inks. The third was to optimize the properties of the formulated inks. Three types of highly conductive organic silver-based inks, silver/rGO ink, silver citrate ink and silver oxalate ink, were developed by using a facile, high yielding and environmentally friendly procedure respectively. The chemical reaction mechanisms in the ink formation and the film formation process were studied in each case. The effects of sintering parameters such as temperature and time on the microstructure and electrical properties of the films have been investigated in detail. In the case of Ag/rGO ink, a remarkable improvement in conductivity was observed, which was attributed to the role of rGO platelets. In the case of silver citrate ink, defects such as the coffee ring effect were eliminated by using solvents containing active

components. An optimal silver oxalate ink was formulated finally for a simple circuit application, producing silver films with good quality and favorable conductivity at a sintering temperature of 150°C.

## Acknowledgement

Time flies. Just a blink, three years have passed and my doctoral project is approaching the end. I am excited as my PhD. dream will come true while I am a little sad since I am about to leave Scotland and those people whom I respect and love. I had imagined a lot of difficulties I might encounter when I started my doctoral project. As expected, some of them turned out to be true, but others were not as hard as I thought. For me, the three-year duration is just like a movie but I really enjoyed it.

First of all, I would like to express my deepest gratitude to my supervisor Dr. Changhai Wang for giving me the opportunity to study here, supervising me and helping me to address the difficulties that I encountered in the research and in the university throughout the past three years. He trained and taught me a lot on idea selection, experimental design, data analysis, paper writing and poster preparation, which are very important for a young person to grow into a scientific researcher.

Secondly, I would like to thank my second supervisor Dr. Valeria Arrighi for providing me the experimental lab and encouraging me. I appreciate your scientific input on my PhD. such as commenting on my papers and suggesting me to write concept notes before trying new ideas. I also appreciate your investment in my personal development. Meanwhile, I would like to thank the Engineering and Physical Sciences Research Council (EPSRC) for offering me the scholarship, without which it would not be possible for me to carry out my study and investigations.

In addition, I would like to thank Dr. Georgina Rosair, Dr. Jim Buckman, Mr. Mark Leonard and Dr. Neil Ross for their assistance in the XRD, EDX and surface profilometry work respectively. I would also like to thank all the staff at the School of Engineering & Physical Sciences for their help in the past years.

Of course, the wonderful movie cannot go well without the participation of nice partners. I am glad that I met them, especially David Watson, Thomas Jones, Adam



ODonnel, Luca Pellegrino, Chris Thomson and John Tobin. Thank you all for the suggestions and help with measurements. I really enjoyed the hard work atmosphere in our lab, sharing ideas and talking jokes. Because of that, I am motivated to try different ideas and have learned a lot.

I also appreciate the opportunities that I got to attend the academic conferences in Paris and London, which really broadened my horizon and enriched my employment career.

A special thank you goes to my closest friend Kexin Wang, with whom I have enjoyed a lot in life in Edinburgh. Thank you for accompanying me, supporting my decisions, and always giving me the push when I needed. Also, I want to thank my flatmates Hongliang Guo, Xia Yan, Piyang Liu and Wenhui Song for their help.

Finally, I would like to thank my parents and my wife for their continuous support and encouragement. I hope I have made you proud.

**ACADEMIC REGISTRY**  
**Research Thesis Submission**

Name:	Wendong Yang		
School:	School of Engineering and Physical Sciences		
Version:	Final	Degree Sought:	PhD in Electronic Engineering

**Declaration**

In accordance with the appropriate regulations I hereby submit my thesis and I declare that:

1. The thesis embodies the results of my own work and has been composed by myself
2. Where appropriate, I have made acknowledgement of the work of others
3. Where the thesis contains published outputs under Regulation 6 (9.1.2) these are accompanied by a critical review which accurately describes my contribution to the research and, for multi-author outputs, a signed declaration indicating the contribution of each author (complete Inclusion of Published Works Form – see below)
4. The thesis is the correct version for submission and is the same version as any electronic versions submitted\*.
5. My thesis for the award referred to, deposited in the Heriot-Watt University Library, should be made available for loan or photocopying and be available via the Institutional Repository, subject to such conditions as the Librarian may require
6. I understand that as a student of the University I am required to abide by the Regulations of the University and to conform to its discipline.
7. Inclusion of published outputs under Regulation 6 (9.1.2) shall not constitute plagiarism.
8. I confirm that the thesis has been verified against plagiarism via an approved plagiarism detection application e.g. Turnitin.

\* *Please note that it is the responsibility of the candidate to ensure that the correct version of the thesis is submitted.*

Signature of Candidate:		Date:	
-------------------------	--	-------	--

**Submission**

Submitted By ( <i>name in capitals</i> ):	WENDONG YANG
Signature of Individual Submitting:	
Date Submitted:	


**For Completion in the Student Service Centre (SSC)**


Received in the SSC by ( <i>name in capitals</i> ):	
<i>Method of Submission</i> ( <i>Handed in to SSC; posted through internal/external mail</i> ):	
<b><i>E-thesis Submitted (mandatory for final theses)</i></b>	
Signature:	
	Date:


## Inclusion of Published Works


### Declaration


This thesis contains one or more multi-author published works. In accordance with Regulation 6 (9.1.2) I hereby declare that the contributions of each author to these publications are as follows:

Citation details	Wendong Yang and Changhai Wang, Graphene and the related conductive inks for flexible electronics, Journal of Materials Chemistry C, 4(30): 7193-7207(2016)
Author 1	Conceived the idea, collected data, wrote and revised the paper
Author 2	Supervisor
Signature:	
Date:	

Citation details	Wendong Yang, Changhai Wang, Valerial Arrighi and Filipe Vilela, One step synthesis of a hybrid Ag/rGO conductive ink using a complexation-covalent bonding based approach, Journal of Materials Science: Materials in Electronics, 28(11): 8218-8230 (2017).
Author 1	Designed the research, performed the experiments, analyzed data, wrote and revised the paper
Author 2	Supervisor
Signature:	
Date:	

Citation details	Wendong Yang, Changhai Wang and Valerial Arrighi. Silver oxalate ink with low sintering temperature and good electrical property. Journal of Electronic Materials, 47(5): 2824-2835 (2018).
Author 1	Designed the research, performed the experiments, analyzed data, wrote and revised the paper
Author 2	Supervisor
Signature:	
Date:	

Citation details	Wendong Yang, Changhai Wang and Valerial Arrighi, Effects of amine types on the properties of silver oxalate ink and the associated film morphology, Journal of Materials Science: Materials in Electronics, 29(24): 20895-20906(2018)
Author 1	Designed the research, performed the experiments, analyzed data, wrote and revised the paper
Author 2	Supervisor
Signature:	
Date:	

Citation details	Wendong Yang, Changhai Wang and Valeria Arrighi, Preparation and characterization of organic silver precursors for conductive ink, ICAPE 2018: 20th International Conference on Advances in Printed Electronics, 2018, 1-5
Author 1	Designed the research, performed the experiments, analyzed data, wrote and revised the paper
Author 2	Supervisor
Signature:	
Date:	

## Table of Contents

<b>Abstract</b> .....	<b>i</b>
<b>Method of Submission</b> .....	<b>iv</b>
<b>E-thesis Submitted</b> .....	<b>iv</b>
<b>Table of Contents</b> .....	<b>vii</b>
<b>List of Figures</b> .....	<b>xi</b>
<b>List of Tables</b> .....	<b>xix</b>
<b>List of Publications</b> .....	<b>xx</b>
<b>Chapter 1 Introduction</b> .....	<b>1</b>
<b>1.1 Introduction</b> .....	<b>1</b>
<b>1.2 Aims and Objectives of the Thesis Work</b> .....	<b>3</b>
<b>1.3 Layout of Thesis</b> .....	<b>3</b>
<b>1.4 Originality and Main Findings</b> .....	<b>5</b>
<i>1.4.1 Originality</i> .....	<b>5</b>
<i>1.4.2 Main Findings</i> .....	<b>5</b>
<b>Chapter 2 Literature Review</b> .....	<b>6</b>
<b>2.1 Flexible Electronics</b> .....	<b>6</b>
<i>2.1.1 Motivation</i> .....	<b>6</b>
<i>2.1.2 Application</i> .....	<b>6</b>
<b>2.2 Conductive Ink</b> .....	<b>9</b>
<i>2.2.1 Ink composition</i> .....	<b>9</b>
<i>2.2.2 Fluid properties</i> .....	<b>10</b>
<i>2.2.3 Electrical property</i> .....	<b>11</b>
<b>2.3 Coffee Ring Effect</b> .....	<b>12</b>
<b>2.4 Substrate</b> .....	<b>13</b>
<i>2.4.1 Polymer films</i> .....	<b>13</b>
<i>2.4.2 Paper</i> .....	<b>14</b>
<b>2.5 Patterning and Sintering</b> .....	<b>14</b>
<i>2.5.1 Patterning methods</i> .....	<b>15</b>
<i>2.5.2 Sintering methods</i> .....	<b>17</b>
<b>2.6 Metal and Graphene Related Conductive Inks</b> .....	<b>19</b>

2.6.1 Silver ink .....	19
2.6.2 Copper ink.....	29
2.6.3 Graphene related ink .....	35
<b>2.7 Conclusions .....</b>	<b>48</b>
<b>Chapter 3 Ag/rGO Hybrid Conductive Ink.....</b>	<b>49</b>
<b>3.1 Introduction .....</b>	<b>49</b>
<b>3.2 Experimental section .....</b>	<b>49</b>
3.2.1 Chemicals and materials .....	49
3.2.2 Ink synthesis .....	50
3.2.3 Deposition and sintering.....	50
3.2.4 Characterization .....	50
<b>3.3 Results and Discussion .....</b>	<b>51</b>
3.3.1 Surface modification of substrate .....	51
3.3.2 PI substrate with thickness of 127 $\mu\text{m}$ .....	52
3.3.3 PEI substrate with thickness of 75 $\mu\text{m}$ .....	54
3.3.4 Ink chemistry.....	57
3.3.5 Thermal behavior of the Ag/rGO inks .....	60
3.3.6 Microstructure of the Ag/rGO ink films.....	61
3.3.7 Electrical performance .....	67
3.3.8 Conductive mechanism .....	70
<b>3.4 Conclusions .....</b>	<b>71</b>
<b>Chapter 4 Silver Citrate Ink Using Two Kinds of Mechanisms in Film Formation</b>	<b>73</b>
<b>4.1 Introduction .....</b>	<b>73</b>
<b>4.2 Experimental Section .....</b>	<b>74</b>
4.2.1 Materials.....	74
4.2.2 Synthesis.....	75
4.2.3 Ink deposition and sintering .....	75
4.2.4 Characterization .....	76
<b>4.3 Results and Discussion .....</b>	<b>76</b>
4.3.1 Characterization of silver precursor .....	76
4.3.2 Ink formulation .....	79
4.3.3 Effects of solvent on the thermal behavior of the ink.....	80
4.3.4 Effects of sintering temperature on microstructure of silver films .....	83
4.3.5 Effects of sintering time on microstructure of silver ink films .....	86

4.3.6 <i>Electrical performance</i> .....	89
4.3.7 <i>Mechanism of silver film formation</i> .....	90
<b>4.4 Conclusions</b> .....	<b>92</b>
<b>Chapter 5 Preparation and Characterization of New Organic Silver Precursors</b> ..	<b>93</b>
<b>5.1 Introduction</b> .....	<b>93</b>
<b>5.2 Experimental Section</b> .....	<b>94</b>
5.2.1 <i>Materials</i> .....	94
5.2.2 <i>Synthesis of organic silver precursors</i> .....	94
5.2.3 <i>Characterization</i> .....	96
<b>5.3 Results and Discussion</b> .....	<b>96</b>
5.3.1 <i>Structure and phase confirmation of silver carboxylates</i> .....	96
5.3.2 <i>Chemical composition and surface morphology</i> .....	100
5.3.3 <i>Thermal behavior of silver carboxylates</i> .....	102
5.3.4 <i>Thermal decomposition mechanism</i> .....	106
<b>5.4 Conclusions</b> .....	<b>107</b>
<b>Chapter 6 Silver Oxalate Ink with Low Sintering Temperature and Good Electrical Property</b> .....	<b>108</b>
<b>6.1 Introduction</b> .....	<b>108</b>
<b>6.2 Experimental Section</b> .....	<b>109</b>
6.2.1 <i>Materials</i> .....	109
6.2.2 <i>Synthesis</i> .....	109
6.2.3 <i>Ink deposition and sintering</i> .....	109
6.2.4 <i>Characterization</i> .....	109
<b>6.3 Results and Discussion</b> .....	<b>110</b>
6.3.1 <i>Characterization of silver oxalate</i> .....	110
6.3.2 <i>Ink formulation</i> .....	111
6.3.3 <i>Ink thermal behavior</i> .....	114
6.3.4 <i>Effect of sintering temperature on microstructure of silver films</i> .....	116
6.3.5 <i>Effects of sintering time on microstructure of silver ink films</i> .....	119
6.3.6 <i>Electrical performance</i> .....	122
<b>6.4 Conclusions</b> .....	<b>123</b>
<b>Chapter 7 Optimization of Silver Oxalate Ink: Effects of Amines</b> .....	<b>124</b>
<b>7.1 Introduction</b> .....	<b>124</b>
<b>7.2 Experimental Section</b> .....	<b>125</b>

7.2.1 Preparation of silver-amine complex ink and film .....	125
7.2.2 Characterization .....	125
<b>7.3 Results and Discussion .....</b>	<b>126</b>
7.3.1 Basic chemical reaction.....	126
7.3.2 Thermal behavior of various complex inks.....	129
7.3.3 Stability, film Morphology and resistivity of various complex inks.....	131
7.3.4 Film quality improvement by blended amines .....	137
<b>7.4 Optimal Silver Ink .....</b>	<b>139</b>
7.4.1 Film microstructure evolution .....	139
7.4.2 Film electrical performance .....	140
<b>7.5 Application .....</b>	<b>141</b>
7.5.1 Conductive pen preparation .....	141
7.5.2 Direct-writing research .....	141
7.5.3 Application.....	142
<b>7.6 Conclusions .....</b>	<b>143</b>
<b>Chapter 8 Conclusions and Future Work .....</b>	<b>144</b>
8.1 Conclusions .....	144
8.2 Future Work.....	146
<b>References .....</b>	<b>147</b>
<b>Appendices .....</b>	<b>161</b>



## List of Figures

Figure 2.1 (a) An RF antenna printed onto corrugated stock; (b) A printed RFID Tag [66] .....	8
Figure 2.2 (a) A4-sized e-book with a printed back plane (Courtesy of Plastic Logic, Cambridge, UK); (b) Flexible 20 layers wiring printed circuit board (PCB) made with inkjet printing (Courtesy of EPSON, Nagano, Japan) [68].....	8
Figure 2.3 (a) Photograph of pre-annealed silver current collectors for an MSC which can also be considered as an MSC with bare silver electrodes, (b) Photograph of a pre-annealed graphene mSC (graphene is on top of silver current collectors). In (a) and (b), the fingers are 1.0 mm wide, 9.4 mm long and interspaced by 0.6 mm. The two large silver pads (on the left) are for electrical connections for electrochemical measurements. The total effective electrode area for each MSC is about 1.6 cm <sup>2</sup> [63] .....	8
Figure 2.4 Surface profiles of silver ink film after sintering (a) coffee ring effect; (b) a flat film without coffee ring using suitable solvent composition [12] .....	12
Figure 2.5 Comparison of the basic properties of the different substrates (+ Good, - Bad; 1. Intrinsic property of such substrate. 2. Planarizing coatings have already been applied on these polymeric films to get $R_a \leq 1$ nm. 3. Temperature resistance can be improved by extra heat stabilizing process. 4. Intrinsic high barrier of metal foils, but usually pin holes are present. 5. Barrier layers have already been applied on these polymeric films) [75] .....	13
Figure 2.6 Screen printing: schematic figures showing a flat-bed screen printing [78] .	15
Figure 2.7 Inkjet printing principles: schematics of (A) CIJ, and DoD inkjet printing with (B) piezoelectric and (C) thermal head [78] .....	16
Figure 2.8 (a) TEM micrograph of silver nanoparticles protected by dodecanoate; (b) Surface profiles of silver ink line; (c) Conductive silver film [6] .....	20
Figure 2.9 (a) TEM image of silver nanoparticles synthesized in PVP/AgNO <sub>3</sub> mass ration of 1:1 with adipoyl hydrazide and dextrose; (b) The printed RFID antenna on paper, chip location close-up view (top); (c) The chip bonded RFID antenna, chip close-up view [86] .....	21
Figure 2.10 (a) Schematic diagram representing the electrosteric repulsion between Ag nanoparticles capped by polyelectrolyte dissociated in high pH aqueous medium; (b) photograph of prepared Ag conductive ink; (c) Optical microscope images and cross-sectional profiles of Ag patterns printed onto PI substrate [88] .....	22
Figure 2.11 (a) schematic illustration for the preparation of conductive lines by a	

pen-on-paper paradigm; (b) the image of the as-prepared nanosilver ink (on the left) [90].....	23
Figure 2.12 (a) Optical image of the silver ink in a vial. (b) 1D array of conductive silver lines (5 $\mu\text{m}$ wide) printed on a silicon substrate via direct-write assembly using a 100 nm nozzle. (c) UV-vis spectrum of the silver ink. (d) TGA curves for the ink heated at 23 and 90 $^{\circ}\text{C}$ in air [8].....	24
Figure 2.13 Schematic illustration what happened when a droplet of PDAC solution was dropped on the silver NPs array, SEM images of the printed drop zone (b); the magnified NPs arrays outside (a) and inside (c) in the droplet zone of PDAC [81].....	26
Figure 2.14 Schematic illustration of the silver NPs self-sintering process (the green lines represented the polymeric stabilizer; the blue spheres represented the sintering agent) [82].....	27
Figure 2.15 Transmission electron micrograph of single copper NP with a thick graphene wrapping of 3 nm and a corresponding schematic illustration [43].....	30
Figure 2.16 Schematic illustration of a single Cu NP synthesis and the formation of a silver shell by the transmetalation reaction [102] .....	31
Figure 2.17 Patterns of the ion ink printed using a roller-ball pen [106].....	32
Figure 2.18 Absorption spectra of the three types of copper complex ink: copper formate, copper acetate, and copper oleate. The inset photographs displayed the visual color of the inks [110].....	33
Figure 2.19 Schematic illustration of the ink preparation method. (a) Graphene is exfoliated from graphite powder in ethanol/EC by probe ultrasonication, (b) centrifugation-based sedimentation to remove residual large graphite flakes, (c) salt-induced flocculation of graphene/EC, (d) An ink for inkjet printing is prepared by dispersion of the graphene/EC powder in 85:15 cyclohexanone/terpineol, and (e) Vial of the prepared graphene ink [115].....	37
Figure 2.20 Schematic illustration of the preparation process of pristine graphene ink and inkjet printing. (a) Layered graphite was immersed in supercritical $\text{CO}_2$ , (b) $\text{CO}_2$ molecules penetrated and intercalated in the interlayer of graphite, (c) forming single or few layer thick graphene sheets, (d) Graphene sheets were stabilized by EC in cyclohexanone, (e) formed stable graphene ink, and (f) printing graphene electrodes on PET and PI substrates [117] .....	38
Figure 2.21 GO ink and morphology. (a) GO dispersed in water at 0.2 wt% as a stable ink, (b) spherical ink droplets generated by piezoelectric nozzles [63].....	40
Figure 2.22 (a) Optical pictures of vials containing GO and rGO dispersions. (b)	

Inkjet-printed graphene oxide film after lift-off from the PET surface. (c) TEM image of the RGO powder [60] .....	40
Figure 2.23 (a) XRD patterns of graphite, graphite oxide(GO), GO/PVA, and RGO/PVA composite, insert showing photographs of well-dispersed GO/PVA (left) and RGO/PVA (right) suspensions, (b) RGO/PVA composite stably dispersed in a mixed solvent with DMF and water for three month (left) and RGO precipitated from the same medium (right) [121].....	41
Figure 2.24 (a) Optical image of EG/PH1000 hybrid ink and molecular structures of EG and PH1000, (b) TEM image of a single graphene sheet from EG/ PH1000 hybrid ink, inset showing the SAED pattern of the single graphene sheet, (c) Raman spectra of graphene flakes from EG and EG/PH1000 hybrid ink ( Inset shows the shift of the G peak), and (d) AFM image of graphene sheets from EG/PH1000 hybrid ink [124]	43
Figure 2.25 The TEM images of the as-synthesized (a) Ag NPs, (b) Ag NP–GO (the inset is a photograph of the Ag NP–GO ink), (c) Ag NTPs, (d) Ag NTP–GO (the inset is the photograph of the Ag NTP–GO ink) and the HRTEM images of the as-synthesized Ag NTPs (e and f), the inset in (f) is a high resolution fast Fourier transform diffraction pattern of Ag NTPs [125] .....	44
Figure 2.26 (a) TEM image of Ag/RGO hybrid with reaction time of 48 h (inset: enlarged TEM view of Ag NPs and EDS of Ag/RGO composite), (b) UV–vis absorption spectra of synthesized Ag/RGO composites from GO after reaction times of 12 h, 24 h and 48 h, and (c) sheet resistance as reaction time (inset: Patterns obtained by inkjet printing on office paper and photo paper) [128] .....	45
Figure 3.1 FT-IR spectra of the PI film treated with different temperatures (a), NaOH concentration (b) and time (c) [49] .....	53
Figure 3.2 Interferometry profiles of PI film with thickness of 127 $\mu\text{m}$ (a for un-treated PI film; b for modified film) [49] .....	54
Figure 3.3 FT-IR spectra of the PEI film treated with different temperatures (a), NaOH concentration (b) and time (c) .....	56
Figure 3.4 Interferometry profiles of PEI film with thickness of 75 $\mu\text{m}$ (a for un-treated PEI film; b for modified film).....	57
Figure 3.5 UV-Vis absorption spectra of rGO and rGO/ethanolamine dispersions (inset is the optical image of these two kinds of dispersion).....	58
Figure 3.6 FT-IR spectra of rGO and rGO after ethanolamine adsorption .....	59
Figure 3.7 UV-Vis absorption spectra of Ag/rGO ink at different heating temperatures	60
Figure 3.8 DSC analysis of Ag ink and Ag/rGO ink.....	60

Figure 3.9 (a) As-prepared Ag/rGO ink; (b, c) Optical microscopy image and surface profile of the sintered Ag/rGO film.....	61
Figure 3.10 XRD patterns of the Ag/rGO films sintered at different temperatures for 60 minutes. Data shifted vertically, for clarity .....	62
Figure 3.11 SEM images of Ag/rGO films sintered at 150, 165, 185, 200, 215 and 230 °C for 60min (inset: 1 and 2 are the corresponding magnified images of figure b and e, 3 corresponds to the image of rGO offered by Graphenea Website) .....	63
Figure 3.12 Change of C/O weight ratio and Ag content in Ag/rGO films as a function of sintering temperature.....	64
Figure 3.13 Raman spectra of the Ag/rGO films sintered at 230°C for 60min.....	64
Figure 3.14 XRD patterns of Ag/rGO films prepared with the inks after sintering for 5min, 15min, 30min, 45min and 60min .....	65
Figure 3.15 SEM images of Ag/rGO films sintered at 230 °C for 5 min, 15min, 60min (a, c and e) and corresponding magnified images (b, d and f) .....	66
Figure 3.16 EDX results of Ag/rGO films formed at 230°C for 5, 15, 30, 45 and 60 minutes respectively.....	67
Figure 3.17 Resistivity variation of the deposited Ag and Ag/rGO films sintered at various temperatures for 60 minutes .....	68
Figure 3.18 Resistivity of the deposited Ag/rGO films as a function of sintering time at 230°C .....	69
Figure 3.19 Flexibility test of Ag/rGO obtained at 150°C and 230°C on PI substrate (Inset is the schematic diagram of bending test) .....	69
Figure 3.20 Schematic illustration of the film formation and conduction process of the Ag/RGO ink during sintering process (a. room temperature, b. below 150°C, c and d) 150-200°C, e) above 200°C).....	70
Figure 4.1 XRD pattern of the as-prepared silver citrate powder .....	77
Figure 4.2 FT-IR spectrum and EDS results of the synthesized silver citrate powder ...	77
Figure 4.3 DSC-TG curve of silver citrate powder.....	78
Figure 4.4 FT-IR spectra of the ethylenediamine and silver-amine complex .....	80
Figure 4.5 (a) Optical images of ink <sub>0</sub> color change during the heating process, (b) DSC curves of the ink with and without ethylene glycol .....	81
Figure 4.6 UV-Vis absorption spectra of silver citrate ink obtained at different temperatures .....	82
Figure 4.7 (a) As-prepared ink <sub>1</sub> ; (b) Surface profile of a sintered silver film from ink <sub>1</sub> ; (c) Optical images of silver films produced from ink <sub>0</sub> and ink <sub>1</sub> ; (d) SEM images of silver	

films produced from ink <sub>0</sub> .....	83
Figure 4.8 XRD patterns of the silver films obtained at different sintering temperatures for 60 minutes. Data shifted vertically, for clarity. ....	84
Figure 4.9 SEM images of silver films sintered for 60 minutes, (a) 125 °C, (b) 140 °C, (c) 155 °C, (d) 170 °C, (e) 185 °C and (f) 200 °C (a <sub>1</sub> and e <sub>1</sub> are high magnification image of a and e) .....	85
Figure 4.10 C and Ag content from EDS results in the films as a function of sintering temperature.....	86
Figure 4.11 XRD patterns of Ag films prepared at 155°C for 5, 15, 30 and 60 min respectively .....	87
Figure 4.12 SEM images of silver films produced at 155 °C for 5, 15, 30 and 60 minutes (a-d, c <sub>1</sub> and d <sub>1</sub> are high magnification image of c and d).....	88
Figure 4.13 EDS results of silver films produced at 155°C for 5, 15, 30 and 60 minutes (a-d).....	89
Figure 4.14 Resistivity of the silver films sintered at various temperatures for 60 minutes .....	89
Figure 4.15 Resistivity of the Ag films as a function of heating time at 155°C .....	90
Figure 4.16 Schematic illustration for the film formation process of the silver ink .....	91
Figure 5.1 FT-IR spectra of five as-prepared silver carboxylates (a. silver carbonate, b. silver oxalate, c. silver itaconate, d. silver tartrate, e. silver glycolate) .....	98
Figure 5.2 XRD patterns of four as-prepared silver carboxylates (a. silver carbonate, b. silver oxalate, c. silver itaconate, d. silver tartrate, e. silver glycolate) .....	100
Figure 5.3 SEM and EDS results of five as-prepared silver carboxylates (a. silver carbonate, b. silver oxalate, c. silver itaconate, d. silver tartrate, e. silver glycolate) .....	102
Figure 5.4 DSC curves of four as-prepared silver carboxylates (a. silver carbonate, b. silver oxalate, c. silver itaconate, d. silver tartrate, e. silver glycolate) .....	104
Figure 5.5 TG curves of four as-prepared silver carboxylates (a. silver carbonate, b. silver oxalate, c. silver itaconate, d. silver tartrate, e. silver glycolate) .....	106
Figure 6.1 DSC traces of as-prepared silver oxalate powders: S <sub>1</sub> powder was prepared using sodium hydroxide, oxalic acid and silver nitrate, S <sub>2</sub> powder was prepared using oxalic acid and silver nitrate .....	111
Figure 6.2 (a) DSC curves of the silver amine complex solutions formulated with various amines; (b) DSC curves of the silver amine complexes prepared by two silver oxalate powders .....	112

Figure 6.3 FT-IR spectra of the butylamine and $[\text{Ag}(\text{C}_4\text{H}_{11}\text{N})_2]_2\text{C}_2\text{O}_4$ solid complex .	113
Figure 6.4 $^1\text{H}$ NMR spectra of the butylamine and solid $[\text{Ag}(\text{C}_4\text{H}_{11}\text{N})_2]_2\text{C}_2\text{O}_4$ complex, D <sub>2</sub> O as solvent.....	114
Figure 6.5 DSC curves of the as-prepared ink .....	115
Figure 6.6 UV-Vis absorption spectra of silver citrate ink heated at different temperatures .....	115
Figure 6.7 (a) As-prepared silver ink; (b) Surface profile of a sintered silver film (130 °C, 60 min) .....	116
Figure 6.8 XRD patterns of the silver films obtained at different sintering temperatures for 60 minutes. Data shifted vertically, for clarity. ....	117
Figure 6.9 SEM images of silver films sintered for 60 minutes, (a) 100 °C, (b) 115 °C, (c) 130 °C, (d) 145 °C, (e) 160 °C (d <sub>1</sub> and f are high magnification images of figure d and e, respectively). ....	118
Figure 6.10 EDS results in the films as a function of sintering temperature, (a) 115 °C, (b) 130 °C and (c) 160 °C .....	119
Figure 6.11 XRD patterns of Ag films prepared at 130°C for 10, 15, 30 and 60 min respectively .....	120
Figure 6.12 SEM images of silver films produced at 130 °C for 10, 15, 30 and 60 minutes (a)-(d) .....	121
Figure 6.13 EDS results of silver films produced at 130°C for (a) 15 and (b) 30 minutes .....	121
Figure 6.14 Resistivity of the silver films sintered at various temperatures for 60 minutes .....	122
Figure 6.15 Resistivity of the Ag films as a function of heating time at 130°C .....	123
Figure 7.1 UV-Vis absorption spectra of the silver oxalate inks prepared using different amines .....	126
Figure 7.2 FT-IR spectra of 1,2-diaminopropane and the formed silver-amine complex .....	127
Figure 7.3 $^1\text{H}$ NMR spectra of 1,2-diaminopropane and the formed silver-amine complex, D <sub>2</sub> O used as solvent for both.....	128
Figure 7.4 DSC curves of the silver oxalate inks prepared using different amines .....	130
Figure 7.5 Optical images of the as-prepared silver oxalate inks storing in a refrigerator at 3°C for different times, (a, a <sub>1</sub> ) ethylenediamine, (b, b <sub>1</sub> ) 1,2-diaminopropane, (c, c <sub>1</sub> ) butylamine, (d) hexylamine, (e) octylamine, (f) ethanolamine.....	131
Figure 7.6 Sheet resistance of silver films sintered at 150°C for 60min from different	

silver oxalate inks (The error for all the measurements is about $0.010\Omega/\square$ ).....	132
Figure 7.7 XRD patterns of silver films sintered at 150°C for 60min from different silver oxalate inks.....	133
Figure 7.8 Optical and SEM images of silver films sintered at 150°C for 60min from different silver oxalate inks, (a, a <sub>1</sub> ) Ethylenediamine, (b, b <sub>1</sub> ) 1,2-diaminopropane, (c, c <sub>1</sub> ) butylamine, (d, d <sub>1</sub> ) hexylamine, (e, e <sub>1</sub> ) octylamine, (f, f <sub>1</sub> ) ethanolamine (c <sub>2</sub> and d <sub>2</sub> are high magnification images of figure c <sub>1</sub> and d <sub>1</sub> , respectively).....	134
Figure 7.9 Schematic illustration of the influences of amine types on morphology of silver film from different silver oxalate inks during sintering process (a) Amines with low boiling point and short carbon chain ; (b) Amines with high boiling point and long carbon chain. For amines with low boiling point and short carbon chain, large changes in concentrations due to the rapid evaporation could cause a broad nucleation event, thereby leading to a film with wide particle size distributions and porous structure. For amines with high boiling point and long carbon chain, they evaporated slowly and can encapsulate the produced silver nanoparticles and restrict their growth, so a dense film with narrow size distributions was produced .....	135
Figure 7.10 EDS results of silver films sintered at 150°C for 60min from different silver oxalate inks, (a) Ethylenediamine, (b) 1,2-diaminopropane, (c) butylamine, (d) hexylamine, (e) octylamine, (f) ethanolamine .....	136
Figure 7.11 Resistivity of silver films sintered at 150°C for 60min from a silver oxalate ink prepared using a blend of butylamine and 1,2-diaminopropane in different volume ratios; (a) 1:0, (b) 4:1, (c) 3:2, (d) 2:3, (e) 1:4 and (f) 0:1 .....	137
Figure 7.12 SEM images of silver films sintered at 150°C for 60min from a silver oxalate ink prepared using a blend of butylamine and 1,2-diaminopropane in different volume, (a) 100% butylamine, (b) 60% butylamine and 40% 1,2-diaminopropane, (c) 100% 1,2-diaminopropane (b <sub>1</sub> is high magnification images of figure b) .....	138
Figure 7.13 SEM and EDS images of silver films sintered at 150°C for (a, d) 10, (b, e) 30 and (c, f) 60min from the optimal silver oxalate ink.....	139
Figure 7.14 Resistivity of silver films sintered at 150°C for 60min from optimal silver oxalate ink .....	141
Figure 7.15 Relationship between deposition time and the dot size (inset, image of dots with different size) .....	142
Figure 7.16 Relationship between the film resistance and writing speed .....	142
Figure 7.17 The conductive effect of silver circuit with different conditions (a, b.	

connected with and without a voltage; c. bent).....	143
Figure S1 FT-IR spectra of ethylenediamine and the formed silver-amine complex ...	161
Figure S2 FT-IR spectra of butylamine and the formed silver-amine complex .....	161
Figure S3 FT-IR spectra of hexylamine and the formed silver-amine complex .....	162
Figure S4 FT-IR spectra of octylamine and the formed silver-amine complex .....	162
Figure S5 FT-IR spectra of ethanolamine and the formed silver-amine complex .....	163



## List of Tables

Table 2.1 OE-A roadmap for organic and printed electronics applications [67].....	7
Table 2.2 Comparison of the reported nano silver inks .....	27
Table 2.3 Comparison of the reported organic silver inks .....	28
Table 2.4 A brief overview of the reported copper nano inks .....	34
Table 2.5 A brief overview of the reported organic copper inks .....	35
Table 2.6 A brief overview of the graphene and related inks.....	46
Table 3.1 Particle sizes of silver nanocrystals in the film at different sintering temperature .....	62
Table 3.2 Particle sizes of silver nanocrystals in the film at different sintering time ....	65
Table 4.1 Physical properties of various solvents .....	75
Table 4.2 Particle sizes of silver nanocrystals in the film sintered at different temperatures .....	84
Table 4.3 Particle size of silver nanocrystals in the films processed at 155°C for different times .....	87
Table 5.1 Thermal behavior analysis of products .....	104
Table 5.2 Theoretical silver content and measured solid content .....	104
Table 6.1 Particle sizes of silver nanocrystals in the film sintered at different temperatures .....	117
Table 6.2 Particle size of silver nanocrystals in the films processed at 130°C for different times .....	120
Table 7.1 Amine types and the decomposition temperatures of the formulated inks ...	130
Table 7.2 Particle size of silver nanocrystals in each film .....	134

## List of Publications

The following papers published in peer-reviewed journals and conferences contribute to the main part of the thesis:

1. **Wendong Yang** and Changhai Wang. Graphene and the related conductive inks for flexible electronics. *Journal of Materials Chemistry C*, **2016**, 4(30): 7193-7207. (SCI, IF: 5.976)
2. **Wendong Yang**, Changhai Wang, Valerial Arrighi and Filipe Vilela. One step synthesis of a hybrid Ag/rGO conductive ink using a complexation-covalent bonding based approach. *Journal of Materials Science: Materials in Electronics*, **2017**, 28(11): 8218-8230. (SCI, IF: 2.324)
3. **Wendong Yang**, Changhai Wang and Valerial Arrighi. An organic silver complex conductive ink using both decomposition and self-reduction mechanism in film formation. *Journal of Materials Science: Materials in Electronics*, **2018**, 29(4): 2771-2783. (SCI, IF: 2.324)
4. **Wendong Yang**, Changhai Wang and Valerial Arrighi. Silver oxalate ink with low sintering temperature and good electrical property. *Journal of Electronic Materials*, **2018**, 47(5): 2824-2835. (SCI, IF: 1.579)
5. **Wendong Yang**, Changhai Wang and Valerial Arrighi. Effects of amine types on the properties of silver oxalate ink and the associated film morphology. *Journal of Materials Science: Materials in Electronics*, **2018**, 29(24): 20895-20906. (SCI, IF: 2.324)
6. **Wendong Yang**, Changhai Wang and Valerial Arrighi. One step preparation of copper-silver self-catalyzed hybrid conductive ink with reduced sintering temperature for flexible electronics. *Journal of Materials Science: Materials in Electronics*, **2019**, (SCI, IF: 2.324)
7. **Wendong Yang**, Changhai Wang and Valeria Arrighi. Preparation and characterization of organic silver precursors for conductive ink. *ICAPE 2018: 20<sup>th</sup> International Conference on Advances in Printed Electronics*, **2018**, 1-5 (conference paper).

# Chapter 1 Introduction

## 1.1 Introduction

With the development of science and technology, there is a high demand for new features in electronic products. The traditional electronic products based on rigid substrates such as glass can no longer meet the portable requirement since they are bulky and fragile. Miniaturization and flexibility of electronic products are expected. Flexible electronic technology offers a new way for manufacturing electronic devices, which creates electrical products by depositing conductive inks on a variety of flexible substrates [1]. This technology is characterized by low-cost, large-area, flexible substrates and is lightweight, which will bring a revolution for the future electronic industry. According to Kamyshny and Magdassi, the flexible electronics market is estimated to exceed \$300 billion over the next 20 years [2]. Clearly, flexible electronics will play a major role in meeting the key challenges in future electronic devices and systems in the coming decades. However, many technical problems have to be solved first in order to have a promising product platform. Among these, the biggest one is to formulate suitable inks that can be patterned using inkjet, screen, flexographic, direct writing or gravure based methods, while providing the required electrical and mechanical performance.

Conductive ink is a crucial material for flexible electronics. It is an ink that results in a patterned object which conducts electricity. Generally, these types of inks contain three constituents: conductive materials, solvents, and additives. Conductive materials play a primary role since they determines the electrical properties of the resulting products.

The basic requirements for a conductive ink are similar to those of standard inkjet inks, but in addition, they should provide good electrical conductivity. There are nine points to consider when designing an optimal conductive ink: 1) Conductivity, 2) Film and morphology, 3) Procedure, 4) Yielding, 5) Stability, 6) Adhesion, 7) Printability, 8) Temperature, 9) Time, 10) Cost and Application. In detail, first, the ink should have conductivity near bulk material with good adhesion to the substrates after post-treatment. The produced film should have a uniform morphology. Second, the synthesis procedure should be simple and high-yielding. Third, the ink should be stable against aggregation and precipitation. Fourth, it should have a good compatibility with the substrate and printer. The printable ink should be low viscosity (8-15 cP), medium surface tension

(25-35 dyne/cm), easy to flow through the nozzle or pen but does not leak from, dry out, or coagulate within the nozzle [2]. Fifth, the ink should be processable at temperatures below 150 °C in 60 minutes, or better 120 °C to be compatible with a wide range of flexible substrates. Last, it should serve for low-cost electronics.

Up to now, numerous kinds of conductive ink with various conductive materials such as polymers [3], carbon nanotube [4, 5], and metal nanoparticles or organic metal complexes [6-37], have been developed for the formation of conductive patterns. Among these, silver-based inks have been the currently favored metal inks and are under rapid development for applications in flexible electronics. Different kinds of silver ink composed of silver nanoparticles (NPs) or organic silver complexes have been used for inkjet printing of conductive traces. However, the high cost, the complex preparation process, and a high heat-processing temperature (generally >150 °C) of such inks limit their wide industrial applications. Copper is also an attractive material for conductive ink application due to its low price and high conductivity. Copper inks are typically synthesized using a suspension of copper nanoparticles (NPs) [38-44]. However, copper NPs are easily oxidized. The presence of copper oxides increases the sintering temperature of NPs and reduces the conductivity [15]. Copper coordination compounds are desirable ink materials as they are inexpensive, easy to prepare and process, compatible with a range of different printing methods and have excellent electrical properties. The thermal decomposition ink of amine complexes of copper formate is an innovation in the development of copper compound based inks [45-51], but this is the only example of this ink system so far. Besides, the relatively high temperature required for decomposition can cause flexible substrates such as polyethylene terephthalate (PET) to deform or alter its optical transmission thereby limiting their use as a low-cost substrate material. Thus there is still a need to develop new types of metal conductive ink.

Graphene has many unique properties, such as high carrier mobility at room temperature, large specific surface area, high Young's modulus and excellent thermal conductivity [52]. To exploit these properties in various kinds of applications, versatile synthetic routes have been developed to prepare graphene and its derivatives [53-59]. Among these methods, chemical reduction of graphene oxide (GO) is the most versatile approach, which incorporates many reactive oxygen-containing groups for further functionalization and tuning of the properties of GO or reduced GO (rGO) sheets. With

the additional attributes, it is desirable to harness the useful properties of graphene and its derivatives in conductive inks. To date, several graphene-related conductive inks have been produced successfully and are applied in different electronic applications such as sensors [60], conductive patterns [61], supercapacitors [62], electrodes [63] and so on.

On the other hand, surface treatment and modification of substrates are often required before ink deposition in order to generate reactive sites or functional groups on the surface to improve the ink deposition quality and the adhesion of the resulting metal films to the substrate. It has been shown that suitable surface treatment techniques can make the surface hydrophilic for easy printing and improving the adhesion of the metal film to the surface of the substrate [64]. Nevertheless, this aspect has not been studied in detail in most of the ink patterning processes. Therefore it is necessary to carry out research in this area.

## **1.2 Aims and Objectives of the Thesis Work**

The aim of this thesis was to develop novel, reliable, low-temperature sintering ( $\leq 150$  °C) and highly conductive (near bulk silver) organic silver based conductive inks for application in the field of flexible electronics.

Towards these, the main objectives can be briefly described as follows:

- Investigate the existing work carried out in the area of conductive inks for flexible electronics.
- Obtain a hydrophilic flexible substrate surface for the ink deposition.
- Formulate organic silver/graphene hybrid ink using a simple method; study its properties and conductive mechanism; elucidate the function of the graphene.
- Synthesize new organic silver precursors with desirable electronic and thermal properties via a facile procedure; study their structure, and thermal stability, and discuss their functions in decreasing the ink sintering temperature.
- Formulate organic silver inks using the as-prepared silver precursors; investigate the effects of sintering parameters on film morphology, chemical composition and conductivity.
- Optimize the obtained organic silver ink system and explore its applications.

## **1.3 Layout of Thesis**

Chapter 2 reviews the research progress of metal and graphene-related conductive inks for flexible electronics. The basic properties required by a conductive ink, such as viscosity, surface tension, wettability and electrical property, are described. The development in the formation and patterning of metal and graphene-related inks is reviewed. The challenges and opportunities have also been discussed.

In Chapter 3, an Ag/rGO hybrid ink was developed by a one-step method which is simple, high throughput and environmentally friendly. The ink was composed of 13.5 wt % of silver and 0.1wt% rGO, showing a good electrical performance on modified flexible substrates after sintering at 230°C. A remarkable improvement in resistivity by a factor of over 200 was observed at 150°C, which is attributed to the role of rGO platelets. A model for the mechanism of conductivity enhancement was proposed. This research provides an idea to improve the conductivity of organic silver inks at low temperature while reducing its cost.

In Chapter 4, a silver citrate ink with decomposition and self-reduction mechanisms in the film formation process was formulated, producing silver films with good conductivity at 155°C. The reaction mechanism between the complexing agent and the silver precursor was investigated and confirmed. The defects that often appear in the films due to bubbling effects were effectively reduced by using solvents containing active components. The effects of sintering temperature and time on the microstructure and electrical properties of the obtained silver films from the ink have been studied using various techniques.

In Chapter 5 and 6, five types of organic silver precursors were synthesized and characterized. It was found that silver oxalate is an ideal precursor for ink application. Then, a silver oxalate ink was synthesized by complexing the as-prepared silver oxalate with butylamine in organic solvents. A highly conductive film with a surface structure consisting of spherical silver nanoparticles was produced from the ink at a sintering temperature of 130°C, and even at 100°C. This research implies that the ink is compatible with most of the temperature-sensitive flexible substrates.

In Chapter 7, the effects of amine types on the thermal property, stability and electrical performance of the formulated silver oxalate ink, were investigated. The underlying mechanism was elucidated. The chemical reactions occurring within the ink and the film

formation process were also studied. An optimal silver oxalate ink was prepared by using blended amines as ligands, producing a uniform silver film with good quality and favorable conductivity at 150 °C. Successful circuit application was demonstrated. The results are important for the design of stable and high conductive silver inks for practical applications.

Chapter 8 provides the conclusions of the study presented in this thesis. Suggestions for future work are also discussed.

## **1.4 Originality and Main Findings**

### ***1.4.1 Originality***

Three types of organic silver-based inks with favorable electrical property, silver/rGO ink, silver citrate ink and silver oxalate ink, were developed by a facile, high yield and environmentally friendly method and are easy for industrial application.

### ***1.4.2 Main Findings***

- For silver/rGO ink, a remarkable improvement of conductivity by a factor of over 200 was observed in Ag/rGO films sintered at 150 °C as compared with that of the Ag films produced using the same formulation and thermal treatment process, while a factor of 10 was observed at 165 °C.
- Regarding silver citrate ink, the active roles of the solvents and the underlying chemical reactions in ink during heating were found and confirmed, respectively.
- For silver oxalate ink, a solid silver complex with lower decomposition temperature was found, which is different from all of the other organic silver complexes that usually exist in liquid form.

## **Chapter 2 Literature Review**

In this chapter, the basic properties of the conductive ink, such as viscosity, surface tension, wettability and electrical property, were elaborated in detail. The development in the formation and patterning of metal and graphene-related inks was reviewed, with particular emphasis on their synthesis, types and properties. The challenges and opportunities have also been discussed. Part of section 2.6 has been published [65].

### **2.1 Flexible Electronics**

#### ***2.1.1 Motivation***

Flexible electronics creates electrically functional devices by depositing conductive inks on a broad range of flexible substrates. Compared to conventional microelectronics, flexible electronics is characterized by low-cost, large area, high-throughput and flexible substrates [66]. It enables roll-to-roll fabrication. Very small series or customized products can be fabricated by using a simple process such as printing. Despite its many benefits, to date, the actual performance of flexible electronics is less advanced when compared with that of conventional electronics. It is therefore believed that this technology is not a substitute for conventional electronics but a complementary technology.

Flexible electronics mainly serves for low-performance and low-cost electronics. The applications can be small electronic products such as smart labels or cards. They are also targeting large area products such as flexible displays.

Flexible electronics involve two subtopics. The first one is the material: the conductive inks and the flexible substrates. The second one is the corresponding patterning and metallization method.

#### ***2.1.2 Application***

Flexible electronics is based on various patterning arts and conductive inks, which are opening up new possibilities for applications. According to the report from OE-A, these applications can be categorized into five groups [67], OLED lighting, organic photovoltaics, flexible displays, electronics and components (memories, batteries, wiring and interconnects, active devices and passive devices) and integrated smart systems (smart cards, RFID tags, sensors and smart textiles). Each category has a potentially huge market. For instance, the worldwide new lighting market is expected to



\$150 billion in 2020, which is comparable to global annual sales of TVs [68]. Table 2.1 shows the application forecast of each category for the next few years [67]. It is obvious that flexible electronics is opening up new possibilities for various applications.

Table 2.1 OE-A roadmap for organic and printed electronics applications [67]

<b>Classification</b>	<b>Existing until 2013</b>	<b>Short term 2014-2016</b>	<b>Medium term 2017-2020</b>	<b>Longer term 2021+</b>
<b>Organic Photovoltaics</b>	<i>Portable chargers</i>	<i>Consumer electronics, Customized mobile power</i>	<i>Specialized building integration, off grid</i>	<i>Building integration, Grid connected PV</i>
<b>Flexible Displays</b>	<i>Flexible segmented displays integrated into smart cards, price labels, bendable color displays</i>	<i>Bendable OLEDs, plastic LCD, in-moulded displays, large-area signage, rollable color displays</i>	<i>Rollable OLEDs with OTFT, transparent rollable displays, flexible consumer electronics</i>	<i>Rollable OLED TVs, telemedicine</i>
<b>OLED Lighting</b>	<i>Design projects</i>	<i>Transparent and decorative lighting modules</i>	<i>Flexible lighting</i>	<i>General lighting technology</i>
<b>Electronics and Components</b>	<i>Primary single-cell batteries, memory for interactive games, ITO-free transparent conductive films</i>	<i>Rechargeable single-cell batteries, transparent conductors for touch sensors, printed reflective display elements</i>	<i>Printed multi-cell batteries, integrated flexible multi-touch sensors, printed logic chips</i>	<i>Directly printed batteries, active and passive devices to Smart Object</i>
<b>Integrated Smart Systems</b>	<i>Garments with integrated sensors, anti theft, brand protection, printed test strips, physical sensors</i>	<i>Integrated systems on garment, large-area physical sensor arrays and mass market intelligent packaging</i>	<i>Textile sensors on fiber, dynamic price displays, RFID smart labels, disposable monitoring devices</i>	<i>OLEDs on textile, fiber-electronics, health monitoring systems and smart buildings</i>

Figure 2.1 shows an example of an RFID antenna printed on corrugated stock and a printed RFID tag [66].



Figure 2.1 (a) An RF antenna printed onto corrugated stock; (b) A printed RFID Tag [66]

Figure 2.2 (a) shows the world's first A4 size e-book fabricated using flexible electronic technique developed by Plastic Logic in 2011 [68]. Since this display has no glass substrate, it cannot be broken like LCDs when it is dropped from a height of 1 m. Figure 2.2 (b) shows a multilayer flexible tag circuit developed by Epson [68]. The entire structure, including the via-hole, was fabricated using inkjet printing. Twenty layers were formed on the film, with a total thickness of 200  $\mu\text{m}$ .



Figure 2.2 (a) A4-sized e-book with a printed back plane (Courtesy of Plastic Logic, Cambridge, UK); (b) Flexible 20 layers wiring printed circuit board (PCB) made with inkjet printing (Courtesy of EPSON, Nagano, Japan) [68]

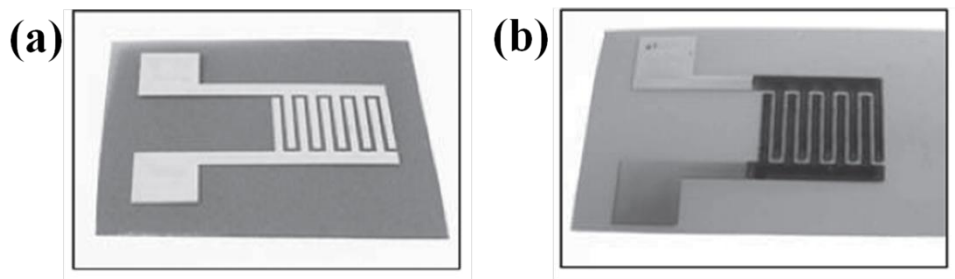


Figure 2.3 (a) Photograph of pre-annealed silver current collectors for an MSC which can also be considered as an MSC with bare silver electrodes, (b) Photograph of a pre-annealed graphene mSC (graphene is on top of silver current collectors). In (a) and (b), the fingers are 1.0 mm wide, 9.4 mm long and interspaced by 0.6 mm. The two large silver pads (on the left) are for electrical connections for electrochemical measurements. The total effective electrode area for each MSC is about 1.6  $\text{cm}^2$  [63]

Figure 2.3 gives an example of micro-supercapacitors (MSCs) fabricated by flexible

electronics technology [63]. Silver nanoparticles were first printed as the current collectors in an interdigitated structure (Figure 2.3 (a)). Then, graphene was printed onto the fingers as the electrodes (Figure 2.3(b)). The printed silver current collectors possess considerable capacitance due to the porous nature resulting from the printed nanoparticles. The technique provides an efficient, low-cost method for fabrication of a variety of graphene-based electronic devices with good performance and it is a promising alternative to the existing approaches for future commercial applications in printed and flexible electronics.

## **2.2 Conductive Ink**

### ***2.2.1 Ink composition***

Conductive ink is an essential material for flexible electronics. It is an ink that results in a patterned object which conducts electricity. The transformation from liquid ink to solid printing may involve drying, curing or melting processes. In principle, these types of inks usually contain several different constituents, which can be divided into three groups: functional materials, solvents, and additives. Functional materials can be metal nanoparticles, conducting polymers, metal complex or inorganic carbon, which plays a primary role in conductivity. Solvents are used to dissolve the components of the ink and to reduce viscosity. Additives complete the required functionality of the mixture, according to different needs.

Up to now, numerous materials have been employed to obtain conductive inks. In terms of conductive polymer inks, most commonly used organic conductors are based on poly(3,4-ethylenedioxythiophene) doped with polystyrene sulphonate (PEDOT: PSS), polythiophene, polypyrroles and polyaniline [3, 18]. However, these inks have limited conductivity due to the material properties. As for metallic inks, silver-based inks have been developed rapidly due to their high conductivity and good stability under ambient conditions. There are two main types: nanosilver inks and organic silver inks [15, 69]. Each has its advantages and deficiencies. Nanosilver inks are composed of silver NPs, organic solvents and some surfactants, which can melt at a much lower temperature than the melting point of the bulk metal silver due to the small size effect of the nanoparticles. Organic silver inks are made of organic silver salt and volatile organic solvent, which can be reduced to metal at low temperature. Copper-based inks are developed as an attractive alternative material to silver-based ink since they are cost-effective and have equivalent conductivity. However, copper nano inks are not stable and are prone to

oxidizing during the synthesis process and usually require a reductive atmosphere or a special sintering method to ensure good conductivity. Organic copper decomposition inks are a good alternative to the copper NP inks. A typical example is the thermal decomposition of the ink containing the amino complexes of copper(II) formate [45], which gives clean decomposition at low temperature without any organic residues, but this is the only example of the ink system. In respect of graphene-related inks, there are four types; graphene ink, graphene oxide ink, graphene/polymer ink, and graphene/metal ink. Graphene ink is composed of graphene, stabilizers, and solvents. The stabilizers might be polycyclic aromatic hydrocarbons, surfactants, polymers or ethyl cellulose. The solvent is water or organic solvents such as terpineol, ethanol or N,N-dimethylformamide (DMF). Compared to graphene ink, GO ink does not require an addition of stabilizing agents, which is an advantage. Graphene/polymer ink can not only address the shortcomings of polymer but can also form a stable and underlying conductive network due to the incorporation of graphene. Similarly, graphene/metal hybrid ink was formulated to take full advantage of these two materials to enhance the conductivity and reduce the concentration of metal particles.

### ***2.2.2 Fluid properties***

The fluid properties of the conductive ink are important because these must be compatible with various patterning technology. The surface tension and viscosity of the ink not only determine the velocity, size, and stability of the ejected droplet but also affect the shape of the droplets impinging on the substrate [70]. These impingement shapes establish the pattern resolution and thickness and further influences its mechanical and electronic properties. Therefore, the rheological parameters of inks, such as viscosity, surface tension and wettability should be controlled in the ink formulation process.

#### **a) Viscosity**

Viscosity is a quantity to measure a fluid's resistance to flow, which is related to the internal friction of a moving fluid. A fluid with a high viscosity flows slowly because its molecular interrelation gives high internal friction [70]. On the contrary, a fluid that has a low viscosity flows easily since there is very little friction in the liquid when it is in motion. An Ostwald viscometer tube (U-tube) was usually employed to measure the viscosity of the conductive inks [70]. For the piezoelectric print heads, the ink viscosity should be in the range of 8-15 cP, while thermal print heads require viscosity below 3 cP

[71].

### **b) Surface Tension**

Surface tension is the force that causes the molecules on the surface of a liquid to be pushed together, minimizing the area. It is also known as interfacial force or interfacial tension. The surface tension of water is 72 dyne/cm and can be reduced to 30-50 dyne/cm by adding some surfactants [70]. A liquid with a low surface tension is easy to wet or to spread across the surface of substrates. This phenomenon is useful to determine whether or not an ink will stay where it is deposited, and how wide it dries [70]. The typical values for industrial printing heads are in the range of 25-35 dyne/cm [71]. Du Noüy ring method is a general technique used to measure the surface tension of a liquid [70].

### **c) Wettability**

Wetting is the ability of a liquid to maintain contact with a solid surface (the substrate). If sufficiently contact is achieved between the two phases, a physical attraction due to inter-molecular forces develops causing the liquid to conform to the surface on a macro and microscale, displacing air and thus minimizing interfacial flaws. Good wettability of a surface is a prerequisite for ensuring good adhesion between the ink and flexible substrates.

### **2.2.3 Electrical property**

Electrical resistivity is an intrinsic property that quantifies how strongly a given material opposes the flow of electric current. A low resistivity indicates a material that readily allows the flow of electric current. In other words, the material has good conductivity. The electrical resistivity of conductive ink is defined as follows:

---

$$\rho = R \cdot A/L \quad (2.1)$$

Where  $\rho$  is resistivity in ohm meter ( $\Omega \cdot m$ ), or micro ohm-centimeter ( $\mu\Omega \cdot cm$ ),  $R$  is the measured resistance of the film resulted from the ink ( $\Omega$ ),  $A$  is its cross-sectional area, and  $L$  is the length. Conductivity is the reciprocal of resistivity:

---

$$\sigma = 1/\rho = L/(R \cdot A) \quad (2.2)$$

It is measured in Siemens per meter ( $S \cdot m^{-1}$ ).

If the length and width of the measured sample are equal, then  $R$  is referred to as "sheet

resistance",  $R_s$  ( $\Omega/\square$ ) and the electrical resistivity equation simplifies to  $\rho = R_s \cdot t$  ( $t$  is the thickness of the ink film).

### 2.3 Coffee Ring Effect

When ink droplets dry on a substrate surface, the solvent evaporation rate at contact lines is higher than that of the interior area. Therefore, there is a net transport of particles toward the edges of the structure. Thus, the solute or particulate matter tends to deposit in a ring-like fashion, or known as the coffee-ring effect [72]. This effect will lead to a strongly non-uniform morphology and performance of patterned devices. To improve the uniformity of the films from the ink, modification of solvent composition has been proposed, providing additional Marangoni flow to counteract the evaporating rate at contact lines [12, 72].

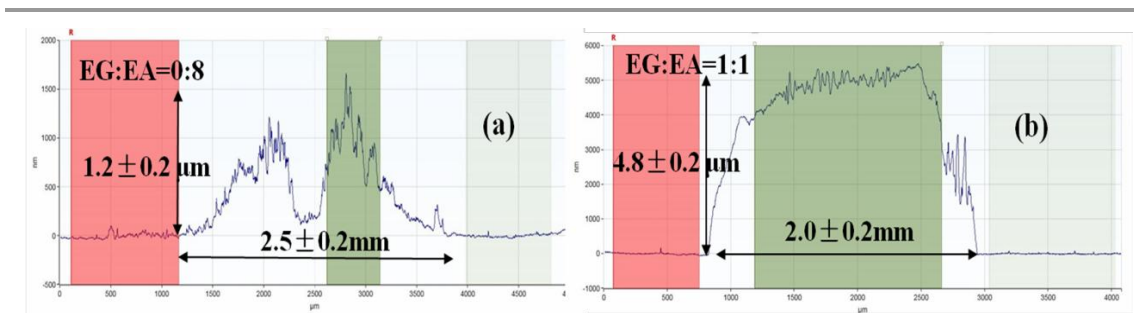


Figure 2.4 Surface profiles of silver ink film after sintering (a) coffee ring effect; (b) a flat film without coffee ring using suitable solvent composition [12]

To date, significant progress has been achieved to control the coffee-ring effects on the obtained features. For instance, using a high boiling solvent with low surface tension, such as ethylene glycol, in silver inks, can reduce the evaporative rate to decrease coffee ring effects on printed conductive tracks [12]. As showed in Figure 2.4, a coffee ring is easily formed from a droplet of the ink containing ethanol (Figure 2.4a). However, by using the mixed solvents with proper evaporation rates, the coffee ring effect can be eliminated (Figure 2.4b). On the other hand, Yunker et al. also showed experimentally that the shape of suspended particles could be used to eliminate the coffee-ring effect [73]. Moreover, the increase in ink viscosity can lead to slow particle motion and hamper the coffee ring formation.

In contrast to reduction of the non-uniformity caused by solvent evaporation, enhanced coffee ring effects have also been used to manipulate the microstructures of conductive thin films for greater transparency. Zhang et al. recently printed silver nanoparticle inks

in various patterns, such as lines and meshes, with enhanced coffee rings by adjusting substrate wettability [74]. The printed rings form a network composed of highly conductive silver rings and create a nearly transparent conductive thin film.

## 2.4 Substrate

Along with the development of ink technologies for flexible electronics, substrates must be designed to meet various requirements. Ideally, such materials must present a unique balance of properties that would make it suitable for all applications. In detail, a flexible substrate must be physically and thermally stable yet flexible, impermeable, smooth yet sufficiently adhesive, transparent, and above all economically viable. Currently, there are a number of materials that meet most of these requirements and have been used as substrates for flexible electronics.

### 2.4.1 Polymer films

Polymer films are extensively used for flexible electronics. Compared to paper substrates, they usually have smooth surfaces, homogeneous properties, and no porosity. This is beneficial in some aspects but is not ideal in other aspects. For instance, the non-absorbing surface is not ideal for the ink deposition.

	Glass	Metal	Paper	PET	PEN	PC	PI	PEI	PVF
Smoothness	++ <sup>1</sup>	++ <sup>1</sup>	0	+ <sup>1</sup>	+ <sup>2</sup>	+ <sup>2</sup>	0	0	0
Temperature Resistance	++	++	0	+ <sup>2</sup>	+ <sup>3</sup>	0	++	++	++
Flexibility	--	++	++	++	++	++	++	++	++
Optical Transmittance	++	--	--	++	++	++	0	0	0
Barrier	++	+ <sup>3</sup>	-	+ <sup>3</sup>	+ <sup>5</sup>	+ <sup>5</sup>	+	+	+
Price	--	+	++	+	0	0	--	-	--

Figure 2.5 Comparison of the basic properties of the different substrates (+ Good, - Bad; 1. Intrinsic property of such substrate. 2. Planarizing coatings have already been applied on these polymeric films to get  $R_a \leq 1$  nm. 3. Temperature resistance can be improved by extra heat stabilizing process. 4. Intrinsic high barrier of metal foils, but usually pin holes are present. 5. Barrier layers have already been applied on these polymeric films) [75]

Polyimide films (PI) are often used as substrates for flexible electronics because they can withstand prolonged exposure to 300 °C and still keep their flexibility. However, the

cost of PI film is relatively high, and the adhesion between PI and the ink is usually poor because there are no functional groups on its surface, which limits their applications. Polyethylene (PE), polycarbonate (PC) and polyethylene terephthalate (PET) are also used as low-cost flexible substrates for flexible electronics. Their softening points are below 150 °C, and therefore they are not compatible with a high temperature sintering process required for ink based metallization. Polytetrafluorethylene (PTFE) has excellent temperature stability and resistance to chemicals. It is, however, expensive and its low surface energy can pose problems with the undesirable printed structure. Figure 2.5 shows the basic properties of different substrates [75]. It can be seen that each material has its advantages and drawbacks. But in general, polymer films and paper are the most favorable materials because they are light and have good flexibility.

#### ***2.4.2 Paper***

Paper-based substrates for printed electronics are interesting for several reasons. They are widely available and inexpensive, while also lightweight, biodegradable and foldable. Besides, the mechanical, physical and chemical properties of paper can be altered by additives, or by changes in the manufacturing process. Therefore, it is possible to tailor papers, adapting them to a specific functional ink or application. Functional electronic components such as thermochromic displays, disposable radio frequency identification (RFID) tags, and cellulose-based batteries, have been fabricated on paper substrates [76]. Simple methods to create devices under ambient conditions are needed to exploit the potential of paper-based flexible electronics.

The primary challenge of using paper as a substrate for ink deposition is that paper is fibrous and non-uniform due to its nature. High porosity and surface roughness of paper surfaces will in most cases render difficulties with reaching the intended functionality. Furthermore, the paper is readily affected by environmental factors such as temperature and humidity that might change mechanical properties and cause dimensional and roughness changes.

### **2.5 Patterning and Sintering**

Two processes are generally involved in ink patterning. One is the transfer of an ink to a flexible substrate and the other is the conductive network formation in the patterned ink



traces. The former involves deposition methods such as screen printing, inkjet printing and direct writing; the latter is a process of sintering the particles together at a suitable temperature. All types of inks require sintering treatment to form well-conducting tracks after being transferred to substrates.

### 2.5.1 Patterning methods

Multiple technologies have been adopted for the ink patterning such as inkjet, aerosol, screen printing and direct writing. Among these, screen printing is the most popular and common method to date due to the ease of printing relatively thick conductor traces that carry large currents. However, line widths below 80-100 $\mu\text{m}$  cannot be obtained by this method [77]. Therefore, new patterning strategies are required.

Figure 2.6 shows a schematic of a typical flat-bed screen printing process. During printing, the ink is first spread over the screen mesh, and then is printed onto the substrates by a squeegee through the open pores of the screen [78].

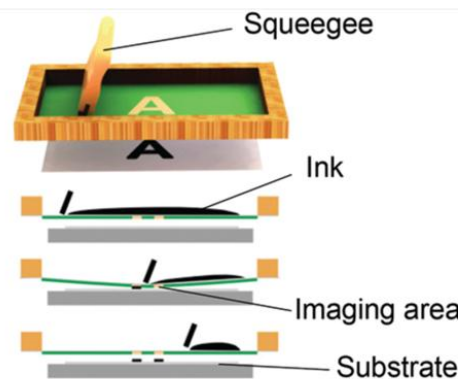


Figure 2.6 Screen printing: schematic figures showing a flat-bed screen printing [78]

Inkjet printing offers a promising approach. Conductive features can be created by printing functional inks with low viscosity and modest surface tension onto various substrates. Fast printing speeds of up to 1m/s can be accomplished, and features sizes as small as 20 $\mu\text{m}$  can be realized in this technology [77]. There are two main technologies in use in contemporary inkjet printers: continuous inkjet (CIJ) and drop-on-demand (DOD) inkjet. In CIJ technology, a stream of charged ink droplets is continuously generated and jetted by high-pressure pump (Figure 2.7A). Then, these droplets are directed by electrostatic deflection plates and selectively printed onto the substrates. In DOD technology, there are two types, the piezoelectric and thermal DOD. In a piezoelectric inkjet process (Figure 2.7B), a voltage is applied to the piezoelectric

material to induce a change in the shape, generating a pressure pulse in the liquid, which forces a droplet of ink from the nozzle. In the thermal inkjet process, a pulse of current is passed through the heating element causing a rapid vaporization of the ink in the chamber and forming a bubble, which further causes a large pressure increase, propelling a droplet of ink onto the paper (Figure 2.7C).

Although inkjet is perhaps the most studied ink printing method, it poses many challenges from a functional material deposition technique, especially for ink formulations, due to the strict range of solution parameters required to ensure successful patterning.

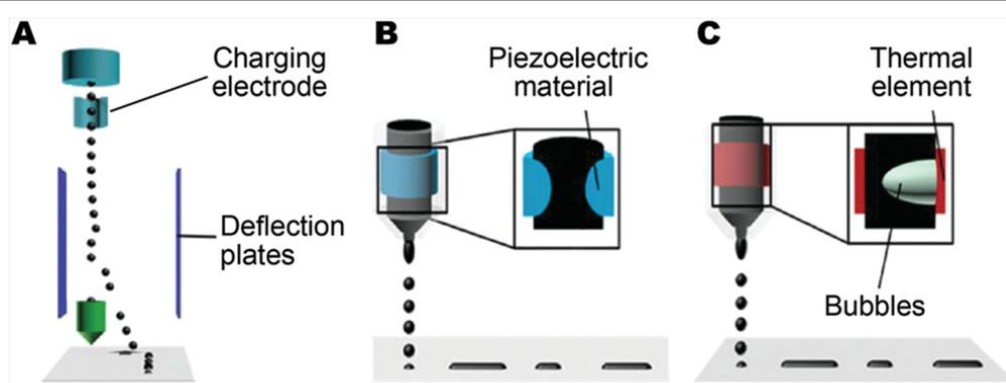


Figure 2.7 Inkjet printing principles: schematics of (A) CIJ, and DoD inkjet printing with (B) piezoelectric and (C) thermal head [78]

Aerosol jet printing is an emerging technique used for flexible electronics. In this method, the ink is first aerosolized and then flow-focused using a sheath gas resulting in printed features with widths as small as  $10\ \mu\text{m}$  [79]. Compared to inkjet printing, aerosol jet printing is more tolerant to wide variations in ink parameters such as surface tension, viscosity and particle size.

Direct ink writing is another emerging technique with unique patterning capabilities. In this technique, a concentrated ink is extruded through a tapered cylindrical nozzle that is translated using a three-axis (x-y-z), robotic motion stage [80]. The ink filaments can maintain a similar size to the nozzle, which ranges from  $0.5\ \mu\text{m}$  to  $1\ \text{mm}$  [77]. The printed feature dimensions are determined by the ink rheology and printing parameters. Inks designed for this method can be modified for fabricating patterns using a pen-on-paper mode. Unique 3D structures can also be fabricated by this technology.

Roll-to-roll (R2R) printing is also a technique that can print features at high speed. This method is suitable for the preparation of large numbers of devices such as RFID tags. However, the resolution of printed features is limited, which is in the range of 50-100 $\mu\text{m}$  [77].

### ***2.5.2 Sintering methods***

Various methods have been employed to transform the as-deposited inks into highly conductive traces, including thermal sintering, chemical sintering, electrical sintering, plasma sintering, microwave sintering and photonic annealing.

Thermal sintering is usually processed on a hotplate or in an oven. The required temperature varies from ink to ink depending on the boiling points of the organic solvents used, the dissociation temperatures of the salts and the degree of conductive network formation. Nearly every conductive ink is processed this way. Usually, heating at 200-350  $^{\circ}\text{C}$  for 10-60 min is required to remove the organic insulating materials from the surface of the NPs, and to obtain sintered metal coatings with resistivity comparable to that of bulk metal, for both silver-based and copper-based inks.

Chemical sintering is an innovative approach, which can trigger the coalescence and sintering of NPs at room temperature. This method is beneficial to some heat-sensitive substrates such as polyethylene terephthalate (PET) and polycarbonate (PC). The development in particle-based inks is the idea of polymer desorption. One example is the use of cationic polymer, which can initiate room temperature coalescence of the silver NPs stabilized with poly(acrylic acid) (PAA) through binding with PAA, yielding traces with good conductivities [81]. The other is to use hydrochloric acid to promote polymer desorption upon drying, leading to coalescence of the particles at room temperature [82]. However, the conductivities obtained by this method approach only half that of bulk silver. Solvent washing is also a method to achieve high conductivities patterns at room temperature, which utilizes a capping agent, such as dodecylamine. Spontaneous sintering of the particles can be observed when the patterned substrate is dipped into a suitable solvent for the capping agent. Although high conductivities result, this method is not practical for inks used in flexible electronics.

Electrical sintering is a method by applying a voltage over the printed structure that causes current flow through the structure, leading to local heating within the film [71].

The resistivity of the patterned film is determined by the sintering voltage used. The main advantages of this method are the short sintering time, which can be less than 1 min, depending on the geometry of the printed area, reduced damage to the substrate due to area-specific heating and real-time monitoring of the sintering process through current measurement. This ability to monitor while sintering allows the desired conductivity to be repeatedly achieved. However, electrical sintering requires contact with the printed film, which may not be ideal for some applications.

Plasma sintering is performed by exposure of printed patterns to low-pressure Ar plasma and electron-cyclotron resonance (ECR) plasma [71]. The sintering process shows a clear evolution starting from the top layer into the bulk. This method has been applied to plastic substrates, and the obtained resistivity of the printed patterns is 10 times higher compared to the resistivity of bulk silver. Meanwhile, it can be utilized in R2R processes.

Microwave sintering is a rapid sintering method. Metals such as Ag, Au and Cu nanoparticles can be sintered quickly by microwave radiation, but they have a very small penetration depth, in the range of 1-2  $\mu\text{m}$  at 2.54 GHz [18]. Therefore, microwave sintering can only be successful if the thickness of the printed object is in the range of the penetration depth. This method is particularly attractive when polymer substrates are used, as they are almost transparent to microwaves, which ensures that the microwaves are absorbed mostly by the metallic nanoparticles, leading to localized heating whilst ensuring minimal damage to the substrate.

Photonic sintering utilizes flash lamps, lasers, and other light sources which deliver energy to the targeted material to be sintered [18]. Absorption of light by the printed material causes heating through the dissipation of non-radiative energy and exothermic photochemical reactions. This heat causes evaporation of the solvent and eventually sintering of adjacent particles. Photonic sintering shows much promise for large-scale manufacturing on low thermal diffusivity substrates, such as plastic and paper. However, it is largely incompatible with glass and silicon due to their comparatively high thermal diffusivities. This method can process copper in an ambient atmosphere without oxidation if the ink is properly designed.

Lasers have also been used to sinter printed metallic films, which induces local,

transient heating through a scanning laser beam leading to a rapid sintering effect. This method is suitable for small areas as the spot size is usually between 20 and 40  $\mu\text{m}$  in diameter and the scan speed is as low as  $0.2 \text{ mm}\cdot\text{s}^{-1}$  [18]. Fast scanning can minimize the heat diffusion effects and provide high-resolution metal tracks without damage to the substrates. Moreover, if the sintering duration is short enough, copper oxidation can be avoided even in the ambient atmosphere.

## **2.6 Metal and Graphene Related Conductive Inks**

### ***2.6.1 Silver ink***

#### **a) Silver NPs ink**

Conductive inks of silver NPs have been attracting much attention and are a popular choice for flexible electronics. Due to the small size effect of the silver NPs, these inks allow formation of bulk silver with excellent conductivity at lower conversion temperatures [83], which are beneficial to the flexible substrates. Such inks are usually composed of silver NPs, organic solvents, and some surfactants. The capability of silver NPs is a critical factor because it determines the electrical and mechanical properties of the resulted conductive patterns.

Two main approaches are usually used to prepare silver NPs: top-down and bottom-up respectively [71]. The top-down or physical methods are usually used to produce silver NPs by breaking the bulk metal silver into small particles. The most widely used methods are based on physical gas-phase approaches. The main disadvantages of top-down methods are the difficulties in obtaining large quantities of uniform silver NPs and high cost [15]. In the bottom-up methods, silver NPs are formed by a reduction reaction in the solution of ionic silver precursors, or by decomposition of molecular silver precursors. Currently, silver NPs used in the inks are mostly prepared by the chemical reduction process. The prepared silver NPs are of various characteristics such as different sizes, diverse morphologies, and good stability. For the required particle size and morphology, the synthesis usually needs to be optimized by varying experimental parameters, such as the type and concentration of reagents, temperature, pH, stabilizers and so on [15].

Aggregation of silver NPs during the synthesis process is an important issue in formulation and needs to be avoided. The electrostatic and steric mechanisms are often used to decrease the aggregation effect, by forming an electrical double layer or a

polymer layer on the surface of the silver NPs [71]. One crucial factor in the electrostatic stabilization method is the surface electrostatic repulsion among the particles, the higher it is, the more stable of the colloidal systems. The Zeta potential ( $\zeta$ ) of the particles is usually used as an indication of the surface potential [71]. The steric stabilization approach is to create a barrier to prevent close contact and aggregation of the NPs. To obtain stable nano silver inks, various stabilizers or capping agents or protectants were used in the preparing process of silver nanoparticles.

Using a sparse ionic protection monolayer, Anto et al prepared gold and silver NPs with an extremely high solvent dispersibility and a low coalescence temperature [84]. These NPs are protected by the mixed ligands comprising the  $\omega$ -functionalized ionic ligand and labile ligand, which is suitable for inkjet and other printing methods to deposit on the substrates that may be solvent and/or temperature-sensitive, such as plastic films.

Shim et al introduced a thermal decomposition method to achieve silver NPs with a high precursor concentration [85]. Highly monodispersed silver nanocrystals were synthesized by thermolysis of silver alkanoate precursors. The capping ligands of these nanoparticles, dodecanoic acid, myristic acid, and palmitic acid, were selected according to the designed sintering temperature of the ink. Silver nanoparticles stabilized with dodecanoic have the lowest thermal decomposition temperature, which could be re-dispersed into organic solvents and formulated into inkjet inks that can be applied to the low-cost fabrication of electronics.

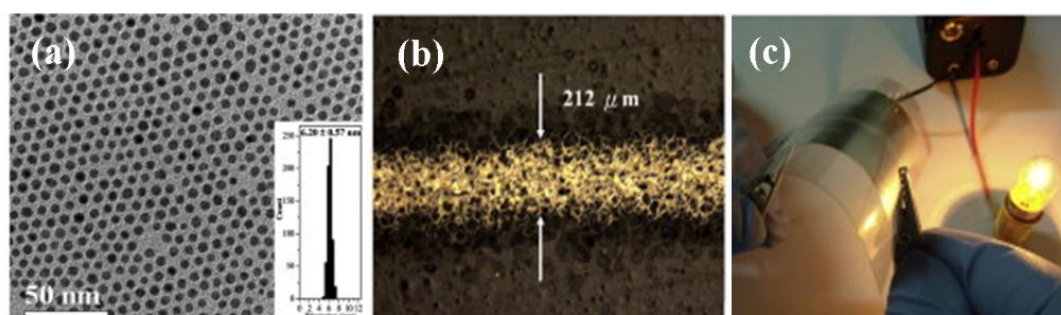


Figure 2.8 (a) TEM micrograph of silver nanoparticles protected by dodecanoate; (b) Surface profiles of silver ink line; (c) Conductive silver film [6]

Chen et al. reported a room-temperature chemical reduction process to fabricate conductive silver features on flexible PET substrates using a suspension of dodecanoate protected silver NPs in cyclohexane, as showed in Figure 2.8 [6]. The research contributes significantly to promoting the application of nanoparticles in the electronic

and information industries. It also provides a solution to address the critical issues of manufacturing 2D conductive patterns by taking advantage of the low-temperature chemical process.

Zhang et al. developed a new reduction system to synthesize mono-dispersed silver NPs at ambient temperature [86]. In this work, adipoyl hydrazide and dextrose were used as reductant and polyvinylpyrrolidone (PVP) was used as the protectant of silver nanoparticles. By controlling the nucleation and growth process, monodisperse silver nanoparticles were obtained on a large scale at a low mass ratio of PVP/ AgNO<sub>3</sub> under ambient temperature (Figure 2.9a), which was highly beneficial to achieve low cost and high conductivity. Conductive inks were formulated by dispersing these silver nanoparticles in a mixture of water, ethanol and ethylene glycol. A series of electric circuits were produced by ink-jet printing such inks on paper, which showed low resistivity in the range of  $9.18 \times 10^{-8}$ - $8.76 \times 10^{-8}$  Ω·m after sintering at 160°C for 30 min (Figure 2.9b and c). These flexible electric circuits have huge potential for the manufacture of low-cost electrodes and sensor devices.

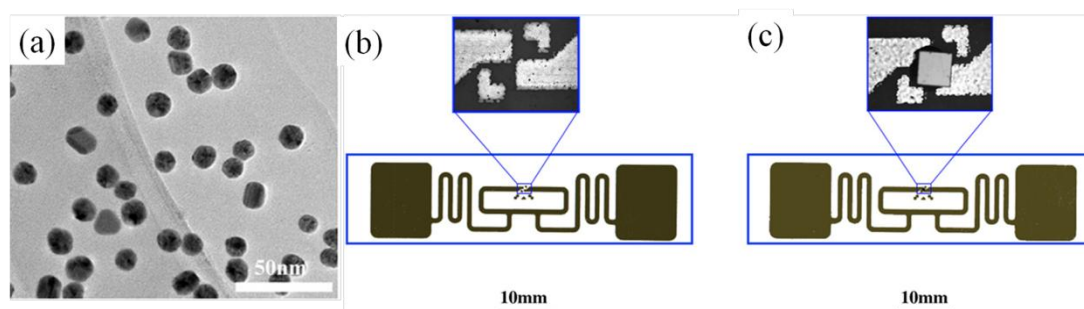


Figure 2.9 (a) TEM image of silver nanoparticles synthesized in PVP/AgNO<sub>3</sub> mass ration of 1:1 with adipoyl hydrazide and dextrose; (b) The printed RFID antenna on paper, chip location close-up view (top); (c) The chip bonded RFID antenna, chip close-up view [86]

Kosmala et al. synthesized a stable aqueous printable silver nano ink by dispersing the as-prepared Ag NPs in water with the help of a co-polymer stabilizer under ultrasound environment [83]. The research showed that ultrasound technique and the copolymer could help to separate the agglomerates of these nanoparticles, thereby leading to stable silver inks. Such inks have been printed on ceramic substrates, and the printed films showed low resistivity ( $<10^{-7}$  Ω·m).

Khondoker et al. developed a conductive ink by using PVP stabilized silver nanoparticles [87]. The ink can be used for inkjet printing of conductive patterns on

cellulose films. The smallest resistivity of the film resulting from the ink was  $16.3 \mu\Omega\cdot\text{cm}$ .

Jeong et al. prepared an aqueous printable silver ink with good dispersion stability [88]. Unlike Kosmala, a kind of anionic polyelectrolyte (PAA), was used to stabilize silver nanoparticles. These nanoparticles capped by PAA were first prepared by chemical reduction, and then they were formulated into nano silver ink. Owing to the electrostatic repulsion effect of the PAA, the prepared ink has good stability. Narrow conductive features on flexible substrate were fabricated by an ink-jet printing method and showed good conductivity after annealing at  $250 \text{ }^\circ\text{C}$ . The creativity in this approach lies in the selection of the stabilizer. The stabilizer, PAA, can adsorb on the surface of silver nanoparticles and offers an electrostatic repulsion force between them, thereby leading to a long-term stable silver ink (Figure 2.10).

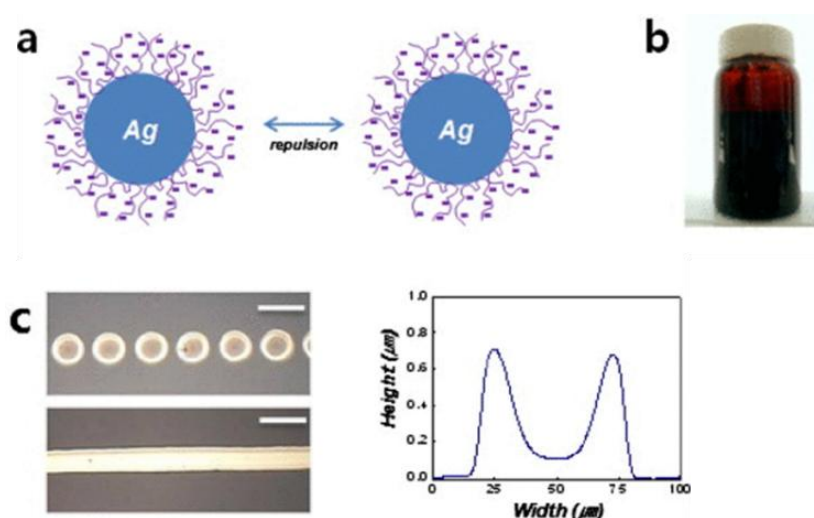


Figure 2.10 (a) Schematic diagram representing the electrostatic repulsion between Ag nanoparticles capped by polyelectrolyte dissociated in high pH aqueous medium; (b) photograph of prepared Ag conductive ink; (c) Optical microscope images and cross-sectional profiles of Ag patterns printed onto PI substrate [88]

Using the same stabilizer, PAA, Shen et al. prepared printable aqueous nanosilver inks with different solid content [89]. Such inks have been successfully printed on paper and polyethylene terephthalate (PET) substrates using a common printer. The printed silver patterns showed good conductivity under ambient conditions, which enabled the fabrication of flexible electronic devices.

By using dodecanoic acid as a capping agent, Liu et al. prepared silver NPs of 5nm in water with relatively good stability [90]. The capping-ligand based silver NPs not only



have a steric hindrance effect but also offer an electrostatic stabilization effect, thus resulting in a stable nanosilver ink. Such ink can be directly written into conductive lines on weighing paper by a facile pen-on-paper paradigm (Figure 2.11), and the trace from the ink could be treated at a low sintering temperature.

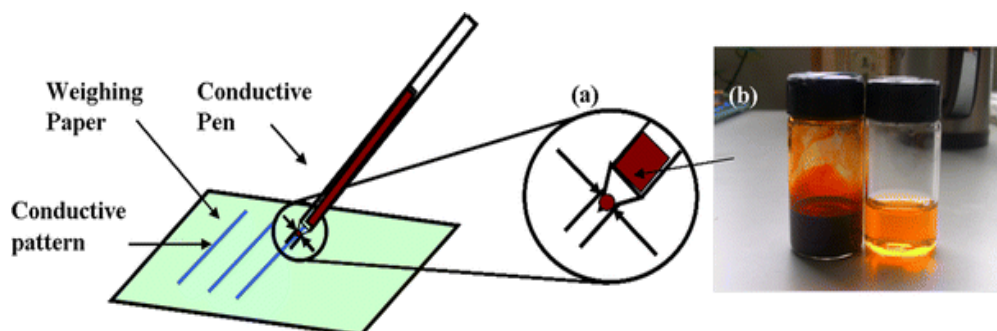


Figure 2.11 (a) schematic illustration for the preparation of conductive lines by a pen-on-paper paradigm; (b) the image of the as-prepared nanosilver ink (on the left) [90]

Although silver nano inks have some merits of high loading and good conductivity, the easy aggregation of NPs could potentially precipitate after storage for some time, thus resulting in instability.

### **b) Organic silver ink**

Organic silver ink has been studied with a great interest because of its flexibility in preparation, good stability and low cost. Organic silver inks are generally composed of organic silver salt or organic silver complex and volatile organic solvent that provide essential rheological properties for patterning. As the silver is generally present in ionic salts in these inks, there is no aggregation of NPs during preparation and storage. After depositing onto substrates, the organic solvent evaporates leaving the silver salt as a deposit, which can be subsequently decomposed by thermal treatment to form conductive metal patterns.

Silver neodecanoate was first used as a precursor to form organic silver inks, which starts to decompose to silver at 125 °C, and full decomposition achieved at 200 °C [91, 92]. Dearden et al. prepared an organic silver ink by dissolving the synthesized silver neodecanoate into xylene for ink-jet printing [92]. They investigated the resistivity as a function of temperature and found that temperature of 150 °C gave the excellent conductivity of 3.0-4.8  $\mu\Omega\cdot\text{cm}$ .

Then, Jahn et al. reported an organic silver ink based on Silver(I)

2-[2-(2-methoxyethoxy)ethoxy] acetate [93]. The ink had a silver content of 9.1 wt% and could be used for piezo ink-jet printing. The printed, photochemical sintered silver features on PET substrates showed a favorable conductivity of  $2.7 \times 10^7 \text{ S}\cdot\text{m}^{-1}$  and superior adhesion to the substrates.

In 2011, Wu et al. formulated an organic silver ink in a mixed solvent by using 1-dimethylamino-2-propanol (DP) as both the protecting and reducing agent for silver nitrate [26]. The printed silver lines showed a resistivity of  $1.73 \pm 0.44 \times 10^{-5} \Omega\cdot\text{cm}$  after sintering at  $100 \text{ }^\circ\text{C}$  for 60 min, which is quite close to the resistivity of bulk silver.

In 2012, Walker et al. developed a low-viscosity and highly conductive organic silver ink based on a modified Tollens' process using silver acetate, ammonium hydroxide and formic acid [8]. The ink was stable, particle-free, and suitable for a wide range of patterning techniques such as direct-writing, ink-jet printing and airbrush-spraying (Figure 2.12). After annealing at  $90 \text{ }^\circ\text{C}$ , the printed electrodes exhibit a conductivity equivalent to that of bulk silver, which is attractive to plastic, paper or textile based electronics applications.

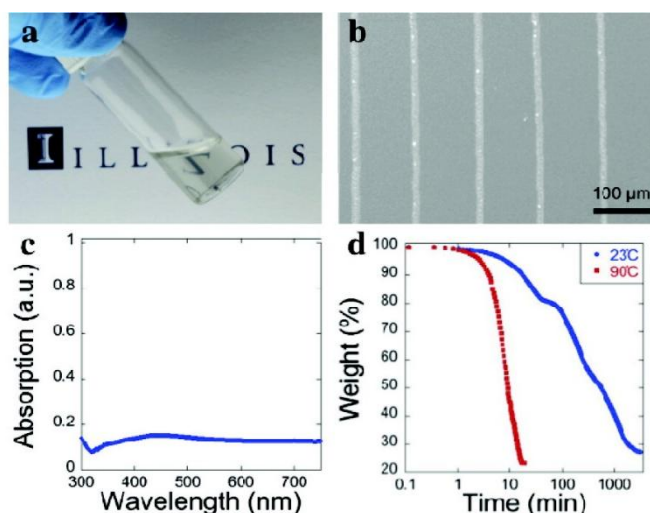


Figure 2.12 (a) Optical image of the silver ink in a vial. (b) 1D array of conductive silver lines ( $5 \mu\text{m}$  wide) printed on a silicon substrate via direct-write assembly using a  $100 \text{ nm}$  nozzle. (c) UV-vis spectrum of the silver ink. (d) TGA curves for the ink heated at  $23$  and  $90 \text{ }^\circ\text{C}$  in air [8]

Chang et al. developed a novel organic silver conductive ink via a complexing process of silver carbonate and isopropyl amine in a glycol-water mixture [13]. Silver ions in the ink can be reduced to metallic silver by glycol in the sintering process, following the typical polyol process. The viscosity of the ink was  $13.8 \text{ mPa}\cdot\text{s}$  and the surface tension

was  $36.9 \text{ mN m}^{-1}$ . After writing the ink on a polyimide (PI) substrate and sintering at  $150 \text{ }^\circ\text{C}$ , the formed film showed a resistivity of  $18 \mu\Omega\cdot\text{cm}$ . However, the ink was unstable in air due to the easy decomposition of the silver complex.

Nie et al. reported an organic silver ink through a complexing process of silver citrate and 1,2-diaminopropane for printing on PET substrates [32]. The ink could be reduced at  $135 \text{ }^\circ\text{C}$ , which was much lower than the  $185 \text{ }^\circ\text{C}$  decomposition temperature of silver citrate. The printed film showed a resistivity of  $17 \mu\Omega\cdot\text{cm}$  after sintering at  $150 \text{ }^\circ\text{C}$  for 50 minutes and possessed excellent adhesive properties.

Chen et al. reported a solution-based  $\beta$ -diketonate silver ink for spin-coating and inkjet printing of highly conductive features on a flexible substrate [14]. Ag films annealed at  $250 \text{ }^\circ\text{C}$  with thicknesses from 64 to 102 nm exhibited resistivities of  $4.625\text{-}9.376 \mu\Omega\cdot\text{cm}$ , which are relatively close to the resistivity of bulk silver.

Dong et al. prepared an organic silver ink using silver oxalate as precursor, ethylamine as a complexant, ethyl alcohol and ethylene glycol as the solvent [27]. The resultant silver film had a resistivity of  $8.4 \mu\Omega\cdot\text{cm}$  after sintering at  $170 \text{ }^\circ\text{C}$  for 30 min. The printed patterns on PI substrate sintered at  $150 \text{ }^\circ\text{C}$  for 30 min showed metalized silver with low resistivity and good adhesion.

### **c) Silver ink metallization**

Both types of the silver inks, the nano ink and the organic silver ink, require post-treatment techniques to form conducting tracks after being transferred to flexible substrates. A number of patterning techniques have been developed for the fabrication of conductive silver patterns.

The most used method is heating in an oven. The temperature required varies from ink to ink depending on the boiling points of organic solvents used, dissociation temperatures of the salts and the contact degree of silver NPs. Sometimes the treating temperature is higher than  $300 \text{ }^\circ\text{C}$ , which is too high to use for flexible substrates. Regarding this, some alternative methods are adopted such as microwave sintering, laser sintering, chemical conversion, electrical sintering, UV radiation and plasma treatment [2, 18, 71]. All of them can provide the desired temperature for the conversion of the ink traces to conductor tracks.

Microwave sintering is a fast, simple and cost-effective method in converting the printed silver patterns into conductors. It offers uniform, fast and volumetric heating which can significantly reduce the sintering time as compared to the conventional heating method for the same ink. Using this method, Perelaer et al. sintered silver NPs on a PI polymer substrate [94].

Ultra-violet light sintering is also used to convert the deposited silver structures because some organometallic silver solution inks have a particular reaction band with the UV light. Valetton et al. reported an organic silver ink which was reduced to silver by exposure to UV light and in the subsequent treatment with a hydroquinone solution at room temperature [95]. Such methods could produce silver patterns with a conductivity of 10% of the bulk silver and opened up the door to the temperature-sensitive polymeric substrates.

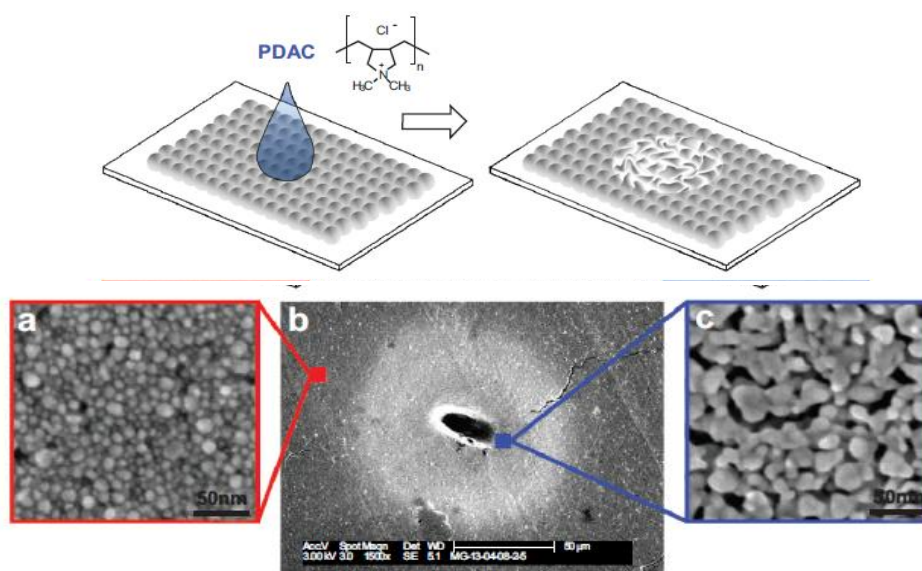


Figure 2.13 Schematic illustration what happened when a droplet of PDAC solution was dropped on the silver NPs array, SEM images of the printed drop zone (b); the magnified NPs arrays outside (a) and inside (c) in the droplet zone of PDAC [81]

The ultimate aim for converting the deposited silver patterns into the corresponding conductive counterparts is to reduce the sintering temperature to be as low as possible and to achieve the best conductivity in the widest range of potential substrates. The use of chemical sintering agents provides a breakthrough in this aspect. Using a cationic polymer, poly(diallyldimethylammonium chloride) (PDAC), the spontaneous coalescence of the silver NPs stabilized with poly(acrylic acid) (PAA) was initiated at

room temperature by Magdassi group, yielding traces with good conductivities (Figure 2.13) [81]. This method allows printing of conductive patterns on temperature-sensitive substrates.

Magdassi group also developed a spontaneous self-sintering method [82]. The ink is composed of silver NPs stabilized by polymer and a low concentration sintering agent; the latter can be a simple electrolyte such as NaCl. During the drying process, the sintering agent can induce the coalescence and sintering of the silver NPs (Figure 2.14). Such a process has led to very high conductivities up to 41% of the conductivity of the bulk silver material.

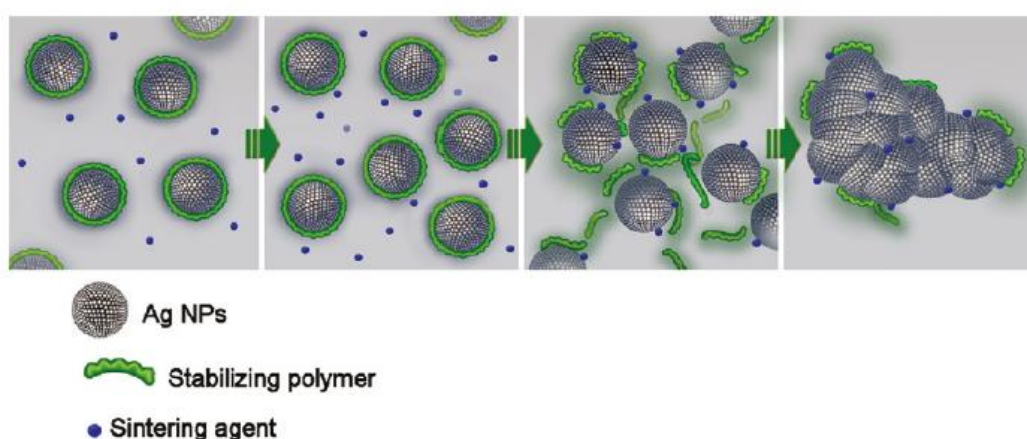


Figure 2.14 Schematic illustration of the silver NPs self-sintering process (the green lines represented the polymeric stabilizer; the blue spheres represented the sintering agent) [82]

Table 2.2 compares the current reported silver nano inks in terms of their ink composition, patterning method and conductivity. As seen, most of silver nano inks require a temperature above 200 °C to achieve a resistivity in the order of  $10^{-6} \Omega \cdot \text{cm}$ , which is not ideal for the ink being used on a variety of flexible substrates. Only the ink with a suitable size, solvent and stabilizer system can be successfully sintered below 200 °C with a resistivity near 5 times of bulk silver. The inks developed in reference [86] and [89] have facile synthesis approaches, good stability, printability and conductivity, exhibiting huge potential for electronics applications. But the sintering temperatures are still high for most of flexible substrates.

Table 2.2 Comparison of the reported nano silver inks

No.	Ink Composition			Patterning Method		Resistivity ( $\mu\Omega \cdot \text{cm}$ )	Ref.
	Silver size	Stabilizer	Solvent	Deposition	Metallization		

(nm)								
1	14	Mixed ligands	DI water and methanol	Suitable for inkjet printing	200°C	for 10		[84]
2	6	Dodecanoic acid	n-tetradecane	Ink-jet printing	250°C for 30 min	6		[85]
3	6.2 (Ag-C <sub>11</sub> H <sub>23</sub> CO <sub>2</sub> )	Dodecanoic acid	cyclohexane	Ink-jet printing	250 °C for 60 min	3.23–4.62		[6]
4	20	PVP	A mixture of ethylene glycol, ethanol and DI water	Ink-jet printing	160 °C for 30 min	8.76-9.18		[86]
5	50	Pluronic F-127	DI water	Ink-jet printing	350 °C for 60 min	20		[83]
6	47	PVP	DI water and diethylene glycol	Electrode printing	200 °C for 20 min	16.3		[87]
7	20	PAA	DI water	Ink-jet printing	250 °C for 60 min	4		[88]
8	30	PAA	DI water and ethylene glycol	Ink-jet printing	180 °C for 15 min	8		[89]

Similarly, Table 2.3 makes a comparison to the current developed organic silver inks. Overall, this type of ink needs specific metal salts to formulate and has a relatively low sintering temperature (~150°C) for conductivity comparable to that of bulk silver. The difficulties are to select appropriate organic salt. The inks reported in reference [8], [27] and [92] have facile synthesis routes, good conductivity and printability, which basically fulfilled the criteria for an optimal ink design.

Table 2.3 Comparison of the reported organic silver inks

No.	Ink Composition		Patterning Method			Resistivity ( $\mu\Omega\cdot\text{cm}$ )	Ref.
	Silver precursor	Complexing agent	Solvent	Deposition	Metallization		
1	Silver neodecanoate	None	Not given	Ink-jet printing	150°C	3-4.8	[92]
2	Silver(I) 2-[2-(2-methoxyethoxy)ethoxy] acetate	Triethylamine	Ethanol-acetonitrile	Ink-jet printing	130°C with UV irradiation, 30 min	9.11	[93]
3	Silver nitrate	1-Dimethylamin o-2-propanol	Ethanol and	Ink-jet printing	100°C for 60 min	17.3	[26]

			ethylene glycol					
4	Silver acetate	Ammonium hydroxide	Aqueous containing formic acid	Ink-jet printing, direct-writing and airbrush-spraying	90°C for 15 min	1.6	[8]	
5	Silver carbonate	Isopropyl amine	Glycol and DI water	Handwriting	150°C for 60 min	18	[13]	
6	Silver citrate	1,2-diaminopropane	Methanol and isopropanol	Ink-jet printing	150°C for 50 min	17	[32]	
7	$\beta$ -diketonate silver	Diethylenetriamine	Hexylamine (containing ethyl cellulose)	Ink-jet printing	250°C for 180 min	4.62-9.37	[14]	
8	Silver oxalate	Ethylamine	Ethyl alcohol and ethylene glycol	Ink-jet printing	170°C for 30 min	8.4	[27]	

### 2.6.2 Copper ink

Copper is a good alternative material for silver due to its low cost, good conductivity, and the reduced electromigration effect. Copper-based inks have been developed to reduce costs compared to the silver-based inks. Various methods have been developed to synthesize copper inks [38-44]. Similarly, with silver-based inks, there are also two types of copper based-inks: copper nano inks and organic copper inks. Each has its advantages and disadvantages.

The major drawback associated with copper NP inks is that they are prone to agglomeration and a high tendency to oxidation under the ambient conditions, which is a serious problem since the oxidized particles require elevated temperatures to sinter and usually have poor electrical conductivities. In order to circumvent the oxidation of Cu NPs, novel methods have been used to improve the material properties. A very successful approach is to stabilize copper NPs by amorphous carbon [96, 97] or graphene [43] or organic polymers [98-101] or core-shell structure [102].



Ang et al. [96] prepared 5 to 10 nm size copper NPs coated by alkanethiols with C8 to C12 chains in ethanol, such a layer is a good barrier to protect copper NPs from oxidation for at least six months. Kanninen et al [97] used the same approach and longer chain compounds of C6 to C18 as a coating and compared the performance of lauric (C12) and oleic (C18) acids. The results showed that the oleic acid-capped particles were superior to the thiol-stabilized particles.

Luechinger et al. reported that copper NPs coated by graphene bi- or tri-layers could resist oxidation under the ambient conditions [43]. Copper NPs of 50 nm coated by the graphene layer of 3 nm in thickness were synthesized by using the reducing flame technique (Figure 2.15). The prepared particles were stable against oxidation at temperatures up to 165°C. The ink formed from these copper NPs enabled conductive patterns.

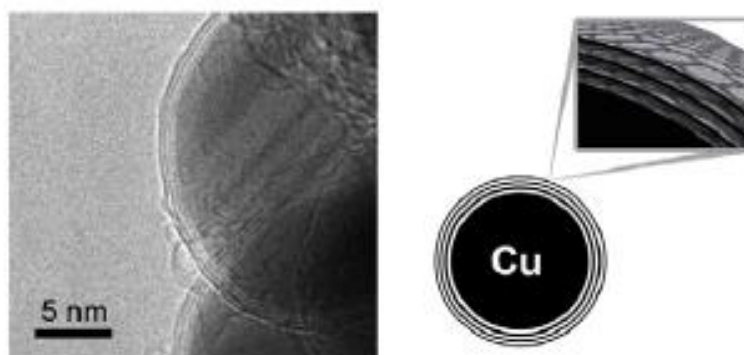


Figure 2.15 Transmission electron micrograph of single copper NP with a thick graphene wrapping of 3 nm and a corresponding schematic illustration [43]

Kobayashi et al. [98] used polypyrrole to coat copper NPs in an aqueous solution. The coated copper NPs were chemically stable, even under air. Pulkkinen et al [99] evaluated two different polymer protecting agents for copper NPs, polyethylene imine and tetraethylenepentamine. However, even under pressing and heating to 250°C, the resistivity of the conductive films was still 3 to 5 times higher than that of the bulk copper.

Liu group developed a simple, large-scale and high-throughput process for the synthesis of copper NPs ink using CuO as a copper source, PVP as a protection agent and hydrazine hydrate as the reductant [100]. As the prepared oblate shape copper NPs sized 80 nm had a better anti-oxidation capability, a good quality conductive film was formed



on glass slides easily at 300 °C using an ink of the copper NPs (20 wt%).

Jeong et al. described an approach to controlling the thickness of the oxide layer on Cu NPs surface by varying the molecular weight of the polymeric capping agents [101]. They confirmed that the oxide layer thickness was the predominant factor determining the electrical conductivity of the granular film of Cu NPs. The synthesized Cu NP ink was used to write conductive features on plastic substrates.

Core-shell structures can also prevent copper NPs from oxidation. Several methods have been used to form the structure, such as electrodeposition, thermal evaporation, and ion exchange. Grouchko et al. [102] synthesized a copper-silver core-shell structure based on a transmetalation reaction on the surface of copper NPs, where the copper atoms were used as the reducing agent for silver (Figure 2.16). The obtained Cu-Ag core-shell NPs displayed good stability below 187°C. The layer of silver could effectively prevent the oxidation of copper core and preserve its metallic characteristic.

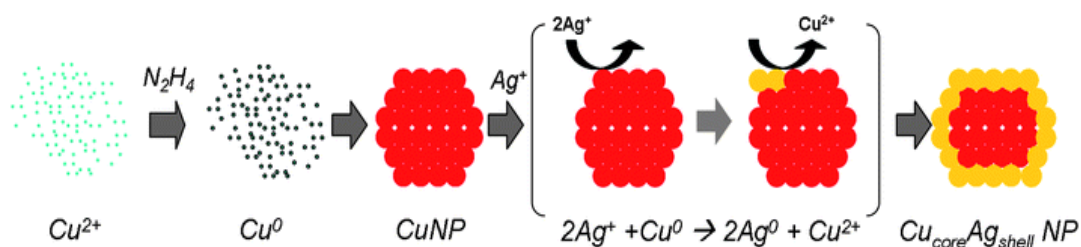


Figure 2.16 Schematic illustration of a single Cu NP synthesis and the formation of a silver shell by the transmetalation reaction [102]

Although some progress has been made to prevent aggregation and undesirable oxidation of copper NP-based inks, most of the synthetic methods are not economically feasible because of the low throughput and poor scalability.

In contrast to the copper nano inks, organic copper inks are stable under an aerobic atmosphere. Thus, organic copper inks are a worthy alternative to copper NP inks. Several organic copper inks have been developed in recent years. The most prominent example is copper formate [45, 50, 51]. The main advantage of such inks is clean decomposition at low temperature without any organic residues.

Yabuki et al. produced a copper conductive film on a glass substrate by the thermal decomposition of the ink containing the complexes of copper (II) formate and

n-octylamine in a nitrogen atmosphere at low temperature [45]. Kim et al. investigated the optimal conditions for reducing the electrical resistivity of copper films made from the organic Cu ink formulated by mixing copper(II) formate and hexylamine [50]. They revealed that the Cu concentration in the inks controlled the porosity and impurity content, and ultimately determined the electrical resistivity of the films.

Besides, copper carboxylate inks derived from citric, hexanoic acid and neodecanoic acid have been reported [42, 103], but both needed post-printing sintering in a reducing atmosphere in order to obtain pure copper structures. Copper glycolate and lactate have also been used to produce copper films [104]. Copper(I) complexes, copper(I) vinyltrimethylsilane hexafluoroacetylacetonate, has been used in inkjet printing process [105].

Recently, Wang et al. reported a particulate-free copper ion ink which offered excellent ion complex stability and dispersion stability [106]. The ink is environmentally friendly and can be written and sintered using intense pulsed light at low temperatures, showing excellent electrical properties. The study gives a new inspiration and may lead to innovative changes in the various industries. Figure 2.17 shows some patterns of the ink written by a roller-ball pen.

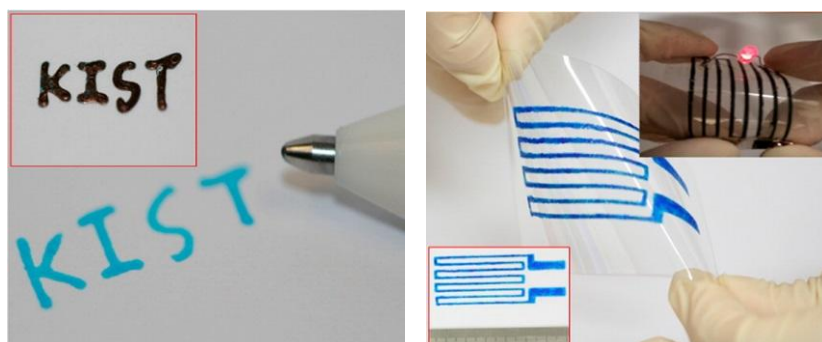


Figure 2.17 Patterns of the ion ink printed using a roller-ball pen [106]

Magdassi et al. reported a copper complex ink with the ability of self-reduction [107]. The ink was of copper formate and 2-amino-2-methyl-1-propanol, and can decompose at 140 °C under a nitrogen environment. It is chemically stable and easy to process in inkjet printing.

Liu group designed a new complex oxidation-reduction process of copper acetate and cyclohexylamine together with formic acid to prepare Cu ink [108]. Although the ink

contained only 9.6 wt% of copper, it still offered good conductivity. The research revealed that formic acid was the most critical factor influencing the conductivity of the film.

Apart from the modification of the ink material properties, selection of a suitable sintering method is also a good solution to the oxidation problem of both copper NPs ink and organic copper ink in the sintering process such as the intense pulsed light sintering and the laser sintering methods [109-112]. For example, Lee et al. obtained conductive copper films with tightly packed, dense structures from a Cu complex ink by laser sintering [111]. Their results showed that the laser sintered film consisted of mainly nanorods with a better crystalline quality than that by a typical thermal process. Araki et al formulated copper inks using copper formate/acetate/oleate as the precursor [110]. Based on the light absorption ability of the inks (Figure 2.18), they adopted the photonic sintering method for the metallization. The formed wires showed a low resistivity of  $5.6 \times 10^{-5} \Omega \cdot \text{cm}$ .

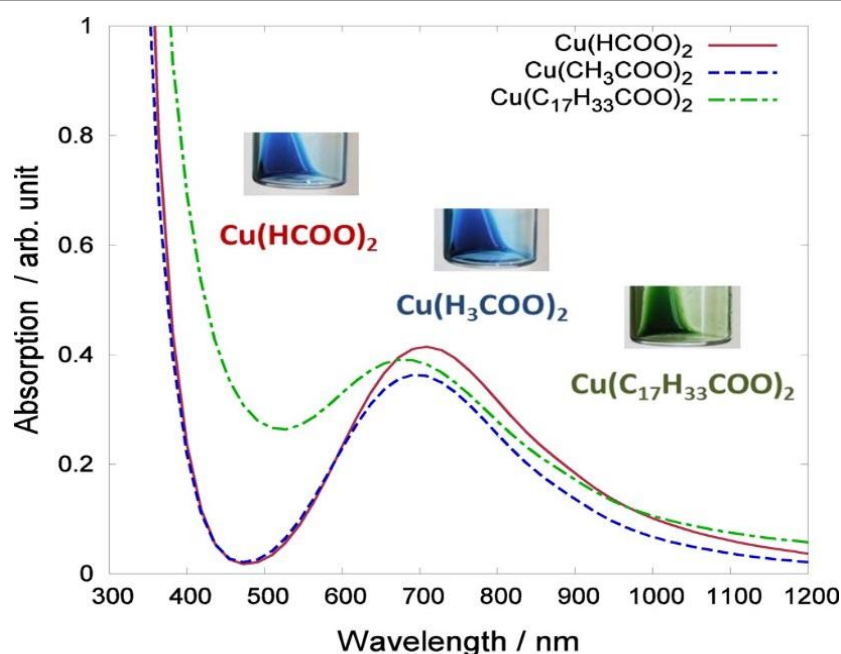


Figure 2.18 Absorption spectra of the three types of copper complex ink: copper formate, copper acetate, and copper oleate. The inset photographs displayed the visual color of the inks [110]

Table 2.4 compares the current reported copper nano inks in terms of their ink composition, patterning method and conductivity. As seen, strong surfactants such as PVP and oleic acid were usually selected to synthesize Cu NPs with less oxidation for the ink application. The drawback along with this method is that temperatures above 250 °C are normally required to remove these stronger surfactants before realizing the

efficient sintering of Cu NPs. Besides, a special sintering method such as vacuum condition or a reductive atmosphere is also needed to prevent the Cu NPs from oxidation and to achieve good conductivity during sintering process. These two points overshadows the low cost advantage of copper nano inks compared to silver nano inks. The ink reported in reference [44] has a facile synthesis route and a low sintering temperature for good conductivity, which is ideal.

Table 2.4 A brief overview of the reported copper nano inks

No.	Ink Composition			Patterning Method		Resistivity ( $\mu\Omega\cdot\text{cm}$ )	Ref.
	Particle size (nm)	Protecting agent	Solvent	Deposition	Metallization		
1	55	PVP	2-(2-butoxyethoxy)ethanol	Ink-jet printing	275°C for 60 min in formic acid atmosphere	3.6	[21]
2	40-50	PVP	Ethyleneglycol	Ink-jet printing	325 °C for 1 h in vacuum	17	[23]
3	42.3/108.3	Oleic acid	Toluene	Ink-jet printing	300 °C in Ar	5.9	[24]
4	50	PVP	Ethanol solution of carboxylic acids	Drop-coating	200 °C for 30 min, N <sub>2</sub>	14.0 ± 4.5	[38]
5	10	Lactic acid and glycolic acid	Ethanol	Drop-coating	200 °C for 60 min, N <sub>2</sub>	9.1 ± 2.0	[39]
6	3.5 ± 1.0	1-amino-2-propanol	Propylene glycol, glycerol	Bar coating	150 °C for 15 min, N <sub>2</sub>	30	[44]
7	35-60	PVP	A mixture of ethylene glycol, 2-methoxyethanol, and methyl alcohol	Ink-jet printing	275°C for 60min in vacuum	11	[101]

Similarly, Table 2.5 makes a comparison to the current developed organic copper inks. Overall, the precursors of this type of inks are very limited and most of them are based on copper(II) formate. The ink reported in reference [107] show good property for ink-jet printing electronics but the sintering temperature is still high. Here, photonic sintering such as intensive pulsed light sintering shows huge advantages to realize the effective sintering of such inks under ambient condition within a millisecond time frame.

Table 2.5 A brief overview of the reported organic copper inks

No.	Ink Composition			Patterning Method	Resistivity ( $\mu\Omega\cdot\text{cm}$ )	Ref.
	Copper precursor	Complexing agent	Solvent	Deposition	Metallization	
1	Copper(II) formate tetrahydrate	n-octyl amine	Toluene	Squeegee coating	140°C for 60min, N <sub>2</sub>	20 [45]
2	Copper(II) formate tetrahydrate	2-Amino-2-methyl-1-propanol	Isopropyl alcohol	Drop coating	350 °C for 30min, N <sub>2</sub>	9.46 [46]
3	Copper acetate	Cyclohexylamine	Ethanol/ethylene glycol mixture	Drop coating	230 °C for 60min, N <sub>2</sub>	22 [49]
4	Copper (II) formate hydrate	Hexylamine	/	Coating	250 °C for 2 min with formic acid	5.2 [50]
5	Copper(II) formate anhydrate	3-dimethylamino-1,2-propanediol	/	Squeegee coating	180 °C for 5min	300 [51]
6	Copper(II) hydroxide	Formic acid and citric acid	DI water	Handwriting	Intensive Pulsed Light Sintering	3.21–5.27 [106]
7	Copper(II) formate tetrahydrate	2-amino-2-methyl-1-propanol	/	Inkjet printing	190 °C for 2 min, N <sub>2</sub>	10.5 [107]
8	Copper formate/acetate/oleate	Diethanolamine	Ethanol	Inkjet printing	Intensive Pulsed Light Sintering	56 [110]
9	Copper formate	Hexylamine and 2-amino-2-methyl-1-propanol	Isopropyl alcohol	Spin coating	Laser sintering	17 [112]

### 2.6.3 Graphene related ink

#### a) Graphene ink

Currently, two routes are taken to prepare stable graphene inks. The first one is to use stabilizers in the ultrasonic exfoliation process of pristine graphene sheets. The second

one is to use stabilizers in the chemical reduction process of GO, which can wrap around the graphene and may sterically or electrostatically hinder restacking. The kinds of stabilizers mainly involve polycyclic aromatic hydrocarbons, surfactants (sodium dodecyl sulphate), polymers (PVP, PVA) and ethyl cellulose. Water or organic solvents such as terpineol, ethanol, N,N-dimethylformamide (DMF), N-methyl-2-pyrrolidone (NMP) and dimethyl sulfoxide (DMSO) are used as the main solvents in ink formulation.

Li and co-workers developed a simple method to formulate stable graphene inks with high concentration and compatible fluidic characteristics based on the combination of solvent exchange and polymer stabilization techniques [62]. Graphene is first exfoliated from graphite flakes in DMF, and then a small amount of polymer (ethyl cellulose) is added into the above dispersion to protect the graphene flakes from agglomeration. Last, the DMF is exchanged with terpineol through distillation. Benefiting from the polymer stabilization, the graphene/terpineol dispersions with a concentration around  $1 \text{ mg mL}^{-1}$  can be stable for at least several weeks. Ethanol was added to tailor the viscosity and surface tension to make the dispersions compatible with inkjet printing. The inks provided well-directed and constant jetting for printing. Del et al. also prepared a graphene ink with multiple graphene layers using the solvent exchange technique, where graphite powders were first exfoliated in DMF and then stabilized using ethyl cellulose [113]. DMF was replaced with terpineol to increase the graphene concentration, as well as to adjust the ink viscosity and to reduce solvent toxicity.

Torrise et al. produced a stable graphene-based ink by liquid phase exfoliation of graphite in NMP and used it to print thin film transistors, with mobilities up to  $95 \text{ cm}^2 \text{V}^{-1} \text{s}^{-1}$ , as well as transparent and conductive patterns, with transmittance of 80% and sheet resistance of  $30 \text{ k}\Omega/\square$  [114]. The liquid phase exfoliated graphene turned out to be an ideal low-cost material for making printable inks. But NMP is still not environmentally benign, which is not good for ink-jet printing process.

Secor et al. developed a novel graphene ink using a graphene/ethyl cellulose (EC) powder that was produced using only room temperature processing methods [115]. The graphene inks were produced by the exfoliation of graphite in ethanol and EC. The processing steps are illustrated in Figure 2.19. The graphene/EC powder allowed the ink to achieve stable inkjet printing of features on a variety of substrates with excellent

morphology. The graphene features showed low resistivity of  $4 \text{ m}\Omega\cdot\text{cm}$  after thermal annealing at  $250 \text{ }^\circ\text{C}$  for 30 minutes while showing uniform morphology, compatibility with flexible substrates, and excellent tolerance to bending stresses. However, this method involved a repetitive and sophisticated process of salt flocculation and redispersion in solvent to obtain the graphene/EC powder, which limits its application. Recently, by changing the EC composition in the graphene exfoliation step, they obtained graphene/EC powders with a graphene composition ranging from 25 to 65 wt% as precursors for graphene inks [116]. These inks are suitable for intense pulsed light annealing and were prepared by dispersion of the graphene/EC in a solvent system composed of cyclohexanone/terpineol (85:15, v/v).

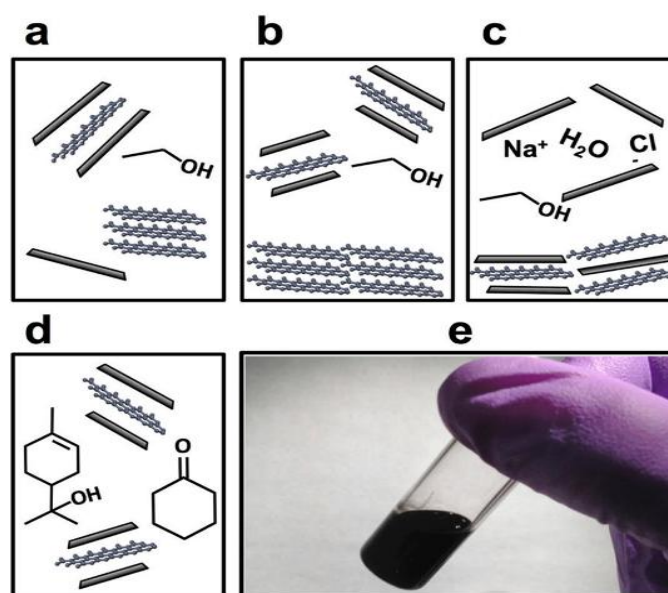


Figure 2.19 Schematic illustration of the ink preparation method. (a) Graphene is exfoliated from graphite powder in ethanol/EC by probe ultrasonication, (b) centrifugation-based sedimentation to remove residual large graphite flakes, (c) salt-induced flocculation of graphene/EC, (d) An ink for inkjet printing is prepared by dispersion of the graphene/EC powder in 85:15 cyclohexanone/terpineol, and (e) Vial of the prepared graphene ink [115]

Gao et al. formulated a pristine graphene based ink with high concentration and stability using a simple and practical method, and fabricated electrodes with high electrical conductivity [117]. The pristine graphene was prepared by exfoliating graphite using an ultrasound-assisted supercritical  $\text{CO}_2$  based method as shown in Figure 2.20. The graphene ink was formulated using cyclohexanone and ethyl cellulose (EC) as the solvent and the stabilizing agent, which was stable for more than 9 months. This long stability is mainly because of the strong hydrophobic interactions between ethyl cellulose and the graphene sheets, thereby inhibiting the aggregation of the graphene.



The sheet resistance of the films printed for 30 times was only  $0.81 \pm 0.2 \text{ k}\Omega/\square$ , and the annealed films had a transmittance of approximately 60%. The resistivity of the printed electrodes on flexible substrates increased slightly after 1000 bending or folding cycles. But the annealing temperature,  $300 \text{ }^\circ\text{C}$ , is still high for most flexible substrates applications.

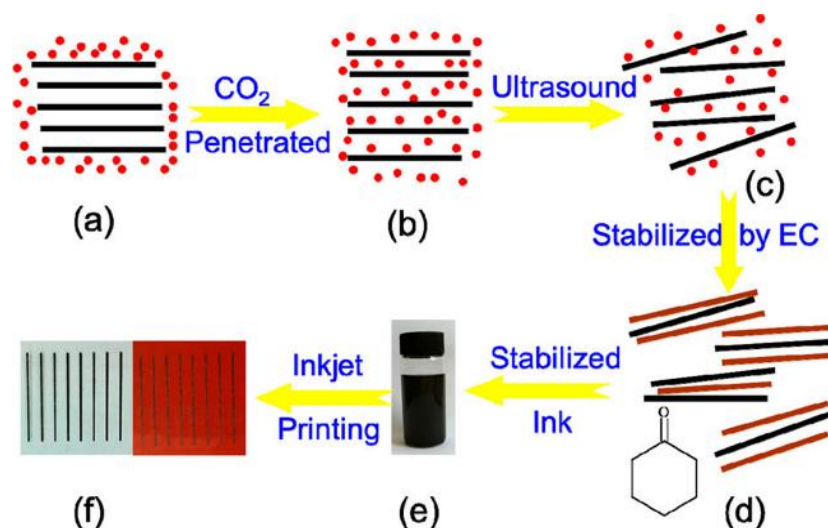


Figure 2.20 Schematic illustration of the preparation process of pristine graphene ink and inkjet printing. (a) Layered graphite was immersed in supercritical CO<sub>2</sub>, (b) CO<sub>2</sub> molecules penetrated and intercalated in the interlayer of graphite, (c) forming single or few layer thick graphene sheets, (d) Graphene sheets were stabilized by EC in cyclohexanone, (e) formed stable graphene ink, and (f) printing graphene electrodes on PET and PI substrates [117]

Lee et al. prepared a highly stable graphene ink by the adsorption of sodium n-dodecyl sulphate (SDS) and adjusting the pH value to 10 [118]. The SDS can yield multiple charged layers, hemi-cylinders, or multiple hemi-spheres, and further it can prevent graphene powder from aggregation. The effect of pH adjustment is to change the charge density of the graphene surface. The graphene dispersions can be stable for more than one month and meet the requirements for inkjet printing. Conductive features were fabricated on a flexible PI film by inkjet printing the stable ink directly on the substrate. The loading of graphene on the PI film showed a linear increase with printing time. The conductivity of the sintered film was improved to  $121.95 \text{ S m}^{-1}$  via a post-heating process, but this value is still low for most electronic devices.

Capasso et al. prepared graphene and graphene a few layer thick based inks suitable for inkjet printing processes on flexible substrates using a low boiling point and environmentally-friendly solvent, ethanol/water mixture [119]. The stable ink formulations were obtained by investigating various rheological properties such as



density ( $\rho$ ), surface tension ( $\gamma$ ) and viscosity ( $\nu$ ). These inks were used to print conductive stripes with sheet resistance of  $13 \text{ k}\Omega/\square$ .

### **b) Graphene oxide ink**

Graphene oxide (GO) has a similar structure as graphene but with oxygen containing groups which results in expansion of interlayer distance in the GO structure, and as a consequence, it makes GO hydrophilic. The abundant oxygen-containing functional groups enable GO to have excellent solution processability and allow efficient assembly of large area films from solution. GO can be easily dispersed in water and polar organic solvents such as DMF, NMP, tetrahydrofuran, and ethylene glycol. Preparation of stable GO dispersions does not require the addition of stabilizing agents which is an advantage over graphene inks.

Shin et al. synthesized a GO ink using a modified Hummers and Offeman method [120]. Exfoliated GO aqueous solution was used as conductive ink, and thermal annealing for the reduction process was performed under vacuum conditions. Graphene nanosheets that consisted of a few atomic layers were successfully patterned on a PET film using this ink after the subsequent thermal reduction. The patterned graphene lines had a much higher resolution compared to other conducting polymers. The graphene-based thin film exhibited sustained electrical conductivity. One disadvantage is that hydrazine vapor was used in the reduction process, which is not desirable due to its high toxicity.

Le et al. produced electrically conductive graphene electrodes using a GO dispersion and the subsequent thermal reduction under  $\text{N}_2$  at  $200 \text{ }^\circ\text{C}$  for 12 hours (Figure 2.21) [63]. Hydrophilic GO dispersed in water was found to be a stable ink for inkjet printing. At room temperature, the viscosity and surface tension of the GO ink were  $1.06 \text{ mPa s}$  and  $68 \text{ mN m}^{-1}$  respectively. In order to jet spherical GO ink droplets, the waveform function of the piezoelectric nozzle operation was adjusted to compensate for the low viscosity and high surface tension of the water-based ink.

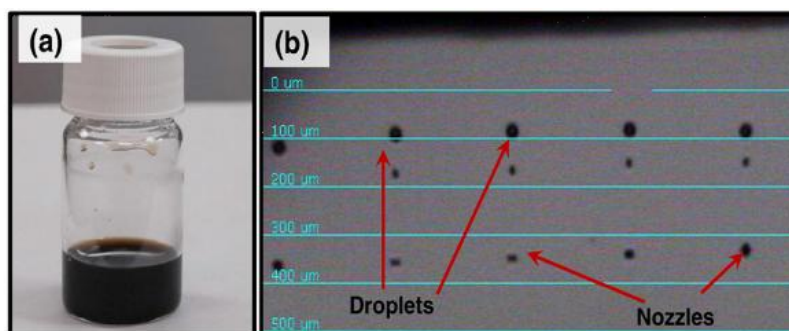


Figure 2.21 GO ink and morphology. (a) GO dispersed in water at 0.2 wt% as a stable ink, (b) spherical ink droplets generated by piezoelectric nozzles [63]

Dua et al. printed rGO platelets by using aqueous surfactant-supported dispersions of GO powder and ascorbic acid as a mild and green reducing agent (Figure 2.22) [60]. The resulting film has electrical conductivity and has fewer defects compared to rGO films obtained using a hydrazine based reduction process.

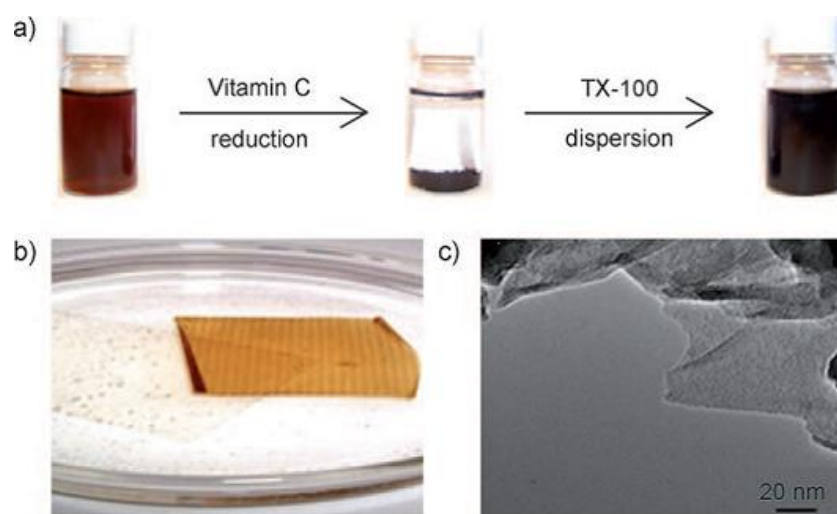


Figure 2.22 (a) Optical pictures of vials containing GO and rGO dispersions. (b) Inkjet-printed graphene oxide film after lift-off from the PET surface. (c) TEM image of the RGO powder [60]

Lim et al. found that poly(vinyl alcohol) (PVA) blended with graphite oxide can enhance exfoliation of the graphite sheets and produce a stable solution for inkjet printing [121]. A homogeneous RGO/PVA colloidal suspension was prepared (Figure 2.23), and PVA played an important role in maintaining the long-term stability of the RGO/PVA suspension required for inkjet printing.

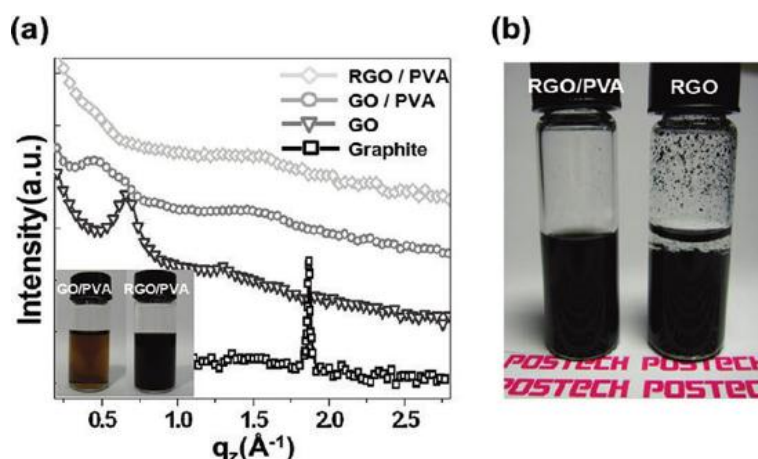


Figure 2.23 (a) XRD patterns of graphite, graphite oxide (GO), GO/PVA, and RGO/PVA composite, insert showing photographs of well-dispersed GO/PVA (left) and RGO/PVA (right) suspensions, (b) RGO/PVA composite stably dispersed in a mixed solvent with DMF and water for three months (left) and RGO precipitated from the same medium (right) [121]

Porro et al. prepared a water-based, environmentally friendly graphene oxide/acrylic ink [122]. The possibility of inkjet printing and subsequently polymerizing the composite resin by irradiation with UV light was studied. The graphene oxide filler, which was strongly hydrophilic due to its heavily oxygenated surface for easy dispersion in water, was reduced by UV irradiation during photo-curing of the polymeric matrix. The network clusters of reduced graphene oxide inside the polymer matrix act as preferential pathways for the mobility of charge carriers, thus leading to an overall decrease of the material's resistivity.

Although the solution processability of GO offers a unique advantage in spin-coating or inkjet printing onto substrates for the large-scale production of graphene based electronic circuits, the graphene reduced from GO by chemical reduction and thermal annealing is reported usually to have more defects and poor conductivity resulting from low carrier mobility, which restricts its use in electronic applications.

### c) Graphene/polymer ink

Conducting polymers are promising materials for supercapacitors due to their high pseudocapacitance. As a typical conducting polymer, polyaniline has long been a widely used material for supercapacitor electrodes due to its ease of synthesis, processability, and special redox activity. However, one of the drawbacks of polyaniline as supercapacitor electrodes is its poor cycling stability. Additionally, polyaniline exhibits only moderate electrical conductivity.

Graphene/polyaniline hybrid materials can address the shortcomings of polyaniline and can also form a stable and underlying conductive network due to the incorporation of graphene. Thus it is attractive to formulate graphene/polyaniline inks to harness these excellent synergistic capacitive properties. Xu et al. formulated graphene/polyaniline inks and produced graphene/polyaniline thin film electrodes from these inks [123]. Nano graphene platelets (NGPs), sodium dodecyl benzene sulfonate (SDBS), polyaniline (PAIN) and water were used to form the inks. In inkjet printing, good control over a number of key film properties including pattern geometry, pattern location, film thickness, and electrical conductivity was achieved.

Liu et al. developed a hybrid ink of exfoliated graphene (EG) and poly (3, 4-ethylenedioxy thiophene) : poly (styrenesulfonate) (PEDOT:PSS) formulation (Clevios PH1000) in DMF [124]. PH1000 was selected as the surfactant due to its conjugated aromatic chains that can strongly anchor onto the graphene surface via  $\pi$ - $\pi$  interactions without disrupting the electronic structure of graphene. PH1000 was also used due to its superior electronic properties and solution compatibility with EG. The resulting hybrid ink was stable for at least 1 month without apparent precipitation. The significant  $\pi$ - $\pi$  interactions between the EG basal plane and PH1000 are believed to produce charge-transfer effects, which were confirmed by Raman spectroscopy (Figure 2.24c). The fabricated graphene films exhibited excellent mechanical properties. The hybrid ink of EG/PH1000 may pave the way to the future development of transparent electrodes for optoelectronics, and other emerging flexible devices such as wearable supercapacitors and electronic skins.

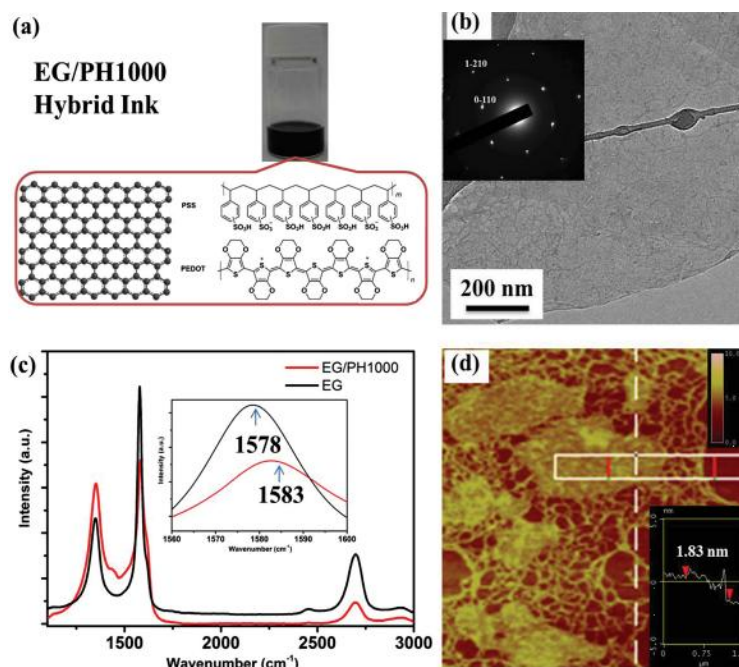


Figure 2.24 (a) Optical image of EG/PH1000 hybrid ink and molecular structures of EG and PH1000, (b) TEM image of a single graphene sheet from EG/ PH1000 hybrid ink, inset showing the SAED pattern of the single graphene sheet, (c) Raman spectra of graphene flakes from EG and EG/PH1000 hybrid ink ( Inset shows the shift of the G peak), and (d) AFM image of graphene sheets from EG/PH1000 hybrid ink [124]

### c) Graphene/metal ink

Recent research has focused on the graphene/metal based composite materials for improving the conductivity of pure graphene ink. It is promising to mix metal nanoparticles and graphene nanosheets together to produce a hybrid ink and thus take full advantage of these two materials to enhance the conductivity and reduce the concentration of metal particles. Some new approaches using metal nanoparticles and graphene or GO/rGO as the ink fillers have been developed. So far the work has been focused on Ag based hybrid systems since the Ag based inks are more cost effective than Pt and Au based metal inks, and they are more stable than Cu based on inks - less prone to oxidation. Therefore Ag nanoparticles have been widely used to decorate graphene and its derivatives in graphene/metal inks.

Li et al. prepared inks of Ag and rGO, one based on a mixture of Ag nano-triangle particles (NTPs) and rGO platelets, and the other containing polyhedral Ag and rGO nanoparticles (Figure 2.25) [125]. They used a process starting from graphene oxide exfoliation, ink formation, printing, to final reduction. Central to this approach was that the ink solvent was only water. The monodispersed Ag nano-triangle platelets (Ag NTPs)

and Ag polyhedral nanoparticles (Ag NPs) could self-assemble on rGO platelets which were also used as the dispersant and stabilizer. Compared with rGO, (Ag NP)-rGO and other rGO-based materials previously reported, the Ag NTP-rGO pattern showed a low sheet resistance of  $170 \Omega/\square$  after reduction with a transmittance of 90.2%. The inkjet printing and reduction process can also be used to obtain other metal-graphene patterns and devices. However the reduction process of this method is not ideal because of the long thermal treatment time of 3 hours at  $110 \text{ }^\circ\text{C}$  in a vacuum oven after the ink printing process.

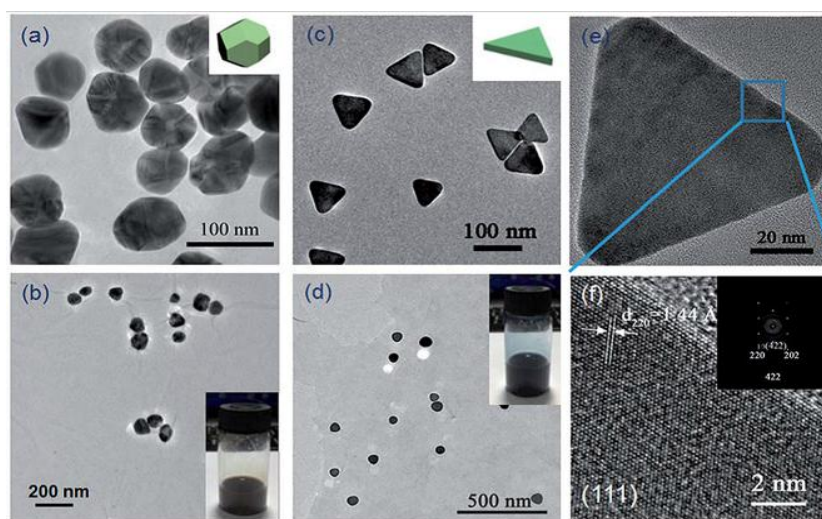


Figure 2.25 The TEM images of the as-synthesized (a) Ag NPs, (b) Ag NP-GO (the inset is a photograph of the Ag NP-GO ink), (c) Ag NTPs, (d) Ag NTP-GO (the inset is the photograph of the Ag NTP-GO ink) and the HRTEM images of the as-synthesized Ag NTPs (e and f), the inset in (f) is a high resolution fast Fourier transform diffraction pattern of Ag NTPs [125]

Annealed graphene nanosheets coupled with Ag organic complex inks have been developed by Chen's group, by dispersing an as-purchased silver based complex and the annealed graphene nanosheets in a mixture of cyclohexanone and terpineol [126]. A resistivity of  $4.62 \times 10^{-4} \Omega \cdot \text{m}$  was achieved after baking at  $300 \text{ }^\circ\text{C}$  for 40 minutes after film deposition. The Ag nanoparticles (NPs) were uniformly distributed on graphene nano-sheets after the post annealing process, which could act as superiorly conductive bridge to further decrease the contact resistance of graphene flakes and the resistivity of the inkjet printed track. The interwoven graphene nanosheets with Ag NPs formed a three-dimensional conductive network in the film with good mechanical robustness. The results provide a possible pathway for future bendable inkjet printed electronic devices.

Xu et al. prepared a hybrid conductive ink composed of Ag NPs and graphene-Ag



nanocomposites for writing electronics [127]. The Ag NPs and graphene-Ag nanocomposites were dispersed in a mixture of ethanol, ethylene glycol and glycerol to form the ink. Owing to the electrical pathway effect of graphene and the decreased contact resistance of graphene interfaces by depositing Ag nanoparticles onto graphene sheets, the concentration of Ag NPs was significantly reduced while maintaining high conductivity at a curing temperature of 100 °C. A typical resistivity value measured was  $1.9 \times 10^{-7} \Omega \cdot \text{m}$ , which is 12 times the value for bulk silver. Even after thousands of bending cycles or rolling, the resistance values of the written tracks only increased slightly.

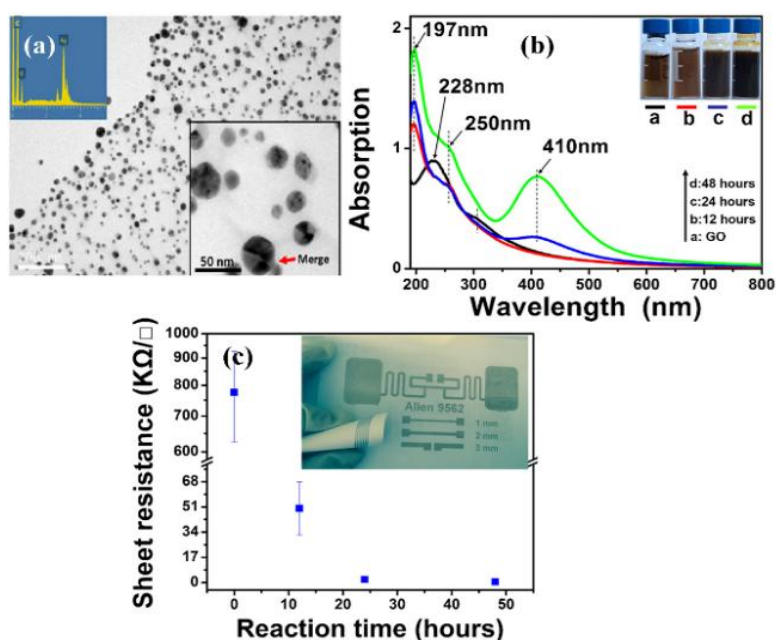


Figure 2.26 (a) TEM image of Ag/RGO hybrid with reaction time of 48 h (inset: enlarged TEM view of Ag NPs and EDS of Ag/RGO composite), (b) UV-vis absorption spectra of synthesized Ag/RGO composites from GO after reaction times of 12 h, 24 h and 48 h, and (c) sheet resistance as reaction time (inset: Patterns obtained by inkjet printing on office paper and photo paper) [128]

Recently Zhang et al. synthesized a Ag/RGO composite with good conductivity and dispersivity as a conductive ink filler for inkjet printing (Figure 2.26) [128]. The conductivity of the Ag/RGO filler could be controlled by changing the reaction time to anchor Ag nanoparticles onto the surface of RGO nanosheets. The Ag NPs served as spacers to prevent the reduced graphene sheets from agglomerating and causing nozzle jam. Multifarious regular patterns with an optimum conductivity of  $2.0 \times 10^3 \text{ S/m}$  and a sheet resistivity of  $0.5 \text{ k}\Omega/\square$  were fabricated using a standard commercial inkjet printer. The Ag/RGO composite was attested to be a suitable material for fabricating printable flexible electronics at 100 °C and developing graphene-based functional electronic devices.

Table 2.6 makes a comparison to the current reported graphene related inks in terms of type, solvent, patterning method and conductivity. Overall, graphene and GO inks show poor electrical performance, which limits their wide application. Hybrid inks formulated using silver NPs with graphene or graphene oxide (GO) would be a possible route for manufacturing of flexible devices and systems. Reference [127] is a good example.

Table 2.6 A brief overview of the graphene and related inks

Type	Solvent	Deposition method	Post-treatment method	Resistivity	Ref.
Graphene ink	Terpineol and ethanol	Inkjet printing	400°C for 30min	200 kΩ/□	[62]
Graphene ink	NMP	Inkjet printing	150°C for 7min	30 kΩ/□	[114]
Graphene ink	Ethanol	Inkjet printing	250°C for 30min	4 mΩ·cm	[115]
Graphene ink	Cyclohexanone	Inkjet printing	300°C for 30min	0.81 kΩ/□	[117]
Graphene ink	DI water	Inkjet printing	400 °C for 3 h in Ar	16.68 Ω·cm	[118]
Graphene ink	Ethanol/DI water	Inkjet printing	60 °C	13 kΩ/□	[119]
GO ink	DI water	Inkjet printing	90 °C for 1 h in a reduction atmosphere	65 Ω/□	[120]
GO ink	DI water	Inkjet printing	200 °C for 12h under a N <sub>2</sub> atmosphere	Less than 1 MΩ	[63]
rGO/PVA ink	DI water and DMF	Inkjet printing	350 °C for 1h under a H <sub>2</sub> /Ar atmosphere	1 mΩ·m	[121]
Graphene/polyaniline	DI water containing SDBS	Inkjet printing	80 °C for 2h	846 Ω/□	[123]
Graphene/PEDOT:PSS Ink	DMF	Spray coating	90 °C	1200 and 500 Ω/□	[124]
Ag/rGO ink	DI water	Inkjet printing	110 °C for 3h	170 kΩ/□	[125]
Graphene /Ag organic complex ink	Cyclohexanone and terpineol	Inkjet printing	300 °C for 40 min	4.62×10 <sup>-4</sup> Ω·m	[126]
Ag/graphene ink	Ethanol, ethylene glycol and glycerol	Handwriting	100 °C for 60min	1.9×10 <sup>-7</sup> Ω·m	[127]
Ag/rGO ink	DI water	Inkjet printing	100 °C for 30 min	5×10 <sup>-4</sup> Ω·m	[128]



#### **2.6.4 Challenges for metal and graphene related inks**

Although various kinds of metal and graphene-related inks have been created and deposited onto different substrates and conductive patterns have been obtained, there are still some distinct shortcomings to be overcome for practical applications.

In terms of silver-based inks, first, silver inks with nanosilver fillers usually require high temperatures (generally  $>200\text{ }^{\circ}\text{C}$ ) to make the ink tracks very conductive and are easy to agglomerate in the synthesis and storage process, while organic silver inks typically exhibit medium conductivity due to the low concentrations of metal precursor. Second, most of the synthetic methods of these inks are not economically feasible because of the cost (i.e. needing centrifugal separation) and safety problem (i.e. toluene or formic acid usually used) as well as low throughput.

As for the copper-based inks, the major drawback associated with the copper NP inks is the easy agglomeration and high tendency to oxidation under the ambient conditions, which is the main problem, since the oxidized particles require elevated temperatures to sinter and usually have poor electrical conductivities. Despite organic copper ink is a worthy alternative to the copper NP ink, distinct shortcomings of such ink make them hard to apply commercially. At present, most organic copper inks require reductive atmospheres (such as hydrogen gas or formic gas) or a special sintering method (intense pulsed light or laser) to make the printed tracks conductive. Besides, they generally use nonpolar solvents, which have compatibility problem with mass production techniques.

In the aspect of graphene-related inks, first, graphene loading is low in the current graphene inks, which is usually in the range of 0.002-1 wt% and therefore poor electrical conduction of the resultant circuit patterns for applications in flexible electronics. Second, GO inks require a thermal reduction process or an alternative method (chemical or photo or thermal) to make the ink tracks conductive, which has cost and safety implications and thus not ideal for industrial applications. Third, there is a compatibility problem between the existing graphene-based inks and the production methods as well as the flexible substrates. What's more, most of these synthetic methods are not economically feasible because of the low throughput and agglomeration in the process of preparation and storage. Last, although some research

has been done to improve the conductivity of graphene by decorating it with silver particles, little work has been conducted successfully in view of the feasibility (both dispersivity and conductivity) of Ag-decorated graphene for the printable ink to fabricate flexible electronics.

## **2.7 Conclusions**

This chapter describes the recent progress of metal and graphene-related inks in the field of flexible electronics, with particular emphasis on their synthesis, types, and properties. As already discussed, the ink materials are crucial for the development of flexible electronics. The ink properties, such as viscosity, surface tension and volatility, determine the printing ability and need to be specifically designed and formulated to meet the requirements of the patterning process. Meanwhile, the ink properties, both wet and dry, are also important. When considering the wettability of metal inks with various substrates, a compatible balance is very important. Hence, further development of novel materials with improved electronic properties and good surface functionalization will impact the field of printed electronics significantly.

The advantages of the metal-based inks are still important. The efforts should be focused on reducing the amount of noble metal and the ink sintering temperature. The rational combination of formulation-processing-sintering of the metal inks would be a direction. Hybrid conductive inks composed of metal NPs and carbon-based materials is also an important route. Metal/graphene hybrid inks may be a possible research direction, which can take full advantage of these two materials to enhance the conductivity and reduce the usage of noble metal.

Clearly, much effort is still enquired to obtain highly stable, high throughput conductive inks using simple and facile procedures and patterns with good conductivity at a temperature below 150 °C on a wide range of flexible substrates for the applications in the field of flexible electronics.

## Chapter 3 Ag/rGO Hybrid Conductive Ink

### 3.1 Introduction

Recently there has been a significant interest in the development of hybrid inks from graphene or its derivatives decorated with silver nanoparticles. Although various kinds of graphene/silver hybrid inks have been created and deposited onto different substrates and conductive patterns have been obtained [125-128], they are still not economically feasible because of the low throughput, the complexity of the process as well as the utilization of toxic chemicals. To date, all of these inks are synthesized based on a two-step process where the silver/graphene or silver/rGO composites are first prepared by a complex chemical reduction process and are then formulated into inks. The process is not facile. Besides, the amount of ink produced by these methods is usually low, which limits their potential for commercial development. Moreover, the chemicals used for synthesizing such inks such as hydrazine or DMF, are not ideal because they are toxic and not environmentally friendly. Therefore, it will be advantageous to develop new hybrid inks using non-toxic solvents and a one-step synthetic method.

In this chapter, the first development of a one-step method for the synthesis of an Ag/rGO hybrid ink composed of organic silver complex and rGO is described. The approach has the following advantages. First, the ink formulation process is only one-step, facile, high throughput as well as environmentally friendly, which is different from all the current existing methods used for synthesizing silver/rGO hybrid inks and are easy for industrial production. Second, the dispersion of rGO in the alcohol based solvent was obtained. Third, the synthesized ink was just composed of 13.5 wt % of silver and 0.1wt% rGO but showed an improved electrical performance on modified PI substrates at a low temperature (150 °C), which is not only increasing conductivity but also reducing costs of organic silver complex inks. The thermal response of the ink has been studied to understand the chemical changes in it. The formation and conductive mechanism of the rGO/Ag films from the ink were investigated, including the sintering temperature, time and the degree of interaction between the Ag particles.

Part of this Chapter has been published [129].

### 3.2 Experimental section

#### 3.2.1 Chemicals and materials

Silver acetate, ethanolamine, ethylene glycol, ethanol and oleic acid were obtained from Sigma-Aldrich and were used as received without further purification. The rGO powder was supplied by Graphenea and was produced by chemical reduction of graphene oxide. The size of the rGO platelets is in the range of 260-295nm. The BET surface area is 422.69-499.85 m<sup>2</sup>/g. The solubility is below 0.1 mg/ml in NMP, DMSO and DMF. The conductivity is above 600 S/m. The chemical compositions are: C (77-87%), H (0-1%), O (13-22%), and N (0-1%). The polyimide (PI, 127μm in thickness) substrate was a Kapton film from DuPont. The polyetherimide (PEI) was Ultem 1000 with 75μm in thickness. For surface modification, these films were cut into square pieces (15mm×15mm) and cleaned with ethanol and de-ionized water to remove particles and organic contamination prior to the surface modification process.

### ***3.2.2 Ink synthesis***

The silver/rGO ink was prepared using a modified process of the previous work [12]: rGO powder (6mg) was first dispersed in a mixed solvent containing ethanol (2ml), ethylene glycol (2.85ml) and oleic acid (0.05ml) by sonication for 30minutes, and then silver acetate (1.6g) was added into the solution. After stirring for 10 minutes, ethanolamine (1.2ml) was added. The mixture was stirred for 60 minutes to form the ink. It is useful to note that the appearance of the solution changed, from the initial suspension to a homogeneous solution. For comparison of the electrical performance of films with rGO, Ag films were obtained using the same ink formulation but without rGO and were produced using the same deposition and sintering processes.

### ***3.2.3 Deposition and sintering***

PI and PEI substrates were modified using an alkaline hydrolysis based method prior to the deposition of the ink. The effects of the factors such as concentration, time and temperature of the alkali solution on the surface of PI were investigated in order to obtain good hydrophilic interaction and binding force between the ink film and the substrates. Then, a drop-coating method was used to deposit the as-prepared Ag/rGO ink onto the surface of the modified films, where the film thickness was controlled by the deposition volume of ink. For metallization, the obtained samples were sintered on a hotplate at selected temperatures for up to 60 minutes.

### ***3.2.4 Characterization***

UV-vis spectra were obtained on an EV300 UV-vis spectrophotometer. Fourier

transform infrared spectra in the range of 400-4000 $\text{cm}^{-1}$  were recorded on a FT-IR spectrometer. The thermal profile was measured under nitrogen atmosphere by differential scanning calorimetry (DSC, TA instrument) at a heating rate of 10  $^{\circ}\text{C}\cdot\text{min}^{-1}$  from room temperature to 300  $^{\circ}\text{C}$ . The crystalline structure of the Ag/rGO films was measured by X-ray diffraction (XRD) using Cu  $\text{K}\alpha$  and  $\lambda=0.15418\text{nm}$ . The surface morphology of the Ag/rGO films was obtained on a Field Emission Scanning Electron Microscope (SEM). The chemical composition was determined on an Oxford X-maxN 150 surface energy disperse spectrometer (EDS). The sheet electrical resistivity was measured using a multi-height probe station (Jandel Engineering, UK) with tungsten probe tips of 1mm of spacing and 60g of maximum force. A Zygo View 5200 white light phase shifting interferometer was used to obtain the surface profiles of the modified and original substrates as well as the thickness of the sintered films.

### **3.3 Results and Discussion**

#### ***3.3.1 Surface modification of substrate***

Adhesion is one of the most important factors in the deposition of conductive inks. Surface treatment and modification of substrates are often required before the ink deposition, to generate suitable reactive sites on the substrate surface, thereby improving the adhesion of the printed ink patterns to the substrates.

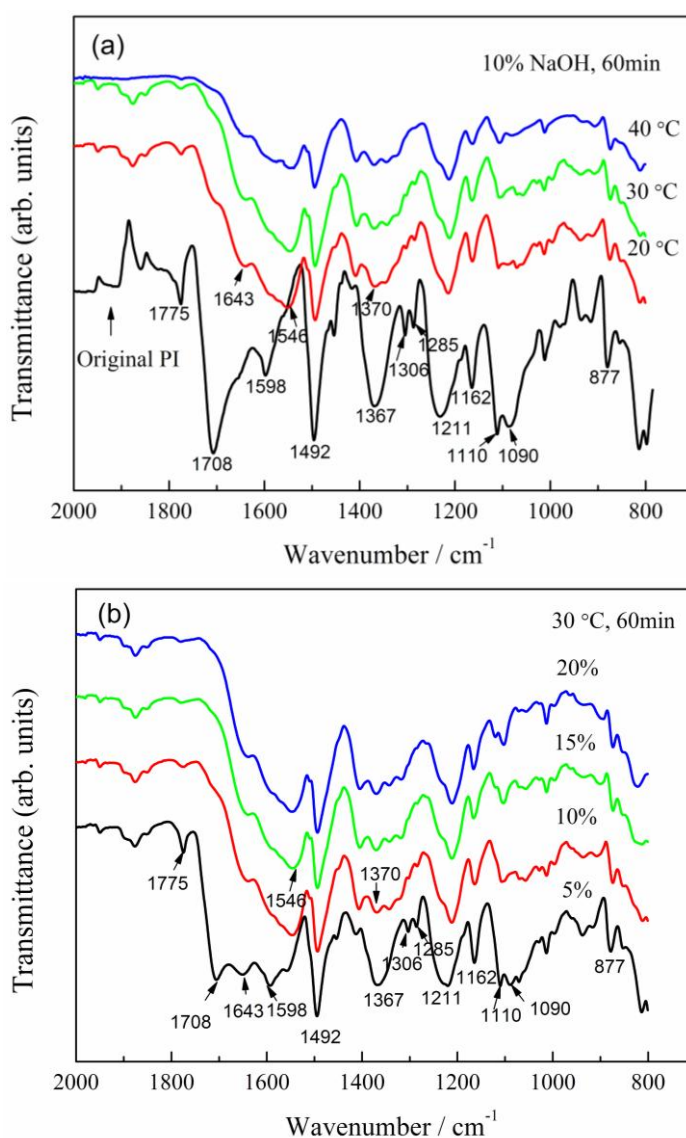
Several techniques have been used to modify the surface of the flexible polymer substrates. These techniques can be classified into two types [64, 130], the physical surface modifications such as surface roughening, and the liquid chemical surface modification such as alkali treatment. The physical surface treatment serves mainly to increase the surface area and to create more sites for mechanical interlocking, while the chemical surface modification method is to create new surface functional groups by exposing the substrates into a chemical or chemical mixture.

As a substrate material, polyimide (PI) is widely used in the printed electronics industry today, because of the low cost and the outstanding properties of high operating temperature, high tensile strength and high dielectric strength. However, the adhesion of the films produced by an ink to PI is generally not good, since there are no functional groups on the surface of the PI film. For a reliable application, the PI surface should be modified to overcome the problem. As Luo described, the PI surface can be modified using a physical method (plasma, ion beam), or a chemical method using a sodium

hydroxide or potassium hydroxide based aqueous solution [131]. Polyetherimide (PEI) has physical properties comparable to PI, which is also a potential substrate for the electronic applications. Here, PI and PEI substrates were processed using a sodium hydroxide aqueous solution based on our previous work [49].

### 3.3.2 PI substrate with thickness of 127 $\mu\text{m}$

Figure 3.1 shows the FT-IR spectra of the original and modified PI films. The characteristic peaks appeared at 820, 1090, 1110, 1162, 1306, 1367, 1492, 1598, 1708 and 1775  $\text{cm}^{-1}$  in the original PI film, are assigned to the out-of-plane deformation vibration of the  $\text{C}_6\text{H}_2$  group, C-O-C stretching (1090, 1110  $\text{cm}^{-1}$ ), C-C bending (1162  $\text{cm}^{-1}$ ), C-N stretching (1306, 1367  $\text{cm}^{-1}$ ), aromatic C=C ring stretching (1492, 1598  $\text{cm}^{-1}$ ), symmetrical stretching and asymmetrical stretching of C=O, respectively. This is in agreement with the FT-IR analysis of polyimide films reported in the reference [132].



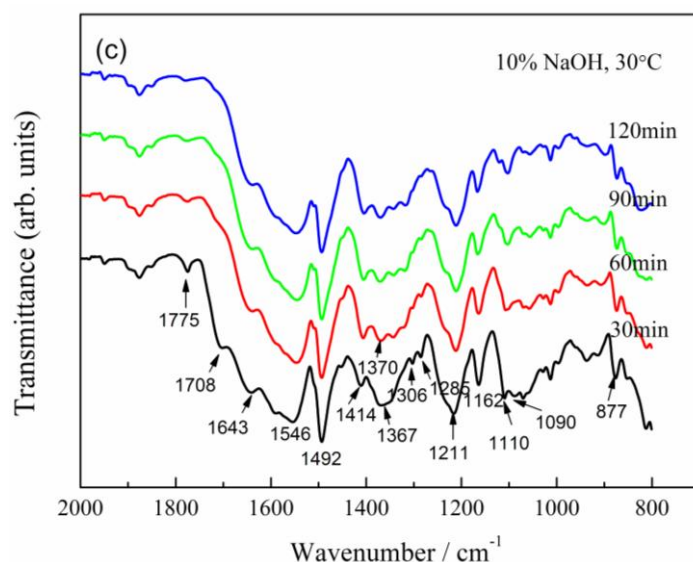
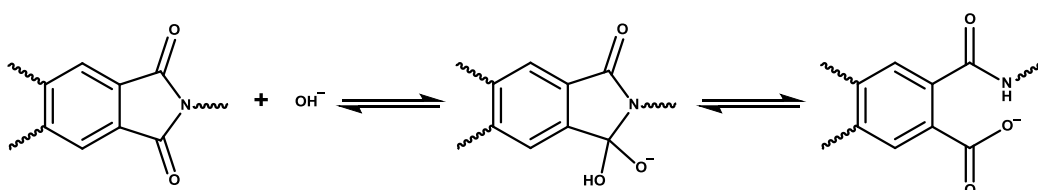


Figure 3.1 FT-IR spectra of the PI film treated with different temperatures (a), NaOH concentration (b) and time (c) [49]

Comparing the results in Figure 3.1 (a), (b) and (c), it can be seen that chemical changes have occurred on the surface of the PI films after the treatment depending on the process temperature and time and the concentration of the alkali solution. The peaks at 1090, 1110, 1162, 1492, 1598  $\text{cm}^{-1}$  become weaker and second the peaks at 820, 1367, 1708 and 1775  $\text{cm}^{-1}$  have disappeared. These IR absorption peaks are all associated with the imide group, indicating the opening of the polyimide ring. Besides, several new peaks appear at 1370, 1546 and 1643  $\text{cm}^{-1}$ . The peaks at 1643 and 1546  $\text{cm}^{-1}$  are attributed to the stretching vibration of the C=O bond and the bending vibration of the N-H bond of the CONH group, indicating the formation of amino compounds on the PI surface. The peak at 1370  $\text{cm}^{-1}$  is attributed to the symmetric stretching of carboxylate groups. These changes indicate the reaction of the hydroxyl groups and the imide rings producing amide structures resulting in surface activation of the PI.



The mechanism of this modification process is described in reference [133] and the above reaction scheme is proposed. The hydroxyl ions diffuse from the alkaline solution into the polyimide substrate, where they nucleophilically attack the carbonyl group, creating an intermediate anion. After transferring a proton from the oxygen to the nitrogen, cleaving of the C–N bond is completed and the carboxyl group is formed.

The evidence of the physical modification can be seen in the comparison of the interferometry profiles between the untreated and the modified PI films (Figure 3.2). It can be seen that the original PI film has a relative smooth surface with some holes on it. After treatment, the surface of the PI film becomes rough and the size of holes on it becomes small. The surface roughness ( $R_a$ ) changed from  $0.029\mu\text{m}$  to  $0.050\mu\text{m}$ , which indicates that the effective surface area of the PI film after modification has increased. Therefore, good hydrophilic interaction and binding between the ink droplet and the surface of the PI film could be obtained.

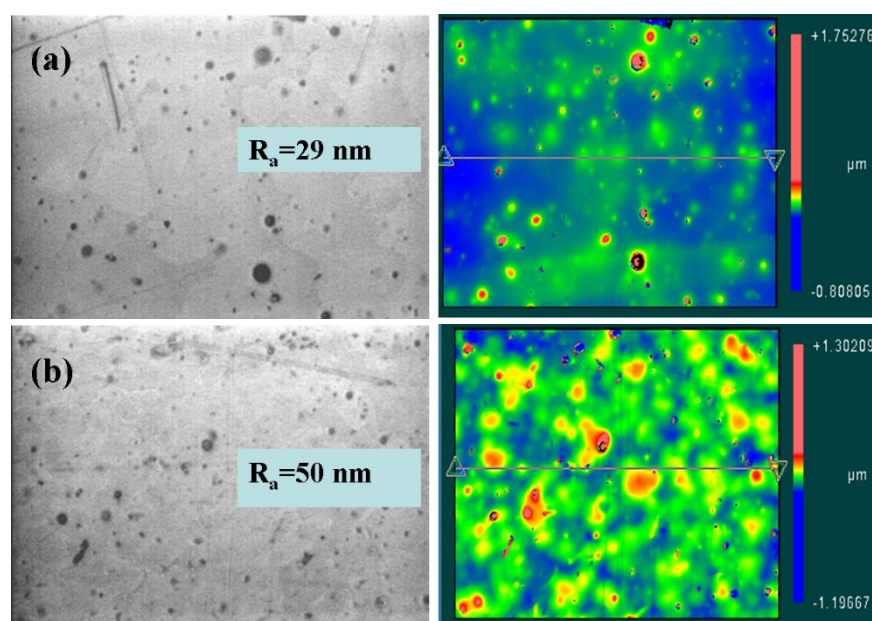


Figure 3.2 Interferometry profiles of PI film with thickness of  $127\mu\text{m}$  (a for un-treated PI film; b for modified film) [49]

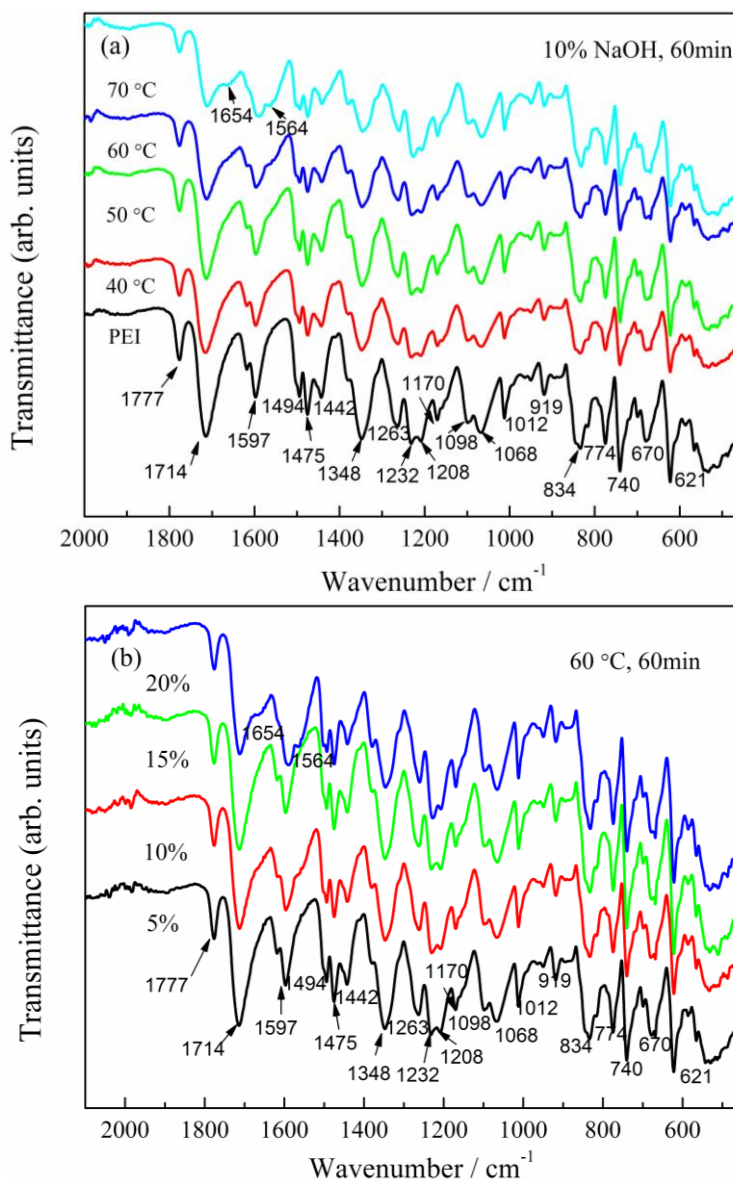
However, in consideration of the structure and properties of the PI material, the treatment time needs to be controlled. The best results for ink deposition were obtained from PI substrates processed at  $30^\circ\text{C}$  for 60 minutes in a solution containing 10% of sodium hydroxide. In this case, the treatment did not appear to affect on the properties of the PI film. The ink droplets could spread well and the resultant films have good adhesion with the PI films.

### 3.3.3 PEI substrate with thickness of $75\mu\text{m}$

Figure 3.3 shows the FT-IR spectra of the original and modified PEI films with a thickness of  $75\mu\text{m}$ . The characteristic peaks appearing around  $834$ ,  $1012$ ,  $1170$ ,  $1263$ ,  $1348$ ,  $1442$ ,  $1475$ ,  $1597$ ,  $1714$  and  $1777\text{ cm}^{-1}$  in the original PEI film, are associated with the out-of-plane C-H bending ( $834\text{cm}^{-1}$ ), C-O-C stretching ( $1012\text{cm}^{-1}$ ), C-C



bending ( $1170\text{ cm}^{-1}$ ), C-O stretching ( $1263\text{ cm}^{-1}$ ), aromatic C-N stretching ( $1348\text{ cm}^{-1}$ ), aromatic C=C stretching ( $1442, 1475\text{ cm}^{-1}$ ), aromatic C=O ring stretching ( $1597\text{ cm}^{-1}$ ), imide carbonyl symmetrical stretching and asymmetrical stretching ( $1714, 1777\text{ cm}^{-1}$ ). After treatment, obvious chemical changes have occurred on the surface of the PEI films. The peaks at  $834, 1012, 1170, 1263, 1348, 1442, 1475, 1597, 1714$  and  $1777\text{ cm}^{-1}$  become weaker and two new peaks at  $1564$  and  $1654\text{ cm}^{-1}$  have appeared. The new peaks at  $1564$  and  $1654\text{ cm}^{-1}$  are attributed to the stretching vibration of the C=O bond and the bending vibration of the N-H bond of the CONH group, indicating the formation of amino compounds on the PEI surface. These changes indicate amide structures were produced, resulting in surface activation of the PEI, which is conducive to the ink wetting and deposition.



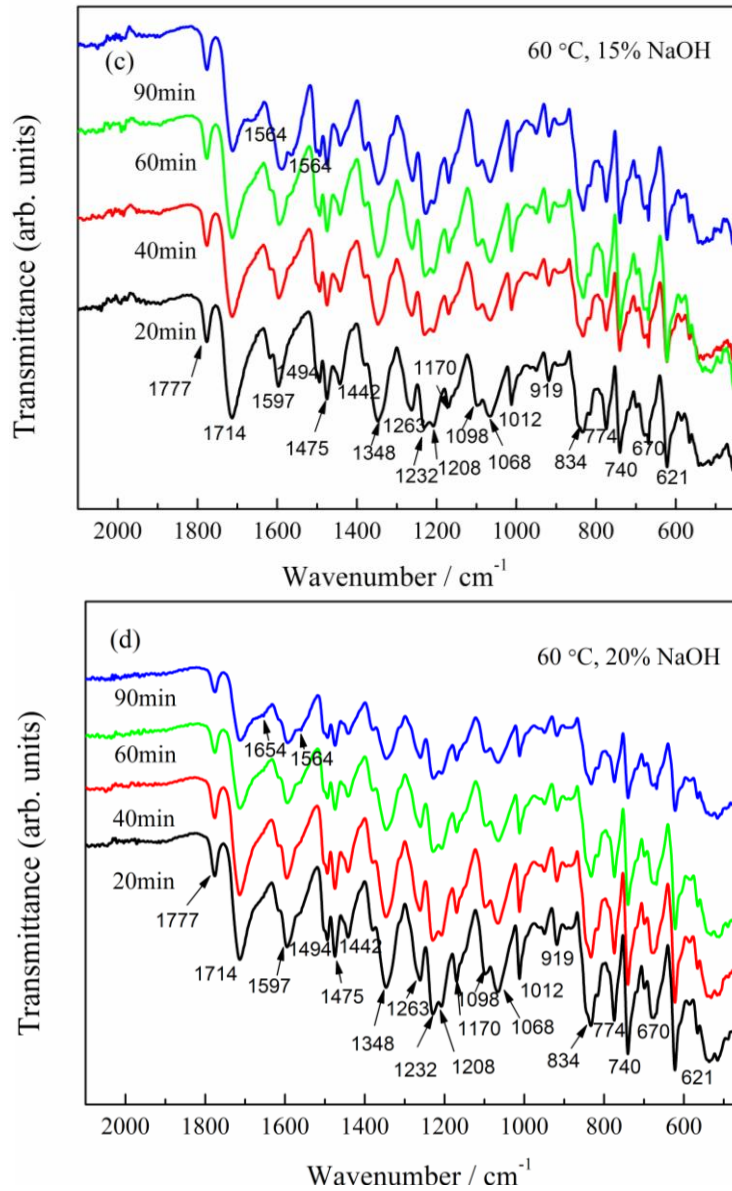


Figure 3.3 FT-IR spectra of the PEI film treated with different temperatures (a), NaOH concentration (b) and time (c)

The results of interferometry profiling of the untreated and the modified PEI films are given in Figure 3.4. Surprisingly, the surface roughness of the modified PEI film is less than the untreated sample. The surface roughness,  $R_a$ , changed from  $0.321\ \mu\text{m}$  to  $0.271\ \mu\text{m}$ , indicating that the effective surface area of the PEI film after modification has decreased.

From the experimental results, it can be seen that the best treatment conditions for PEI material are: 15% of sodium hydroxide solution,  $60^\circ\text{C}$  and 90 minutes. In consideration of the spread-ability of the ink and the characteristics of the substrates materials as well as the modification conditions, the PI substrate with the thickness of  $127\ \mu\text{m}$  was only

chosen for the subsequent ink deposition.

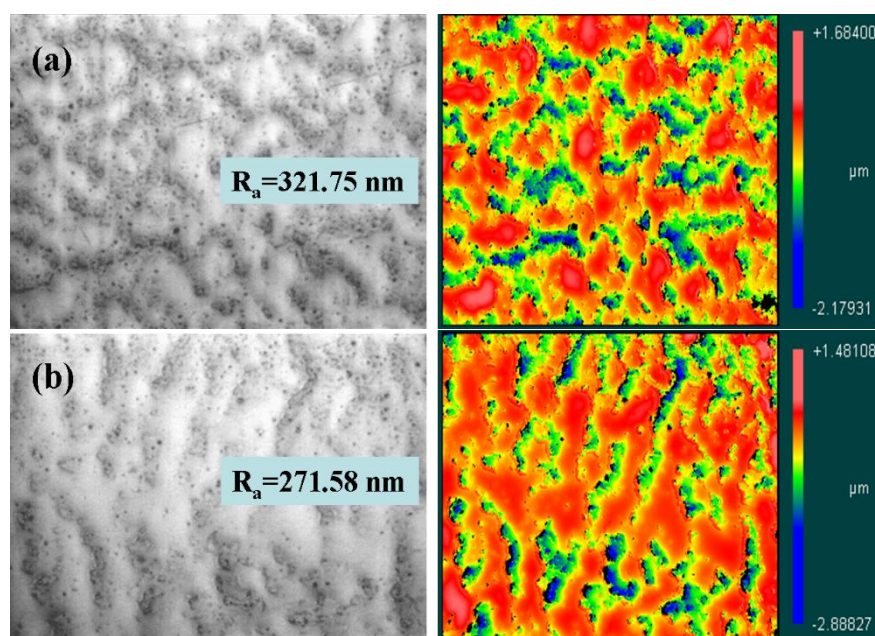
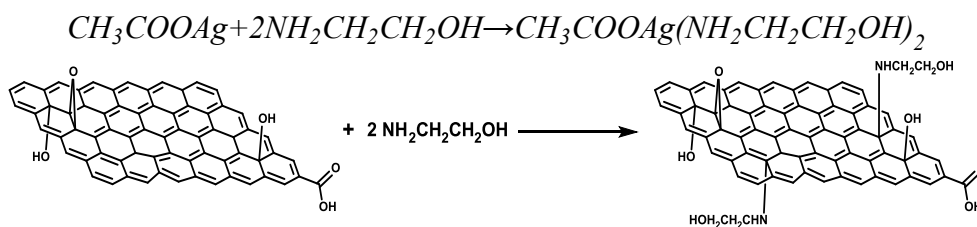


Figure 3.4 Interferometry profiles of PEI film with thickness of 75  $\mu\text{m}$  (a for un-treated PEI film; b for modified film)

### 3.3.4 Ink chemistry

The ink was formulated through a complexation-covalent bonding process of silver acetate and ethanolamine together with the nano rGO. Silver acetate was chosen as the silver precursor since this compound has poor solubility in the solvent medium (alcohol in this case) and so the reaction rate can be controlled. Ethanolamine was used to increase the silver content of the ink and to improve the dispersibility of rGO in the alcohol solvent. rGO was used to study its effect on the conductivity of the resultant Ag/rGO films and to reduce the amount of silver in the film thus reducing the ink cost in electronic applications. Ethanol was used to adjust the surface tension of the ink and Ethylene glycol was chosen as a reduction agent [13] and a co-solvent to suppress the undesirable coffee ring effect in film formation.

The chemical reaction mechanism leading to formation of the Ag/rGO ink is described below. The lone pair of electrons on the nitrogen of ethanolamine can coordinate with silver acetate to form a silver organic complex, at room temperature, which has good solubility in alcohols due to the presence of OH groups [12]. At the same time ethanolamine can react with the rGO to yield rGO decorated with amino group; the latter has better dispersibility in alcohols due to the effects of electrostatic repulsion and volume exclusion between the decorated rGO sheets.



In order to verify the interaction between rGO and ethanolamine, UV-vis spectra and FT-IR spectra were obtained for samples of dispersions of rGO and rGO/ethanolamine in ethanol respectively.

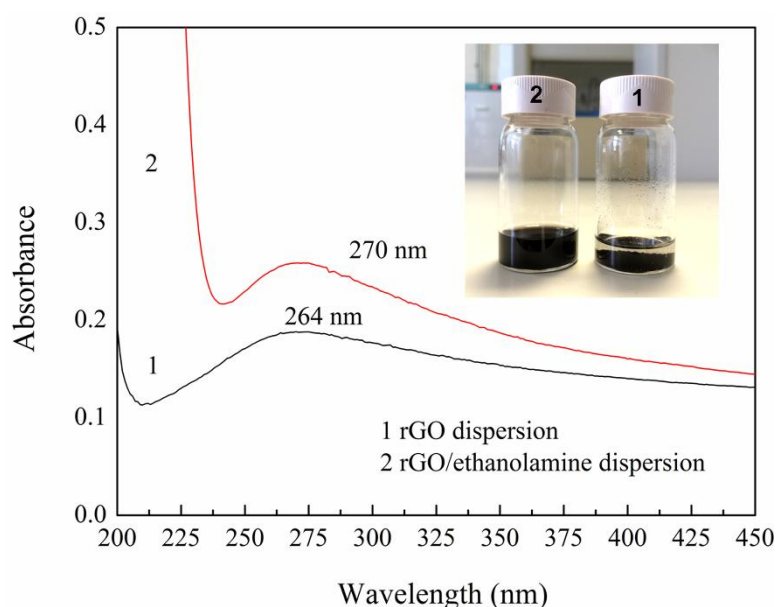


Figure 3.5 UV-Vis absorption spectra of rGO and rGO/ethanolamine dispersions (inset is the optical image of these two kinds of dispersion)

As showed in Figure 3.5, the rGO dispersion shows a typical absorption peak at 264 nm, as reported in the previous work [134]. This absorption peak is attributed to the  $n-\pi^*$  transition of C-O bonds on the surface of rGO. However, in the presence of ethanolamine, the absorption is slightly red-shifted from 264 to 270 nm, indicating that some new groups were introduced on the rGO surface and possibly due to the interaction with ethanolamine.

Figure 3.6 shows the IR spectra of rGO powder dried from the dispersions of rGO and rGO/ethanolamine in alcohol. It can be seen that several new peaks are visible in the sample with ethanolamine. The broad bands between  $3100$  and  $3700\text{ cm}^{-1}$  are attributed to the vibrations of O-H and N-H. Two peaks at  $2933$  and  $2870\text{ cm}^{-1}$  were attributed to the asymmetric and the symmetric  $\text{CH}_2$  stretch, respectively. The broadening of the band at  $1645\text{ cm}^{-1}$  can be assigned to N-H vibrations. The peak at  $1430\text{ cm}^{-1}$  and  $1350$

$\text{cm}^{-1}$  indicates in-plane bending vibrations of the methyl group. The C-O stretching vibration is at  $1055 \text{ cm}^{-1}$ . All of the differences show that the amino groups from ethanolamine can be adsorbed on the rGO surface, thereby resulting in its good dispersibility in a hydrophilic solvent. It has been shown in the previous study of functionalization of graphene with ethanolamine that the latter can react with the hexatomic rings of graphene oxide through covalent bonding [135], in this case it should be with the hexatomic rings of rGO.

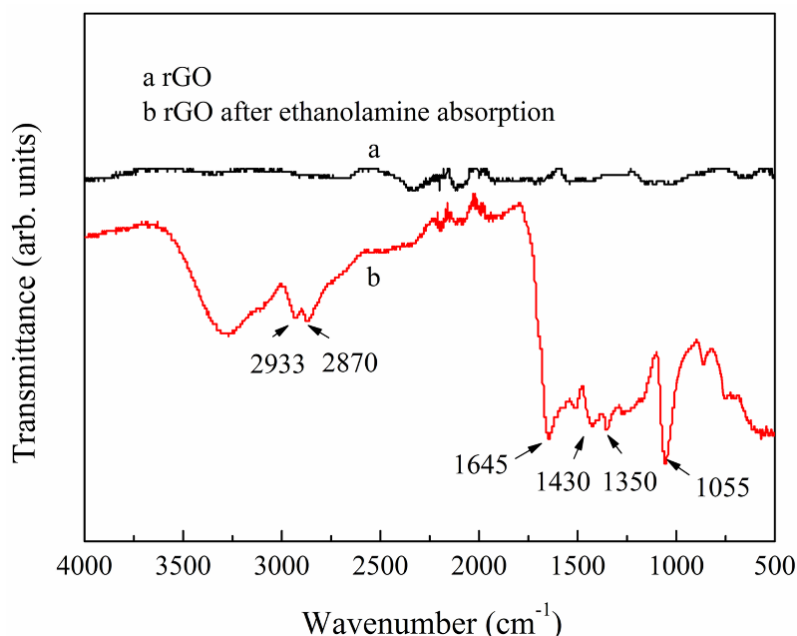


Figure 3.6 FT-IR spectra of rGO and rGO after ethanolamine adsorption

In order to determine the initiation of the complex chemical reactions with temperature, the UV-vis spectra of the ink were obtained after the ink was heated to a selected temperature, as shown in Figure 3.7. At temperatures below  $120^\circ\text{C}$ , there is only one absorption peak associated with the silver carboxylate-amine complex, which is at  $217\text{nm}$ . However, after the ink was heated to  $120^\circ\text{C}$  the absorption spectrum is very different, the peak at  $217\text{nm}$  disappears and a weak peak at  $303\text{nm}$  is observed. This peak is associated with silver nanostructures but different from conventional silver nanoparticles [136]. Based on the results and our previous work [12, 13], it can be deduced that the ink underwent simultaneous change of solvent components and reduction of the silver ion complex at elevated temperatures and in the process ethylene glycol changes to acetaldehyde and triggers the reduction of silver complex. This is the initiation of the conversion process from the deposited ink film to the formation of conductive Ag/rGO film after thermal sintering.

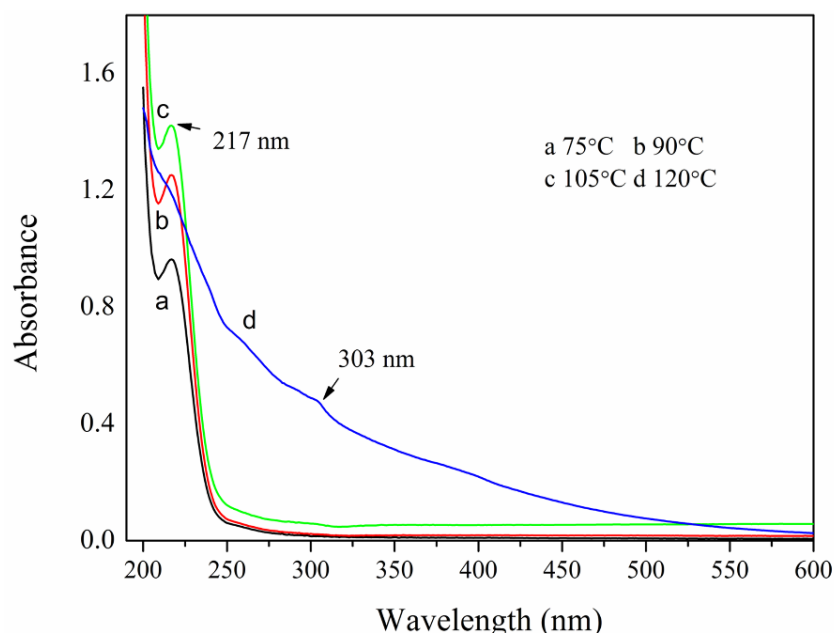


Figure 3.7 UV-Vis absorption spectra of Ag/rGO ink at different heating temperatures

### 3.3.5 Thermal behavior of the Ag/rGO inks

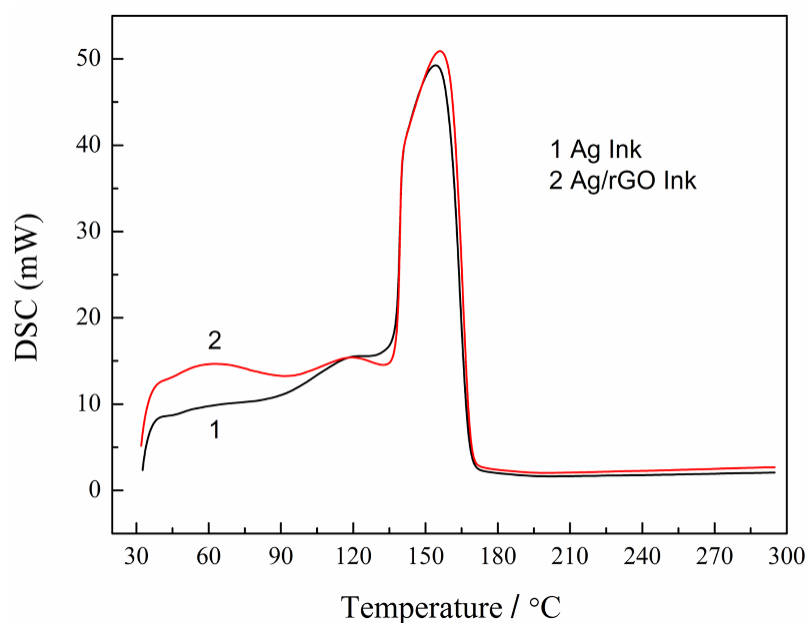


Figure 3.8 DSC analysis of Ag ink and Ag/rGO ink

DSC analysis was carried out to investigate the thermal decomposition behavior of the as-prepared Ag and Ag/rGO inks as shown in Figure 3.8. The two endothermic peaks, at 60°C and 120°C, are related to the evaporation and decomposition of the solvents. The third endothermic peak at about 165°C is attributed to the formation of elemental silver, which is much lower than the decomposition temperature of the silver acetate powder. This is because the lone pair electrons of the nitrogen atoms of ethanolamine can



effectively combine with the silver to form a silver-amine complex with a lower redox potential which determines the decomposition temperature. This is similar to the thermal behavior of the other silver salt based inks [32] and it is also consistent with the previous analysis of the results in Figure 3.7.

### 3.3.6 Microstructure of the Ag/rGO ink films

Ag/rGO films were produced by drop-coating of the ink on the modified PI substrates. The sintering process was carried out on a hotplate in a chamber. Based on the results of DSC and UV-vis analysis of the ink, temperatures between 135°C and 245°C were used for thermal sintering. Figure 3.9 shows the as-prepared Ag/rGO ink, the corresponding optical microscopy image and surface profile of the sintered Ag/rGO film. It can be seen that the sintered film with an average thickness of  $3 \pm 0.3 \mu\text{m}$  had relatively uniform surface structure, with silver nanoparticles accumulated at the center.

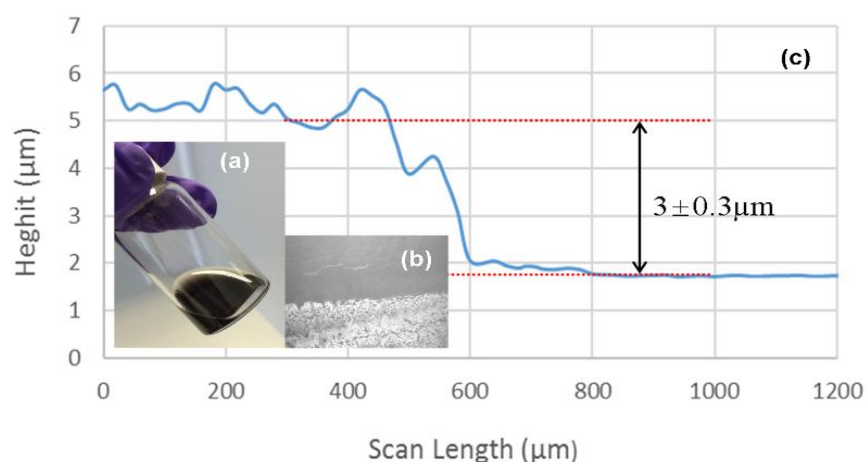


Figure 3.9 (a) As-prepared Ag/rGO ink; (b, c) Optical microscopy image and surface profile of the sintered Ag/rGO film

Figure 3.10 presents the XRD results of the Ag/rGO films sintered at different temperatures for 60 minutes (measured in  $2\theta$  from  $25^\circ$  to  $85^\circ$ ). The peaks for Ag at  $2\theta$  equal to  $38.2^\circ$ ,  $44.4^\circ$ ,  $64.5^\circ$ ,  $77.5^\circ$  and  $81.6^\circ$  were observed in all of the films which indicate that the silver ions are transformed to silver crystals. The reflection peaks are indexed as the (111), (200), (220), (311) and (222) crystal planes of the silver face-centered cubic (fcc) crystal structure. The XRD characteristic of the rGO powder is also shown in Figure 3.10 (the bottom) which is a broad diffraction peak around  $24^\circ$ . However, this peak is not present in the characteristics of the Ag/rGO films which may be the result of the low content and diffraction intensity of rGO in the film. The peak intensities of the silver increased with the sintering temperature. This is because the

increase in crystallization of the silver NPs in the film as the level of sintering was increased.

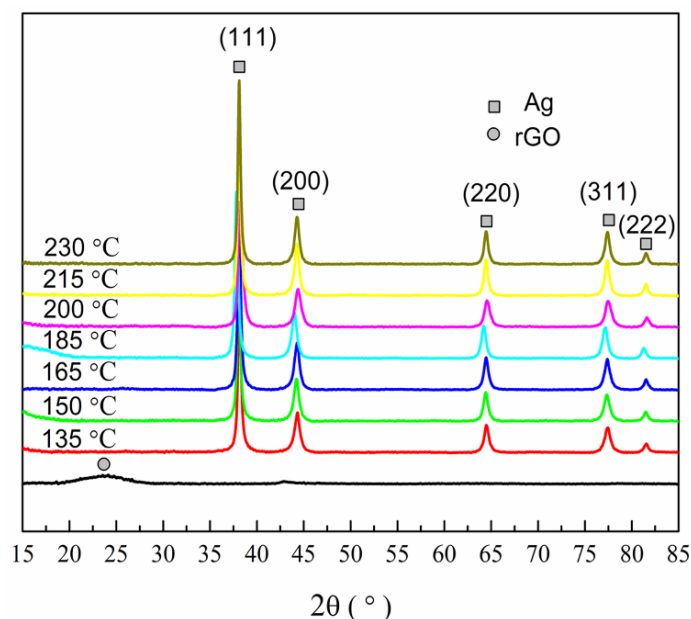


Figure 3.10 XRD patterns of the Ag/rGO films sintered at different temperatures for 60 minutes.  
Data shifted vertically, for clarity

The particle sizes of the silver nanocrystals in the films formed at 135°C, 165°C, 215°C and 230°C were calculated using the Debye-Scherrer equation,

$$d=0.89\lambda/\beta\cos\theta \quad (3.1)$$

Where  $d$  is the particle size,  $\lambda$  is the x-ray wave length (0.15418nm),  $\theta$  is the Bragg angle and  $\beta$  corresponds to the full width at half-maximum (FWHM). The results are given in Table 3.1.

Table 3.1 Particle sizes of silver nanocrystals in the film at different sintering temperature

Sintering temperature (°C)	2θ (Degrees)	FWHM (β)	Size (nm)
135	38.155	0.396	21.01
165	38.118	0.377	22.06
215	38.099	0.362	22.97
230	38.109	0.358	23.24

It can be seen that the average particle size of silver nanocrystals in the film increased with the sintering temperature but the change is not significant.



The SEM images of the Ag/rGO films sintered at different temperatures are shown in Figure 3.11. It can be seen that the morphologies of the Ag/rGO films change with the sintering temperature.

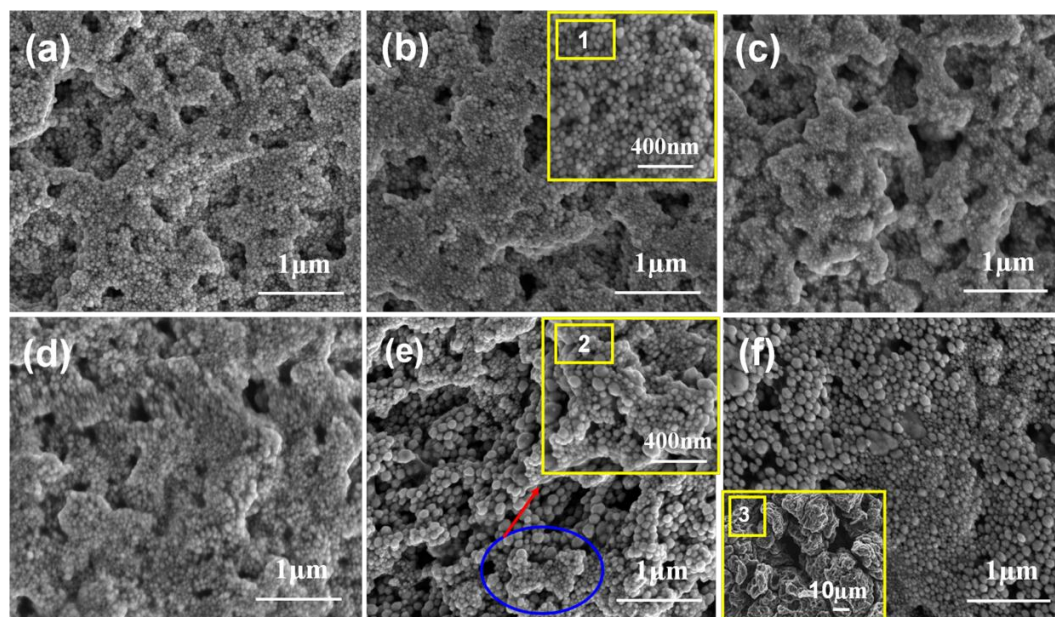


Figure 3.11 SEM images of Ag/rGO films sintered at 150, 165, 185, 200, 215 and 230 °C for 60min (inset: 1 and 2 are the corresponding magnified images of figure b and e, 3 corresponds to the image of rGO offered by Graphenea Website)

At lower sintering temperatures (150°C, 165°C), fewer silver nanoparticles were produced. These are relatively small (Figure 3.11a, b) and surrounded by organic molecules (e.g. ethylene glycol,  $T_b=197^\circ\text{C}$ ). The average size of these silver nanoparticles is measured to be about 23nm from the magnified image (inset 1), which is basically in line with values calculated from the XRD data. At higher sintering temperatures (185°C, 200°C), more silver NPs were produced. The film seems to be made up of many layers where silver NPs were supported (Figure 3.11c). By combining information from the rGO images offered by Graphenea (Figure f3), it can be deduced that these supporting layers are the graphene particles. In addition, it should be noted that pores and voids among the NPs became fewer and smaller at this stage, stacking density was also improved (Figure 3.11d). Sintering at higher temperatures (215°C, 230°C) made the silver nanoparticles grow forming larger particles through neck connection (Figure e2) and further improving the stacking density of the film. By comparing Figure f3, Figure b1 and Figure e2, it can be deduced that in the sintering process, silver ions were reduced into silver NPs and rGO serve as medium to support

and bridge between them.

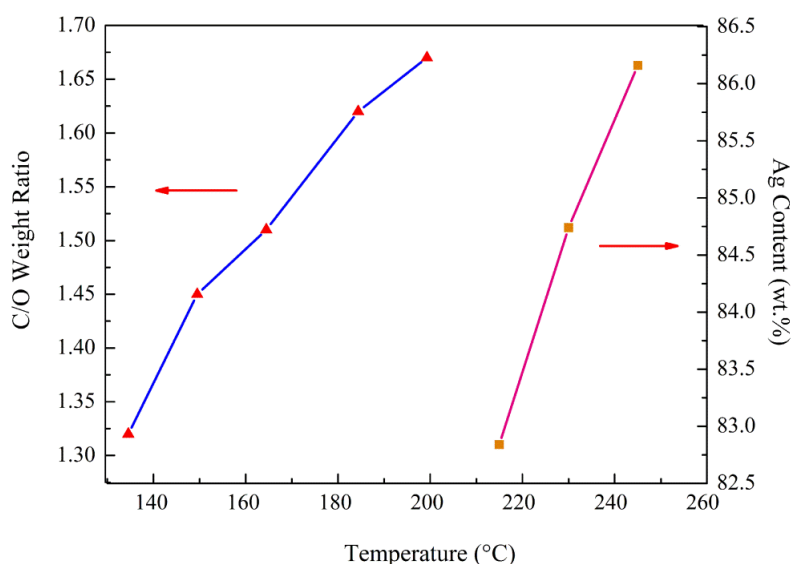


Figure 3.12 Change of C/O weight ratio and Ag content in Ag/rGO films as a function of sintering temperature

Figure 3.12 shows the results of C/O ratio and Ag content from EDS based analysis. It can be seen that the C/O ratio increases rapidly as sintering temperature was increased from 150°C to 200°C, indicating that the decomposition and volatilization of organic molecules mainly occurred at this stage. Above 200 °C, the Ag content increased from 82.76 wt% to 86.17 wt%, indicating that most of the organic molecules were decomposed and volatilized and the  $\text{Ag}^+$  ions were reduced to  $\text{Ag}^0$ .

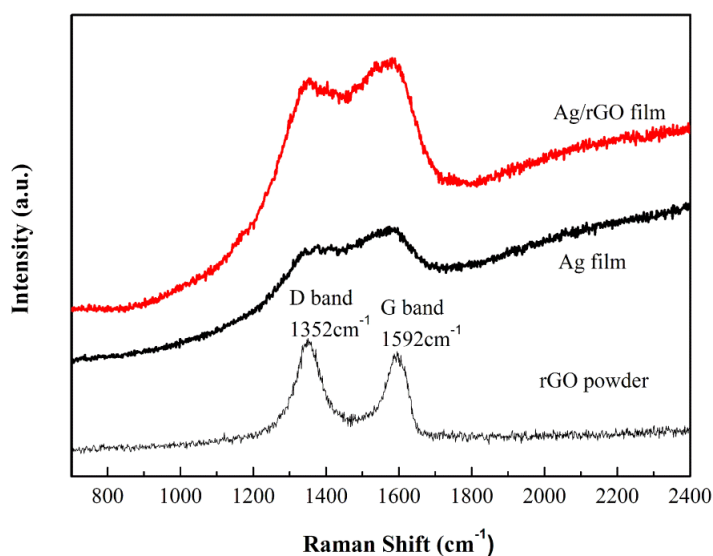


Figure 3.13 Raman spectra of the Ag/rGO films sintered at 230°C for 60min

Figure 3.13 shows the Raman spectra of Ag/rGO film sintered at 230°C. The D band

and G band appeared at  $1352\text{cm}^{-1}$  and  $1592\text{cm}^{-1}$  are consistent with that of rGO powder, indicating that the rGO exists in the film after sintering.

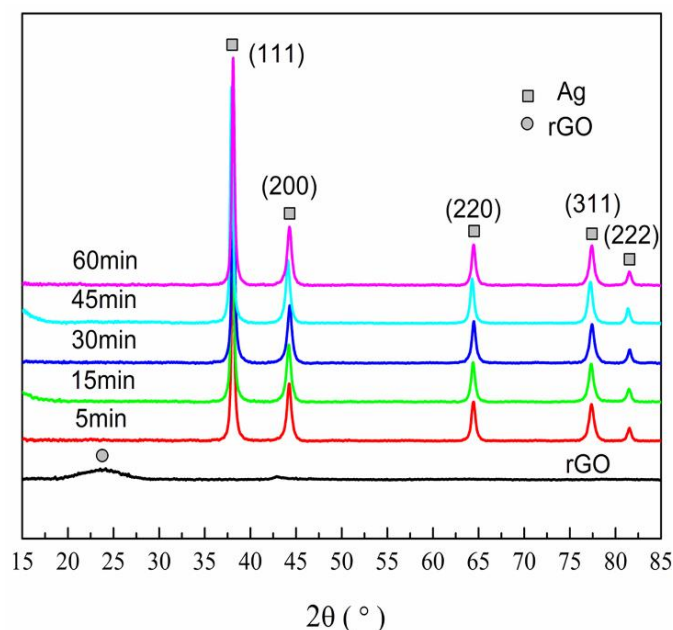


Figure 3.14 XRD patterns of Ag/rGO films prepared with the inks after sintering for 5min, 15min, 30min, 45min and 60min

Considering the boiling point of the ink solvents and the thermal stability of PI substrates, the temperature of  $230^{\circ}\text{C}$  was selected to study the effect of sintering time on the microstructure of the Ag/rGO films. The samples were obtained by sintering the ink films on modified PI substrates for 5, 15, 30, 45 and 60 minutes and were evaluated by SEM and XRD methods.

Table 3.2 Particle sizes of silver nanocrystals in the film at different sintering time

Sintering time (min )	2θ (Degrees)	FWHM (β)	Size (nm)
5	38.035	0.368	22.59
60	38.109	0.358	23.24

As shown in Figure 3.14, silver ions could be transformed to silver crystals within 5 minutes. With the increasing sintering time, the peak intensity also increases, indicating that more metallic silver was formed. The particle sizes of silver nanocrystals in the films formed were calculated using equation (3.1) and the results are shown in Table 3.2. The increase in particle size is very small.

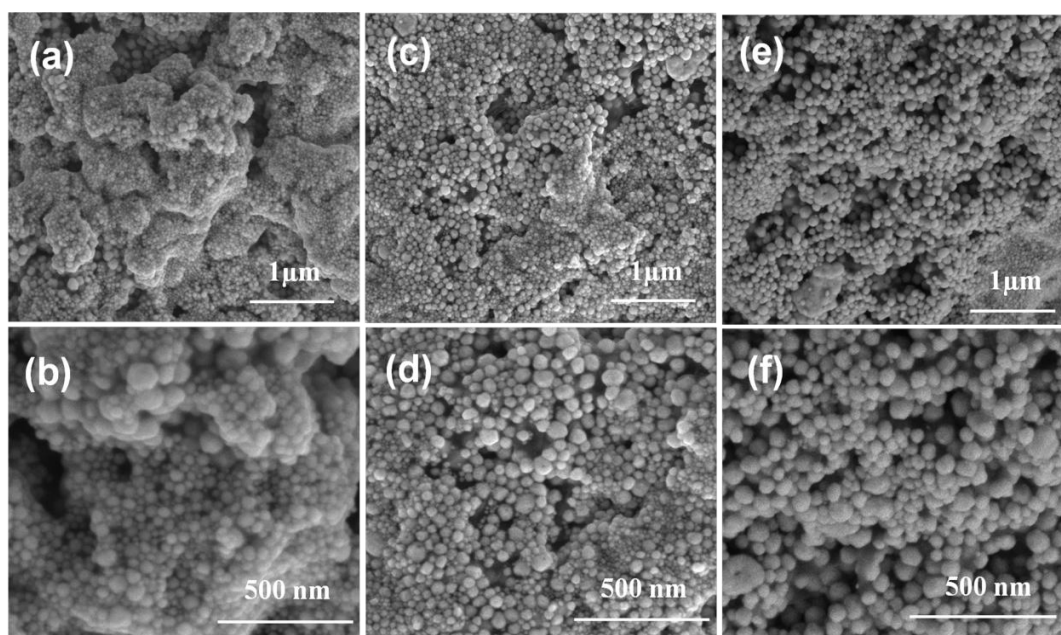


Figure 3.15 SEM images of Ag/rGO films sintered at 230 °C for 5 min, 15min, 60min (a, c and e) and corresponding magnified images (b, d and f)

The SEM images in Figure 3.15 show the microstructures of Ag/rGO films produced using different sintering times. Significant differences in the morphologies of Ag/rGO films can be observed. When the sintering time was 5 minutes, silver nanoparticles were produced but still surrounded by organic molecules (Figure 3.15b). Besides, there are many holes in the film and it is not uniform (Figure 3.15a). With the increase of the sintering time, more silver particles were generated (Figure 3.15c). Meanwhile, the contact degree among the particles and the stacking density were improved due to the evaporation of the solvents and decomposition of the organic silver complexes (Figure 3.15d). When the sintering time was 60 min, more silver nanoparticles were produced and formed a dense structure (Figure 3.15e, f). It is worth noting that the supporter, rGO, could not be observed in the film, which may be covered by the produced silver NPs.

The chemical compositions of the Ag/rGO films sintered at 230°C for 5, 15, 30, 45 and 60 minutes were studied by EDS, the results are shown in Figure 3.16. Clearly, three elements (C, O, and Ag) were found existing in the films, which is in accordance with the original chemical compositions of the compounds in the ink. As the sintering time was increased from 5 to 60 minutes, the Ag content increased from 80.16 wt% to 86.17 wt%, the content of C decreased from 11.44 wt% to 7.98 wt% while the content of O decreased from 8.4 wt% to 5.85 wt%. The results indicate that organic molecules were decomposed and volatilized mostly and the reduction of silver complex was continued

to a large extent. The small amount of organic residue may be from the OA ( $T_b=360\text{ }^\circ\text{C}$ ).

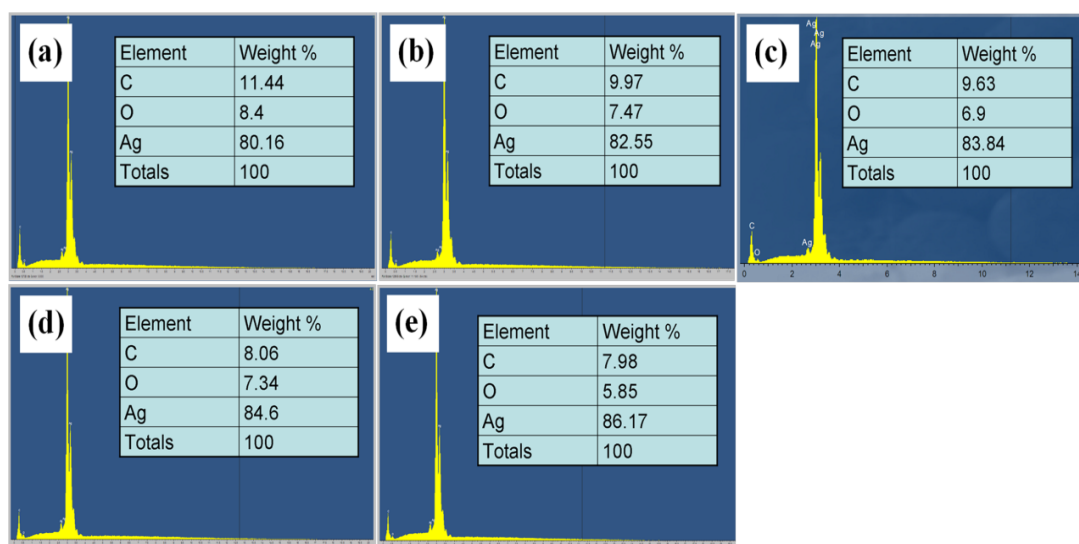


Figure 3.16 EDX results of Ag/rGO films formed at 230°C for 5, 15, 30, 45 and 60 minutes respectively

Based on the ink formulation, the carbon percentage of oleic acid in the ink can be calculated as 1.31%. Using the %C value in films obtained at 230°C for 60 min sintering, 7.98%, in the above EDS results, the amount of C from other chemicals (rGO and solvents) in the film is estimated to be 6.67%. As the amount of rGO in the ink is very small, so it mostly comes from the residual solvent. This is similar to the result of organic silver ink reported in reference [13] where there was 4.29wt% of C left in the sintered film. This is also a reason why silver/rGO ink cannot achieve the same electric properties as bulk silver.

According to the DSC, UV-vis, SEM and EDS results, it can be deduced that, during sintering process, the films underwent a series of processes including solvent evaporation, reduction of silver ions and neck connection of the silver nanoparticles during the sintering process.

### 3.3.7 Electrical performance

For comparison of the electrical performance of films with rGO, Ag films were obtained using the same ink formulation but without rGO. The Ag films were produced using the same deposition and sintering processes for the Ag/rGO films. The resistivities of the Ag and Ag/rGO ink films were calculated from the measured sheet resistance and film thickness using following equation:

$$\rho = R_s \cdot t \quad (3.2)$$

Where  $\rho$  is the resistivity,  $R_s$  is the sheet resistance of the Ag or Ag/rGO film,  $t$  is the average thickness of the Ag and Ag/rGO film which was measured to be about  $3 \pm 0.3 \mu\text{m}$ .

Calculated resistivity values for the Ag and Ag/rGO films are plotted in Figure 3.17 as a function of sintering temperature. In both cases the resistivity decreases rapidly by several orders of magnitude as the sintering temperature was increased from  $150^\circ\text{C}$  to  $245^\circ\text{C}$ . The resistivity of the Ag films decreased from  $188.75 \Omega \cdot \text{cm}$  to  $1.78 \times 10^{-5} \Omega \cdot \text{cm}$ , while the resistivity of Ag/rGO film decreased from  $0.728 \Omega \cdot \text{cm}$  to  $1.47 \times 10^{-5} \Omega \cdot \text{cm}$ . Below  $150^\circ\text{C}$ , the resistivity is very high and is beyond the sensitivity of the 4-probe instrument. The Ag/rGO film has much lower resistivity than the Ag film when the sintering temperature is below  $230^\circ\text{C}$  with the maximum enhancement by a factor of 200 achieved at the sintering temperature  $150^\circ\text{C}$ . It is worth noting that the resistivity of Ag/rGO film sintered at  $T < 165^\circ\text{C}$  was below  $10^{-4} \Omega \cdot \text{cm}$ , which is sufficient for some applications and the sintering temperature is comparable with heat-sensitive flexible substrates such as PET. The enhancement in film conductivity will be discussed in section 3.3.8.

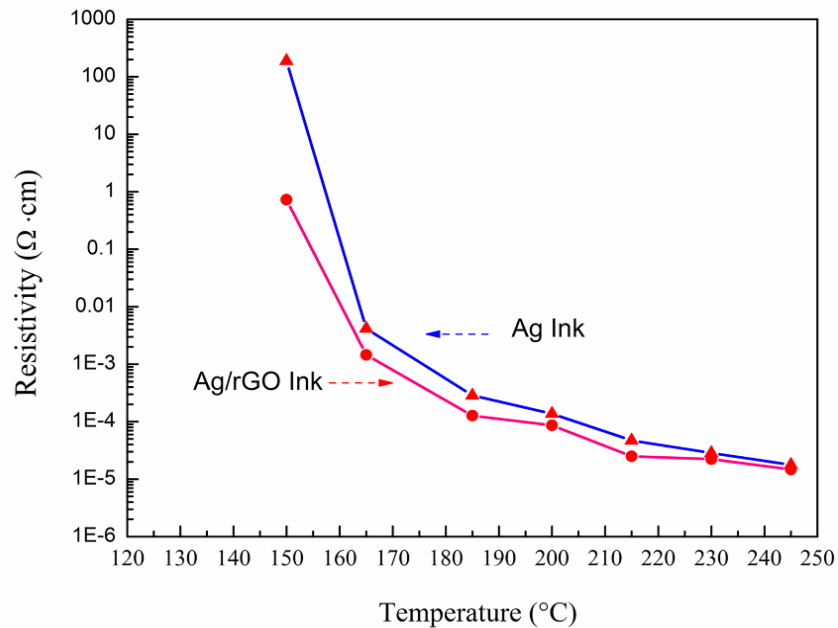


Figure 3.17 Resistivity variation of the deposited Ag and Ag/rGO films sintered at various temperatures for 60 minutes

Figure 3.18 shows the effect of sintering time on the resistivity of the films at the

sintering temperature of 230°C. The resistivity decreased by a factor of about 5 for both of the Ag and Ag/rGO films when the sintering time was increased from 5 minutes to 60 minutes. However the reduction of resistivity in the Ag/rGO film is much faster than in the Ag film, reaching the same value in 30 minutes as compared to 60 minutes in the case of the Ag film. Therefore the results highlight another advantage of using the Ag/rGO hybrid ink for formation of conductive tracks for electronic and energy storage devices and sensors.

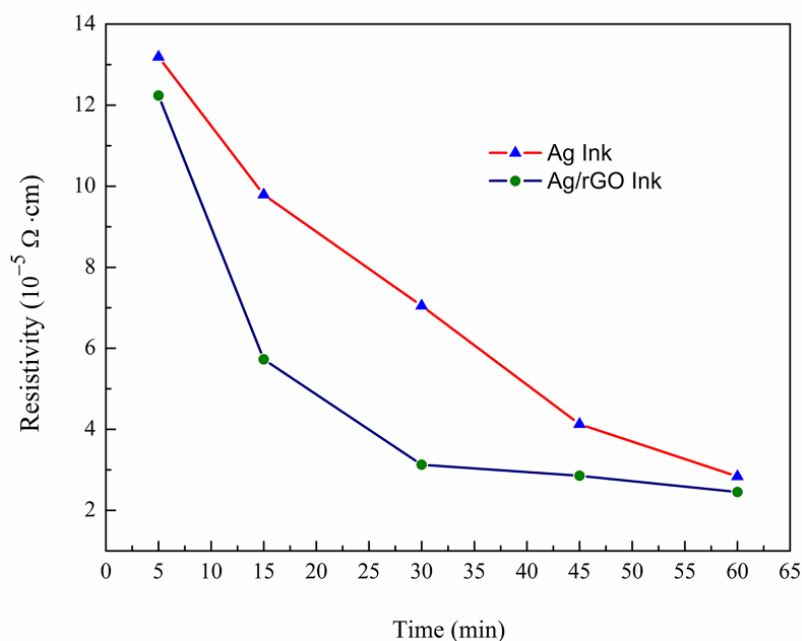


Figure 3.18 Resistivity of the deposited Ag/rGO films as a function of sintering time at 230°C

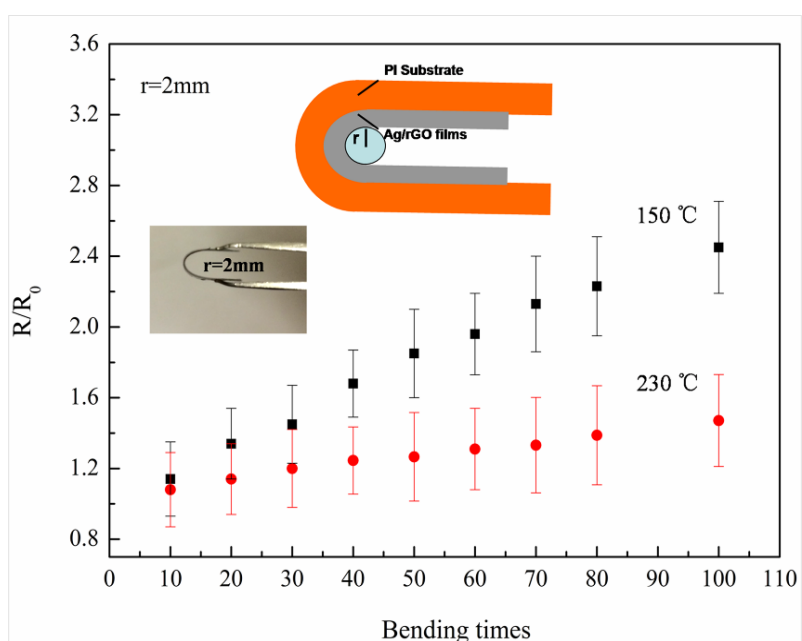


Figure 3.19 Flexibility test of Ag/rGO obtained at 150°C and 230°C on PI substrate (Inset is the schematic diagram of bending test)



Apart from the electrical performance, flexibility is another important characteristic, which was also assessed, as shown in Figure 3.19. The cyclical bending tests were conducted on the Ag/rGO film obtained at 150°C and 230°C (1.5cm×7.5mm), respectively. The way to evaluate is to compress the sample according to the given radii of curvature ( $r=2\text{mm}$ ).  $R_0$  and  $R$  stood for the sheet resistance of the Ag/rGO film before and after bending tests. It can be seen that resistances of the film obtained at 230°C experienced a slow increase after 100 times of bending, implying the films have good flexibility. The resistances of the film obtained at 150°C increased about 2 times after 100 times of bending, which may be the result of limited contact area between silver nanoparticles in the film.

### 3.3.8 Conductive mechanism

The conduction mechanisms of conductive inks are mainly explained in terms of two theories: percolation threshold theory [137] and the tunneling or field emission effect [138, 139]. In the percolation theory, there is a dramatic decrease in resistivity when the fraction of the particles in the ink film reaches a critical value. In the tunneling effect, electrons in one particle can penetrate the potential barrier and reach the next particle within a critical separation distance. Conductive channels are formed before direct contact between particles. The conduction mechanism of the silver/rGO ink should be a combination of these two processes.

Figure 3.20 shows an illustration of intermediate processes occurring in the transformation of the Ag/rGO ink into a conductive film during the sintering process.

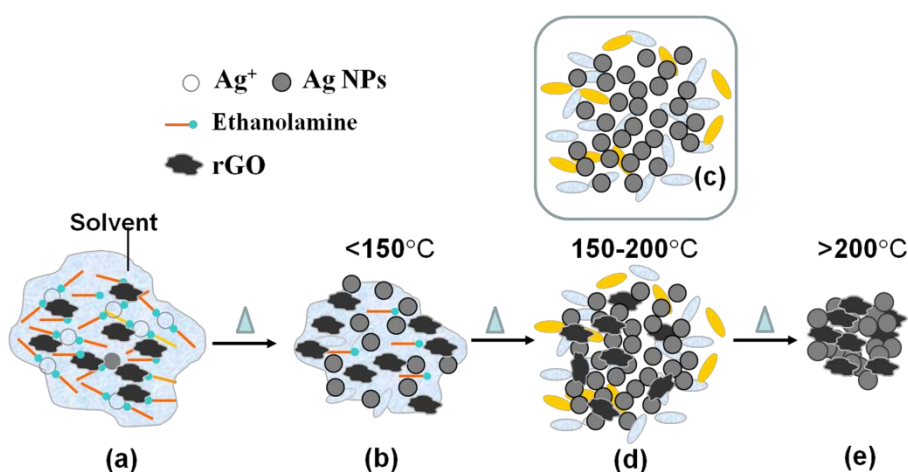


Figure 3.20 Schematic illustration of the film formation and conduction process of the Ag/rGO ink during sintering process (a. room temperature, b. below 150°C, c and d) 150-200°C, e) above 200°C)



At a lower sintering temperature ( $<150^{\circ}\text{C}$ ), fewer silver particles are produced by the reduction of ethylene glycol. These are likely to be surrounded by organic molecules such as ethanolamine ( $T_b=170^{\circ}\text{C}$ ) and oleic acid ( $T_b=360^{\circ}\text{C}$ ) and, as indicated by SEM images, have limited contact area (Figure 3.20b) since the temperature is below the boiling point of these solvents. Therefore the NPs cannot form a continuous conductive network and the resistivity is very high.

When the temperature is above  $150^{\circ}\text{C}$ , more organic molecules were decomposed and vaporized and more silver particles are generated. The silver particles form clusters resulting in an improved contact and film density. Moreover, the thickness of the surrounding organic layer separating the silver particles is decreased, which enable the quantum tunneling effect to occur and electrons can cross the barrier between the adjacent silver particles through thermal vibration to form electron paths [139], so the resistivity decreases greatly (Figure 3.20c). In this process, rGO platelets play an important role in serving as a bridge for charge transfer between silver nanoparticles, thus improving the conductivity of the film due to its high carrier mobility and excellent thermal conductivity (Figure 3.20d). Therefore, the resistivity of Ag/rGO film decreases more drastically than that of Ag films at the same sintering temperature.

Finally when the sintering temperature is above  $200^{\circ}\text{C}$ , the resistivity decreases slowly, this indicates that the percolation threshold is reached. In this case almost no solvent is left in the film and all  $\text{Ag}^+$  ions have been reduced to  $\text{Ag}^0$ . The silver particles form a continuous conductive track and cover the rGO (Figure 3.20e). So the resistivity of both films is similar and the effect of rGO is less significant at higher sintering temperatures.

### 3.4 Conclusions

A one-step method for the synthesis of a Ag/rGO hybrid ink was developed based on the amino complexation and the covalent bonding process of silver ions and rGO. The synthesized ink was composed of 13.5 wt % of silver and 0.1wt% rGO and showed good electrical performance on modified PI substrates after sintering ( $2.45 \times 10^{-5} \Omega \cdot \text{cm}$  for  $230^{\circ}\text{C}$ ). Successful dispersion of rGO in the alcohol based solvent was achieved by using rGO platelets decorated with amino groups. A hydrophilic substrate surface was obtained. A remarkable improvement of resistivity by a factor of above 200 was observed in Ag/rGO films sintered at  $150^{\circ}\text{C}$  as compared with that of the Ag films

produced using the same formulation and thermal treatment process. The increase of conductivity in Ag/rGO films from the hybrid ink at low temperatures was attributed to the role of rGO platelets in forming bridges to facilitate charge transfer between the silver particles.

## Chapter 4 Silver Citrate Ink Using Two Kinds of Mechanisms in Film Formation

### 4.1 Introduction

As described in chapter 2, organic silver inks have received increasing attention in recent years. Generally, such inks consist of organic silver precursor or organic silver complex and volatile organic solvent. Since silver is usually in an ionic form within the ink, there is no aggregation issue during preparation, storage and patterning process, which is a key advantage.

To date, silver acetate [8, 12], silver carbonate [13], silver oxalate [27],  $\beta$ -diketonate silver [14], silver 2-[2-(2-methoxyethoxy)ethoxy] acetate [93], silver nitrate [140] and silver hexafluoroacetylacetonate cyclooctadiene [141] have been used as silver precursors to formulate organic silver inks. Each precursor has its advantages and disadvantages. For instance, the first three have a relatively high decomposition temperature and can decompose in the presence of light.  $\beta$ -diketonate silver and 2-[2-(2-methoxyethoxy)ethoxy] acetate silver are stable but the synthesis is relatively complex. As for the volatile organic solvents, alcohols, especially low molecular weight ones, are usually preferred because they are less toxic and are easy to evaporate without leaving residues in the resulting film, which is beneficial for the final conductivity. Furthermore, they usually contain hydroxyl groups with a certain amount of reduction capability which is also beneficial for film formation. Among the complexing agents, amines, cyanides and thiocyanate are usually considered since they can solubilize and stabilize the silver precursors in the alcohols based solvents.

Compared with silver acetate, nitrate or carbonate, silver citrate seems to be an ideal precursor for use in silver organic ink, which were found to have excellent ink stability property as well as can promote silver reduction at lower temperatures [32, 142]. However, there are only two studies carried out using this material [32, 143]. Nie et al. [32] synthesized their ink using silver citrate as a precursor and 1, 2-diaminopropane as complex agent whereas Chen et al. [143] used silver citrate as a catalyst for the growth of copper films. Although interesting results have been obtained in both cases, further research is still required. In the first case, the ink was formulated using only short chain alcohols as the solvents (methanol and isopropanol), which were not ideal. It is well known that films derived from inks containing such solvents often suffer from serious

coffee ring effects because these solvents can easily form an outward convective flow in the area contacting with a substrate during sintering; the flow causes the small particles formed in the ink droplet to move to the edge region, resulting in a ring shape pattern [144]. Also, there was no detailed description of ink formulation, film formation and conduction. Furthermore, the chemical reactions leading to ink formation based on such material (silver citrate) are not clear. In addition, the film from such inks usually has voids and cracks due to bubbling effects [27] resulting from the fast solvent evaporation of these solvents and the decomposition of silver complex, which should be avoided. Last, there is little investigation of the effects of the constituents such as solvents in the ink on its properties. Therefore, it is necessary to develop a silver citrate based ink and elucidate its formulation and conductive mechanism as well as to investigate the role of each constituent in the ink.

In this chapter, an organic silver ink with self-reducible and decomposable properties was formulated by a complexation process in mixed solvents using silver citrate as the silver precursor and ethylenediamine as the complexing agent, which showed good conductivity after sintering at 155°C. The physical phase, chemical composition and thermal behavior of the silver citrate precursor were studied. The effect of the solvent on the thermal property of the formulated ink was investigated in order to understand the chemical reactions in the film formation process. The effects of sintering temperature and time on the microstructure and electrical properties of the silver films from the ink were studied. The defects such as voids and cracks as well as the coffee rings, which are often associated with films produced from organic silver inks, were reduced significantly by using both decomposition and self-reduction mechanisms in film formation.

This Chapter has been published [145].

## **4.2 Experimental Section**

### ***4.2.1 Materials***

Silver nitrate ( $\text{AgNO}_3$ ), sodium citrate tribasic dihydrate ( $\text{C}_6\text{H}_5\text{O}_7\text{Na}_3 \cdot 2\text{H}_2\text{O}$ ), ethylenediamine ( $\text{C}_2\text{H}_8\text{N}_2$ ), ethylene glycol ( $\text{C}_2\text{O}_2\text{H}_6$ ) and 2-propanol ( $\text{C}_3\text{H}_8\text{O}$ ) were obtained from Sigma-Aldrich and were used as received without further purification. The physical properties of the various solvents used in this study are listed in Table 1. The substrate was a Kapton polyimide film from DuPont (500 HN, 127  $\mu\text{m}$  in

thickness). Before application, the films of 15mm×15mm were cleaned with ethanol and de-ionized water to remove particles and organic contamination and dried in an oven.

Table 4.1 Physical properties of various solvents

Chemicals	Viscosity ( $\eta$ , mPa·s)	Surface tension ( $\gamma$ /mN·m <sup>-1</sup> )	Boiling point (T <sub>b</sub> /°C)	$\rho$ /g·cm <sup>-3</sup>	Possible problem
<b>2-Propanol</b>	2.431	21.7	82.45	0.7855	Coffee ring effect
<b>Ethylene glycol</b>	25.66	46.49	197.85	1.1115	Solvent contraction effect
<b>Ethylenediamine</b>	1.7	42	116	0.90	/

#### 4.2.2 Synthesis

The silver organic decomposition ink used in this study was prepared by dissolving the synthesized silver citrate into a mixture of organic solvents. The process is as follows: silver nitrate (1.7 g, 0.01 mol) and sodium citrate dehydrate (1.1 g, 0.0037 mol) were first dissolved in 30 ml of de-ionized water, respectively, then mixed by continuous stirring for 1 h at room temperature without light. The product, silver citrate, was collected by vacuum filtration and then washed with de-ionized water for three times and ethanol twice, dried at 40 °C for 6 h in an oven and stored both away from light. The obtained silver citrate powder was 1.603 g, which is less than the theoretical product (1.709g), this indicates that silver citrate is sparingly soluble in de-ionized water and ethanol.

For ink preparation, 0.5 g of the obtained silver citrate was dispersed in 2 ml of a mixed solvent containing 2-propanol (1.25 ml) and ethylene glycol (0.75 ml). After stirring for 10 minutes, ethylenediamine (0.5 ml) was added at once. The mixture was stirred for 60 minutes to form the ink, named as ink<sub>1</sub>. It is useful to note that the appearance of the solution changed, from the initial suspension to a homogeneous transparent solution with an orange color. The silver content in the ink was about 10 wt%.

#### 4.2.3 Ink deposition and sintering

The as-prepared ink was deposited on the PI films by a drop-coating method, and sintered at selected temperatures for up to 60 minutes. The film thickness was controlled by the volume of ink solution deposited onto the PI film.

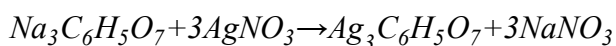
#### 4.2.4 Characterization

Ultraviolet-visible (UV-Vis) absorption spectra were recorded on a Lambda 25 UV-Vis spectrophotometer using water as solvent. Fourier transform infrared (FT-IR) spectra in the range of 400-4000  $\text{cm}^{-1}$  were recorded on a Thermo Scientific Nicolet iS5 FT-IR spectrometer. The thermal profiles of the powder and ink were measured under nitrogen atmosphere by differential scanning calorimetry (DSC, TA instrument) using aluminum pans at a heating rate of 10  $^{\circ}\text{C min}^{-1}$  from room temperature to 250  $^{\circ}\text{C}$  and a nitrogen flow rate of 80  $\text{ml}\cdot\text{min}^{-1}$ . X-ray diffraction (XRD) analysis was conducted by using Cu  $K\alpha$  and  $\lambda = 0.15418$  nm. Grain sizes of silver crystallites were calculated using Scherrer's formula. The morphologies of the silver films after sintering were observed on a FEI Quanta 3D Scanning Electron Microscope (SEM). The chemical composition was determined on an Oxford X-maxN 150 surface energy disperse spectrometer (EDS). The sheet electrical resistivity was measured using a 4-point probe method (Jandel Engineering, UK). The thickness of the sintered films was measured using a Zygo View 5200 white light phase shifting interferometer.

### 4.3 Results and Discussion

#### 4.3.1 Characterization of silver precursor

Silver citrate was chosen as the silver precursor since it has a relatively lower decomposition temperature, which is beneficial in ink application to some temperature-sensitive polymer substrates. Also, this compound contains one OH group that can increase its solubility in alcohols. The silver citrate used in this study was prepared through a typical ion exchange method as shown below:



As an important component of the ink, the characteristic of the as-prepared silver citrate powder was investigated using FT-IR, XRD, EDS and DSC-TG techniques to confirm its physical phase, chemical composition, and thermal decomposition temperature.

Figure 4.1 shows the XRD pattern of the as-prepared silver citrate powder measured in  $2\theta$  from  $20^{\circ}$  to  $85^{\circ}$ . The main peaks appeared at  $7.749^{\circ}$ ,  $15.003^{\circ}$ ,  $21.603^{\circ}$ ,  $29.062^{\circ}$ ,  $31.249^{\circ}$ ,  $38.783^{\circ}$ ,  $43.951^{\circ}$  and  $48.375^{\circ}$ . The results are in good agreement with the JCPDS No.01-0030 for silver citrate. No diffraction peaks from any other impurities

were detected, indicating that the above reaction took place completely and the silver citrate powder was prepared successfully.

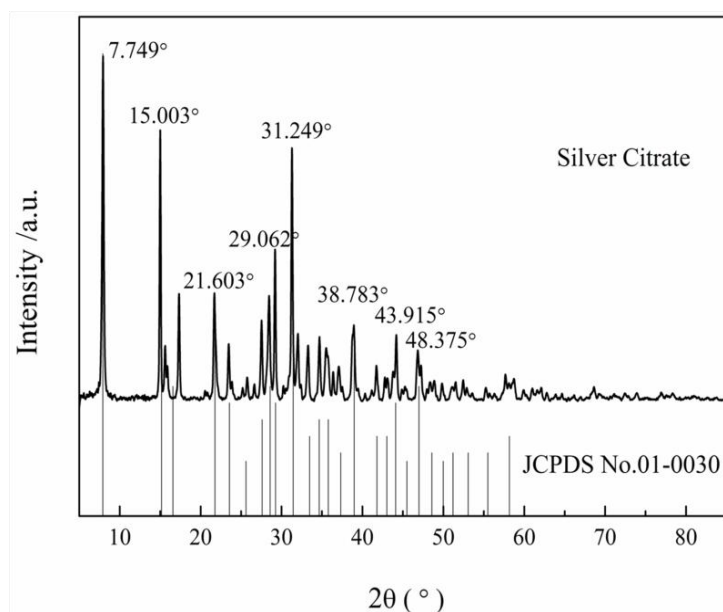


Figure 4.1 XRD pattern of the as-prepared silver citrate powder

Figure 4.2a shows the IR spectrum of the as-prepared silver citrate powder. A broad feature around  $3200\text{ cm}^{-1}$  is attributed to the O-H stretching vibration. Two sharp bands at  $1537$  and  $1401\text{ cm}^{-1}$  are attributed to the asymmetric stretch vibration and the symmetric stretch vibration of C=O in the carboxyl group (-COO-), respectively. The band at  $1073\text{ cm}^{-1}$  is from C-O stretch. These features confirm that silver citrate has a structure of carboxylates.

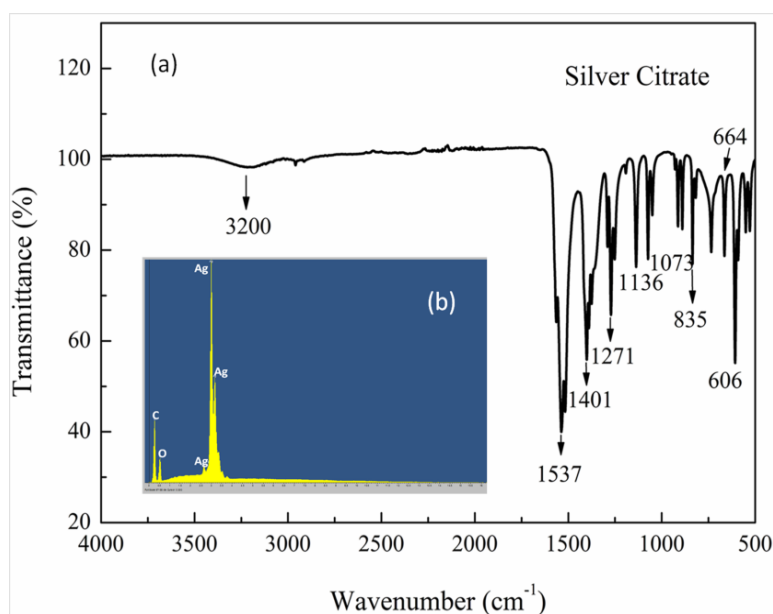


Figure 4.2 FT-IR spectrum and EDS results of the synthesized silver citrate powder

It has been reported that the wave number difference ( $\Delta$ ) between the asymmetric  $\nu_{as}$   $\text{CO}_2^-$  stretch peak and the symmetric  $\nu_s$   $\text{CO}_2^-$  stretch peak in the carboxylate complex can be used to identify the type of interaction between the carboxylate moiety and  $\text{Ag}^+$  ions [146]. Unidentate complexes exhibit the largest  $\Delta$  values ( $200\text{-}320\text{cm}^{-1}$ ). Chelating (bidentate) complexes have the smallest  $\Delta$  values ( $<110\text{cm}^{-1}$ ). The medium  $\Delta$  values ( $140\text{-}190\text{cm}^{-1}$ ) for bridging complexes are greater than those of chelating complexes, and close to the ionic values. Based on these observations, it is concluded that the carboxylate moiety and  $\text{Ag}^+$  ions interacts in a bridging manner ( $\Delta$  value:  $1537\text{-}1401 = 136\text{cm}^{-1}$ ).

The chemical composition was identified by EDS as shown in Figure 4.2b. Evidently, three elements (C, O, and Ag) exist in the powder as expected from the chemical structure.

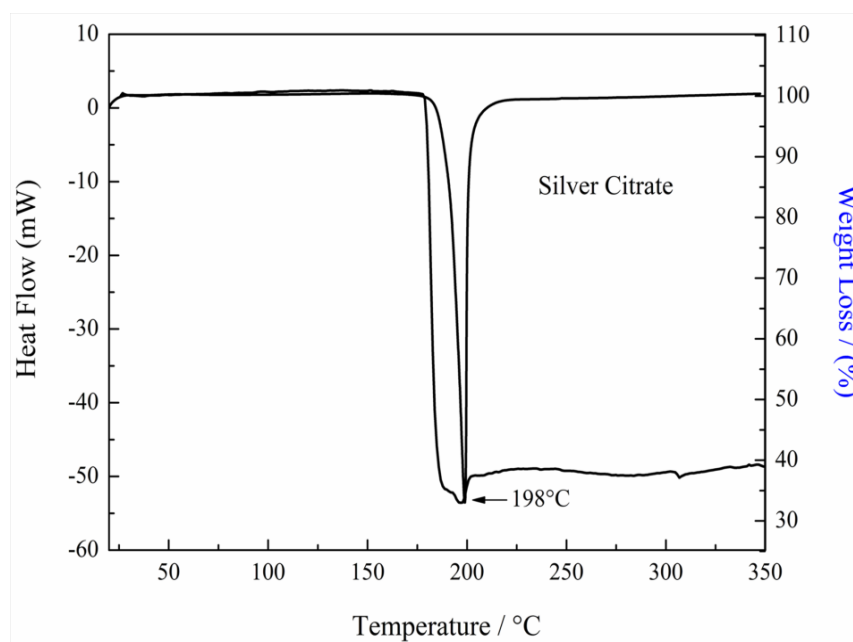


Figure 4.3 DSC-TG curve of silver citrate powder

Figure 4.3 shows the thermal behavior of the as-prepared silver citrate powder. The DSC curve shows an exothermic peak at 198 °C, relating to the thermal decomposition of the silver citrate, which is similar to the behavior of other silver carboxylates but the decomposition temperature is lower than that of them [27]. This is a preferred property. From the TG curve, it can be seen that the powder starts to lose weight at 175 °C and a maximal rate of weight loss occurs at 200 °C. The total weight loss was about 40 wt%, indicating that the left weight is 60wt%. This is basically in line with the proportion occupied by silver in the silver citrate (63.19wt%). All of the results demonstrate that

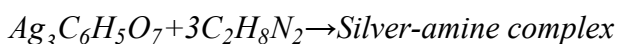


silver citrate is an ideal precursor material for ink formulation.

#### 4.3.2 Ink formulation

For ink preparation, ethylenediamine, a small molecule bi-dentate aliphatic amine with low boiling point (116 °C), was chosen as the ligand to increase the silver content of the ink since it can form a complex that has higher solubility than pure silver citrate and to improve film formation efficiency as well as to decrease the ink sintering temperature [147]. Reduced organic content in the metal-ligand complex can make the sintering process easier and faster since the energy and time required to evaporate the organic content are reduced [142]. 2-Propanol, a volatile alcohol, was used as the ink solvent to adjust the rheological properties as it has lower surface tension and viscosity, which is beneficial to ink deposition. Ethylene glycol was selected as a reduction agent and a co-solvent. The preparation details were given in the experimental section and the prepared ink was named as ink<sub>1</sub>.

The sparingly soluble silver citrate can be dissolved in the organic solution containing ethylenediamine with no difficulty, mainly via the following complexing process, resulting in a soluble complex.



FT-IR was employed to investigate and confirm this complexation mechanism. As the solvents will have some influence in both spectra, the complex was prepared using only silver citrate and ethylenediamine in a stoichiometric ratio without adding any solvents. It was found that the solid silver citrate became dissolvable when ethylenediamine was added, indicating that the above reaction occurred. The silver amine complex formed from ethylenediamine will go through the subsequent sintering process.

Figure 4.4a shows the IR spectrum of ethylenediamine. The absorption peaks at 3352 and 3276 cm<sup>-1</sup> correspond to the asymmetric and symmetric stretch of the NH<sub>2</sub> groups. The two peaks at 2920 and 2852 cm<sup>-1</sup> are assigned to the asymmetric CH<sub>2</sub> stretch and the symmetric CH<sub>2</sub> stretch. The peak at 1594 cm<sup>-1</sup> is associated with NH<sub>2</sub> bending vibration. Figure 4.4b shows the spectrum of the complex. It is worth noting that a new OH stretching vibration peak and a new C-O stretching vibration peak appear at 3675 cm<sup>-1</sup> and 1059 cm<sup>-1</sup>, respectively, which are from the silver citrate. In combination with

the FT-IR spectrum of silver citrate powder, it can be seen that the positions of these two peaks change, which might be the result of complexation between the silver atom and amino group. All peaks associated with  $\text{NH}_2$  group have a red-shift, from 3352 to 3339  $\text{cm}^{-1}$ , 3276 to 3269  $\text{cm}^{-1}$  and 1594 to 1556  $\text{cm}^{-1}$ , implying that a coordination process occurred on the bond of  $\text{NH}_2$ . Here, ethylenediamine can donate electron from the amino group to the silver atom of silver citrate, decreasing the electron density of the amino group and thus resulting in red-shift of the  $\text{NH}_2$  stretch. These changes indicate that the ethylenediamine forms a complex with silver citrate.

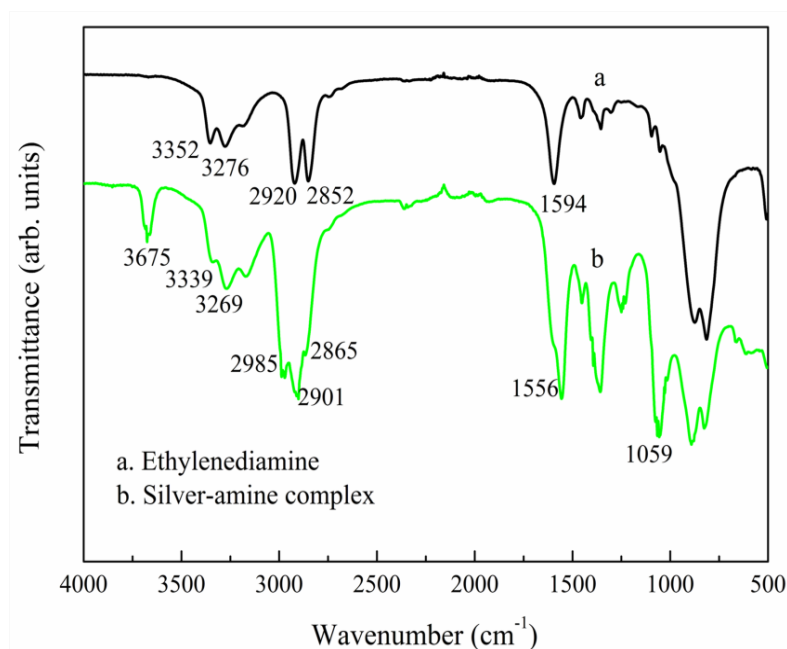


Figure 4.4 FT-IR spectra of the ethylenediamine and silver-amine complex

#### 4.3.3 Effects of solvent on the thermal behavior of the ink

The solvent used in the ink determines the quality of the resultant films and should meet various requirements, such as stability, uniform surface morphology of the formed film and conductivity.

As a solvent of the ink, ethylene glycol has reducibility [13, 147]. In order to investigate whether this mechanism is still active in  $\text{ink}_1$  and to better understand the effect of the solvent on thermal decomposition, an ink, named  $\text{Ink}_0$ , was prepared using the same ink formulation method but replacing ethylene glycol with ethanol. DSC analysis was carried out to investigate the thermal decomposition behavior of both inks and the results are shown in Figure 4.5.

The DSC curves of  $\text{Ink}_0$  show two major peaks at 62°C and 155°C. The first one is

attributed to solvent evaporation. Since the ink color changes from initially light yellow to black, and then to metallic silver during the heating process (Figure 4.5a), it can be deduced that the second peak arises from the decomposition of the complex. Based on the results reported in reference [13] and the color of silver oxide, the change should be associated with the transition of silver ion complex to silver oxide and finally to elemental silver.

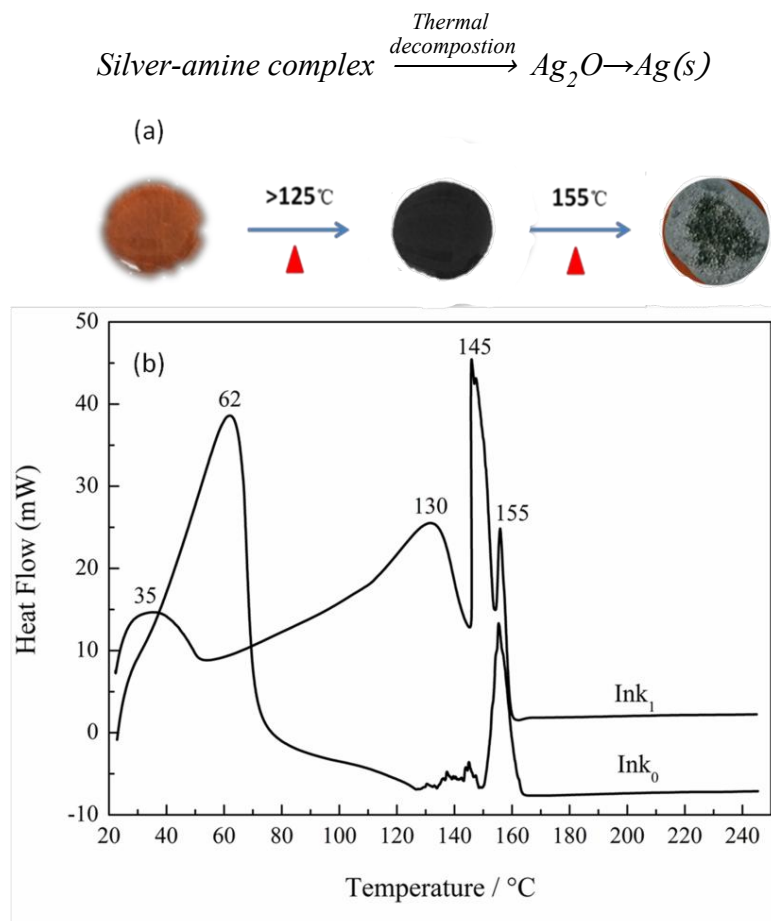
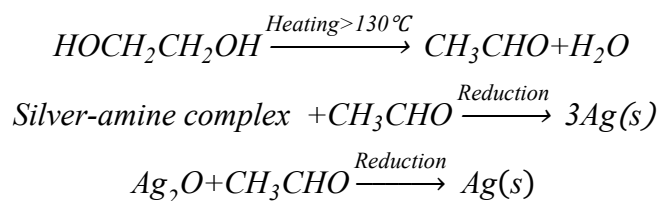


Figure 4.5 (a) Optical images of ink<sub>0</sub> color change during the heating process, (b) DSC curves of the ink with and without ethylene glycol

However, the ink containing ethylene glycol (Ink<sub>1</sub>) shows a different behavior, although the ink color changes were similar to that of ink<sub>0</sub> in the sintering process. The first peak below 50°C is attributed to the evaporation of 2-propanol. The second and third peaks, appeared at 130°C and 145°C, are new features. From the work in reference [13], below 150°C ethylene glycol can decompose to glycolaldehyde that can reduce silver ions to metallic silver. So these two peaks are attributed to the decomposition of ethylene glycol and reduction of the complex ion or Ag<sub>2</sub>O derived from the above reaction. Therefore, it can be deduced that the reduction effect of ethylene glycol occurs in this system.



From the above analysis, it can be concluded that two reaction processes are simultaneously active in our ink system: (1) decomposition and (2) reduction. The latter is the dominant effect. Therefore the ethylene glycol not only acts as the co-solvent but also functions as a reduction agent. This is different from previous work which was based only on the decomposition effect [32]. The decomposition and reduction temperature are both lower than that of the silver citrate powder.

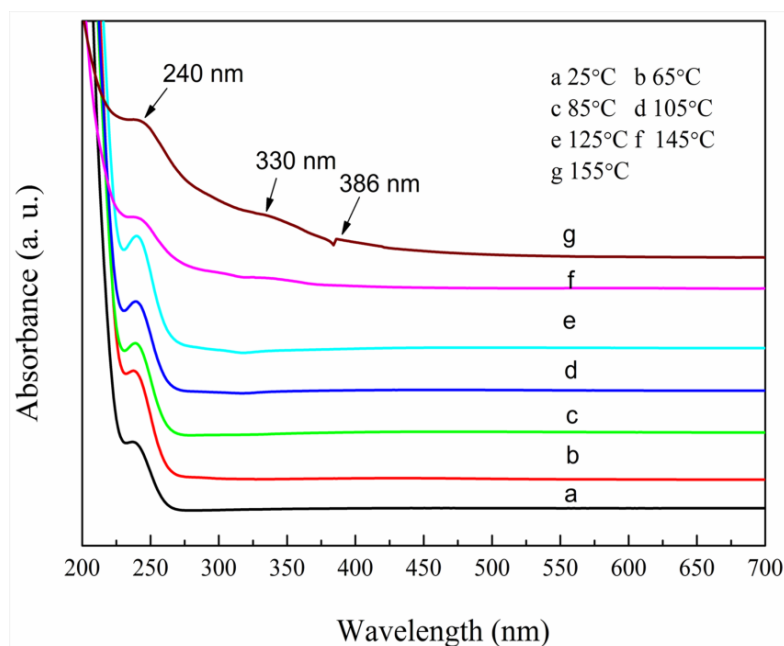


Figure 4.6 UV-Vis absorption spectra of silver citrate ink obtained at different temperatures

UV-Vis absorption peaks are sensitive to the metal nanoparticles, and this is especially true for silver nanoparticles. The UV-Vis technique can be used to detect the atomic, ionic, and cluster states of silver, which exhibit different characteristic absorption bands [148]. The absorption band of  $Ag^+$  is in the 190-230 nm spectral range, silver atoms  $Ag^0$  (or containing  $Ag_2O$ ) absorb in the 250-330 nm region, and small  $Ag_n$  clusters at 330-360 nm and 440-540 nm. Light absorption by silver nanoparticles manifests pronounced resonance bands at 380-450 nm due to the excitation of surface plasmon resonances (SPRs) [149]. Therefore, UV-Vis spectroscopy was employed to study the temperature dependent absorption characteristics as shown in Figure 4.6.

From the results in Figure 4.6, it can be seen that at temperatures below 125°C, there is only one sharp absorption band around 240 nm, which is from the complex according to previous description. However, when the ink is heated above 145°C, the absorption band at 240 nm broadens and two new absorption bands appear at 330 nm and 386 nm. These bands are associated with the formation of Ag<sub>2</sub>O, silver atoms or silver clusters and silver nanostructures, respectively. In other words, the complex is reduced and decomposed into elemental Ag.

Based on these results, it can be deduced that the ink<sub>1</sub> underwent simultaneous the change of solvent components and the decomposition/reduction of silver complex at elevated temperatures. In the process ethylene glycol generates glycolaldehyde and triggers the reduction of the silver complex ion or Ag<sub>2</sub>O to Ag.

#### 4.3.4 Effects of sintering temperature on microstructure of silver films

Silver films were produced by drop-coating of ink<sub>1</sub> on the cleaned PI substrates. The sintering process was carried out on a hotplate in a chamber. Based on the DSC results and UV-Vis analysis of the ink, selected temperatures between 125 °C and 200 °C were used for the thermal sintering. XRD, SEM/EDS and Zygo interferometer were used to evaluate the produced silver films.

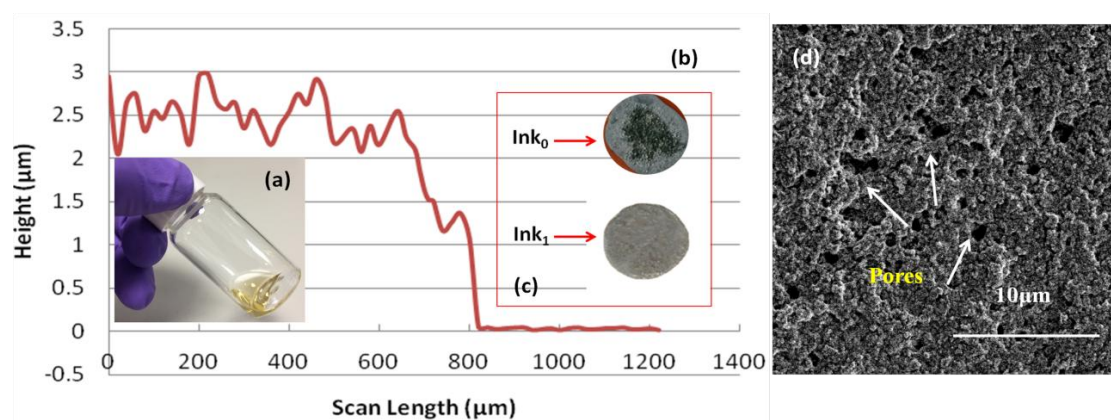


Figure 4.7 (a) As-prepared ink<sub>1</sub>; (b) Surface profile of a sintered silver film from ink<sub>1</sub>; (c) Optical images of silver films produced from ink<sub>0</sub> and ink<sub>1</sub>; (d) SEM images of silver films produced from ink<sub>0</sub>

Figure 4.7 shows the optical image of ink<sub>1</sub> and a corresponding silver film surface profile (sintered at 155 °C) where the thickness was about 2.5±0.5μm. The optical image of silver films produced from Ink<sub>0</sub> was also given for comparison. Clearly, the film from Ink<sub>1</sub> has a continuous surface without pores or a coffee ring effect of ink<sub>0</sub> caused by the fast evaporation of solvents with lower boiling point, indicating the

positive effect of ethylene glycol as a co-solvent.

Figure 4.8 shows the crystalline structure of the silver films obtained at different sintering temperatures for 60 min. Diffraction peaks were observed at  $2\theta$  values of  $38.2^\circ$ ,  $44.4^\circ$ ,  $64.5^\circ$ ,  $77.5^\circ$  and  $81.6^\circ$  and were the same in all of the films. The results indicate that the complex was transformed to silver crystals. The diffraction peaks are indexed as the (111), (200), (220), (311) and (222) crystal planes of the face-centered cubic (fcc) crystal structure of silver.

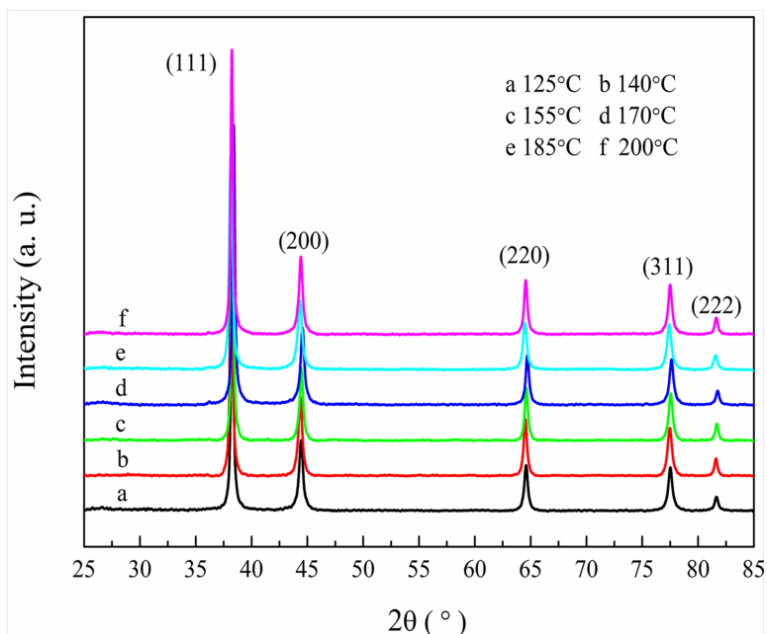


Figure 4.8 XRD patterns of the silver films obtained at different sintering temperatures for 60 minutes. Data shifted vertically, for clarity.

The crystallite sizes of the silver nanoparticles in the films formed at  $125^\circ\text{C}$ ,  $155^\circ\text{C}$  and  $185^\circ\text{C}$  were calculated using the Debye-Scherrer equation given in chapter 3. The average particle size of silver nanocrystals in the film increases with the sintering temperature. However, this change is not significant.

Table 4.2 Particle sizes of silver nanocrystals in the film sintered at different temperatures

Sintering temperature ( $^\circ\text{C}$ )	$2\theta$ (Degrees)	FWHM ( $\text{\AA}$ )	Size (nm)
125	38.274	0.314	26.11
155	38.403	0.289	28.98
185	38.238	0.278	29.34

Figure 4.9 shows the SEM images of the silver films sintered at different temperatures. It can be seen that the morphology of the films changes with the sintering temperature,



which is a result of the fast evaporation of solvent and thermal decomposition and reduction of the complex. At lower sintering temperatures (125°C, 140°C), the films show voids and cracks (Figure 4.9a and a<sub>1</sub>) and silver nanoparticles produced are small. As the film is partly wet at 125°C, these nanoparticles were still to be surrounded by organic molecules as will be shown in the results of EDS measurements. At the sintering temperatures of 155°C and 170°C, the defects on the film surface become less pronounced and the grain boundary becomes obvious (Figure 4.9d). Sintering at higher temperatures (180°C, 200 °C) leads to larger silver nanoparticles formed through neck connection (Figure 4.9e<sub>1</sub> and f).

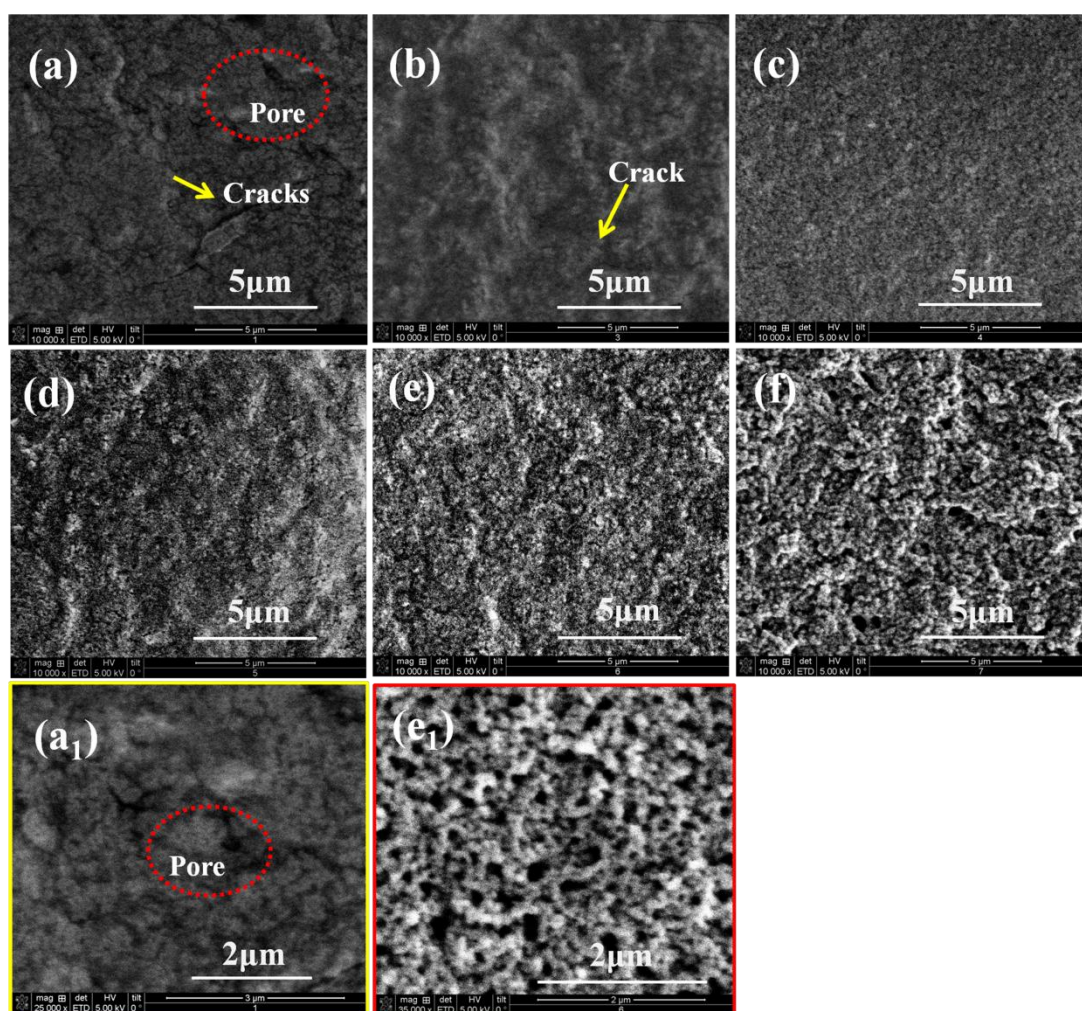


Figure 4.9 SEM images of silver films sintered for 60 minutes, (a) 125 °C, (b) 140 °C, (c) 155 °C, (d) 170 °C, (e) 185 °C and (f) 200 °C (a<sub>1</sub> and e<sub>1</sub> are high magnification image of a and e)

In the previous work by Dong et al. [27], fast solvent evaporation and bubbling caused by CO<sub>2</sub> or H<sub>2</sub>O formation from decomposition of the silver complex were the reason for the presence of pores and cracks in the silver films. However this phenomenon is not obvious in our ink system. It is believed that this is suppressed by a simultaneous

self-reduction mechanism during the film formation and the decomposition effect. The self-reduction effect due to the presence of ethylene glycol produces silver nanoparticles that fill in the pores and cracks, compensating for the bubbling defects from the decomposition of the silver salt. This is a key advantage of the ink developed in this work.

The sintering temperature plays two roles in the film formation process: (i) it aids solvent evaporation and (ii) it triggers chemical reactions in the ink to produce silver nanoparticles and subsequently nanocrystals.

Figure 4.10 shows the C and Ag content from EDS results in the sintered films. The C content decreases rapidly as the sintering temperature was increased from 125°C to 200°C, indicating that the decomposition and volatilization of organic molecules mainly occurred at this stage. The Ag content increased from 72.63 wt% to 88.5 wt% over the same temperature range. This indicates that most of the organic molecules were decomposed and vaporized and the  $\text{Ag}^+$  ions were reduced to  $\text{Ag}^0$ .

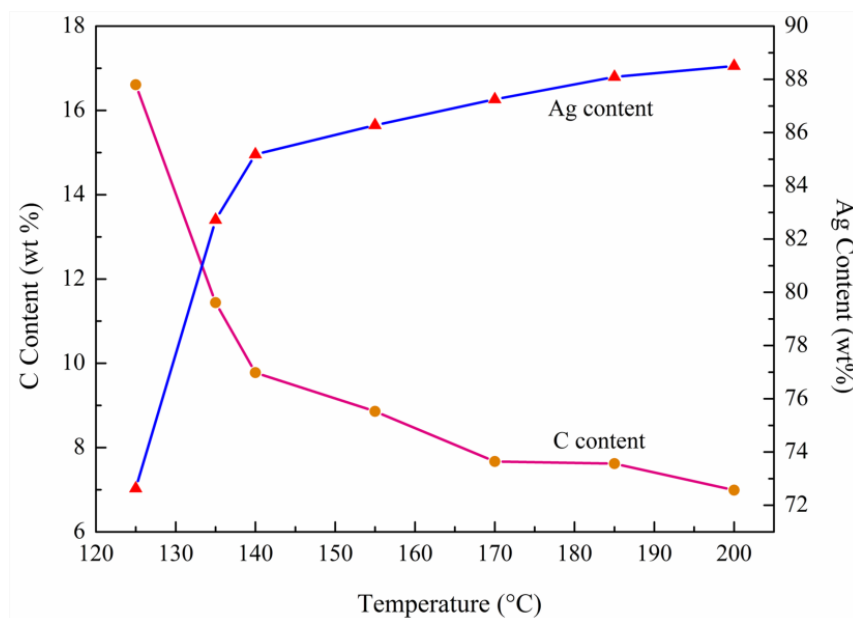


Figure 4.10 C and Ag content from EDS results in the films as a function of sintering temperature

#### 4.3.5 Effects of sintering time on microstructure of silver ink films

The effect of sintering time on the microstructure of silver films from ink<sub>1</sub> was also investigated. The samples were obtained by heating the ink<sub>1</sub> films on PI substrates at 155°C for 5, 15, 30 and 60 minutes and were then evaluated by SEM, XRD and EDS methods.



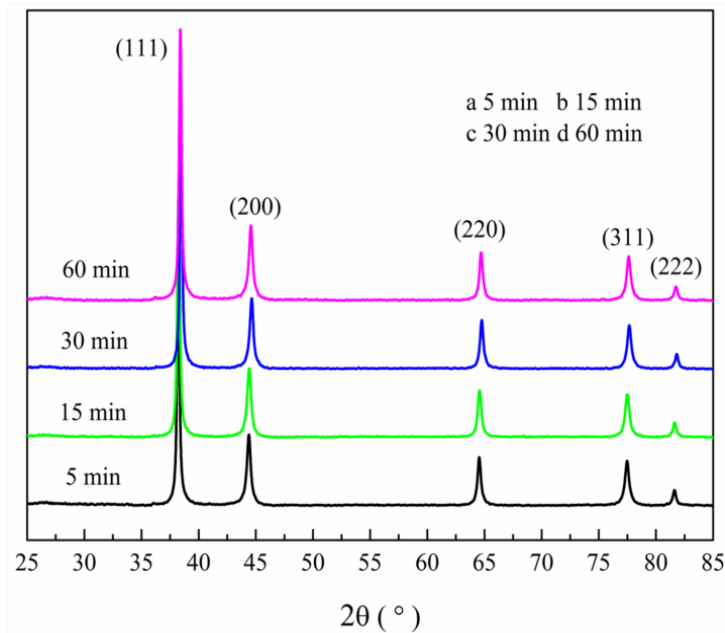


Figure 4.11 XRD patterns of Ag films prepared at 155°C for 5, 15, 30 and 60 min respectively

As shown in Figure 4.11, it can be seen that silver ions could be transformed to silver nanocrystals within 5 minutes. With increasing sintering time, the intensity also increases, indicating that more metallic silver was formed. The particle sizes of silver nanocrystals in the films were calculated using equation (4.1) and the results are shown in Table 4.3. The increase in particle size as the heating time increases is very small. This means that the nucleation and growth of silver nanocrystals is less dependent on the heating time.

Table 4.3 Particle size of silver nanocrystals in the films processed at 155°C for different times

Sintering time (min )	2θ (Degrees)	FWHM (β)	Size (nm)
10	38.210	0.294	27.63
45	38.164	0.286	28.24
60	38.403	0.289	28.98

The SEM images in Figure 4.12 show the microstructures of the silver films produced at 155 °C for different times. Some differences in the morphologies can be observed. The film heated for 5 min has some cracks on its surface. Silver nanoparticles produced seem to be surrounded or covered by organic molecules (Figure 4.12a). With increasing time, the films show relatively more compact microstructures consisting of small silver particles with better film uniformity (Figure 4.12b). The film sintered for 30 min has a porous surface profile consisting of many silver particles. The grain boundaries become less obvious. More particles are in contact at this time (Figure 4.12c and c<sub>1</sub>). When the

sintering time reaches 60 minutes, more silver nanoparticles are produced to form larger silver nanoparticles and produce a relatively complete film (Figure 4.12d and d<sub>1</sub>).

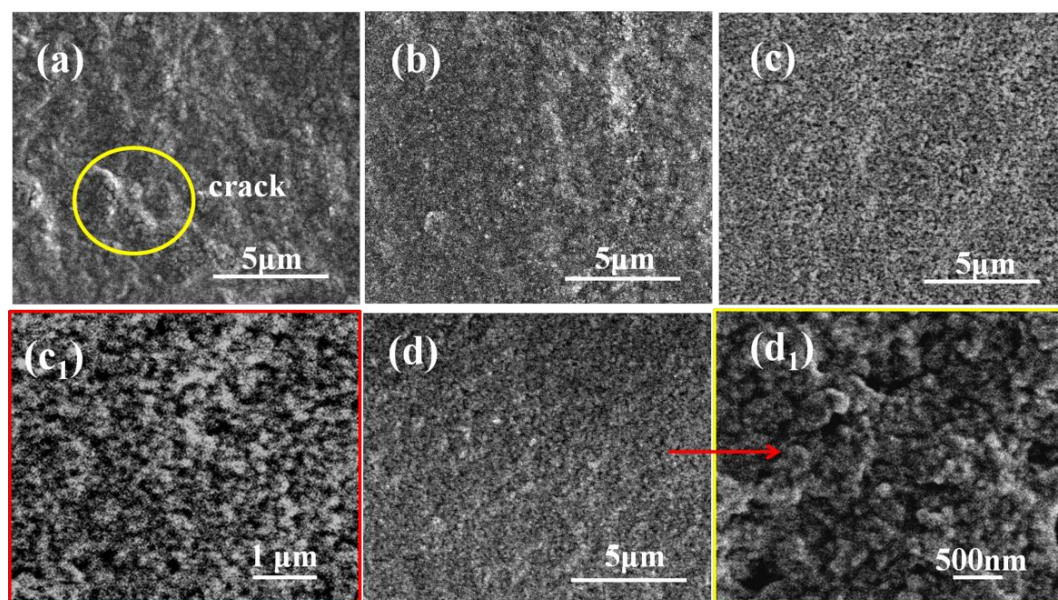


Figure 4.12 SEM images of silver films produced at 155 °C for 5, 15, 30 and 60 minutes (a-d, c<sub>1</sub> and d<sub>1</sub> are high magnification image of c and d)

As discussed before, the film morphology is dependent on the solvent evaporation rate and thermal decomposition or reduction of the silver-amine complex. At 155 °C, the solvent evaporates quickly resulting in an uneven film when the sintering time was 5 minutes. As will be shown in section 4.3.6, the film conductivity was low indicating insufficient formation of Ag particles from the complex. For the sintering time of 15 minutes, the film is less uneven as there is material redistribution due to decomposition and reduction of the complex in the film. Further increase in sintering time results in improved surface morphology (Figure 4.12 c and d).

EDS analysis was also used to illustrate this phenomenon, as shown in Figure 4.13. Clearly, three elements (C, O, and Ag) were found in the films after heating at 155 °C. As the heating time was increased from 5 to 60 minutes, the Ag content increased from 81.70 wt% to 86.28 wt% and the content of C decreased from 12.37 wt% to 8.86 wt% while the oxygen content decreased from 5.93 wt% to 4.86 wt%. The results indicate that the organic molecules were decomposed and volatilized mostly within 15 minutes and the decomposition or reduction reaction of the complex continued to a large extent within 60 minutes.

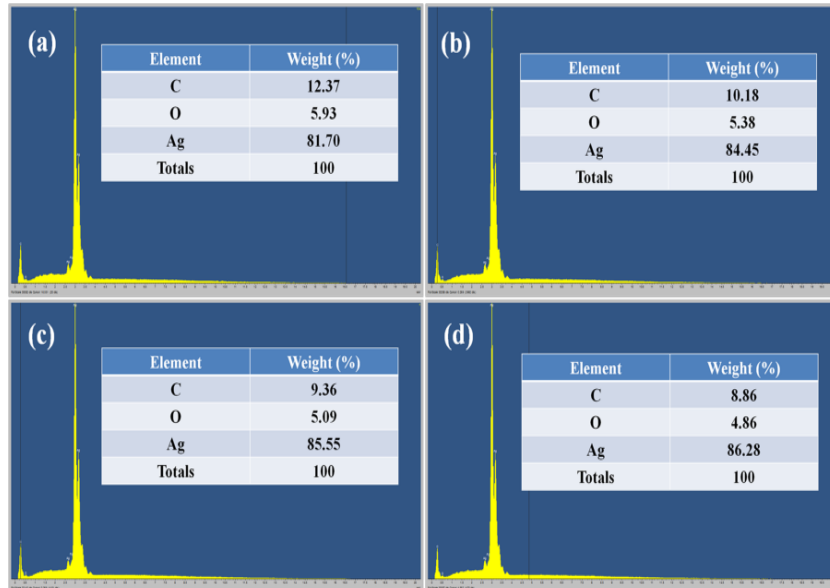


Figure 4.13 EDS results of silver films produced at 155°C for 5, 15, 30 and 60 minutes (a-d)

#### 4.3.6 Electrical performance

The resistivities of the silver films obtained by heating at various temperatures for 60 minutes were calculated from the measured sheet resistance and film thickness ( $2.5 \pm 0.5 \mu\text{m}$ ) using the equation showed in chapter 3. The values are shown in Figure 4.14 as a function of sintering temperature.

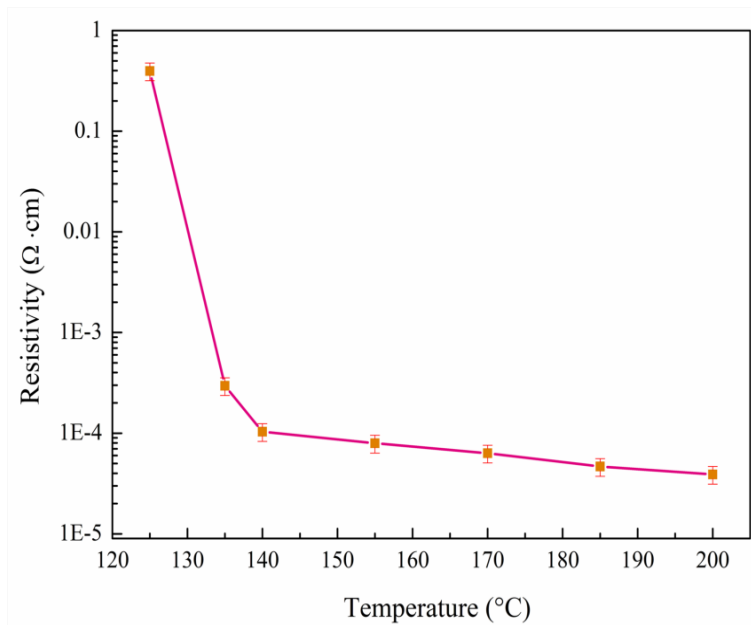


Figure 4.14 Resistivity of the silver films sintered at various temperatures for 60 minutes

It can be seen that the resistivity decreases rapidly by several orders of magnitude from  $0.4 \Omega \cdot \text{cm}$  at 125  $^{\circ}\text{C}$  to  $3.9 \times 10^{-5} \Omega \cdot \text{cm}$  at 200  $^{\circ}\text{C}$ . Below 125  $^{\circ}\text{C}$ , the film was not totally dry and showed a high resistivity that is beyond the sensitivity of the 4-probe instrument.

The resistivity decrease can be explained based on the effects of the temperature in the film formation process. At lower temperature, not all solvent has evaporated and the formation of silver is not complete, so the film has high resistivity. Conversely, at higher temperature, solvent evaporation is fast and more silver nanocrystals can be formed to improve the stacking density of Ag nanoparticles in the film. The pores are eliminated by using both decomposition and self-reduction effects in the sintering process. A continuous and uniform film with better particle stacking density is obtained and hence good film conductivity. It is worth noting that film resistivity of  $10^{-5} \Omega \cdot \text{cm}$  can already be achieved at sintering temperatures below  $150^\circ\text{C}$ . This shows that the organic silver ink can be compatible with the temperature sensitive flexible substrates such as PET or PEN.

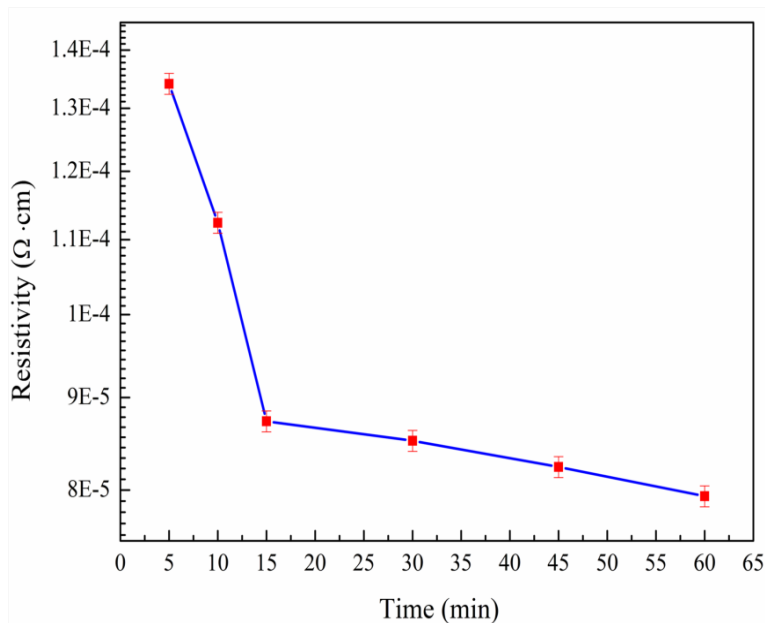


Figure 4.15 Resistivity of the Ag films as a function of heating time at  $155^\circ\text{C}$

The resistivities of the films heated at  $155^\circ\text{C}$  for different times are shown in Figure 4.15. The resistivity decreases by only one order of magnitude from  $1.34 \times 10^{-4} \Omega \cdot \text{cm}$  to  $7.94 \times 10^{-5} \Omega \cdot \text{cm}$  when the sintering time increases from 5 to 60 minutes. This is in agreement with previous analysis of film formation based on the decomposition or reduction of the complex as described in section 4.3.5.

#### ***4.3.7 Mechanism of silver film formation***

Based on the above analysis, it is clear that the electrical performance is correlated with the microstructures of each film. So it is necessary to understand the underlying mechanism. The sintering of the decomposable organic silver ink is generally

considered as a particle formation process after solvent evaporation [150]. When the ink deposit is heated, the decomposition of the silver precursor generally starts at the temperature above the boiling point and the decomposition temperature of the solvent. Therefore, in most cases, silver particles are produced in situ in the absence of solvent. However, as the ink formulation and the parameters used in the sintering process are usually different, the evolution of the microstructures is also different.

According to the DSC results and the physical properties of the chemicals used (Table 4.1), the process of film formation can be illustrated using the schematic diagram shown in Figure 4.16.

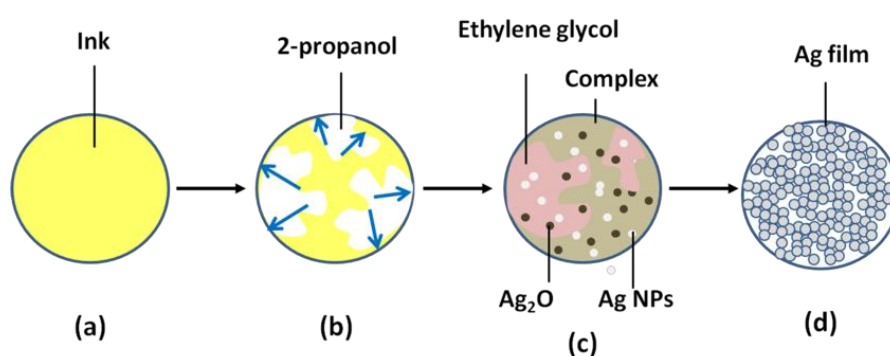


Figure 4.16 Schematic illustration for the film formation process of the silver ink

When the sintering temperature is around  $125^{\circ}\text{C}$ , evaporation of the solvent is dominant with 2-propanol and the unreacted ethylenediamine evaporating rapidly due to their low boiling points ( $82.45^{\circ}\text{C}$  and  $116^{\circ}\text{C}$ , respectively). Usually, this evaporation can induce a vapor recoiling force at the interface with the substrate, pushing the liquid droplets into isolated islands, and finally forming clusters of various sizes (Figure 4.16b). Due to the high thermal stability of the silver complex, the solvent would evaporate in each cluster before decomposing. If there is no high boiling point solvent in the ink, the silver particles produced by thermal decomposition of the silver complex would be largely restricted in these isolated islands and a discontinuous film is formed. Ideally, a sufficient amount of unevaporated solvent should be left in the film when the thermal decomposition of silver complex begins. In ink<sub>1</sub>, as ethylene glycol has a relatively high boiling point ( $T_b=197.85^{\circ}\text{C}$ ) and therefore it is left in the film to facilitate decomposition of the silver organic complex to silver nanoparticles, resulting in a continuous microstructure. However, due to the low heating temperature, fewer silver NPs are produced, which are still coated by organic molecules; a conductive film could not be formed. Therefore, the electrical performance was poor and the sheet resistance

was too high to be measured by the 4-probe device.

When the temperature was increased to 155°C, the silver complex starts to decompose into Ag<sub>2</sub>O. At the same time the glycolaldehyde as produced by ethylene glycol, reduces the Ag<sub>2</sub>O and the silver complex into silver nanoparticles (Figure 4.16c) serving as nucleus for the subsequent thermal decomposition event. In addition, the thickness of the surrounding organic layer separating the silver particles is also decreased due to the evaporation and decomposition effects, which enables the quantum tunneling effect to occur [139]. Meanwhile, the pores and voids among the NPs become less in quantity and size so a homogeneous film with densely packed silver nanoparticles is formed (Figure 4.16d). Hence good film conduction (low resistivity) is obtained.

At sintering temperatures above 155 °C, further improvement in film quality and conductivity can be obtained but the resistivity of the film decreases slowly, indicating that almost no solvent is left in the film and all Ag<sup>+</sup> ions have been reduced to Ag<sup>0</sup>.

#### **4.4 Conclusions**

In summary, a silver citrate ink with self-reducible and decomposable mechanisms for film formation was achieved. The results showed that good film conductivity can be obtained from the ink at a low sintering temperature of 155 °C, with a resistivity value of  $7.94 \times 10^{-5} \Omega \cdot \text{cm}$ . Defects such as pores and cracks as well as the coffee ring effect were eliminated. This is achieved by exploiting both self-reduction and decomposition mechanisms in the film formation process. The active role of ethylene glycol in the ink solvents and the underlying chemical changes during the heating process were clarified, where the ink underwent simultaneous change of solvent components and the decomposition/reduction of silver complex at elevated temperatures. The effects of sintering temperature and time on the microstructure and electrical properties of the silver ink films were studied in detail and the relationship between them was demonstrated. The residual levels of organic solvents, the decomposition/reduction degree of silver-amine complex as well as the contact area of produced silver nanoparticles, are three dominate factors affecting the conductivity of silver films.

## Chapter 5 Preparation and Characterization of New Organic Silver Precursors

### 5.1 Introduction

As an important component of the organic silver ink, the selection of the silver precursor is very critical since this affects the thermal, electrical and mechanical properties of the subsequent ink. As described in Chapter 2 and 4, variety of organic silver salt precursors have been chosen to formulate organic silver inks. Silver neodecanoate was first adopted, which starts to decompose to silver at 125°C, and full decomposition was achieved at 200°C [91, 92]. Then, 2-[2-(2-methoxyethoxy) ethoxy] acetate silver was synthesized to develop the organic silver ink [93]. In 2012, Nie et al. prepared an organic silver ink using silver citrate and 1, 2-diaminopropane [32]. Walker et al. developed a conductive silver ink based on silver acetate [8]. Chang et al. prepared a novel ink of silver carbonate in the glycol-water mixture [13]. In 2013, Chen et al. reported a solution-based  $\beta$ -diketonate silver ink for inkjet printing [14]. Yu et al. synthesized a transparent and high-efficiency organic silver ink with silver acetate as a silver carrier, ethanolamine as additive and dimethylformamide or formic acid as the reduction agent [147]. Recently, Dong et al. prepared organic silver inks using silver tartrate and various amines in ethyl alcohol [150]. Black et al. synthesized an organic silver ink with silver hexafluoroacetylacetonate cyclooctadiene as a precursor [141]. Overall, each precursor has its advantages and disadvantages. For instance, silver neodecanoate, silver acetate, silver carbonate and silver tartrate have a relatively high decomposition temperature and can decompose in the presence of light.  $\beta$ -diketonate silver and 2-[2-(2-methoxyethoxy)ethoxy] acetate silver are stable but the synthesis is relatively complex. Therefore it is still necessary to develop new organic silver precursors with desirable properties for ink application.

In this chapter, five types of organic silver precursors, silver carbonate, silver oxalate, silver tartrate, silver itaconate and silver glycolate, were synthesized using an ion exchange method. Various characterization methods were employed to investigate their physical phase, chemical composition, morphologies and thermal decomposition behavior. It was found that silver oxalate had the ideal thermal property and showed the lowest decomposition temperature, which will enable the subsequent ink to be applied on a variety of polymer flexible substrates.

Part of this Chapter has been published [151].

## 5.2 Experimental Section

### 5.2.1 Materials

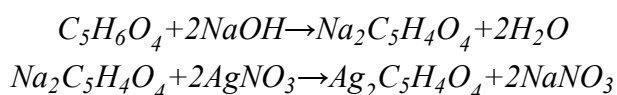
Silver nitrate ( $\text{AgNO}_3$ ), itaconic acid ( $\text{C}_5\text{H}_6\text{O}_4$ ), oxalic acid ( $\text{H}_2\text{C}_2\text{O}_4$ ), sodium carbonate ( $\text{Na}_2\text{CO}_3$ ), sodium hydroxide ( $\text{NaOH}$ ), sodium tartrate dibasic dihydrate ( $\text{C}_4\text{H}_4\text{Na}_2\text{O}_6$ ), ethylenediamine ( $\text{C}_2\text{H}_8\text{N}_2$ ), ethylene glycol ( $\text{C}_2\text{O}_2\text{H}_6$ ) and ethanol ( $\text{C}_2\text{H}_6\text{O}$ ) were obtained from Sigma-Aldrich and were used as received without further purification.

### 5.2.2 Synthesis of organic silver precursors

Five kinds of silver carboxylates possessing ideal structural characteristics were prepared through an ion exchange method. Among them, silver itaconate, silver oxalate, silver tartrate and silver glycolate were synthesized by using their corresponding organic acid sodium salt and silver nitrate, while silver carbonate was produced through the reaction of sodium carbonate and silver nitrate directly. The detailed processes and related chemical reactions are as follows:

#### a) Silver itaconate

Itaconic acid (0.65g) and sodium hydroxide (0.4g) were dissolved in 20ml of deionized water respectively, the solutions mixed and stirred for 30min at room temperature. Then, 10ml of silver nitrate solution (1.7g  $\text{AgNO}_3$ ) was added to the above mixture. After an hour of stirring in the absence of light, the product with white color was collected by vacuum filtration and washed with water for three times and ethanol twice, dried at 40 °C for 8 h in an oven and stored away from light. The obtained silver itaconate is about 1.491g with a yield of 86.7%.



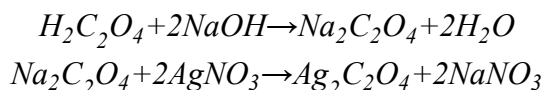
#### b) Silver oxalate

Oxalic acid (0.45g) and sodium hydroxide (0.4g) were each dissolved in 10ml of deionized water. The solutions were mixed and stirred for 30 min at room temperature. Then, 10ml of silver nitrate solution (1.7g  $\text{AgNO}_3$ ) was added to the above mixture. After an hour of stirring in the absence of light, the white product, silver oxalate, was collected by vacuum filtration and washed with water for three times and with ethanol



twice, dried at 40 °C for 8 h in an oven and stored away from light. The obtained silver oxalate was about 1.440g with a yield of 94.8%.

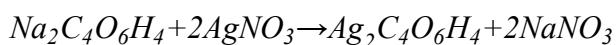
---



### c) Silver tartrate

Sodium tartrate dibasic dihydrate (1.15g) was dissolved in 10ml of deionized water. Then, 10ml of silver nitrate solution (1.7g AgNO<sub>3</sub>) was added to the above solution. After an hour of stirring in the absence of light, the white product was collected by vacuum filtration and washed with water for two times and ethanol once, dried at 40 °C for 8 h in an oven and stored away from light. The obtained silver tartrate was about 1.438g with a yield of 79.1%.

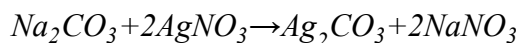
---



### d) Silver carbonate

Sodium carbonate (0.53g) was dissolved in 10ml of deionized water. Then, 10ml of silver nitrate solution (1.7g AgNO<sub>3</sub>) was added to the above solution. After an hour of stirring in the absence of light, the yellow product was collected by vacuum filtration and washed with water for two times and ethanol once, dried at 40 °C for 8 h in an oven and stored away from light. The obtained silver oxalate powder was about 1.037g with a yield of 75.7%.

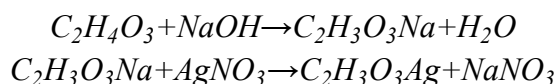
---



### e) Silver glycolate

Glycolic acid (0.76g) and sodium hydroxide (0.4g) were dissolved in 10ml of deionized water respectively, the solutions mixed and stirred for 30 min at room temperature. Then, 10ml of silver nitrate solution (1.7g AgNO<sub>3</sub>) was added to the above mixture. After an hour of stirring in the absence of light, the white product, silver glycolate, was collected by vacuum filtration and washed with water for three times and ethanol once, dried at 40 °C for 8 h in an oven and stored away from light.

---



### 5.2.3 Characterization

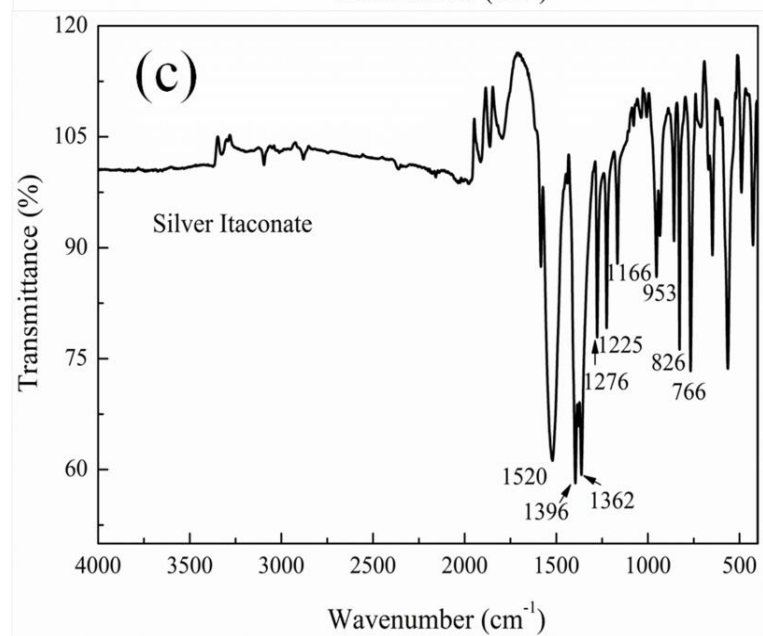
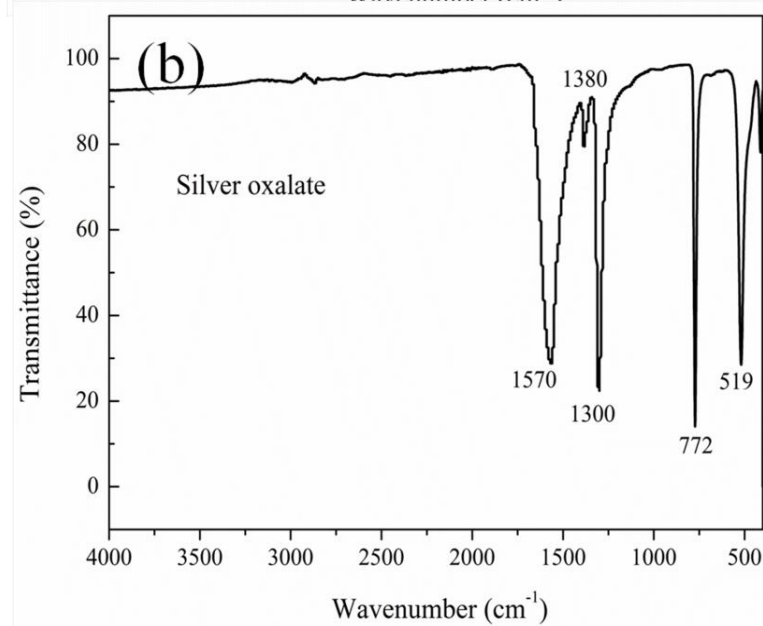
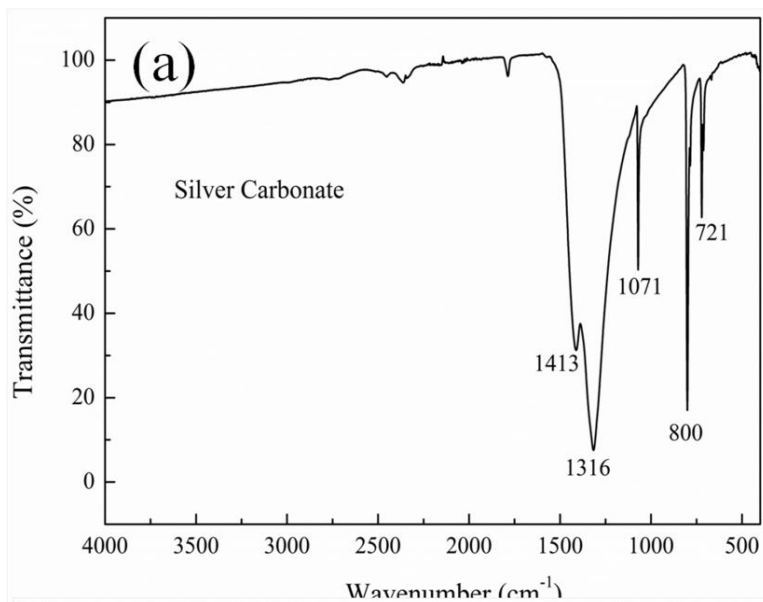
The crystallite phases of the obtained silver carboxylate powders were identified by X-ray diffraction (XRD) using Cu K $\alpha$  radiation ( $\lambda = 0.15418$  nm). The thermal decomposition behaviors were investigated by differential scanning calorimetry (DSC) and thermogravimetry (TG) at a heating rate of 10 °C·min<sup>-1</sup> from room temperature to 250 °C under a nitrogen atmosphere. A fourier transform infrared (FT-IR) spectrometer (Thermo Scientific Nicolet iS5) were used to analyze the chemical structures of the prepared powders. A surface energy disperse spectrometer (EDS, Oxford X-maxN 150) was used to analyze the chemical composition. The surface morphologies were observed using a FEI Quanta 3D Scanning Electron Microscope (SEM).

## 5.3 Results and Discussion

### 5.3.1 Structure and phase confirmation of silver carboxylates

As a component of the ink, the selection of silver precursors is very important because it determines the final thermal and electrical properties of the ink. To some extent, silver aliphatic carboxylates unsaturated, branched and/or substituted with hydroxyl group, are the most preferred precursor materials because they are easy to be transformed into silver atom at low temperature via decarboxylation reaction. Considering this, five types of silver carboxylate possessing the above structural characteristics were prepared and were then investigated to select the most ideal one for the subsequent ink preparation. FT-IR and XRD were first employed to confirm the structure and physical phase of each powder.

Figure 5.1 shows the IR spectra of five as-prepared powders. For silver carboxylates, the peak in the range of 1650 cm<sup>-1</sup> to 1550 cm<sup>-1</sup> is attributed to the asymmetric stretching vibration of C=O in the carboxyl group (-COO-) while the peak in the range of 1440 and 1350 cm<sup>-1</sup> is from C=O symmetric stretching vibration. The peaks from 800 to 200 cm<sup>-1</sup> arise from vibrations of the metal-O group and the band around 1073 cm<sup>-1</sup> is from the C-O stretch. The broad peak around 3200 cm<sup>-1</sup> is assignable to the O-H stretching vibration. Taking silver tartrate for an example, the broad feature around 3230 cm<sup>-1</sup> is attributed to the stretching vibration of O-H. Two sharp peaks at 1610 and 1560 cm<sup>-1</sup> are attributed to the asymmetric stretch vibration of C=O whilst the peak at 1370 cm<sup>-1</sup> is from the symmetric stretch vibration of C=O. These features indicate that silver tartrate has a structure of carboxylate substituted with hydroxyl. Similarly, the IR spectra of the other three powders could also confirm that they are silver carboxylates.



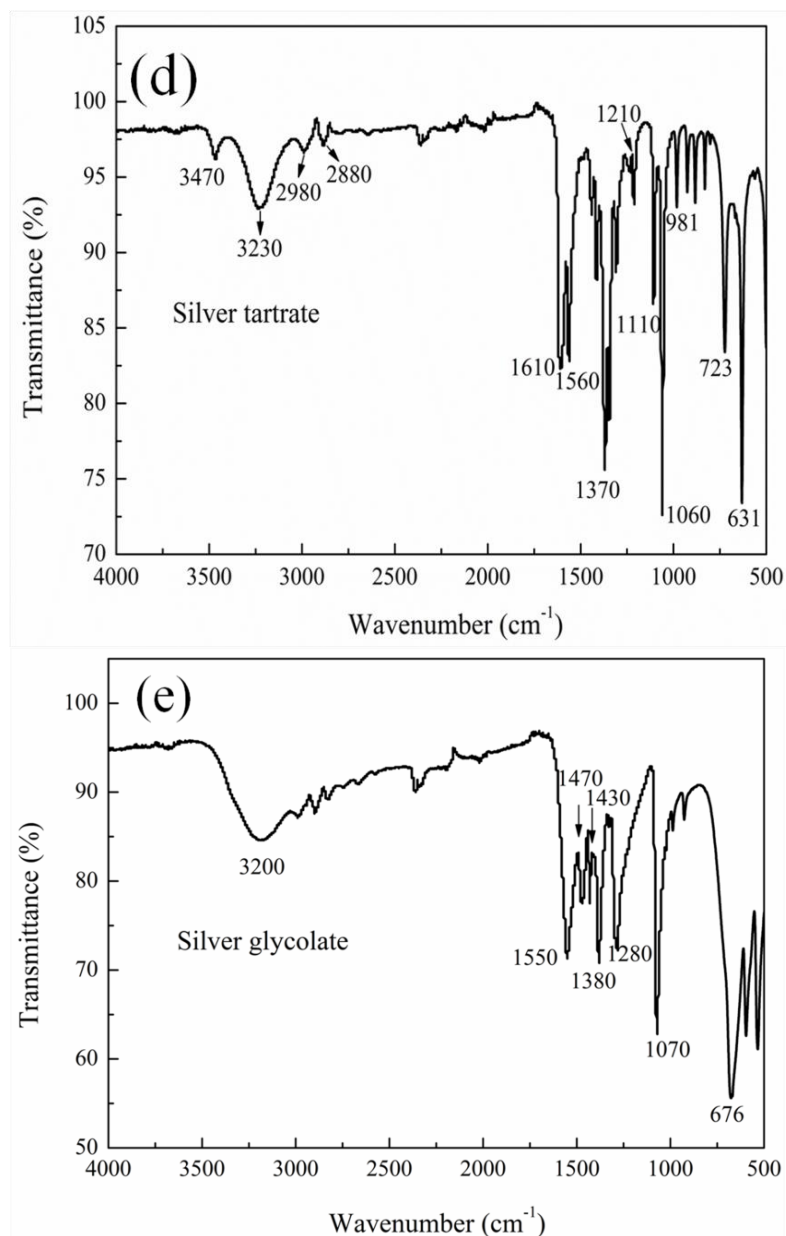
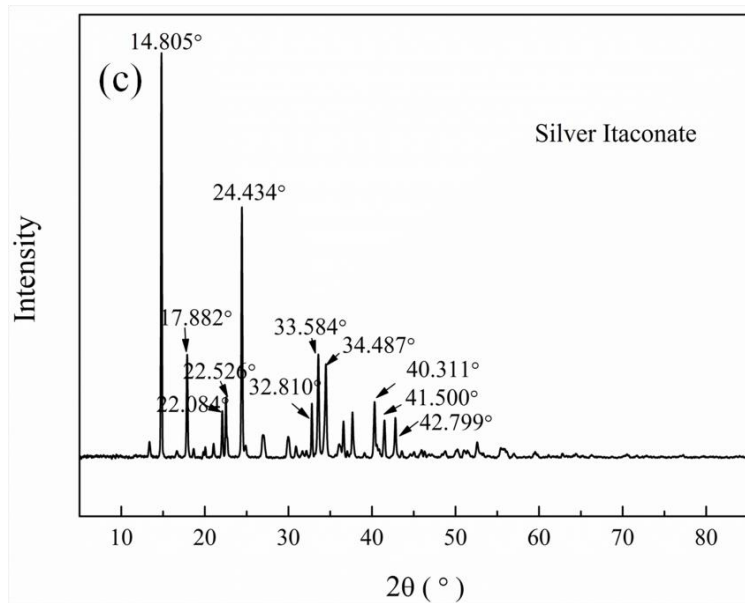
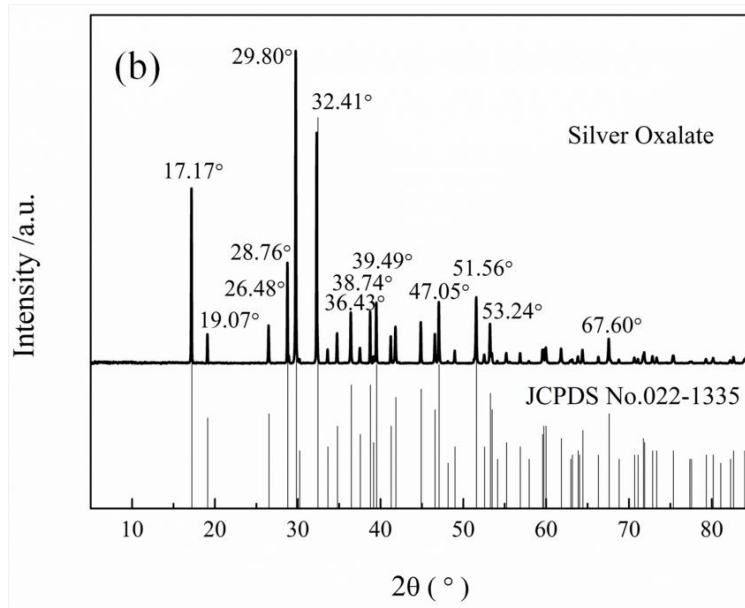
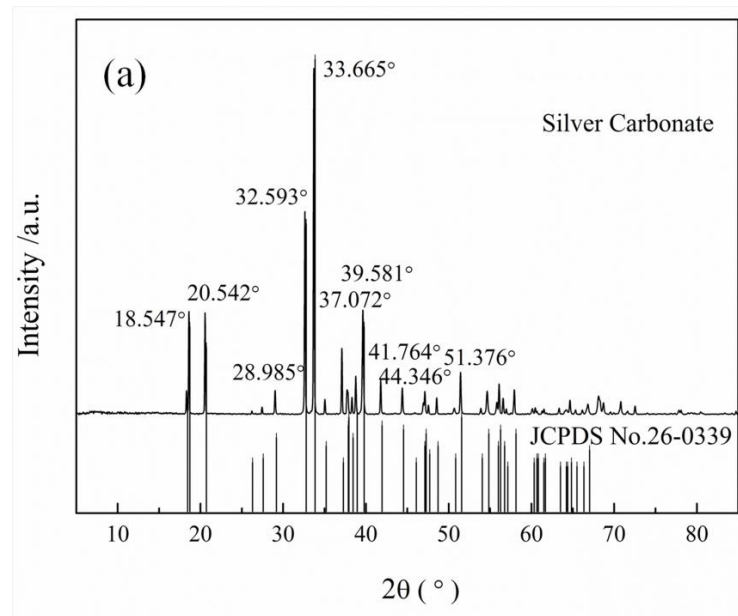


Figure 5.1 FT-IR spectra of five as-prepared silver carboxylates (a. silver carbonate, b. silver oxalate, c. silver itaconate, d. silver tartrate, e. silver glycolate)

Figure 5.2 gives the XRD patterns of the five as-prepared silver carboxylate powders. The results of silver carbonate, silver oxalate and silver tartrate are all in good agreement with that of their standard card, JCPDS No.26-0339, JCPDS No.022-1335 and JCPDS No.01-0441. No diffraction peaks from any other impurities were detected, indicating that the reaction was completed and these three kinds of powders were prepared successfully. For silver itaconate, its card is not available in the XRD database but in combination with the results of DSC/TG shown later, this can be confirmed as there is only one exothermic peak on the DSC curve and 63.46wt% of the remaining weight in TG curve is basically in line with the proportion of silver in the silver itaconate (62.75wt%). The same goes for silver glycolate.



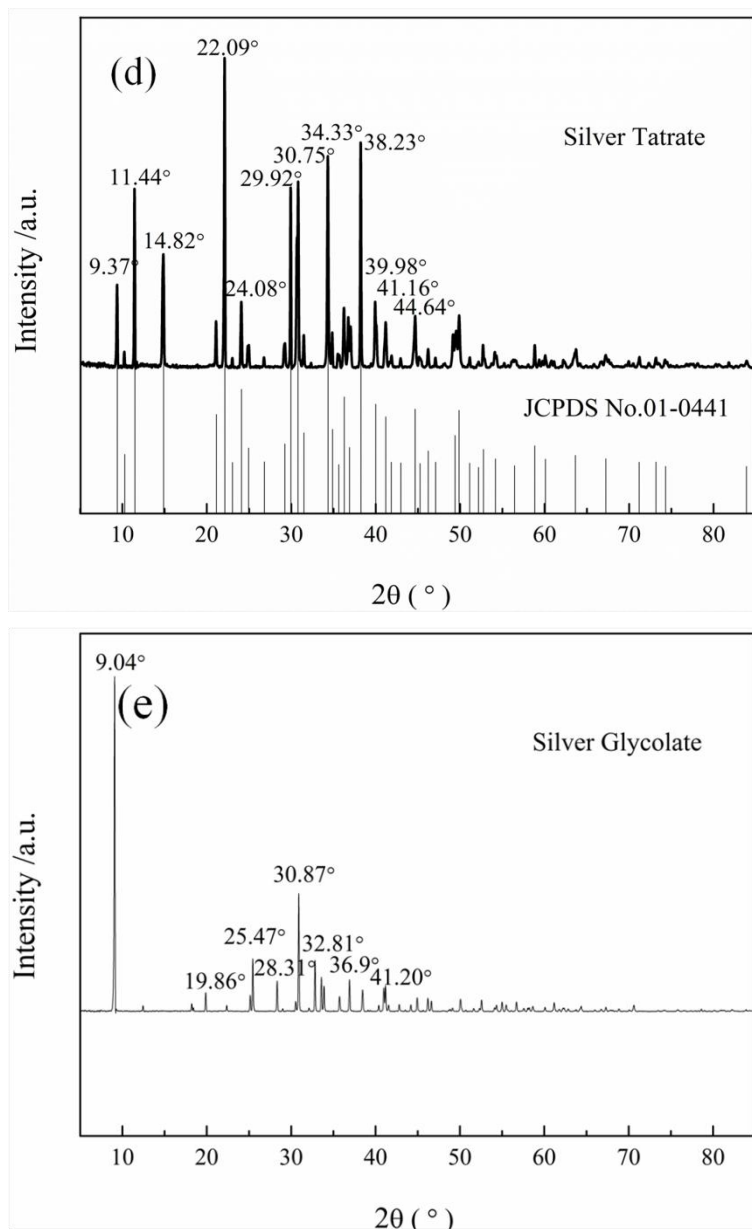
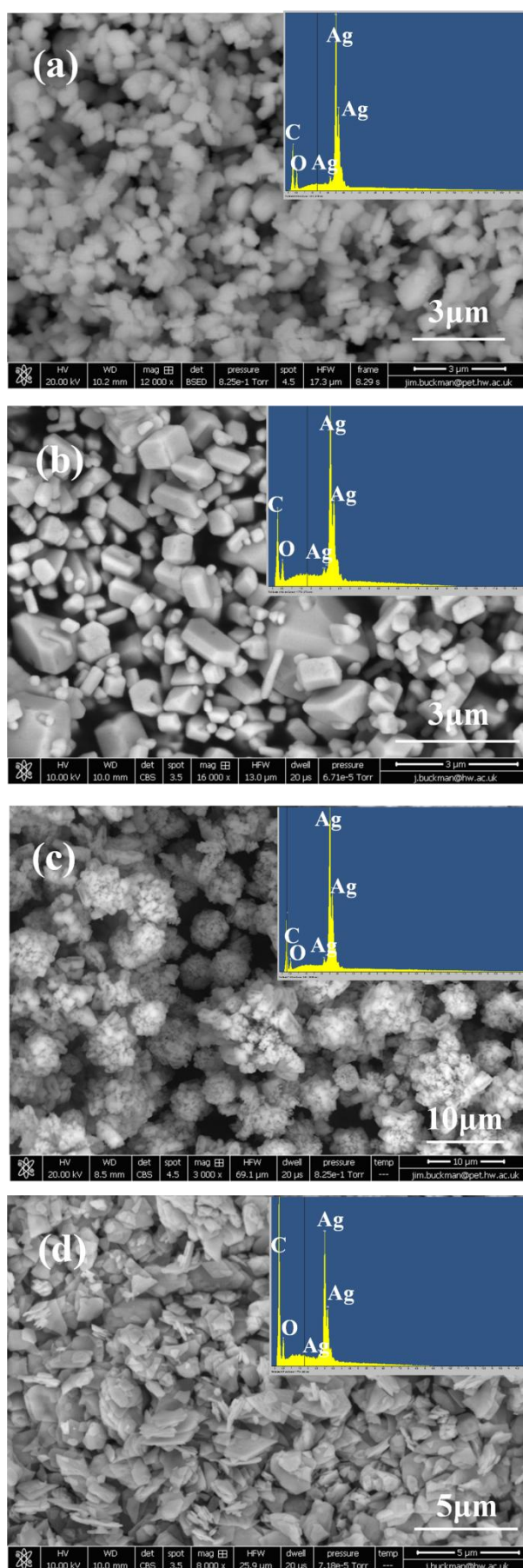


Figure 5.2 XRD patterns of four as-prepared silver carboxylates (a. silver carbonate, b. silver oxalate, c. silver itaconate, d. silver tartrate, e. silver glycolate)

### 5.3.2 Chemical composition and surface morphology

The morphology and chemical composition of the prepared powders were identified by SEM/EDS measurements as shown in Figure 5.3. Clearly, the five powders have different morphologies. Silver carbonate shows oblique crystal structure with uniform particle size while the silver oxalate has a hexagonal columnar morphology with two kinds of particle size, which is in agreement with the DSC results in section 5.3.3 where two peaks were observed. Silver itaconate shows a flowerlike morphology that is assembled by well-defined rectangular crystals and silver tartrate has a flake structure. Silver glycolate presents a spindle-shaped crystal structure that has a big particle size. The EDS measurements show that three elements (C, O, and Ag) exist in all powders,

which are consistent with the original chemical composition of the compounds.



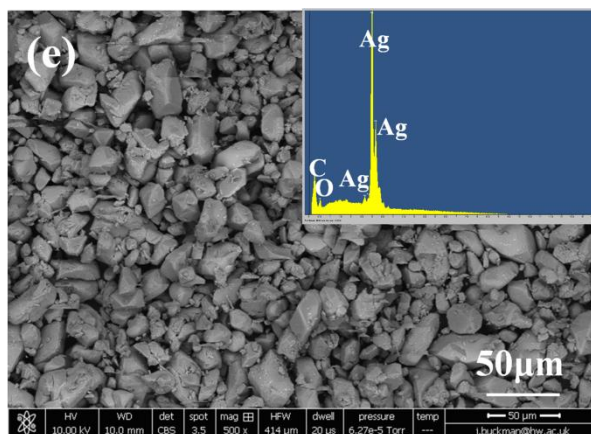
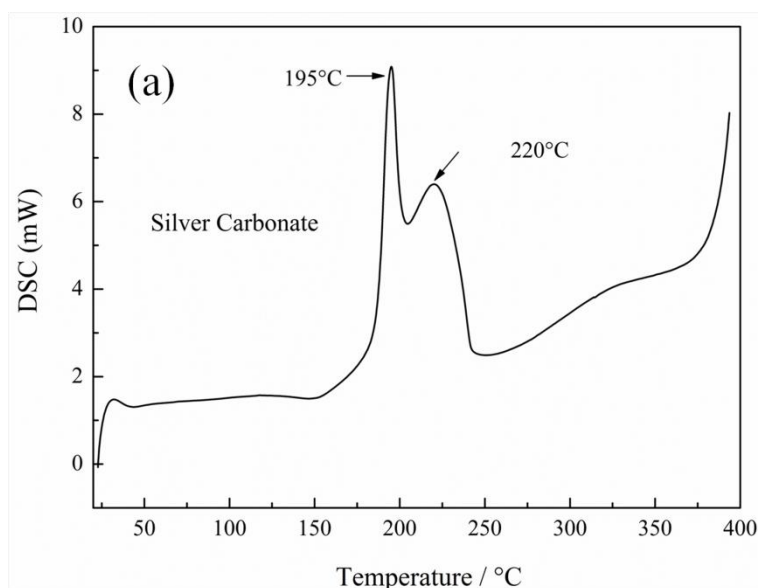


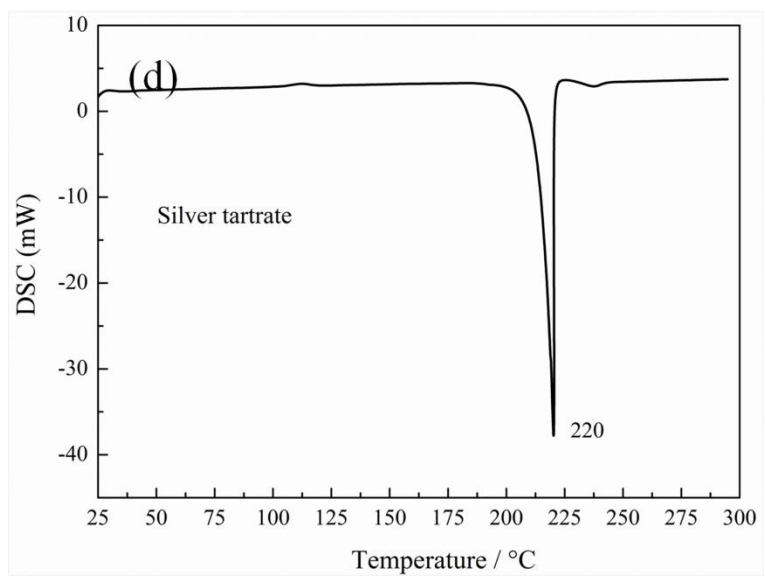
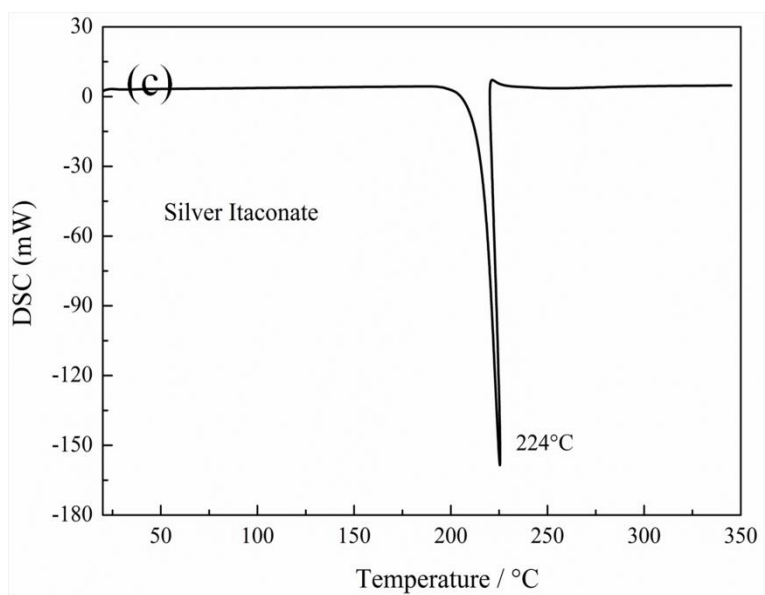
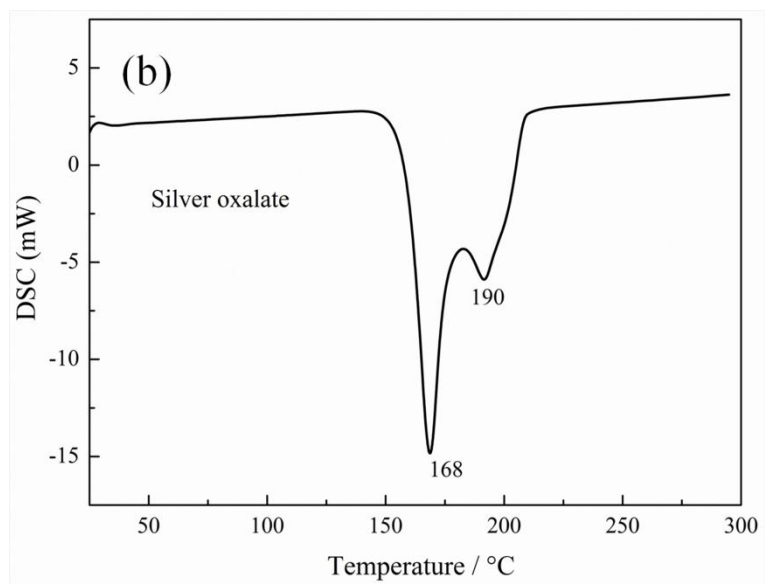
Figure 5.3 SEM and EDS results of five as-prepared silver carboxylates (a. silver carbonate, b. silver oxalate, c. silver itaconate, d. silver tartrate, e. silver glycolate)

### 5.3.3 Thermal behavior of silver carboxylates

Figure 5.4 and 5.5 show the thermal behaviors of the five as-prepared powders. In the DSC curves, silver itaconate and silver tartrate have only one exothermic peak relating to the thermal decomposition of their powders, respectively. Silver carbonate has a complex thermal behavior and a high decomposition temperature compared to others. Silver glycolate displays an endothermic peak and an exothermic peak relating to the dehydration and the thermal decomposition of its powder. Silver oxalate shows two endothermic peaks at 168 °C and 190 °C respectively. Table 5.1 summarizes the initial, the maximum and the end thermal decomposition temperatures of each powder. Clearly, silver oxalate has the lowest decomposition temperature.







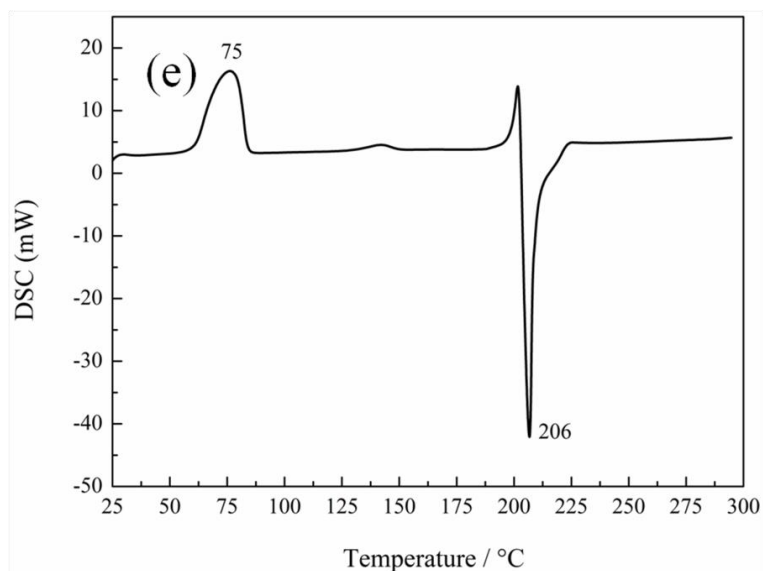


Figure 5.4 DSC curves of four as-prepared silver carboxylates (a. silver carbonate, b. silver oxalate, c. silver itaconate, d. silver tartrate, e. silver glycolate)

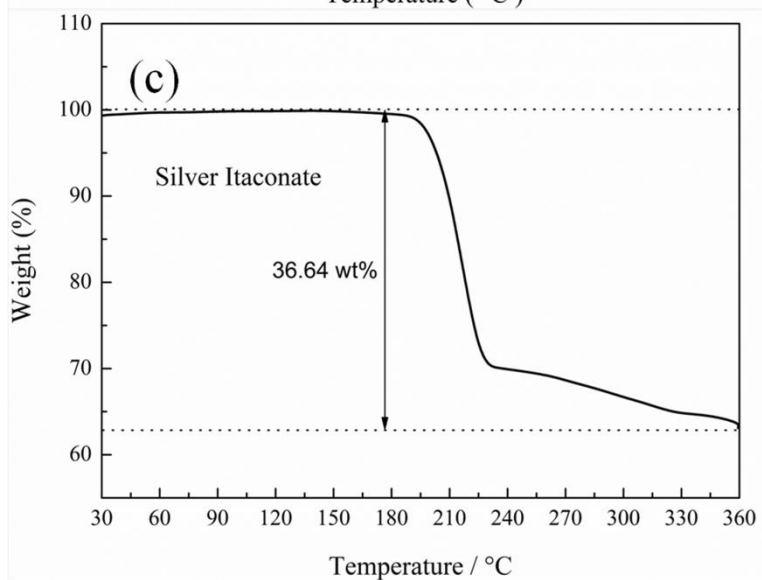
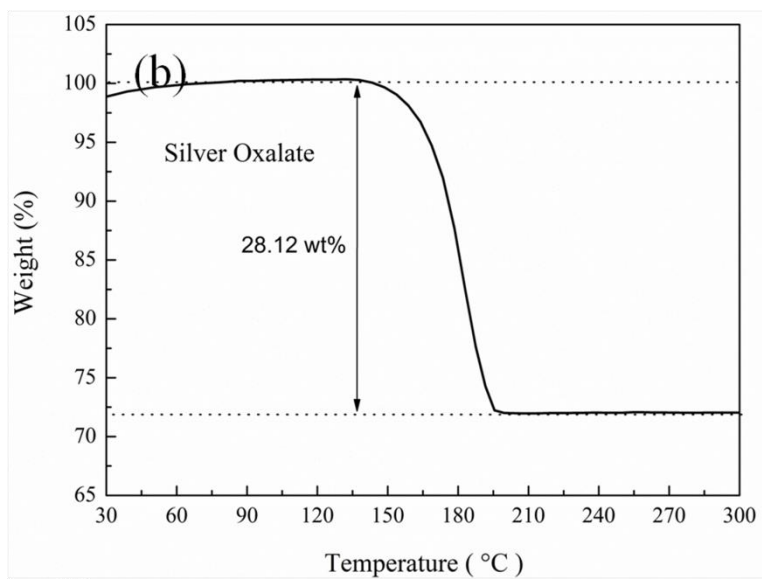
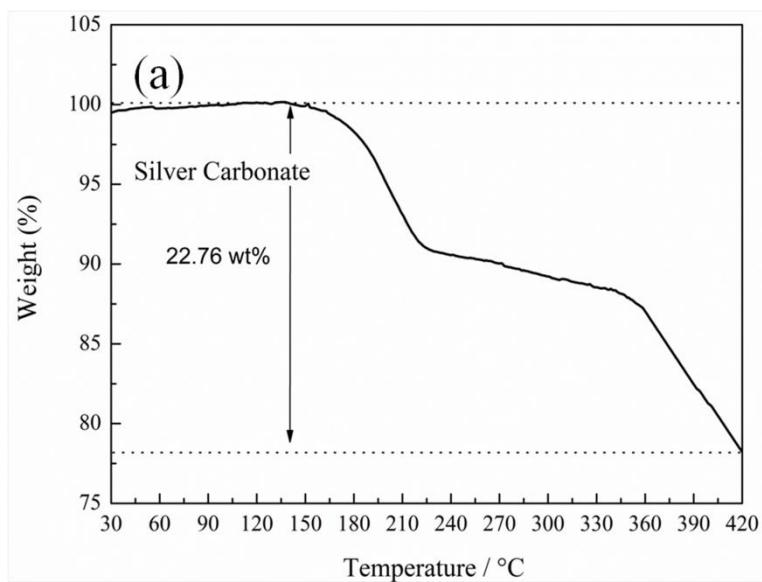
Table 5.1 Thermal behavior analysis of products

Sample	T <sub>Initial</sub> / °C	T <sub>Max</sub> / °C	T <sub>End</sub> / °C
Silver carbonate	150	220	420
Silver oxalate	150	190	200
Silver itaconate	200	224	230
Silver tartrate	200	220	237
Silver glyconate	190	206	225

As for the TG curves, it can be seen that the residual weight of the first four powders is basically in line with the proportion of silver in their complex (Table 5.2), indicating that the decomposition product was almost metal silver. For silver glyconate, the silver weight left is higher than the theoretical value, which is due to the incomplete decomposition. The silver weight left by silver carbonate was the most, but the associated temperature is too high for the ink application. Silver oxalate powder starts to decompose at 150 °C and the weight left is about 71.88wt%, which is expected. As for the reason why they present different thermal behavior, it should be related to their structures.

Table 5.2 Theoretical silver content and measured solid content

Sample	Ag content % (Theoretical)	Ag content % (Measured)
Silver carbonate	78.24%	77.24%
Silver oxalate	71.02%	71.08%
Silver itaconate	62.75%	63.36%
Silver tartrate	59.30%	60.90%



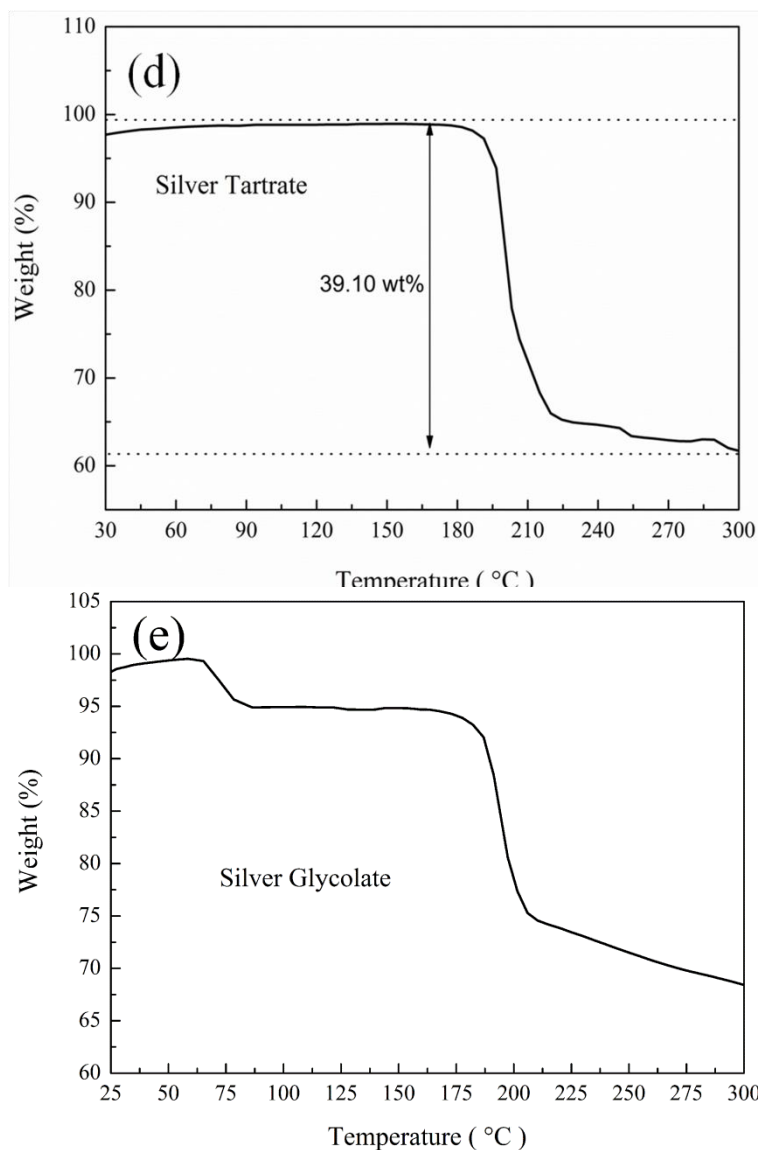


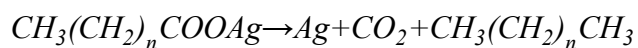
Figure 5.5 TG curves of four as-prepared silver carboxylates (a. silver carbonate, b. silver oxalate, c. silver itaconate, d. silver tartrate, e. silver glycolate)

All results demonstrate that silver oxalate powder is an ideal precursor material for ink preparation.

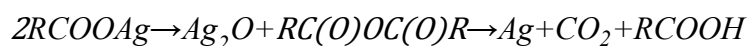
#### 5.3.4 Thermal decomposition mechanism

As for the thermal decomposition mechanism of silver carboxylates, there is not a unified view or theory but surely is likely to be related to their molecular structures.

Some studies believed that silver carboxylates thermally decompose to the metallic silver and volatile products depending on the carboxylate residue at a wide range of temperatures [152, 153]. The following scheme of the decomposition reaction was proposed:



However, others suggested that there are two stages in the thermal decomposition process of silver carboxylates [154]. The first stage is the formation of the silver (I) oxide and the anhydride of the corresponding acid. The anhydride and silver oxide are then transformed into the final products: RCOOH and Ag<sup>0</sup>.



#### 5.4 Conclusions

In summary, five types of organic silver precursors were synthesized via an ion exchange method. FT-IR, XRD, SEM/EDX and DSC-TG were employed to confirm their physical phase, chemical composition, morphologies and thermal decomposition temperature. Among them, silver oxalate has higher silver content and lowest decomposition temperature, which is an ideal precursor material for the ink preparation.

## Chapter 6 Silver Oxalate Ink with Low Sintering Temperature and Good Electrical Property

### 6.1 Introduction

In Chapter 5, silver oxalate was shown to be an ideal precursor for formulating organic silver ink because it has higher silver content, low decomposition temperature and can be easily prepared. However, there is only one report in the literature using this material as an ink precursor. Dong et al. synthesized their ink using silver oxalate as a precursor and ethylamine as the complexing agent [27]. The silver film sintered at 170 °C for 30 min had a resistivity of 8.4  $\mu\Omega\cdot\text{cm}$ . Although interesting results have been obtained in this case, the developed ink is still not ideal and some improvement is needed. Firstly, the silver oxalate decomposition depends on the preparation method [142, 155]. Dong et al. only investigated one approach to prepare the silver oxalate powder which gives a relatively high decomposition temperature (210 °C). Different methods or procedures should be studied to produce silver oxalate powders with a lower thermal decomposition temperature, which is beneficial to the subsequent ink property. Secondly, only one kind of amine, ethylamine, was used as the ink complexing agent. It is well known that the type of amine is a key factor in determining the thermal decomposition temperature of the silver complex in the ink [150]. Appropriate amine complexes which could significantly decrease sintering temperature and make inks usable on plastic substrates need to be investigated. Thirdly, the reaction mechanisms in ink formulation and the metallization process based on such a material have not been studied in detail. Lastly, the ink sintering temperature for obtaining better electrical performance, 170 °C, is still high for an application with some low-cost polymer-based flexible substrates such as polyethylene terephthalate (PET). Therefore, it is necessary to develop a silver oxalate ink that can produce silver film with favorable conductive properties below 170 °C and to elucidate its formulation mechanism.

In this chapter, a silver oxalate ink was formulated in a mixed organic solvent by using the as-prepared silver oxalate and butylamine. The resultant silver films showed favorable conductivity on a polyimide substrate after sintering at 130°C, and even at temperatures as low as 100°C. Silver oxalate powders with good properties were prepared. The effect of changing the amine compound on the thermal properties of the formulated ink was investigated. The chemical reactions occurring within the ink and the film formation process were studied. Surprisingly, a solid silver amine complex was

found. The effects of sintering temperature and time on the microstructure and electrical properties of the silver films prepared from the inks were also investigated in detail.

This Chapter has been published [156].

## **6.2 Experimental Section**

### **6.2.1 Materials**

Silver nitrate ( $\text{AgNO}_3$ ), oxalic acid ( $\text{H}_2\text{C}_2\text{O}_4$ ), sodium hydroxide ( $\text{NaOH}$ ), ethylenediamine ( $\text{C}_2\text{H}_8\text{N}_2$ ), 1,2-diaminopropane ( $\text{C}_3\text{H}_{10}\text{N}_2$ ), butylamine ( $\text{C}_4\text{H}_{11}\text{N}$ ), ethylene glycol ( $\text{C}_2\text{O}_2\text{H}_6$ ) and ethanol ( $\text{C}_2\text{H}_6\text{O}$ ) were purchased from Sigma-Aldrich and were used as received without further purification. Polyimide films (PI) used as substrates in this study was obtained from DuPont (Kapton 500 HN, 127  $\mu\text{m}$  in thickness). Before application, 15mm $\times$ 15mm PI samples were cleaned with de-ionized water and ethanol, and then dried.

### **6.2.2 Synthesis**

The silver organic inks used in this study were prepared in organic solvents using silver oxalate and butylamine. Silver oxalate, named as  $S_1$ , was synthesized using the method described in chapter 5. For ink preparation, 0.152 g of the obtained  $S_1$  powder was first dispersed in 0.75 ml of a mixed solvent containing ethanol (0.375 ml) and ethylene glycol (0.375 ml). After stirring for 5 minutes, butylamine (0.192 ml) was added. The mixture was then stirred for 60 minutes to form the ink. The appearance of the solution changed during this period, from the initial suspension to a homogeneous transparent solution. The silver content in the ink was about 10 wt%.

### **6.2.3 Ink deposition and sintering**

The as-prepared ink was deposited on the PI films by drop coating, and sintered at selected temperatures for up to 60 minutes. The film thickness was controlled by the volume of ink solution deposited onto the PI film.

### **6.2.4 Characterization**

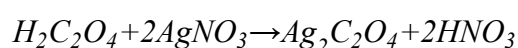
The thermal behaviors of the powder and ink were investigated by differential scanning calorimetry (DSC, TA instrument) at a heating rate of 10  $^\circ\text{C}\cdot\text{minute}^{-1}$  from room temperature to 250  $^\circ\text{C}$  and a nitrogen flow rate of 80  $\text{ml}\cdot\text{minute}^{-1}$ . Ultraviolet-visible

(UV-Vis) absorption spectra were obtained on a Lambda 25 UV-Vis spectrophotometer using water as solvent. Fourier transform infrared (FT-IR) spectra in the range of 400-4000  $\text{cm}^{-1}$  were recorded on a Thermo Scientific Nicolet iS5 FT-IR spectrometer. X-ray diffraction (XRD) analysis was recorded by using Cu  $K\alpha$  and  $\lambda = 0.15418$  nm. The sizes of the silver nanocrystallites were calculated using Scherrer's formula. The morphologies of the silver films after sintering were observed on a FEI Quanta 3D Scanning Electron Microscope (SEM). The chemical composition was determined on an Oxford X-maxN 150 surface energy disperse spectrometer (EDS). The sheet electrical resistivity was measured using a 4-point probe method (Jandel Engineering, UK). The thickness of the sintered films was measured using a Dektak surface profilometer and was used to calculate the equivalent bulk resistivity.

## 6.3 Results and Discussion

### 6.3.1 Characterization of silver oxalate

As a key component of the ink, the characteristic of the silver oxalate powder was important since it determines the ink properties such as thermal decomposition behavior. According to the work carried out by Boldyrev et al., silver oxalate decomposition depends upon its preparation method [155]. For the purpose of comparison, another procedure was also employed to obtain silver oxalate powder (named  $S_2$ ). This involved using only silver nitrate and oxalic acid as the reaction materials. The reaction equation is as follows.



The thermal behavior of the as-prepared silver oxalate powders,  $S_1$  and  $S_2$ , was studied by DSC in  $N_2$  atmosphere under the same conditions. As shown in Figure 6.1, the DSC curve of the  $S_1$  powder displays two major endothermic peaks at 166°C and 185°C, while the  $S_2$  trace gives two peaks at 224°C and 234°C. All of these peaks are attributed to the decomposition of silver oxalate. The presence of two different peaks in each curve may be related to the size and structure as well as morphology of the as-prepared powders. Obviously, the decomposition temperature of the  $S_1$  powder is lower than that of  $S_2$ , which is a preferred property for the subsequent ink. Therefore, the preparation method of  $S_1$  powder was selected for the following studies.



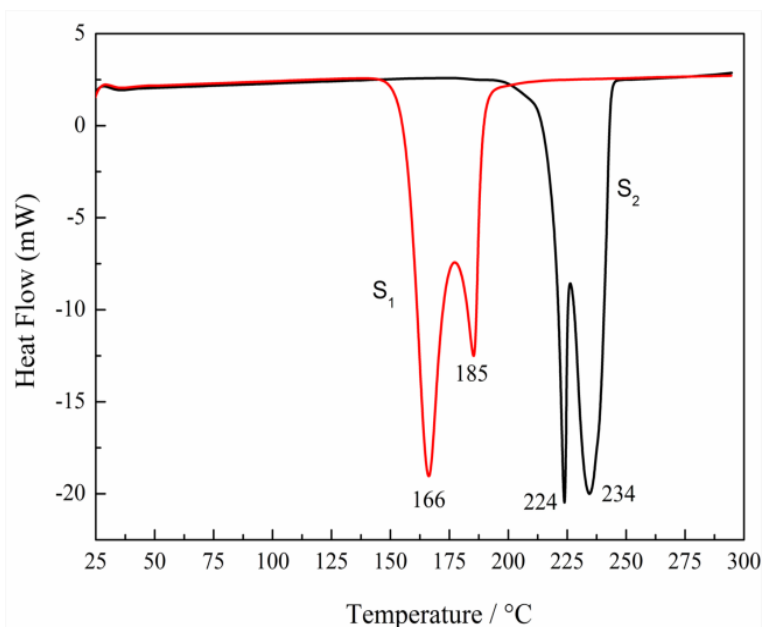


Figure 6.1 DSC traces of as-prepared silver oxalate powders: S<sub>1</sub> powder was prepared using sodium hydroxide, oxalic acid and silver nitrate, S<sub>2</sub> powder was prepared using oxalic acid and silver nitrate

### 6.3.2 Ink formulation

The effect of using different amines on the thermal properties of the silver amine complex solution was investigated. The as-prepared solid silver oxalate powder was dissolved in an aqueous solution containing 1,2-diaminopropane, ethylenediamine and butylamine to form the corresponding complex, named solution 1, solution 2 and solution 3, respectively. In order to make a reasonable comparison, the weight of silver oxalate and water were the same in each solution and the Ag/amine molar ratios were kept at a constant value of 1:2.5. The results are given in Figure 6.2a.

The first peak, around 100 °C, is mainly attributed to water evaporation, whereas the peaks at temperatures above 100 °C correspond to the thermal decomposition of the silver amine complexes. Clearly, the solution containing butylamine has the lowest decomposition temperature (around 109°C), which is a very desirable feature. The low thermal decomposition temperature of the silver-amine complex makes it possible for the subsequent ink to be sintered at a much lower temperature, which is advantageous for patterning conductive features on temperature-sensitive substrates [150]. Therefore, for ink preparation, butylamine, a small molecule with low boiling point (77 °C), was chosen as the ligand to dissolve the silver oxalate in the organic solvents and to decrease the decomposition temperature of the complex. Also, using this type of amine, the sintering process would become faster since silver amine complex with less organic

content could be formed, requiring less energy and time to evaporate the organic content.

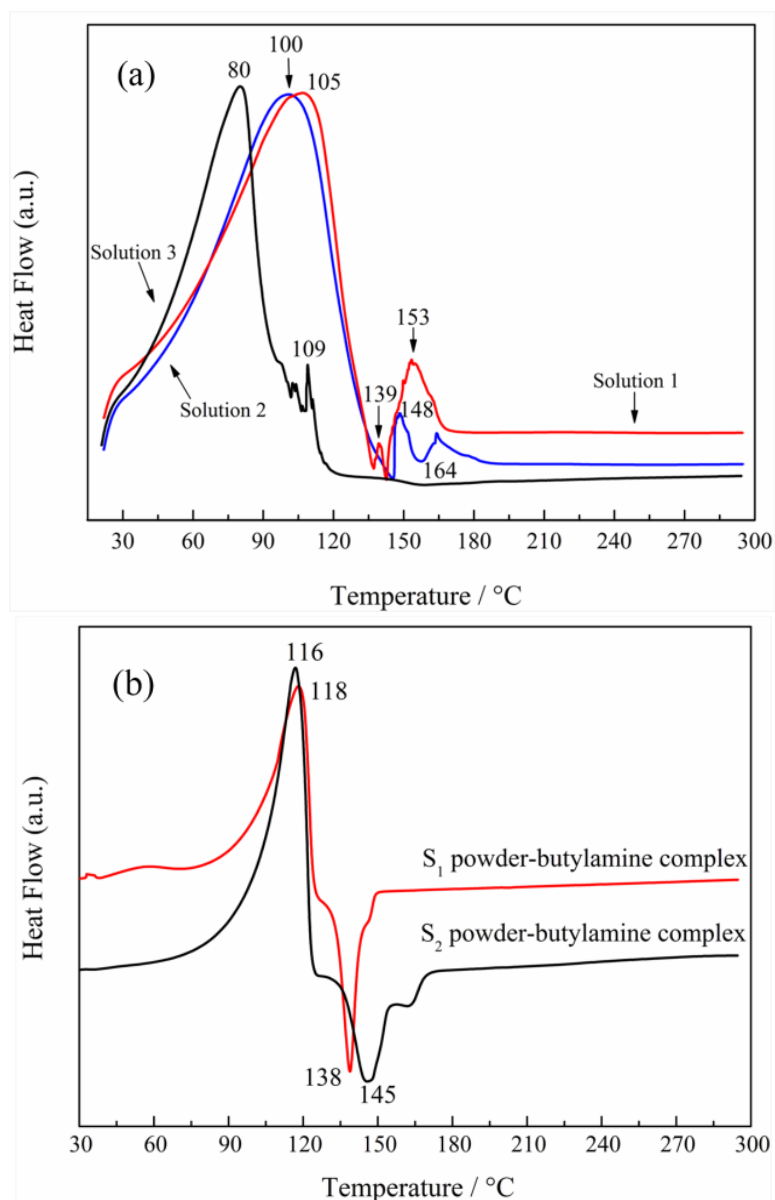
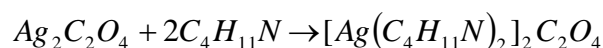


Figure 6.2 (a) DSC curves of the silver amine complex solutions formulated with various amines; (b) DSC curves of the silver amine complexes prepared by two silver oxalate powders

Herein, the decomposition behavior of the complexes formulated using S<sub>1</sub> and S<sub>2</sub> silver oxalate powders and butylamine were also investigated on the DSC instrument, as shown in Figure 6.2b. It can be seen that two of the complexes have similar thermal behaviors while the complex from S<sub>1</sub> powder gives a relatively lower decomposition temperature (138°C), thereby S<sub>1</sub> powder was chosen as the ink precursor material. It should be noted here that both complexes were found to be existing in solid state, which is different from all the other organic silver complexes that usually exist in liquid form.

Ethanol was used as the solvent of the ink and ethylene glycol as a co-solvent to suppress the undesirable coffee ring effect caused by ethanol in the film sintering process [12].

It was found that the sparingly soluble  $S_1$  powder could be easily dissolved in the organic solution containing butylamine, mainly via the following complexing reaction, resulting in a soluble complex, which might exist in the form of molecules of  $[\text{Ag}(\text{C}_4\text{H}_{11}\text{N})_2]^{2+}$  and  $(\text{C}_2\text{O}_4)^{2-}$  in the organic solvents:



FT-IR and  $^1\text{H-NMR}$  were employed to investigate and confirm this mechanism. For the measurements, the complex sample was prepared using only  $S_1$  powder and butylamine in a stoichiometric ratio. FT-IR and  $^1\text{H-NMR}$  were used to characterize this complex, and the spectra are shown in Figure. 6.3 and 6.4, respectively.

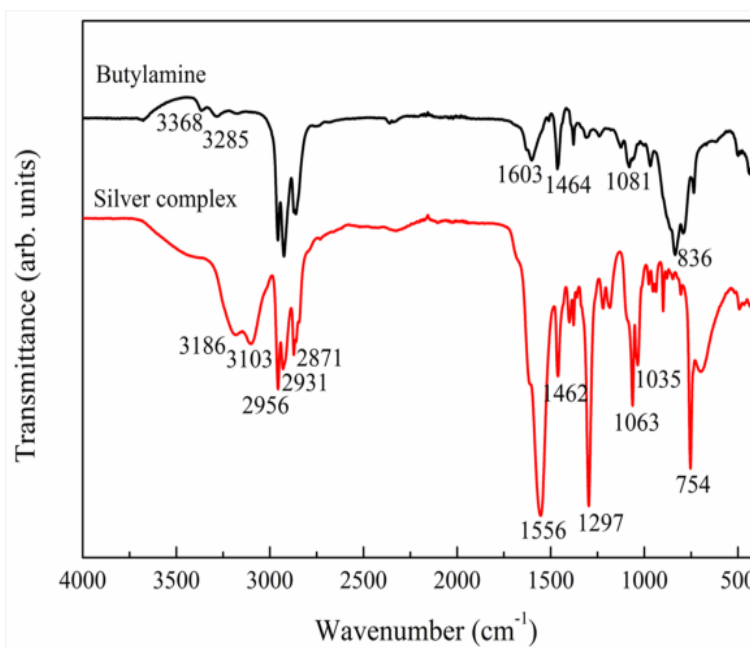


Figure 6.3 FT-IR spectra of the butylamine and  $[\text{Ag}(\text{C}_4\text{H}_{11}\text{N})_2]_2\text{C}_2\text{O}_4$  solid complex

In the spectrum of butylamine, the absorption peaks at 3368 and 3285  $\text{cm}^{-1}$  correspond to the asymmetric and the symmetric stretch of the  $\text{NH}_2$  group. The two peaks at 2956 and 2931  $\text{cm}^{-1}$  correspond to the asymmetric stretch of  $\text{CH}_3$  and  $\text{CH}_2$  groups, respectively. The peak at 2865  $\text{cm}^{-1}$  relates to the symmetric stretching mode of  $\text{CH}_2$ . The peak at 1603  $\text{cm}^{-1}$  and 1464  $\text{cm}^{-1}$  belong to the scissoring vibration of the  $\text{NH}_2$  group and scissoring vibration of  $\text{CH}_2$ , respectively. As for the complex of  $S_1$ , it is worth

noting that the peaks associated with  $\text{NH}_2$  groups undergo a dramatic red-shift, from  $3368$  to  $3186\text{ cm}^{-1}$ ,  $3285$  to  $3103\text{ cm}^{-1}$ . The carbonyl peak appears at  $1556\text{ cm}^{-1}$ , which is from the silver oxalate. These changes indicate that the butylamine reacts with silver oxalate to form a complex, which donates electrons from the amino group to the silver atoms, decreasing the electron density of the amino groups and therefore resulting in a red-shift of the  $\text{NH}_2$  stretching peak.

The  $^1\text{H-NMR}$  results of the butylamine and the solid  $[\text{Ag}(\text{C}_4\text{H}_{11}\text{N})_2]_2\text{C}_2\text{O}_4$  complex in Figure 6.4 also confirm this reaction process. The chemical shift changes of  $\text{CH}_2$  connected to  $\text{NH}_2$  are very significant, from  $2.61$ - $2.66$  to  $2.76$ - $2.81$ , indicating the formation of the complex.

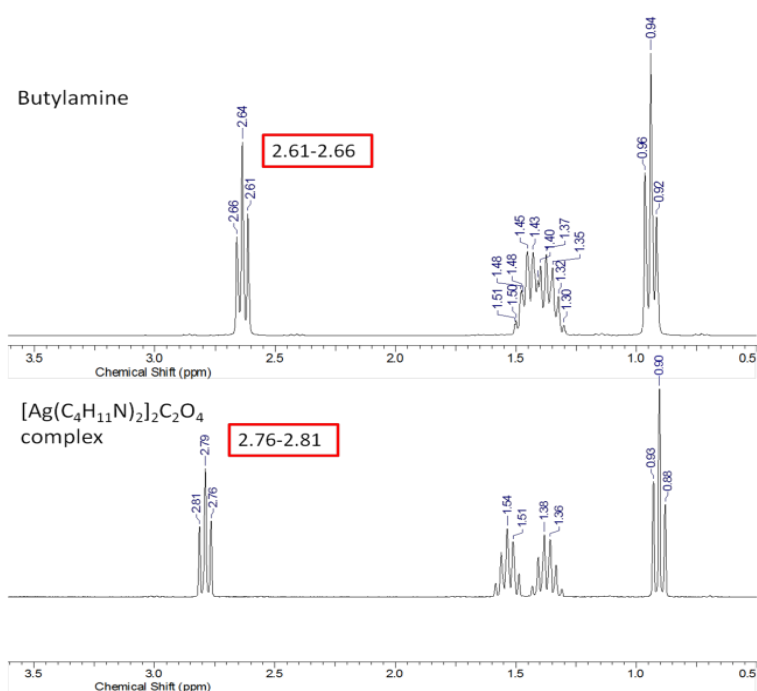


Figure 6.4  $^1\text{H-NMR}$  spectra of the butylamine and solid  $[\text{Ag}(\text{C}_4\text{H}_{11}\text{N})_2]_2\text{C}_2\text{O}_4$  complex,  $\text{D}_2\text{O}$  as solvent

### 6.3.3 Ink thermal behavior

DSC analysis was carried out to investigate the temperature window for thermal decomposition of the as-prepared ink. As shown in Figure 6.5, there are three peaks on the DSC curve of the silver ink. The first peak at  $100^\circ\text{C}$  is likely due to evaporation of ethanol and unreacted amine in the ink. The second peak at  $117^\circ\text{C}$  is attributed to the decomposition of the silver complex whereas the third peak at  $140^\circ\text{C}$  might be from evaporation of ethylene glycol and coalescence of silver nanoparticles produced [27]. It should be noted that the decomposition temperature of the as-prepared ink is much

lower than that of the silver oxalate powder. This is most probably because the lone pair electrons in nitrogen of butylamine can effectively combine with the silver ion to form a silver-amine complex with a lower redox potential, which reduces the decomposition temperature [32].

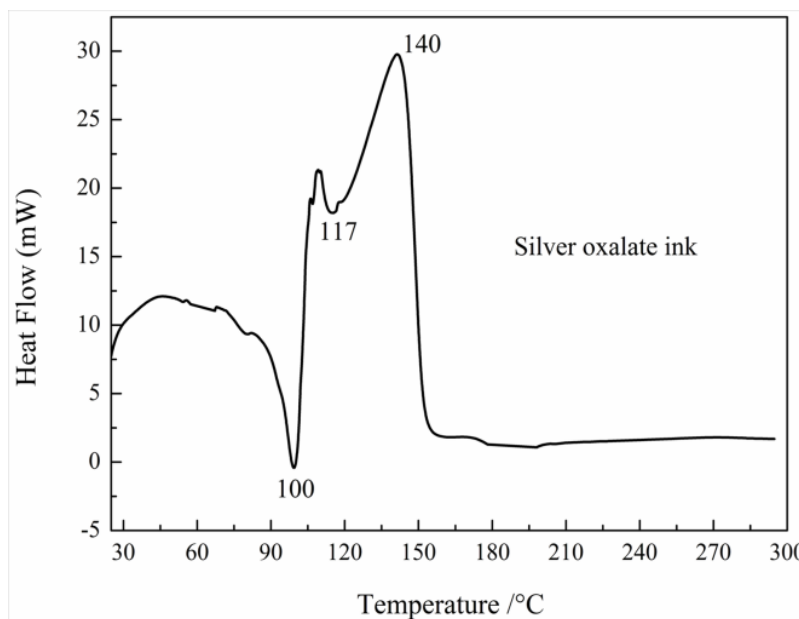


Figure 6.5 DSC curves of the as-prepared ink

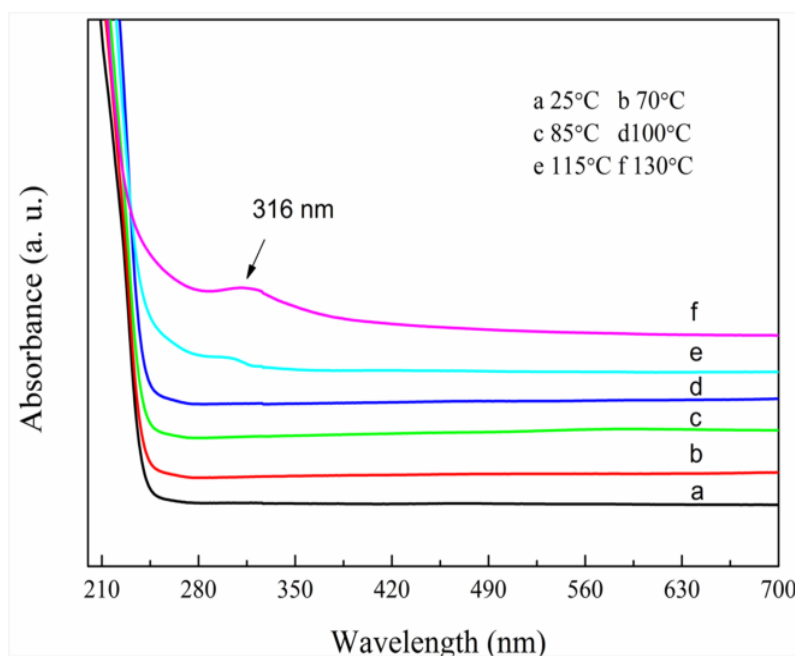


Figure 6.6 UV-Vis absorption spectra of silver citrate ink heated at different temperatures

UV-Vis spectroscopy was used to investigate the temperature-dependent absorption characteristics of the ink, as shown in Figure 6.6. For samples prepared at temperatures below 115°C, no absorption peak is observed in the UV spectra. However, when for ink is heated above 115°C, an absorption peak appears around 315 nm. As silver atoms

absorb in the 250-330 nm region, this peak is associated with the formation of  $\text{Ag}^0$  [148]. In other words, the  $[\text{Ag}(\text{C}_4\text{H}_{11}\text{N})_2]_2\text{C}_2\text{O}_4$  is decomposed into elemental Ag.

Based on the results discussed so far, it can be concluded that, during heating, solvent evaporation occurs first, followed by decomposition of the silver complex at elevated temperatures.

#### 6.3.4 Effect of sintering temperature on microstructure of silver films

Silver films were prepared on the cleaned PI substrates by a drop-coating method. The sintering process was carried out on a hotplate in a chamber. According to the DSC results and UV-Vis analysis of the ink, temperatures between 100 °C and 160 °C were chosen for thermal sintering.

Figure 6.7 gives an optical image of the as-prepared silver ink and the surface profile of a silver film after sintering. It can be seen that the thickness of the sintered silver film was about  $1.3 \pm 0.3 \mu\text{m}$ . As expected the film has a continuous surface without suffering from coffee ring effect caused by the fast evaporation of ethanol [12].

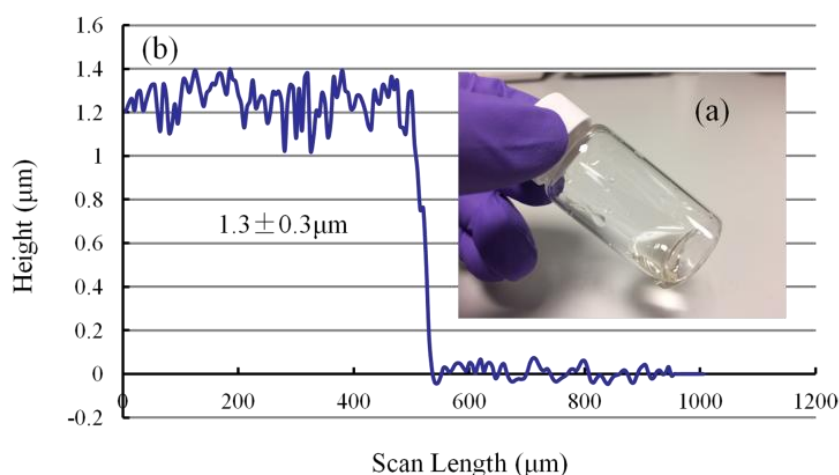
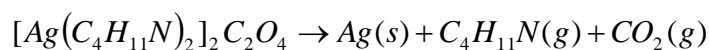


Figure 6.7 (a) As-prepared silver ink; (b) Surface profile of a sintered silver film (130 °C, 60 min)

X-ray diffraction was used to determine the crystalline structure of the silver films obtained at different sintering temperatures for 60 min (Figure 6.8). The results are in agreement with the values for a face-centered cubic (fcc) crystal structure of silver. The peaks at 38.2 °; 44.4 °; 64.5 °; 77.5 ° and 81.6 ° correspond to the (111), (200), (220), (311) and (222) crystal planes of Ag NPs, respectively, and were the same in all the films. No diffraction peaks from any other impurities were detected, revealing the formation of well-crystallized silver films.



It should be noted that  $[Ag(C_4H_{11}N)_2]_2C_2O_4$  could be transformed to silver crystals at 100°C, which is a key advantage of the ink developed in this work.

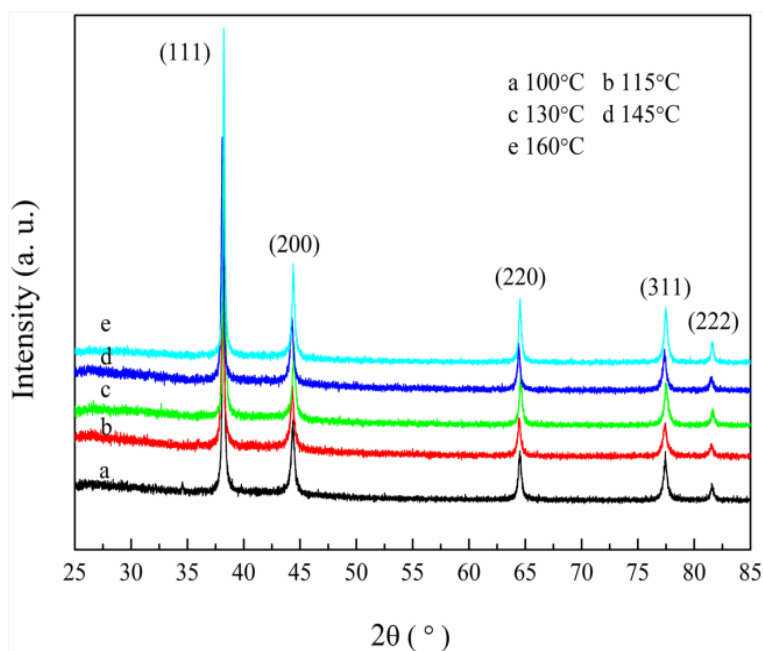


Figure 6.8 XRD patterns of the silver films obtained at different sintering temperatures for 60 minutes. Data shifted vertically, for clarity.

The crystallite sizes of the silver nanoparticles in the films formed at 100°C, 130°C and 160°C were determined from the XRD data (Debye-Scherrer equation). The results are given in Table 6.1.

Table 6.1 Particle sizes of silver nanocrystals in the film sintered at different temperatures

Sintering temperature (°C)	2θ (Degrees)	FWHM	Size (nm)
100	38.211	0.237	35.125
130	38.286	0.222	35.433
160	38.231	0.199	41.835

Clearly, the crystallite sizes of the silver nanoparticles in the film increases gradually with increasing temperature, from 35.125nm to 41.835nm. This can be attributed to the nucleation and growth of the silver grains. It is known that nucleation of silver particles occurs in the initial stage of sintering followed by subsequent grain growth [27]. The higher the sintering temperature, the larger the crystallite size since a large number of

crystal nuclei would form, followed by a fast growth. For sintering at a high temperature (160°C), solvent evaporation is fast, which enables fast growth of silver nanocrystals, thereby resulting in a relatively large size.

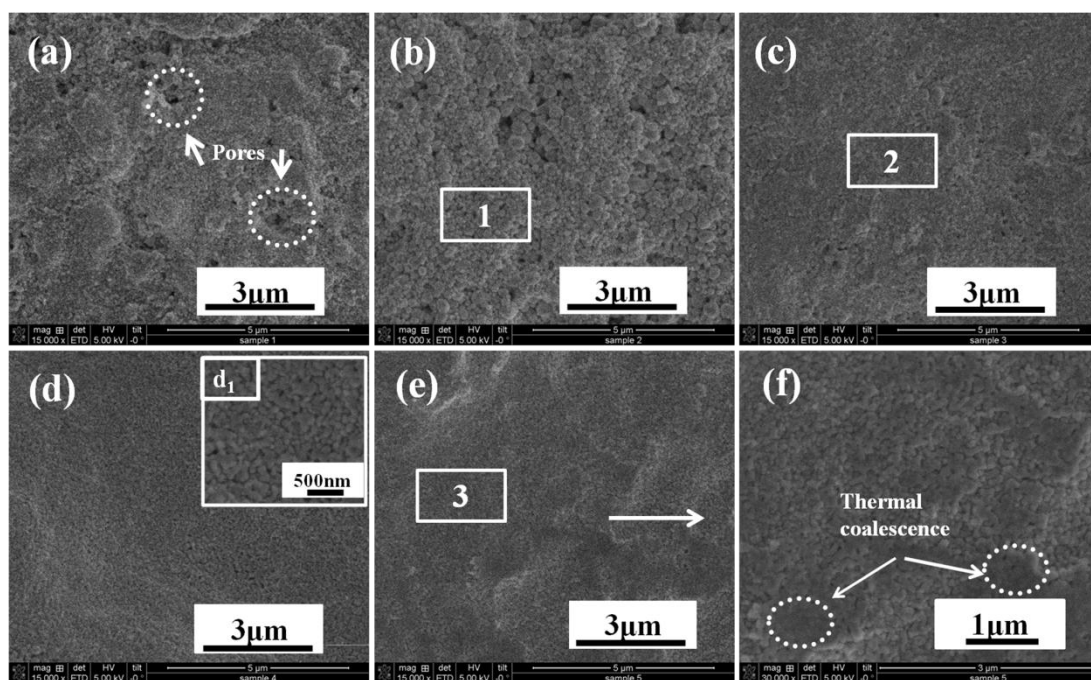


Figure 6.9 SEM images of silver films sintered for 60 minutes, (a) 100 °C, (b) 115 °C, (c) 130 °C, (d) 145 °C, (e) 160 °C (d<sub>1</sub> and f are high magnification images of figure d and e, respectively).

Surface microstructures of silver films obtained at different temperatures were evaluated by SEM (Figure 6.9). All the films show interconnected domains of silver nanoparticles. This feature is a result of fast solvent evaporation and thermal decomposition of the  $[\text{Ag}(\text{C}_4\text{H}_{11}\text{N})_2]_2\text{C}_2\text{O}_4$  complex [27]. At lower sintering temperatures (100°C, 115°C), evaporation of solvent component which could release bubbles is dominant because of its low boiling point and the decomposition of complex producing silver nanoparticles is secondary. The bubbles need to go through the films consisting of silver nanoparticles, so the films are not uniform and have pores (Figure 6.9 a and b), though the produced silver nanoparticles could connect with each other. At sintering temperatures of 130°C and 145°C, more silver particles are produced (Figure 6.9 c and d). The films become uniform with less defects, the particles are homogeneous and the stacking density is increased (Figure 6.9d<sub>1</sub>). Sintering at higher temperatures (160°C) leads to formation of large particles due to the neck connection of silver nanoparticles produced (Figure 6.9f), resulting in a dense film.



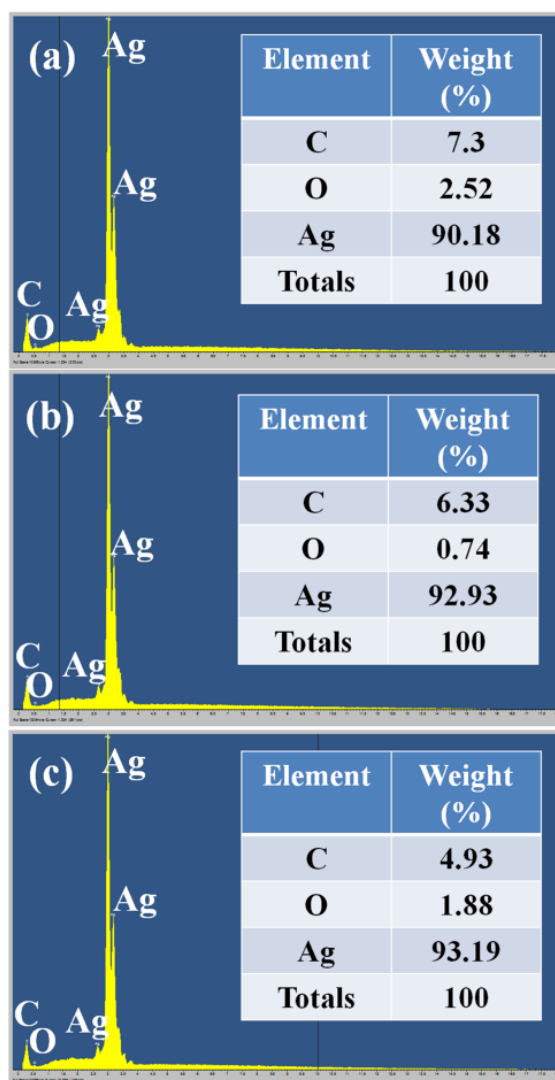


Figure 6.10 EDS results in the films as a function of sintering temperature, (a) 115 °C, (b) 130 °C and (c) 160 °C

The chemical composition of the silver films obtained at 115, 130 and 160 °C was determined from the EDS surface energy spectra (the samples taken from the area 1, 2 and 3 in Figure 6.9). As Fig.6.10 shows, three elements (C, O and Ag) were detected. With increasing sintering temperature, the content of Ag increased from 90.18 wt% to 93.19 wt% and the content of C decreased from 7.3 wt% to 4.93 wt%, indicating that  $[\text{Ag}(\text{C}_4\text{H}_{11}\text{N})_2]_2\text{C}_2\text{O}_4$  has almost fully decomposed to silver.

### 6.3.5 Effects of sintering time on microstructure of silver ink films

The effect of sintering time on the microstructure of the silver films was also studied. The samples were prepared by heating the ink on PI film at 130°C for 10, 15, 30 and 60 minutes and were characterized by XRD, SEM and EDS.

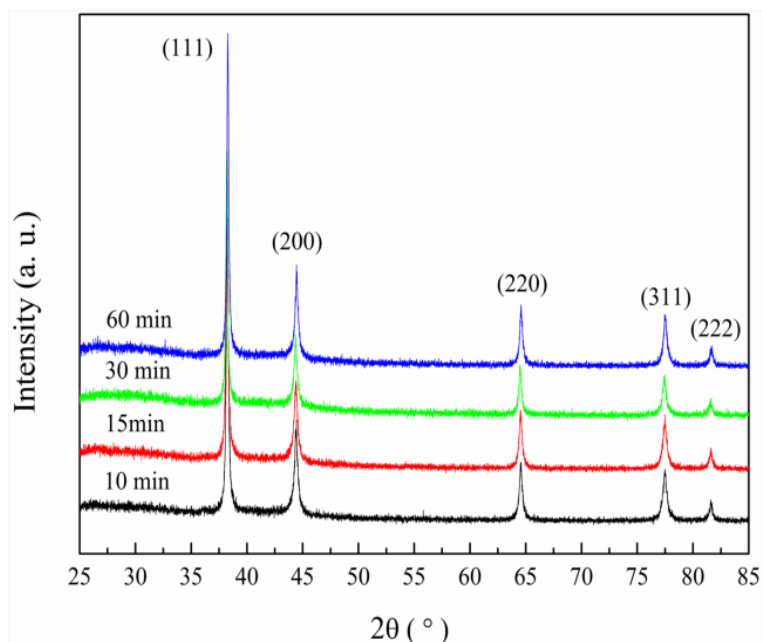


Figure 6.11 XRD patterns of Ag films prepared at 130°C for 10, 15, 30 and 60 min respectively

As shown in Figure 6.11, silver nanocrystals could be produced within 10 minutes. The particle size calculated using XRD data increases as the heating time increases (Table 6.2).

Table 6.2 Particle size of silver nanocrystals in the films processed at 130°C for different times

Sintering time (minutes)	2θ (Degrees)	FWHM (β)	Size (nm)
10	38.239	0.224	37.168
30	38.193	0.216	38.538
60	38.231	0.199	41.835

Figure 6.12 shows the microstructure of the silver films produced at 130 °C for different sintering times. It can be seen that the film sintered for 5 minutes is not uniform and there are some pores on its surface. The particles have irregular shapes and some of them seem to be covered by an organic layer (Figure 6.12a). With increasing time, the films show a compact microstructure consisting of small silver particles with better film uniformity (Figure 6.12b). The film sintered for 30 min has a uniform surface profile consisting of many silver particles, in contact with each other (Figure 6.12c). After 60 minutes, a compact and uniform microstructures consisting of homogeneous spherical silver particles is formed (Figure 6.12d).

The change in film morphology can be easily understood, which is related to solvent evaporation and thermal decomposition of the silver complex. When the sintering time

is 5 minutes, solvent evaporation is inadequate, thereby resulting in an uneven film consisting of many small silver particles. For a sintering time of 15 minutes, the film is uniform as there is material redistribution due to decomposition of silver complex in the film. Further increase in sintering time results in improved surface morphology (Figure 6.12d).

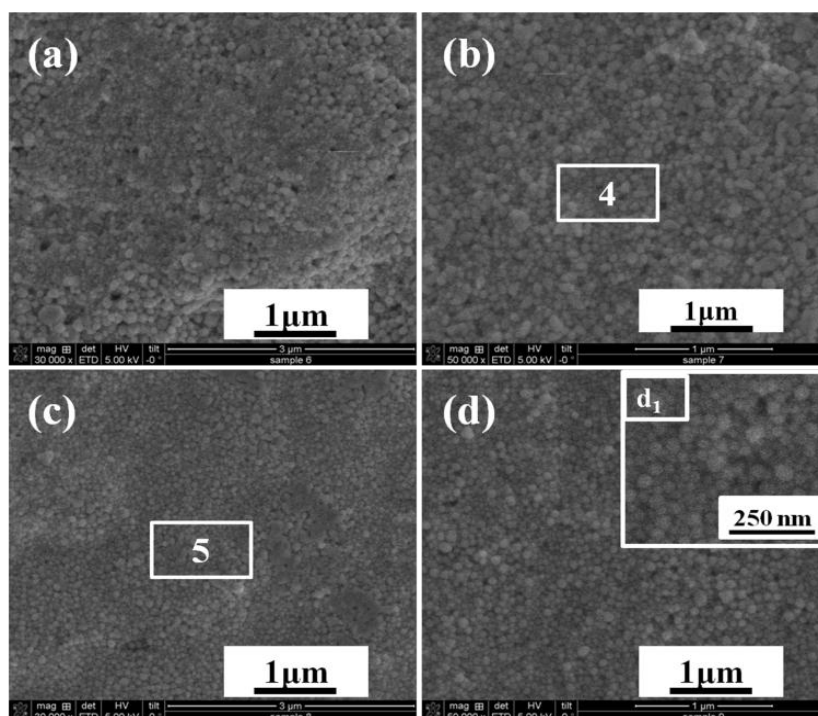


Figure 6.12 SEM images of silver films produced at 130 °C for 10, 15, 30 and 60 minutes (a)-(d)

EDS analysis was employed to investigate the changes in chemical composition, as shown in Figure 6.13. The samples were taken from area 4 and 5 of Figure 6.12. As the heating time was increased from 15 to 30 minutes, no obvious changes in Ag and C content are observed. The results indicate that the organic molecules were decomposed and volatilized mostly within 15 minutes; the decomposition of silver-amine complex continued to a large extent.

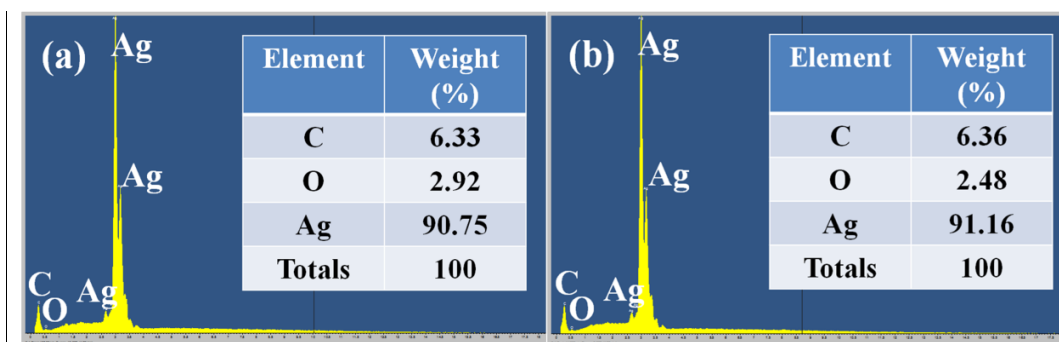


Figure 6.13 EDS results of silver films produced at 130°C for (a) 15 and (b) 30 minutes

### 6.3.6 Electrical performance

The resistivities of the silver films obtained at various temperatures were calculated using the measured sheet resistance and film thickness ( $1.3 \pm 0.3 \mu\text{m}$ ).

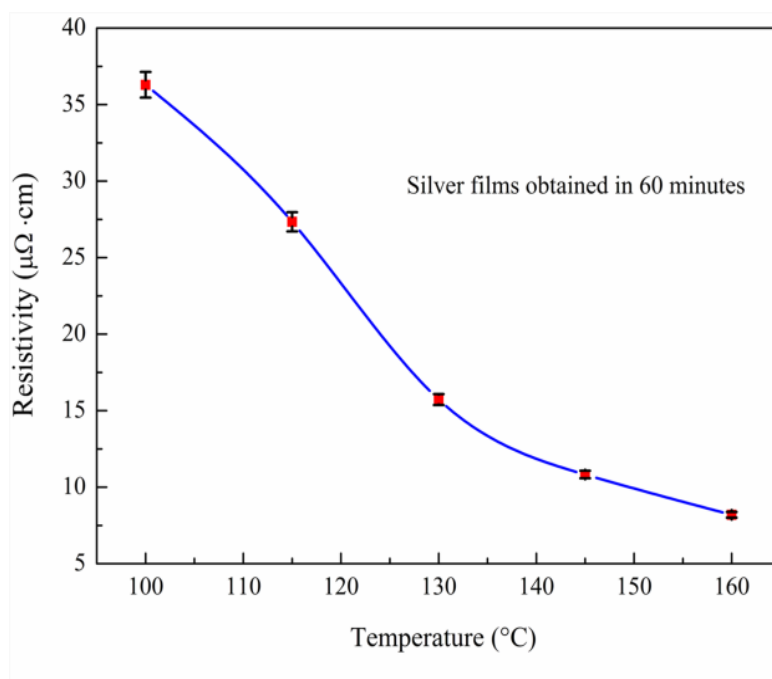


Figure 6.14 Resistivity of the silver films sintered at various temperatures for 60 minutes

From Figure 6.14, it can be seen that the resistivity of the silver films decreases gradually as the temperature increases, from  $36.29 \mu\Omega \cdot \text{cm}$  at  $100^\circ\text{C}$  to  $8.19 \mu\Omega \cdot \text{cm}$  at  $160^\circ\text{C}$ . Below  $100^\circ\text{C}$ , measurements could not be carried out as the film was not totally dry and the sheet resistance was out of the measurement range of the 4-probe instrument.

At lower sintering temperatures, the solvent evaporation is insufficient and the formation of silver is not complete, so the resistivity is relatively high. In contrast, at higher temperatures, solvent evaporation is complete and more silver nanocrystals can be formed to improve the stacking density of Ag nanoparticles in the film, resulting in a continuous and uniform film with better particle accumulation; therefore, good film conductivity was obtained.

The resistivities of the films sintered at  $130^\circ\text{C}$  for different times are shown in Figure 6.15. As the sintering time increases from 5 to 60 minutes, the resistivity decreases gradually from  $24.10 \mu\Omega \cdot \text{cm}$  to  $15.72 \mu\Omega \cdot \text{cm}$ , reaching a value equivalent to 10 times of bulk silver ( $1.59 \mu\Omega \cdot \text{cm}$ ). After 30 minutes, the improvement in resistivity is more than

37%. The decrease in resistivity with time can also be explained by the fact that more silver nanoparticles are generated, become larger and are more closely connected.

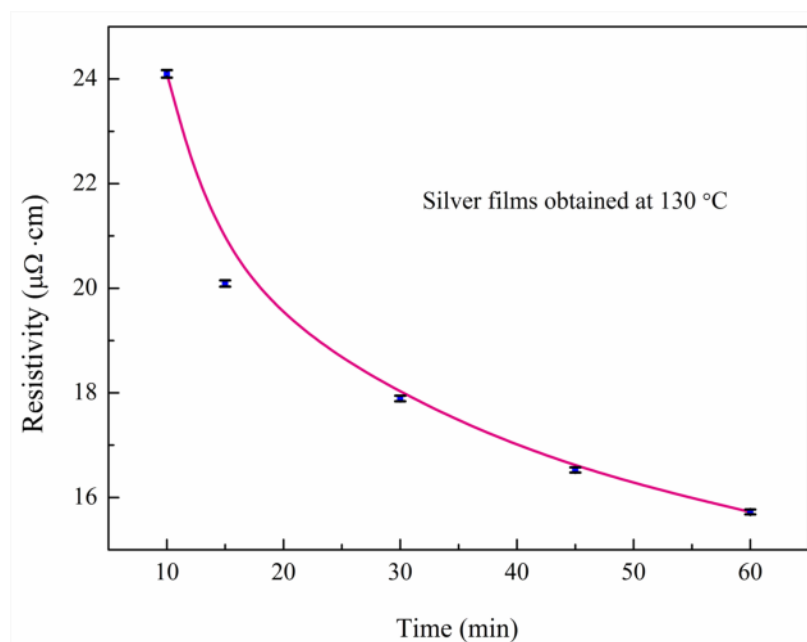


Figure 6.15 Resistivity of the Ag films as a function of heating time at 130°C

It is worth noting that film resistivity of  $10^{-5} \Omega \cdot \text{cm}$  can already be achieved at sintering temperatures around 100 °C. This shows that the silver ink can be used for a variety of polymer flexible substrates such as polyethylene terephthalate.

#### 6.4 Conclusions

In summary, a silver oxalate ink was prepared in a mixture of ethanol and ethylene glycol using the as-prepared silver oxalate as precursor and butylamine as a complexing ligand. Silver film with low resistivity ( $15.72 \mu\Omega \cdot \text{cm}$ ) could be produced on PI substrates at a sintering temperature of 130°C. Silver oxalate precursor with good properties was obtained and an amine complex was formed to produce the ink. The films on PI substrates sintered at a range of temperatures and time durations were analyzed in terms of their morphology and resistivity, where the underlying relationship between them was demonstrated. Three factors are mainly responsible for the conductivity of the produced silver films, which are the residual level of organic solvents, the degree of the decomposition of silver-amine complex and the contact area of silver nanoparticles.

## Chapter 7 Optimization of Silver Oxalate Ink: Effects of Amines

### 7.1 Introduction

Up to now, alkylamines are mainly selected as the ligands for silver oxalate in development of low-temperature sintering organic silver ink. Dong et al. synthesized a silver oxalate ink using ethylamine as a ligand [27]. It was found that the silver oxalate could be dissolved in the organic solution of ethylamine with no difficulty and the obtained ink can produce silver film with a resistivity of  $8.4\mu\Omega\cdot\text{m}$  at the sintering temperature of  $170\text{ }^\circ\text{C}$  for 30min. Zope et al. reported a silver oxalate ink using ethylenediamine as a ligand [157]. Silver conductive traces can be produced with a resistivity of  $4.26 \times 10^{-8}\Omega\cdot\text{m}$ , which is 2.7 times that of bulk silver. In Chapter 6, we reported a silver oxalate ink using butylamine as a ligand [156].

Although interesting results have been obtained in these cases, the studies were only focused on a specific ink formulation. The role of amines in silver oxalate based inks was barely studied. Based on the research of Chapter 6, it can be deduced that the type of amine is critical in ink formulation since it not only affects the solubility of silver oxalate in organic solvents but also affects the thermal sintering temperature of the silver ink. Therefore, it is interesting to study the effect of amine types on the properties of the formulated ink and to elucidate their functions as well as to formulate an optimal silver oxalate ink producing favorable conductive films for flexible electronics application.

In this chapter, the effects of amine types on the thermal property, stability and electrical performance of the formulated silver oxalate inks were investigated in detail. We demonstrated that highly conductive silver films with controlled microstructure features can be achieved by selection of amine types. The underlying mechanism is elucidated. The chemical reactions occurring within the ink and the film formation process were also studied. An optimal silver complex ink was prepared by using a blend of amines as ligands, producing highly conductive silver films at  $150\text{ }^\circ\text{C}$ . Successful circuit application was demonstrated. The research may provide insight into endeavors aimed at developing silver complex inks.

Part of this Chapter has been published [158].

## 7.2 Experimental Section

### 7.2.1 Preparation of silver-amine complex ink and film

Silver nitrate ( $\text{AgNO}_3$ ), oxalic acid ( $\text{H}_2\text{C}_2\text{O}_4$ ), sodium hydroxide ( $\text{NaOH}$ ), ethylenediamine ( $\text{C}_2\text{H}_8\text{N}_2$ ), 1,2-diaminopropane ( $\text{C}_3\text{H}_{10}\text{N}_2$ ), butylamine ( $\text{C}_4\text{H}_{11}\text{N}$ ), hexylamine ( $\text{C}_6\text{H}_{15}\text{N}$ ), octylamine ( $\text{C}_8\text{H}_{19}\text{N}$ ), ethanolamine ( $\text{C}_2\text{H}_7\text{NO}$ ), ethylene glycol ( $\text{C}_2\text{O}_2\text{H}_6$ , EG) and ethanol ( $\text{C}_2\text{H}_6\text{O}$ , EA), were purchased from Sigma-Aldrich and were used without further purification. Polyimide films (PI) of  $127\ \mu\text{m}$  in thickness were obtained from DuPont and were used as substrates. Before application,  $15\text{mm}\times 15\text{mm}$  PI samples were cleaned using deionized water and ethanol to remove the particles and organic contaminations on the surface.

Silver organic inks were prepared in a mixture of EG and EA via a complexing reaction of the silver oxalate and different amines. Silver oxalate was prepared using the method described in Chapter 5. For ink preparation, the obtained silver oxalate (0.152g) was dispersed in a mixed solvent containing ethanol (0.375 ml) and ethylene glycol (0.375 ml). After stirring for 5 minutes, amines with different alkyl-chain lengths were added separately. The mixture was stirred for 60 minutes to form different silver-amine complex inks. In order to make a reasonable comparison, the weight of silver oxalate and solvent were the same in each ink and the Ag/amine molar ratios were kept at a constant value of 1:2.

A drop-coating method was used to prepare the film. Two drops of each ink were deposited and spread evenly on the surface of  $15\text{mm}\times 15\text{mm}$  PI substrates using a disposable transfer pipettes (3.2ml, Thermo Scientific™ Samco™). Then the obtained wet films were sintered at selected temperatures within 60 minutes for metallization.

### 7.2.2 Characterization

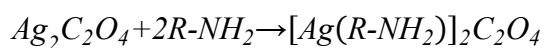
Ultraviolet-visible (UV-Vis) absorption spectra were recorded on a Lambda 25 UV-Vis spectrophotometer. Ethylene glycol was used as the solvent since it does not produce any turbidity in the ink dissolution or dilution process when compared with ethanol. The UV-Vis absorption spectra were obtained from a sample of the ink after dilution by approximately 500 times and quartz cuvettes were used to contain the samples. Fourier transform infrared (FT-IR) spectra were obtained on a Thermo Scientific Nicolet iS5 FT-IR spectrometer. Thermal behaviors of all inks were investigated with a thermal analyzer (TA instrument) using aluminum pans at a heating rate of  $10\ \text{°C}\cdot\text{min}^{-1}$  from

room temperature to 300 °C and a nitrogen flow rate of 80 ml·min<sup>-1</sup>. X-ray diffraction (XRD) analysis was conducted by using Cu K $\alpha$  radiation. Surface morphologies of the sintered silver films were observed via a FEI Quanta 3D Scanning Electron Microscope (SEM) and chemical composition was confirmed by an Oxford X-maxN 150 surface energy disperse spectrometer (EDS). The sheet resistivity was measured using a 4-point probe system (Jandel Engineering, UK). The thickness of the film was measured by a Dektak surface profilometer so as to calculate its volume resistivity.

## 7.3 Results and Discussion

### 7.3.1 Basic chemical reaction

The complexes of silver oxalate with different alkylamines were formed via the following chemical reaction process: the amino group (-NH<sub>2</sub>) of amine molecules coordinates with the silver atom and subsequently form the complex.



As amines are weakly reducing, UV-visible spectroscopy was first used to investigate the as-prepared inks, as shown in Figure 7.1.

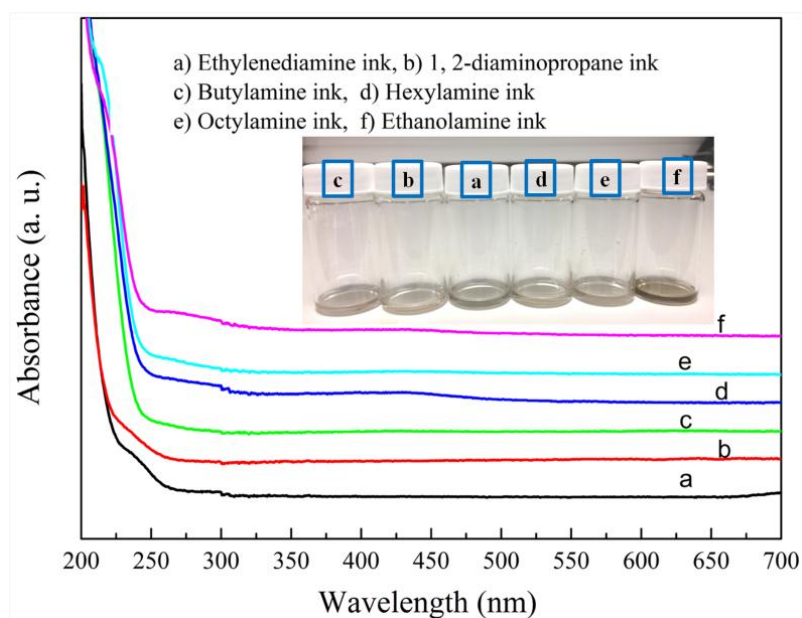


Figure 7.1 UV-Vis absorption spectra of the silver oxalate inks prepared using different amines

As expected, no absorption peak for silver nanoparticles appeared in the wavelength range between 380nm and 450nm [149, 159], implying that the complex was formed and existed in the form of ions in the ink. The optical images of freshly prepared inks are also shown in Figure 7.1 (the inset). It can be seen that the inks formulated using



1,2-diaminopropane, butylamine, hexylamine and octylamine in each case, were colorless and transparent. Inks from ethylenediamine and ethanolamine both had color. As for the reason, we believe that it is associated with the absorption and reduction properties of the amine. Ethylenediamine is faint yellow. Also, unlike other monodentate amines used in this work, the bidentate ethylenediamine has greater reducing capacity [157] and will reduce a small number of silver complex ions into colored  $\text{Ag}_2\text{O}$  from the effect of the heat released from the complexation process [13], thereby resulting in a colored ink. Since the molecular structure of ethanolamine is similar to that of ethylenediamine, so the ink also has color. However, as the amount of the reduced  $\text{Ag}_2\text{O}$  is very low and furthermore the UV-Vis absorption spectra were obtained from a sample of the ink after dilution by approximately 500 times, therefore the effect of absorption of  $\text{Ag}_2\text{O}$  is not observable in the spectra. The different absorption intensities are relative values and the data traces were shifted for clarity.

FT-IR spectroscopy and  $^1\text{H-NMR}$  were used to investigate and confirm the above reaction mechanism. As all the selected amines have similar complexing behavior with silver oxalate, herein 1,2-diaminopropane was only chosen to make an elucidation, the FT-IR result is shown in Figure 7.2 (FT-IR spectra of the rest are listed in the appendices).

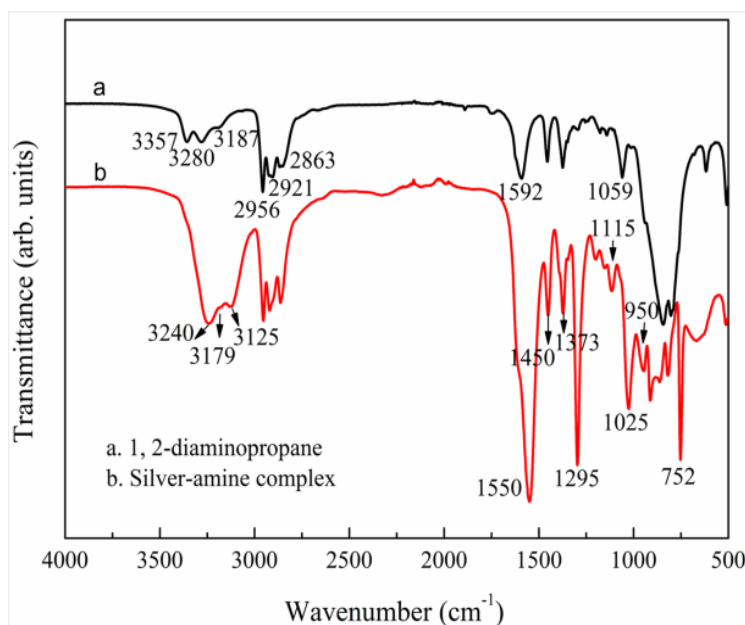


Figure 7.2 FT-IR spectra of 1,2-diaminopropane and the formed silver-amine complex

The absorption peaks appeared at 3357 and 3280  $\text{cm}^{-1}$  in the spectrum of 1,2-diaminopropane were attributed to the asymmetric and the symmetric stretching

vibration of NH<sub>2</sub> groups. Two peaks at 2956 and 2921 cm<sup>-1</sup> were assigned to the asymmetric stretch of CH<sub>3</sub> and CH<sub>2</sub>, respectively. The peak at 2863cm<sup>-1</sup> related to the symmetric stretching mode of CH<sub>2</sub>. After complexation, it is worth noting that the peaks associated with the NH<sub>2</sub> groups undergo a dramatic red-shift, from 3357 to 3240 cm<sup>-1</sup>, 3280 to 3179 cm<sup>-1</sup>. This indicates the decrease of vibration frequencies of the amine group [160]. Besides, a new carbonyl peak appears at 1550 cm<sup>-1</sup>, which is from the silver oxalate. These changes could be explained as follows: the amino group donated electrons to the silver ion after the reaction of 1,2-diaminopropane and silver oxalate, which decreased the electron density of the amino group and thus caused the shift of infrared absorption to lower wave number [143]. The result implies that the formulation of the silver ink was achieved by a facile complexing reaction.

It should be mentioned here that in order to avoid the influence from the solvents, the complex for the FT-IR measurement was prepared using only silver oxalate and 1,2-diaminopropane in a stoichiometric ratio (The Ag/amine molar ratio is 1:2). The chemical formula of the complex is  $[Ag(R-NH_2)]_2C_2O_4$ .

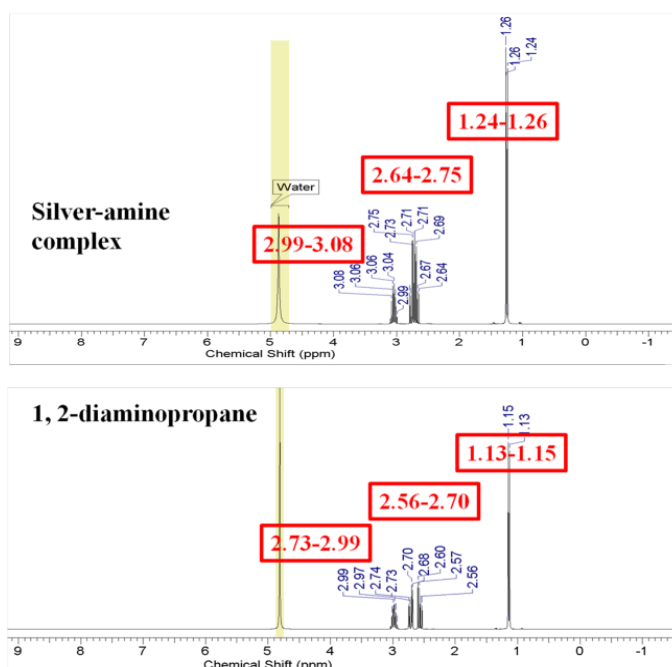


Figure 7.3 <sup>1</sup>H-NMR spectra of 1,2-diaminopropane and the formed silver-amine complex, D<sub>2</sub>O used as solvent for both

The <sup>1</sup>H-NMR results of the obtained complex also confirmed the reaction process, as shown in Figure 7.3. The position of the hydrogen in the methyl group of 1,2-diaminopropane shifted from the range of 1.13-1.25 to 1.24-1.26. The position of

the hydrogen in the methylene and methyne group of 1, 2-diaminopropane shifted from the range of 2.56-2.70 to 2.64-2.75 and 2.73-2.99 to 2.99-3.08. These chemical shift changes indicated that the silver-amine complex was formed.

The solubility of silver oxalate in the organic solvents containing each type of amine was also investigated. It was found that silver oxalate dissolved quickly in the solvents containing ethylenediamine, 1,2-diaminopropane, butylamine and ethanolamine separately, within 5 minutes. However, in the solvents of hexylamine and octylamine, the dissolvable rate was slow and more time was necessary. These differences indicated that the solubility of silver oxalate in the organic solvents is strongly related to the types of amines and their alkyl chain lengths. The longer is the hydrocarbon chain, the slower the dissolution. This can be illustrated by the electron-donating capacity of nitrogen atom in the amino group and the basicity difference as well as the hydrocarbon chain lengths of amines. The stronger is the electron donation, the stronger its ability to coordinate with silver ions [150], and therefore the silver oxalate could dissolve quickly in the solvents containing ethylenediamine and 1,2-diaminopropane. For the ink derived from silver-ethanolamine complex, since this complex contained one OH group, hence its solubility was increased. For hexylamine and octylamine, although they have strong electron-donating capacity resulted from the long carbon chain lengths, the steric-hindrance effect was also strong. Therefore, their ability for complexing and dissolving the silver oxalate was weaker than that of butylamine.

### ***7.3.2 Thermal behavior of various complex inks***

Thermal behavior of various silver-amine inks was investigated by DSC analysis; the results are given in Figure 7.4 and Table 7.1. It can be seen that all inks have a primary endothermic peak at a temperature around 150°C, which is attributed to the decomposition of silver-amine complexes. The broad peak at the temperature below 90°C is assigned to the evaporation of ethanol and free amine in the ink. This is in agreement with the previous research on silver-amine complex inks [27, 32, 150]. The inks derived from ethylenediamine and 1,2-diaminopropane with shorter carbon-chain lengths, have similar thermal behaviors, giving a relatively high decomposition temperature (146 and 144°C, respectively). The inks derived from butylamine, hexylamine and octylamine that have longer carbon-chain lengths, displayed similar thermal behaviors, showing a low decomposition temperature below 135°C. As for the ink from ethanolamine, it has a complex thermal decomposition behavior and the final

endothermic peak appeared at 185°C, which is high for application with the low temperature flexible substrates such as PET.

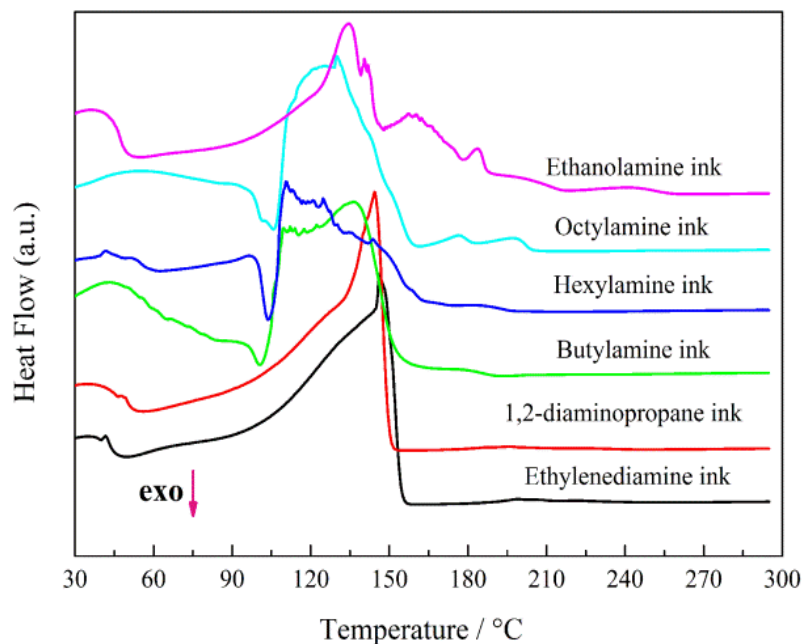


Figure 7.4 DSC curves of the silver oxalate inks prepared using different amines

Table 7.1 Amine types and the decomposition temperatures of the formulated inks

Amine	Alkyl Chain length $\times$ amine	T <sub>Max</sub> / °C
Ethylenediamine	2 $\times$ 2	146
1,2-diaminopropane	3 $\times$ 2	144
butylamine	4 $\times$ 1	135
hexylamine	6 $\times$ 1	122
octylamine	8 $\times$ 1	128
ethanolamine	2 $\times$ 1	135

From the above analysis, it can be seen that the thermal decomposition temperature of silver-amine complex inks is also correlated with the types of amines and their alkyl chain lengths. The variation in thermal decomposition temperature of the inks is a direct reflection of the thermal stability of the silver-amine complex [150]. The complex with low thermal stabilities usually gives rise to lower decomposition temperatures. It is known that the thermal stability of the silver-amine complex was mainly affected by the steric hindrance, which decreases with increasing size of the side groups in the amines [150]. Thus, when amines with long carbon-chain lengths, such as butylamine, hexylamine and octylamine, were used to prepare the ink, the decomposition

temperature of the corresponding ink decreased significantly. This is beneficial for applying the ink on a variety of substrates. For ethylenediamine and 1,2-diaminopropane with short carbon-chain lengths and more amino numbers, they have a stronger capacity to coordinate with silver ions due to the stronger capacity of donating electrons, and as a consequence, the complex formed have higher thermal stability. Here, it should be noted that although amines with longer carbon-chain lengths could decrease the ink decomposition temperature, their boiling points are high and that would increase the temperature in film formation process to remove them. Considering this point, no attempt was made to study amines with much longer alkyl carbon chains. As butylamine and 1,2-diaminopropane have lower boiling temperatures of 78°C and 117.3°C respectively and the resulted inks have lower decomposition temperatures in comparison with that of the other inks, these two amines were chosen for the subsequent ink formulation work.

### 7.3.3 Stability, film Morphology and resistivity of various complex inks

To evaluate the stability of various silver-amine inks, preservation with different time durations were made and optical images were obtained and shown in Figure 7.5.

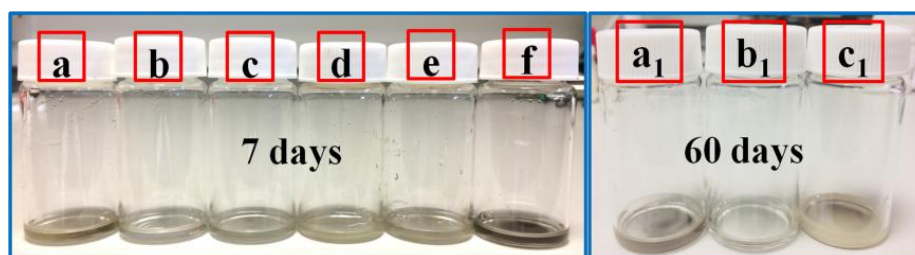


Figure 7.5 Optical images of the as-prepared silver oxalate inks storing in a refrigerator at 3°C for different times, (a, a<sub>1</sub>) ethylenediamine, (b, b<sub>1</sub>) 1,2-diaminopropane, (c, c<sub>1</sub>) butylamine, (d) hexylamine, (e) octylamine, (f) ethanolamine

After storing in a refrigerator at 3°C for one week, only the inks from 1,2-diaminopropane (Figure 7.5b) and butylamine (Figure 7.5c) had no color change and sediment or educts. The long-term stability of these two inks was also tested by storing in refrigerator at 3°C for up to 60 days (Figure 7.5b<sub>1</sub> and c<sub>1</sub>). Clearly, there were educts on the bottle wall of the ink formulated using butylamine (Figure 7.5c<sub>1</sub>) while the ink from 1,2-diaminopropane (Figure 5b<sub>1</sub>) was still transparent without any color change, implying good stability and hence long shelf life.

Based on the analysis of the DSC results, the temperature of 150°C was chosen to sinter the as-prepared silver-amine complex inks to investigate the relationship between the resistivity and amine types. The obtained silver films were tested by a four-probe method and the results are shown in Figure 7.6. Notably, the sheet resistance of the film is dependent on the types of amines and its alkyl-chain lengths. The film from the ink prepared using butylamine showed the lowest sheet resistance (0.066Ω/□), while the film derived from ethanolamine ink had high sheet resistance that was beyond the measurement range of the four-probe instrument. The film sheet resistance derived from ethylenediamine ink was higher (0.322Ω/□) than that of the ink derived from 1,2-diaminopropane (0.105Ω/□) but was much lower than that of hexylamine (1.077Ω/□) and octylamine (20.679Ω/□) derived inks. The error for all the sheet resistance measurements is about 0.010Ω/□.

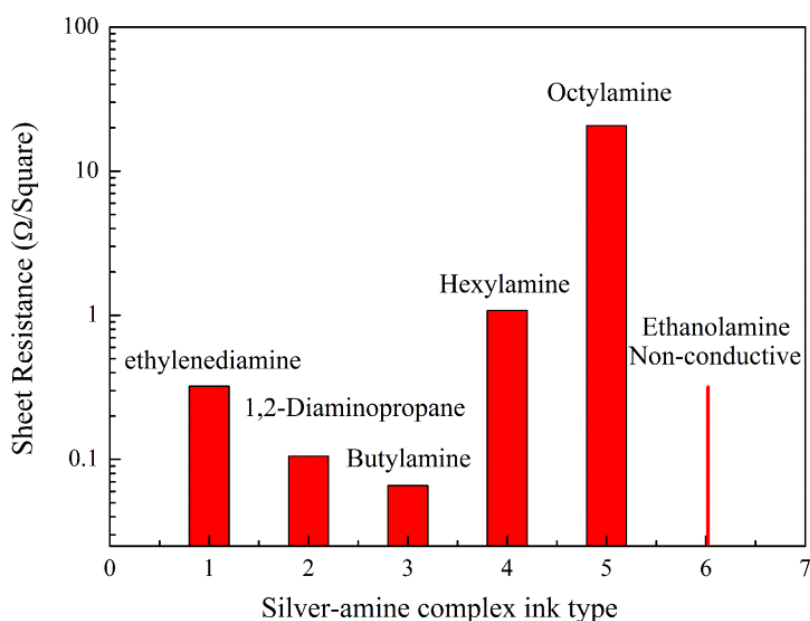


Figure 7.6 Sheet resistance of silver films sintered at 150°C for 60min from different silver oxalate inks (The error for all the measurements is about 0.010Ω/□)

Since the weightings of silver oxalate and solvent were the same in each ink, the Ag/amine molar ratios were kept at a constant value, only two drops of each ink were used to produce the films and the temperature selected for sintering was relatively high, there was not much difference in the thicknesses of the films derived from ethylenediamine, 1,2-diaminopropane and butylamine inks. For the film from ethanolamine ink, it was not conductive. Considering these, an average thickness of 1.43μm was used as an estimated valuation of the film for resistivity calculation. In combination with the results of sheet resistance, it is easy to see that the resistivity of

the films from amines with different alkyl chain lengths but one amino number, increased as the chain length was increased, while the resistivity of films from amines with two amino numbers but different alkyl chain lengths decreased with the increase of chain length.

X-ray diffraction and SEM were then used to probe the crystalline structure and surface microstructure of the obtained silver films from various complex inks (Figure 7.7 and Figure 7.8) to gain insight into the underlying reasons for various sheet resistances of films from different inks.

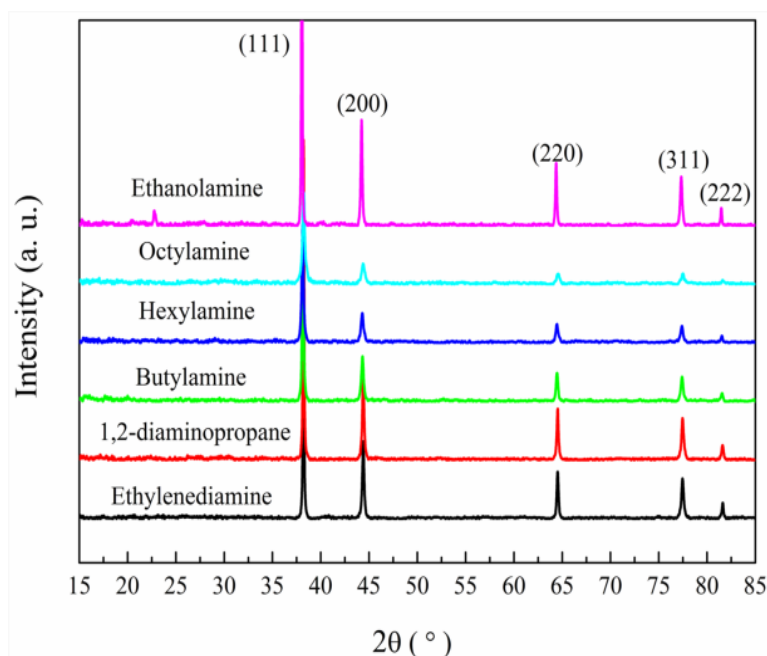
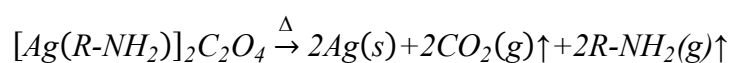


Figure 7.7 XRD patterns of silver films sintered at 150°C for 60min from different silver oxalate inks

It can be seen that all the XRD data is in good agreement with the standard powder diffraction card for a face-centered cubic (fcc) crystal structure of silver (JCPDS No.03-065-2871) and no diffraction peaks from other impurities were detected, indicating that the silver-amine complex was transformed into silver crystals and the following reaction occurred.



The films from the inks of hexylamine and octylamine showed relative weak peaks at  $2\theta$  values of about  $38.2^\circ$ ,  $44.4^\circ$ ,  $64.5^\circ$ ,  $77.5^\circ$  and  $81.6^\circ$ , indicating a low crystalline structure. The films from inks of ethylenediamine, 1, 2-diaminopropane and butylamine



showed sharp peaks, corresponding to a well-crystallized silver film.

Table 7.2 Particle size of silver nanocrystals in each film

Amine	2 $\theta$ (Degrees)	FWHM	Size (nm)
Ethylenediamine	38.211	0.148	54.94
1,2-diaminopropane	38.211	0.151	53.84
butylamine	38.157	0.204	39.59
hexylamine	38.120	0.237	33.94
octylamine	38.230	0.323	25.23

Here, the crystallite size of the silver nanoparticles in each film was calculated using the Debye-Scherrer equation to further confirm the statement, which was shown in Table 7.2. Clearly, the films from the ethylenediamine and 1,2-diaminopropane inks have better crystallinity than the other ones.

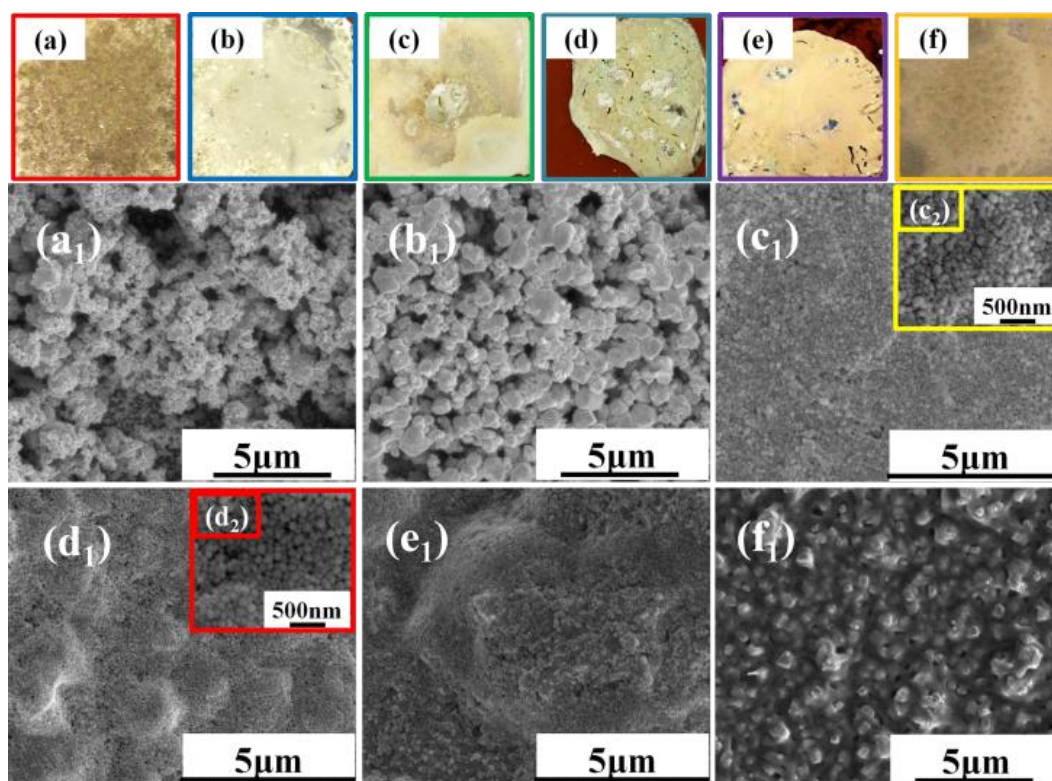


Figure 7.8 Optical and SEM images of silver films sintered at 150°C for 60min from different silver oxalate inks, (a, a<sub>1</sub>) Ethylenediamine, (b, b<sub>1</sub>) 1,2-diaminopropane, (c, c<sub>1</sub>) butylamine, (d, d<sub>1</sub>) hexylamine, (e, e<sub>1</sub>) octylamine, (f, f<sub>1</sub>) ethanolamine (c<sub>2</sub> and d<sub>2</sub> are high magnification images of figure c<sub>1</sub> and d<sub>1</sub>, respectively).

Figure 7.8 shows the optical and SEM images of the films produced from six different types of silver-amine inks. It can be seen that the films have diverse morphologies,



where the microstructures were quite different in terms of particle morphology, size and the degree of contact.

The silver film, derived from ethylenediamine ink, showed an irregular crystal structure consisting of small and big particles and had many voids and poor connection between the particles (Figure 7.8a and a<sub>1</sub>), while the silver films produced from the butylamine and hexylamine derived inks presented a uniform and dense surface structure consisting of spherical silver nanoparticles (Figure 7.8c<sub>2</sub> and d<sub>2</sub>) and few voids as well as good contact between the particles. Besides, there was a significant solvent shrink effect for the hexylamine ink in the sintering process and because of this the formed film does not cover the substrate completely. The silver film derived from 1,2-diaminopropane ink showed a loose surface morphology that was composed of big silver crystals and some voids (Figure 7.8b and b<sub>1</sub>). The silver film from octylamine and ethanolamine derived inks had structures that were composed of few silver particles surrounded by a large amount of residues from the solvents.

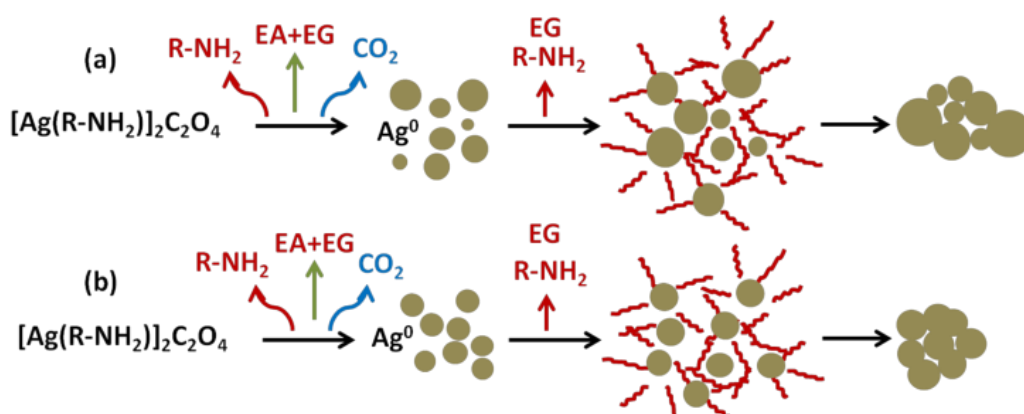


Figure 7.9 Schematic illustration of the influences of amine types on morphology of silver film from different silver oxalate inks during sintering process (a) Amines with low boiling point and short carbon chain ; (b) Amines with high boiling point and long carbon chain. For amines with low boiling point and short carbon chain, large changes in concentrations due to the rapid evaporation could cause a broad nucleation event, thereby leading to a film with wide particle size distributions and porous structure. For amines with high boiling point and long carbon chain, they evaporated slowly and can encapsulate the produced silver nanoparticles and restrict their growth, so a dense film with narrow size distributions was produced

The influences of amine types on microstructure morphology of silver films from different silver oxalate inks during the sintering process, were analyzed and shown schematically in Figure 7.9. For the silver-amine complex ink, the sintering process is a type of in situ particle synthesis process [150]. For amines with short carbon chain

lengths, they have a low boiling point and their silver complexes have high decomposition temperature so that the amine in the ink would evaporate prior to the decomposition of the silver-amine complex during the sintering process. The decrease of amine concentration could cause a broad nucleation event (Figure 7.9a) and leading to coalescence of the particles [161]. Low concentrations of amine will restrict the mobility of particles. Besides, evaporation of ethanol in solvent occurred at this time. Both effects can produce bubbles that need to go through the films consisting of silver nanoparticles, so the films have pores (Figure 7.8a<sub>1</sub> and 8b<sub>1</sub>) [27]. On the contrary, in terms of the amines with a long-chain, they evaporate slowly and the unevaporated amine would encapsulate the produced silver particles and restrict their growth [161], yielding a film with narrow particle size distributions (Figure 7.9b, Figure 7.8c<sub>1</sub>, 7.8d<sub>1</sub> and 7.8e<sub>1</sub>). For the film derived from ethanolamine, as ethanolamine has a higher boiling point of 170 °C, thereby most of them still left in the film, surrounding the silver particles and separating them from the connection between each other (Figure 7.8f<sub>1</sub>). This is why its film is not conductive.



Figure 7.10 EDS results of silver films sintered at 150°C for 60min from different silver oxalate inks, (a) Ethylenediamine, (b) 1,2-diaminopropane, (c) butylamine, (d) hexylamine, (e) octylamine, (f) ethanolamine

The chemical composition of the films derived from inks formulated with various amines was identified by EDS surface energy spectrum, which can be seen in Figure 7.10. Clearly, three elements (C, O, and Ag) were detected in each film, which is in accordance with the original chemical composition of the compounds. The film from 1,2-diaminopropane derived ink had the highest Ag content with 96.03% and fewer

organic residues while the Ag content in the film produced by ethanolamine based ink was the least and the amount of organic residue is up to 40%, which is in agreement with the previous analysis.

Based on the above analysis, it can be concluded that highly conductive silver films from silver-amine complex inks with controlled microstructure features can be achieved by selection of appropriate amines. The ink formulated using 1,2-diaminopropane has good stability and complete and uniform surface structure consisting of big silver crystals but with some voids and a relatively high sintering temperature necessary for decomposition of the complex. The ink formulated using butylamine has a dense structure consisting of small silver crystals and low sintering temperature for decomposition of the complex but the film surface is not uniform and the ink is not stable after long time storage (60 days).

#### 7.3.4 Film quality improvement by blended amines

According to the above experimental results and the previous work by Wu et al. [162], Dong et al. [150] and Yabuki et al. [163], a blend of butylamine and 1,2-diaminopropane was chosen to improve the film quality of the ink.

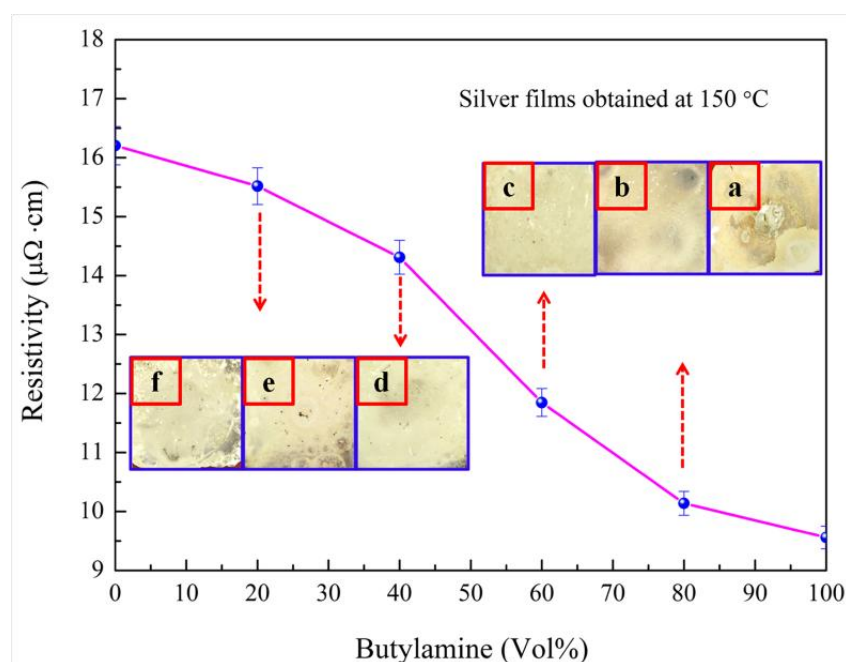


Figure 7.11 Resistivity of silver films sintered at 150°C for 60min from a silver oxalate ink prepared using a blend of butylamine and 1,2-diaminopropane in different volume ratios; (a) 1:0, (b) 4:1, (c) 3:2, (d) 2:3, (e) 1:4 and (f) 0:1

The resistivity and surface morphology of the film sintered at 150 °C from silver oxalate

ink prepared using a blend of butylamine and 1,2-diaminopropane in different ratios, are shown in Figure 7.11 and Figure 7.12 respectively. The molar ratio of blended amines to silver oxalate in the ink was kept at 2:1 and the x-axis shows the volume fraction of butylamine in the blended amines. The Y-axis shows the corresponding resistivity of the film from blended amines.

Clearly, the resistivity of the film decreased with the increased volume of butylamine in the blended amine. Meanwhile, the film quality was also improved (Figure 7.11 inset) along with a surface change from loose to dense distribution of silver particles. However, there is an optimum ratio where the film quality and resistivity have the best balance, which was 60% butylamine and 40% 1,2-diaminopropane.

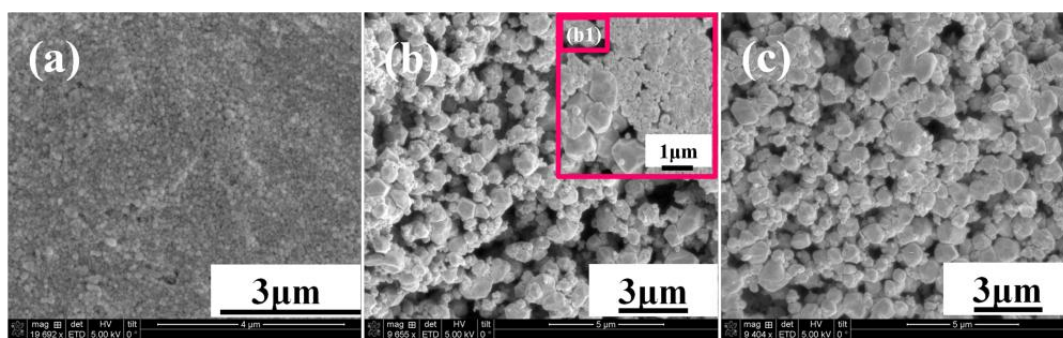


Figure 7.12 SEM images of silver films sintered at 150°C for 60min from a silver oxalate ink prepared using a blend of butylamine and 1,2-diaminopropane in different volume, (a) 100% butylamine, (b) 60% butylamine and 40% 1,2-diaminopropane, (c) 100% 1,2-diaminopropane (b<sub>1</sub> is high magnification images of figure b)

SEM was employed to investigate the surface morphology differences of the films sintered at 150 °C with butylamine of 0%, 60% and 100% in the blended amines, the results are shown in Figure 7.12. The surface morphology of the film derived from the ink containing butylamine only showed a uniform and dense surface structure consisting of spherical silver nanoparticles with small size and good contact. By contrast, the film derived from the ink containing 1,2-diaminopropane only has a much loose microstructure that is composed of well-defined silver particles with large size. The film produced from the complex ink with 60% butylamine and 40% 1,2-diaminopropane had a mean particle size that is between the values of the inks containing 100% butylamine or 1,2-diaminopropane. In further analysis, the crystallite size of silver nanoparticles in each film was calculated by using its XRD data. Indeed, the structure of the film from the blended amine had the particle size (49.57nm) between that of the silver-1,2-diaminopropane complex ink (53.84nm) and that of the silver-butylamine

complex ink (39.59nm). It should be noted here that the crystallite size of silver nanoparticles calculated using the XRD data belongs to the primary particle and is different from the size shown in the SEM images because the latter is from aggregated particles (secondary particles).

Since a packed structure with smaller particles filling the space between bigger particles could be obtained (Figure 7.12b<sub>1</sub>) because of the balance of the high nucleation rate and the weakened Ostwald ripening effect [162], the film quality was improved significantly.

## 7.4 Optimal Silver Ink

### 7.4.1 Film microstructure evolution

Figure 7.13 (a-c) shows the changes in surface morphology of the silver films derived from the optimal ink (60% butylamine and 40% 1,2-diaminopropane) at a temperature of 150 °C for different sintering time.

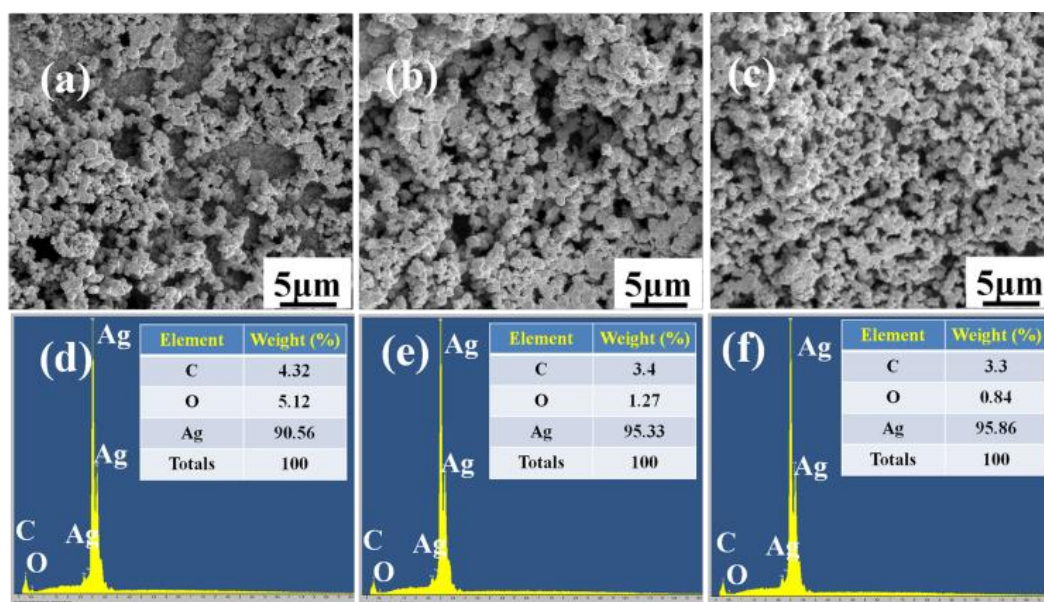


Figure 7.13 SEM and EDS images of silver films sintered at 150°C for (a, d) 10, (b, e) 30 and (c, f) 60min from the optimal silver oxalate ink

The film sintered for 10 min is not uniform and consisted of big particles and small ones on their surface. These particles have irregular shapes and have a wide range of sizes (Figure 7.13a). With the increase of the sintering time, the films showed a microstructure that mainly consists of big particles and have some voids on its surface (Figure 7.13b). The film sintered for 60 min had a flat surface profile where big silver

particles have good contact with each other. Meanwhile, the voids became less (Figure 7.13c). As discussed before, the film morphology is dependent on the solvent and free-amine evaporation rate and thermal decomposition of the silver complex. When the sintering time is 10 minutes, solvent evaporation and decomposition of the silver-amine complex both are inadequate, thereby resulting in an uneven film consisting of small silver particles generated mainly by the silver-butylamine complex. For a sintering time of 30 minutes, the film is uniform as there is material redistribution due to decomposition of silver-1, 2-diaminopropane complex in the film. Further increase in sintering time results in improved surface morphology as the small particles could be connected to the larger particles.

The arrangement of this surface microstructure was related to particle nucleation and growth. In this case, nucleation of small particles produced from the decomposition of silver-butylamine complex occurred in the first stage, and then the growth of the particles followed. In the last stage, nucleation and growth of big silver particles due to silver-1, 2-diaminopropane complex occurred in the remaining ink. Thus, the film formed by using blend amines produced two sizes of particles.

EDS analysis was employed to investigate the changes in chemical composition, as shown in Figure 7.13 (d-e). As the sintering time was increased from 10 to 30 minutes, obvious changes in Ag and C content were observed. After 30min, the change was not much, indicating that the organic molecules were decomposed and volatilized mostly and the decomposition of silver-amine complex continued to a large extent.

#### ***7.4.2 Film electrical performance***

The resistivity of the silver films obtained at various times from the optimal silver ink was calculated from the measured sheet resistance and film thickness ( $1.5\pm 0.3\mu\text{m}$ ) and the results are given in Figure 7.14. As the sintering time was increased from 10 to 60 minutes, the resistivity decreased gradually from  $16.44\ \mu\Omega\cdot\text{cm}$  to  $11.84\ \mu\Omega\cdot\text{cm}$ . After 30 minutes, there is no significant improvement in resistivity. Thus, sintering for 30min was long enough to form a film with favorable conductivity. The decrease in resistivity with time can also be explained by the fact that more silver nanoparticles are generated, becoming larger and more closely connected. The resistivity of the film stored for 9 months from the optimal silver ink was also measured to be  $13.14\mu\Omega\cdot\text{cm}$ , which was only a slight decrease, indicating that the film has good stability.



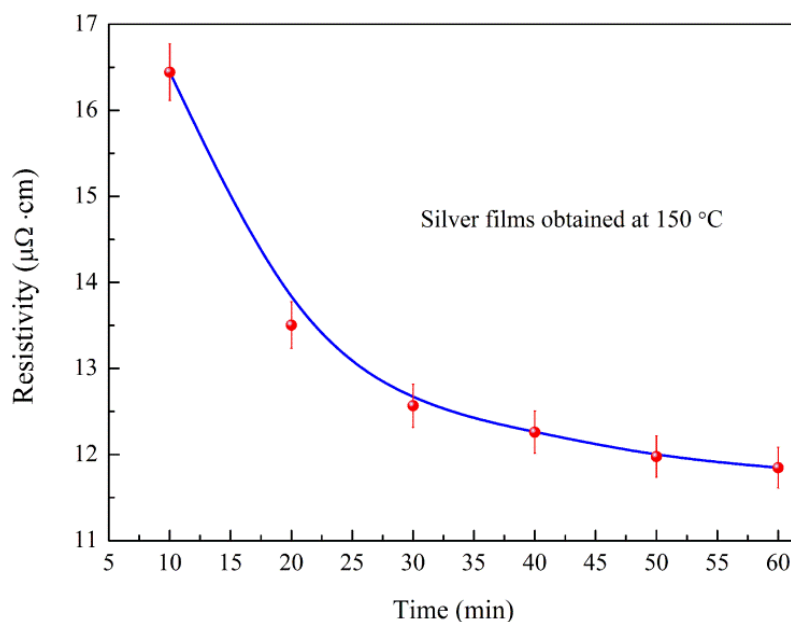


Figure 7.14 Resistivity of silver films sintered at 150°C for 60min from optimal silver oxalate ink

## 7.5 Application

### 7.5.1 Conductive pen preparation

Gel-ink pen which is composed of a hollow cylinder with 12.3cm in length and 3.8mm in diameter, and a pen-head with 1.2cm in length and 1 mm in diameter was purchased from Beijing M&G Stationery Store. For the application, the pen was washed with deionized water and ethanol, and then filled with the as-prepared ink for writing conductive tracks.

### 7.5.2 Direct-writing research

The dimensional stability of the written dots was investigated, shown in Figure 7.15. It can be seen that the dot size increases with the increase of deposition time. This means that the ink has low viscosity and surface tension, and flows out of the pen head easily.

Figure 7.16 reveals the relationship between the film resistance and the writing speed. As the writing speed was increased from 0.25 cm/s to 2.25cm/s, the resistance increased rapidly. This is easy to be understood. The faster is the writing, the smaller the ink amount deposited on the substrate. Thus, considering the pattern resolution, short deposition time (2s) and fast writing speed (0.25cm/s) should be adopted when preparing a pattern.

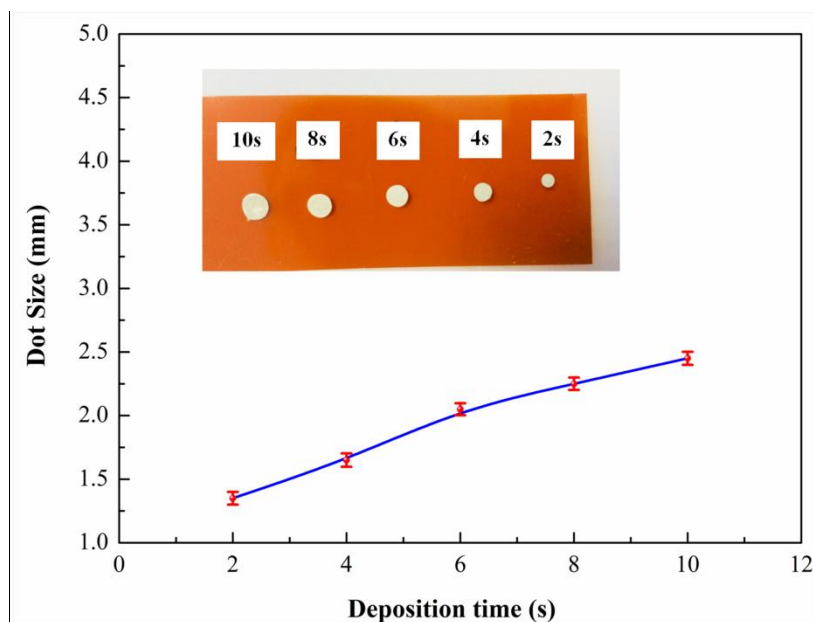


Figure 7.15 Relationship between deposition time and the dot size (inset, image of dots with different size)

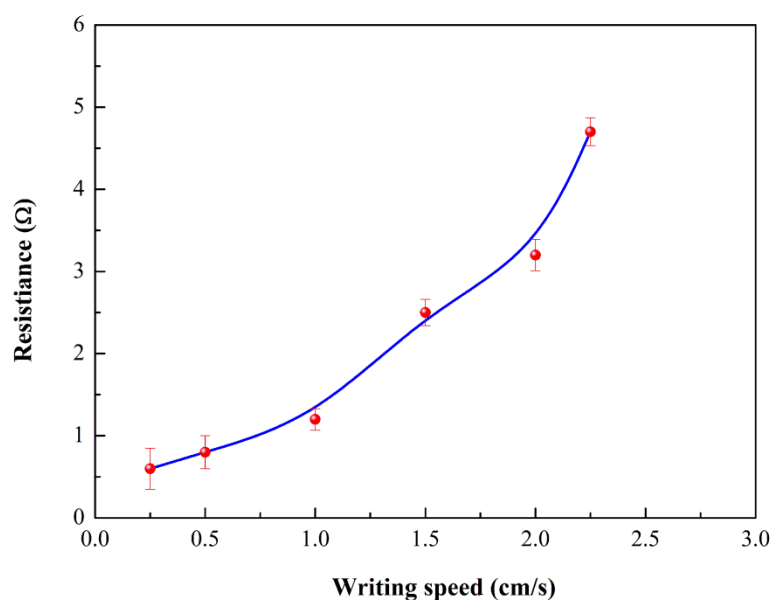


Figure 7.16 Relationship between the film resistance and writing speed

### 7.5.3 Application

For practical application, a simple circuit was directly made on a PI substrate by drawing the optimal silver ink using the pen (Figure 7.17). After connecting an LED (MCL053GD, 20mA, 2.1V) to the written circuit from the silver ink and using a DC voltage of 5V and a protective resistor of 150  $\Omega$ , the LED was operated successfully, even when the PI film and hence the circuit was bent. The current of the circuit was 19.6mA. The circuit operation demonstrates useful conductivity of the silver lines.



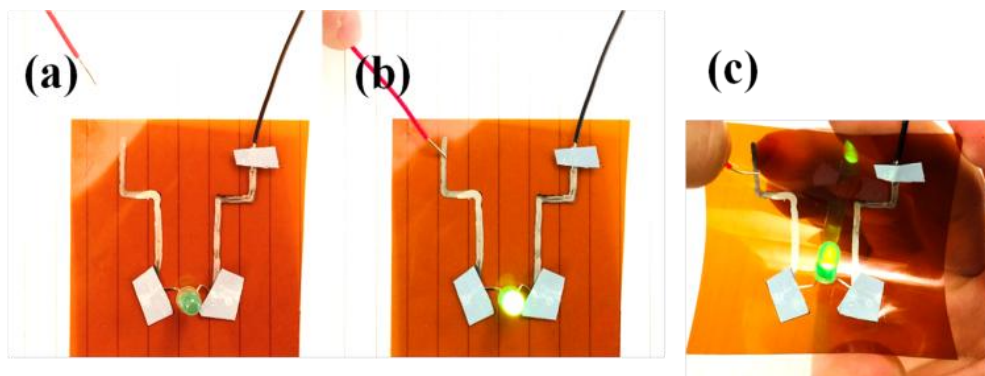


Figure 7.17 The conductive effect of silver circuit with different conditions (a, b. connected with and without a voltage; c. bent)

## 7.6 Conclusions

In summary, four monoamines and two diamines were used to formulate silver oxalate inks, where the amine types on the thermal property, stability and electrical performance of the resulted inks were studied. The results show that the ink properties are strongly related to the amine used in each case as the latter determines the decomposition temperature of the ink. It is also shown that it has a strong influence on the morphology of the resultant film during sintering process. Appropriate selection of amines can lead to highly conductive silver films. The chemical reactions occurring within the ink and the film formation process were also studied. An optimal silver oxalate ink was synthesized by using blended amines as the ligands finally, producing a silver film with good quality and conductivity at 150 °C.

## Chapter 8 Conclusions and Future Work

### 8.1 Conclusions

Undoubtedly, flexible electronics represents an important direction of future electronics and are opening up novel and different applications. However, the successful development of flexible electronics, as a supplement to the silicon-based microelectronics, depends on the development of new materials.

In this thesis, firstly, the development of the formation and patterning of metal and graphene related inks was reviewed. The challenges and opportunities during the development of flexible electronics have been discussed. Further development will be focused on the preparation and optimization of conductive ink materials, especially on the metal-based inks. A rational combination of formulation-patterning-sintering of inks would be a necessary direction. Metal hybrid ink, such as copper-silver or silver-graphene, is also a possible route, which can strike a balance between cost, synthesis process, conductivity and long-term stability.

Secondly, an Ag/rGO hybrid ink was formulated by a one-step method, showing a good electrical performance after sintering at 230 °C with a resistivity of 24.5  $\mu\Omega\cdot\text{cm}$ . A remarkable reduction in resistivity by a factor of above 200 has been observed in Ag/rGO films sintered at 150 °C as compared with that of the Ag films, which was attributed to the role of rGO nanoplatelets in forming bridges to facilitate charge transfer between the silver particles. The research results indicate that it is possible to improve the conductivity of organic silver ink at low sintering temperature while reducing its cost.

Favorable conductivity at temperatures around 150°C is desirable as it would widen the application of silver organic inks on a variety of flexible substrates. Towards this aim, a silver citrate ink with decomposition and self-reduction mechanisms was then developed. It has been shown that the ink is capable of producing silver films with good uniformity and electrical performance (79.4  $\mu\Omega\cdot\text{cm}$ ) on polymer substrates after sintering at 155°C. The active role of the solvent and the underlying chemical changes in the film formation process were clarified. The defects such as voids and cracks as well as coffee ring effect, which are often associated with films from organic silver inks, were effectively eliminated by using both mechanisms in the film formation process.

For organic silver ink, the selection of silver precursors was critical because it determines the final thermal and electrical properties of the ink. Therefore, five types of organic silver precursors were synthesized and investigated subsequently. It was found that silver oxalate had the ideal thermal property and showed the lowest decomposition temperature. An ink was then formulated using as-prepared silver oxalate and butylamine, which could produce silver films with low resistivity ( $15.72 \mu\Omega\cdot\text{cm}$ ) after sintering at  $130^\circ\text{C}$ . Silver oxalate powders with good properties and a solid amine complex with lower decomposition temperature were obtained, both differing from those reported in the literature. The influence of the factors on the electrical properties of the produced silver films such as sintering temperature and time was studied and the relationship between them was demonstrated.

Amine is also a critical factor in ink formulation since it can decrease the sintering temperature of organic silver precursors via forming a soluble silver-amine complex, making the ink suitable for a variety of plastic substrates. Therefore, the effects of amine types on the properties of the formulated silver oxalate ink were studied in detail. It was found that highly conductive silver films from silver-amine complex inks with controlled microstructure features can be achieved by selection of appropriate amines. The ink formulated using 1,2-diaminopropane has good stability and uniform surface structure but with some voids and a relatively high sintering temperature necessary for decomposition of the complex. The ink formulated using butylamine has a dense structure and low sintering temperature for decomposition of the complex but the ink is not stable after long time storage. An optimal silver oxalate ink was finally designed and formulated using a blend of butylamine and 1,2-diaminopropane as ligands to improve the quality and the electrical performance of the resultant film, which could produce silver films with good quality and conductivity at  $150^\circ\text{C}$  (resistivity  $11.84 \mu\Omega\cdot\text{cm}$ ). A simple circuit was successfully made on a polyimide substrate by drawing conductive traces using a pen.

From the above results, it can be seen that the resistivity around  $10^{-5}\Omega\cdot\text{cm}$  has already been obtained in each case, higher than that of bulk silver ( $1.59 \mu\Omega\cdot\text{cm}$ ), but can meet the electrical requirements of most electronic products. As for the reason, it is associated with the characteristics of organic silver precursors and sintering parameters as well as the organic residues. Comparing with Ag/rGO hybrid ink and silver citrate ink, the

optimal silver oxalate ink has the best performance in the research work since it can produce silver films with a resistivity equivalent to 10 times of bulk silver at a relatively low temperature (150°C) in 15minutes.

## **8.2 Future Work**

Although progress has been made in the development of organic silver inks using non-toxic solvents by simple synthetic methods and favorable conductivity has been achieved at low sintering temperature, the printability of the obtained inks is still an issue to be solved in order to obtain patterns with high resolution for practical applications.

So further research should be carried out in the following areas: (i) the fluidic properties of as-prepared silver inks, such as viscosity, surface tension and wettability, should be specifically adjusted to make the inks compatible with a commercial printer and a flexible substrate; (ii) it is necessary to study the printability of the as-prepared silver inks, where the printing parameters are carefully controlled to obtain tracks or patterns with high resolution and good quality; (iii) simple electronic or energy storage devices can be fabricated using the ink-jet printing to test the performance of the inks; and (iv) new sintering methods can be explored for energy efficient manufacturing of flexible electronics.

## References

1. Z. Yin, Y. Huang, N. Bu, X. Wang and Y. Xiong, *Inkjet printing for flexible electronics: Materials, processes and equipments*, Chinese Science Bulletin, **55**, 3383-3407 (2010).
2. A. Kamyshny and S. Magdassi, *Conductive nanomaterials for printed electronics*, Small, **10**, 3515-3535 (2014).
3. N. Perinka, C. H. Kim, M. Kaplanova and Y. Bonnassieux, *Preparation and characterization of thin conductive polymer films on the base of PEDOT: PSS by ink-jet printing*, Physics Procedia, **44**, 120-129 (2013).
4. W. R. Small, Inkjet Printing of Transparent, *Electrically conducting single-walled carbon-nanotube composites*. Small, **3**, 1500-1503 (2007).
5. J. W. Han, B. Kim, J. Li and M. Meyyappan, *Carbon nanotube ink for writing on cellulose paper*, Materials Research Bulletin, **50**, 249-253 (2014).
6. C. N. Chen, C. P. Chen, T. Y. Dong, T. C. Chang, M. C. Chen, H. T. Chen and I. G. Chen, *Using nanoparticles as direct-injection printing ink to fabricate conductive silver features on a transparent flexible PET substrate at room temperature*, Acta Materialia, **60**, 5914-5924 (2012).
7. S. Magdassi, M. Grouchko, O. Berezin and A. Kamyshny, *Triggering the sintering of silver nanoparticles at room temperature*, ACS nano, **4**, 1943-1948 (2010).
8. S. B. Walker and J. A. Lewis, *Reactive silver inks for patterning high-conductivity features at mild temperatures*, Journal of the American Chemical Society, **134**, 1419-1421 (2012).
9. S. Jeong, H. C. Song, W. W. Lee, Y. Choi, S. S. Lee and B. H. Ryu, *Combined role of well-dispersed aqueous Ag ink and the molecular adhesive layer in inkjet printing the narrow and highly conductive Ag features on a glass substrate*, The Journal of Physical Chemistry C, **114**, 22277-22283 (2010).
10. R. Shankar, L. Groven, A. Amert, K. W. Whites and J. J. Kellar, *Non-aqueous synthesis of silver nanoparticles using tin acetate as a reducing agent for the conductive ink formulation in printed electronics*, Journal of Materials Chemistry, **21**, 10871-10877 (2011).
11. B. Y. Ahn, D. J. Lorang and J. A. Lewis, *Transparent conductive grids via direct writing of silver nanoparticle inks*, Nanoscale, **3**, 2700-2702 (2011).
12. W. D. Yang, C. Y. Liu, Z. Y. Zhang, Y. Liu and S. D. Nie, *One step synthesis of uniform organic silver ink drawing directly on paper substrates*, Journal of Materials

- Chemistry, **22**, 23012-23016 (2012).
13. Y. Chang, D. Y. Wang, Y. L. Tai and Z. G. Yang, *Preparation, characterization and reaction mechanism of a novel silver-organic conductive ink*, Journal of Materials Chemistry, **22**, 25296-25301 (2012).
  14. C. N. Chen, T. Y. Dong, T. C. Chang, M. C. Chen, H. L. Tsai and W. S. Hwang, *Solution-based  $\beta$ -diketonate silver ink for direct printing of highly conductive features on a flexible substrate*, Journal of Materials Chemistry C, **1**, 5161-5168 (2013).
  15. W. Yang, C. Liu and C. Wang, *Synthesis and patterning of metal-based inks*, Science Letters Journal, **4**, 178 (2015).
  16. H. H. Lee, K. S. Chou and K. C. Huang, *Inkjet printing of nanosized silver colloids*, Nanotechnology, **16**, 2436 (2005).
  17. J. G. Bai, K. D. Creehan and H. A. Kuhn, *Inkjet printable nanosilver suspensions for enhanced sintering quality in rapid manufacturing*, Nanotechnology, **18**, 185701 (2007).
  18. G. Cummins and M. P. Y. Desmulliez, *Inkjet printing of conductive materials: a review*, Circuit World, **38**, 193-213 (2012).
  19. I. Jung, Y. H. Jo, I. Kim and H. M. Lee, *A simple process for synthesis of Ag nanoparticles and sintering of conductive ink for use in printed electronics*, Journal of electronic materials, **41**, 115-121 (2012).
  20. S. Jeong, H. C. Song, W. W. Lee, Y. Choi and B. H. Ryu, *Preparation of aqueous Ag Ink with long-term dispersion stability and its inkjet printing for fabricating conductive tracks on a polyimide film*, Journal of Applied Physics, **108**, 102805 (2010).
  21. Y. Lee, J. R. Choi, K. J. Lee, N. E. Stott and D. Kim, *Large-scale synthesis of copper nanoparticles by chemically controlled reduction for applications of inkjet-printed electronics*, Nanotechnology, **19**, 415604 (2008).
  22. Y. Mou, H. Cheng, H. Wang, Q. Sun, J. Liu, Y. Peng and M. Chen, *Facile preparation of stable reactive silver ink for highly conductive and flexible electrodes*, Applied Surface Science, **475**, 75-82 (2019).
  23. B. K. Park, D. Kim, S. Jeong, J. Moon and J. S. Kim, *Direct writing of copper conductive patterns by ink-jet printing*, Thin Solid Films, **515**, 7706-7711 (2007).
  24. S. Jeong, S. H. Lee, Y. Jo, S. S. Lee, Y. H. Seo, B. W. Ahn, G. Kim, G. E. Jang, J. U. Park and B. H. Ryu, *Air-stable, surface-oxide free Cu nanoparticles for highly conductive Cu ink and their application to printed graphene transistors*, Journal of

Materials Chemistry C, **1**, 2704-2710 (2013).

25. I. K. Shim, Y. S. Oh and J. W. Joung, *Core-shell structure metal nanoparticles and its manufacturing method*, Google Patents, (2009).
26. J. T. Wu, S. L. C. Hsu, M. H. Tsai and W. S. Hwang, *Inkjet printing of low-temperature cured silver patterns by using AgNO<sub>3</sub>/1-dimethylamino-2-propanol inks on polymer substrates*, The Journal of Physical Chemistry C, **115**, 10940-10945 (2011).
27. Y. Dong, X. Li, S. Liu, Q. Zhu, J. G. Li and X. Sun, *Facile synthesis of high silver content MOD ink by using silver oxalate precursor for inkjet printing applications*, Thin Solid Films, **589**, 381-387 (2015).
28. Q. J. Huang, W. F. Shen, Q. S. Xu, R. Q. Tan and W. J. Song, *Properties of polyacrylic acid-coated silver nanoparticle ink for inkjet printing conductive tracks on paper with high conductivity*, Materials Chemistry and Physics, **147**, 550-556 (2014).
29. J. T. Wu, S. L. C. Hsu, M. H. Tsai, Y. F. Liu and W. S. Hwang, *Direct ink-jet printing of silver nitrate-silver nanowire hybrid inks to fabricate silver conductive lines*, Journal of Materials Chemistry, **22**, 15599-15605 (2012).
30. D. Y. Wang, Y. Chang, Q. S. Lu and Z. G. Yang, *Nano-organic silver composite conductive ink for flexible printed circuit*, Materials Technology: Advanced Performance Materials, **30**, 54-59 (2015).
31. Y. L. Tai, Z. G. Yang and Z. D. Li, *A promising approach to conductive patterns with high efficiency for flexible electronics*, Applied Surface Science, **257**, 7096-7100 (2011).
32. X. Nie, H. Wang and J. Zou, *Inkjet printing of silver citrate conductive ink on PET substrate*, Applied surface science, **261**, 554-560 (2012).
33. D. Y. Wang, Y. Chang, Y. X. Wang, Q. Zhang and Z. G. Yang, *Green water-based silver nanoplate conductive ink for flexible printed*, Materials Technology, **31** (1), 32-37 (2016).
34. Y. H. Choi, J. Lee, S. J. Kim, D. H. Yeon and Y. Byun, *Highly conductive polymer-decorated Cu electrode films printed on glass substrates with novel precursor-based inks and pastes*. Journal of Materials Chemistry, **22**, 3624-3631 (2012).
35. Y. I. Lee and Y. H. Choa, *Adhesion enhancement of ink-jet printed conductive copper patterns on a flexible substrate*, Journal of Materials Chemistry, **22**, 12517-12522 (2012).

36. T. Yonezawa, H. Tsukamoto, Y. Q. Yong, M. T. Nguyen and M. Matsubara, *Low temperature sintering process of copper fine particles under nitrogen gas flow with Cu<sup>2+</sup>-alkanolamine metallacycle compounds for electrically conductive layer formation*, RSC Advances, **6**, 12048-12052 (2016).
37. T. Y. Dong, H. Wu, C. Huang, J. M. Song, I. G. Chen and T. H. Kao, *Octanethiolated Cu and Cu<sub>2</sub>O nanoparticles as ink to form metallic copper film*, Applied Surface Science, **255**, 3891-3896 (2009).
38. D. Deng, Y. Cheng, Y. Jin, T. Qi and F. Xiao, *Antioxidative effect of lactic acid-stabilized copper nanoparticles prepared in aqueous solution*, Journal of Materials Chemistry, **22**, 23989-23995 (2012).
39. D. Deng, Y. Jin, Y. Cheng, T. Qi and F. Xiao, *Copper nanoparticles: aqueous phase synthesis and conductive films fabrication at low sintering temperature*, ACS Appl. Mater. Interfaces, **5**, 3839-3846 (2013).
40. J. S. Kang, H. S. Kim, J. Ryu, H. T. Hahn, S. Jang and J. W. Joung, *Inkjet printed electronics using copper nanoparticle ink*, Journal of Materials Science: Materials in Electronics, **21**, 1213-1220 (2010).
41. X. F. Tang, Z. G. Yang and W. J. Wang, *A simple way of preparing high-concentration and high-purity nano copper colloid for conductive ink in inkjet printing technology*, Colloids and Surfaces A: Physicochemical and Engineering Aspects, **360**, 99-104 (2010).
42. Y. Kim, B. Lee, S. Yang, I. Byun, I. Jeong and S. M. Cho, *Use of copper ink for fabricating conductive electrodes and RFID antenna tags by screen printing*, Current Applied Physics, **12**, 473-478 (2012).
43. N. A. Luechinger, E. K. Athanassiou and W. J. Stark, *Graphene-stabilized copper nanoparticles as an air-stable substitute for silver and gold in low-cost ink-jet printable electronics*, Nanotechnology, **19**, 445201 (2008).
44. Y. Hokita, M. Kanzaki, T. Sugiyama, R. Arakawa and H. Kawasaki, *High-Concentration Synthesis of Sub-10-nm Copper Nanoparticles for Application to Conductive Nanoinks*, ACS Appl. Mater. Interfaces, **7**, 19382-19389 (2015).
45. A. Yabuki, N. Arriffin and M. Yanase, *Low-temperature synthesis of copper conductive film by thermal decomposition of copper-amine complexes*, Thin Solid Films, **519**, 6530-6533 (2011).
46. D. H. Shin, S. Woo, H. Yem, M. Cha, S. Cho, M. Kang, S. Jeong, Y. Kim, K. Kang and Y. Piao, *A Self-reducible and alcohol-soluble copper-based metal-organic decomposition ink for printed electronics*, ACS Appl. Mater. Interfaces, **6**,



- 3312-3319 (2014).
47. T. Qi, Z. Zhang, Y. Li, J. Wang and F. Xiao, *A low temperature self-reducible copper hydroxide amino-alcohol complex catalyzed by formic acid for conductive copper films*, J. Mater. Chem. C, **6**, 11320-11327 (2018).
  48. W. Xu, X. Dai, T. Zhang and T. Wang, *Dual effects of water on the performance of copper complex conductive inks for printed electronics*, Chemical Engineering Science, **190**, 40-47 (2018).
  49. W. D. Yang, C. H. Wang, V. Arrighi, C. Y. Liu and D. Watson, *Microstructure and electrical property of copper films on a flexible substrate formed by an organic ink with 9.6% of Cu content*, Journal of Materials Science: Materials in Electronics, **26**, 8973-8982 (2015).
  50. S. J. Kim, J. Lee, Y. H. Choi, D. H. Yeon and Y. Byun, *Effect of copper concentration in printable copper inks on film fabrication*, Thin Solid Films, **520**, 2731-2734 (2012).
  51. A. Yabuki, Y. Tachibana and I. W. Fathona, *Synthesis of copper conductive film by low-temperature thermal decomposition of copper-aminediol complexes under an air atmosphere*, Materials Chemistry and Physics, **148**, 299-304 (2014).
  52. K. S. Kim, Y. Zhao, H. Jang, S. Y. Lee, J. M. Kim, K. S. Kim, J. H. Ahn, P. Kim, J. Y. Choi and B. H. Hong, *Large-scale pattern growth of graphene films for stretchable transparent electrodes*, Nature, **457**, 706-710 (2009).
  53. X. Li, W. Cai, J. An, S. Kim, J. Nah, D. Yang, R. Piner, A. Velamakanni, I. Jung and E. Tutuc, *Large-area synthesis of high-quality and uniform graphene films on copper foils*, Science, **324**, 1312-1314 (2009).
  54. P. W. Sutter, J. I. Flege and E. A. Sutter, *Epitaxial graphene on ruthenium*, Nature materials, **7**, 406-411 (2008).
  55. N. Xiao, X. Dong, L. Song, D. Liu, Y. Tay, S. Wu, L. J. Li, Y. Zhao, T. Yu and H. Zhang, *Enhanced thermopower of graphene films with oxygen plasma treatment*, ACS Nano, **5**, 2749-2755 (2011).
  56. D. Li, M. B. Mueller, S. Gilje, R. B. Kaner and G. G. Wallace, *Processable aqueous dispersions of graphene nanosheets*, Nature nanotechnology, **3**, 101-105 (2008).
  57. Y. Hernandez, V. Nicolosi, M. Lotya, F. M. Blighe, Z. Sun, S. De, I. McGovern, B. Holland, M. Byrne and Y. K. Gun'Ko, *High-yield production of graphene by liquid-phase exfoliation of graphite*, Nature nanotechnology, **3**, 563-568 (2008).
  58. C. Vallés, C. Drummond, H. Saadaoui, C. A. Furtado, M. He, O. Roubeau, L. Ortolani, M. Monthieux and A. Pénicaud, *Solutions of negatively charged graphene*

- sheets and ribbons*, Journal of the American Chemical Society, **130**, 15802-15804 (2008).
59. M. Lotya, Y. Hernandez, P. J. King, R. J. Smith, V. Nicolosi, L. S. Karlsson, F. M. Blighe, S. De, Z. Wang and I. McGovern, *Liquid phase production of graphene by exfoliation of graphite in surfactant/water solutions*, Journal of the American Chemical Society, **131**, 3611-3620 (2009).
  60. V. Dua, S. P. Surwade, S. Ammu, S. R. Agnihotra, S. Jain, K. E. Roberts, S. Park, R. S. Ruoff and S. K. Manohar, *All-organic vapor sensor using inkjet-printed reduced graphene oxide*, Angewandte Chemie, **122**, 2200-2203 (2010).
  61. L. Huang, Y. Huang, J. Liang, X. Wan and Y. Chen, *Graphene-based conducting inks for direct inkjet printing of flexible conductive patterns and their applications in electric circuits and chemical sensors*, Nano Research, **4**, 675-684 (2011).
  62. J. Li, F. Ye, S. Vaziri, M. Muhammed, M. C. Lemme and M. Ostling, *Efficient inkjet printing of graphene*, Advanced Materials, **25**, 3985-92 (2013).
  63. L. T. Le, M. H. Ervin, H. Qiu, B. E. Fuchs and W. Y. Lee, *Graphene supercapacitor electrodes fabricated by inkjet printing and thermal reduction of graphene oxide*, Electrochemistry Communications, **13**, 355-358 (2011).
  64. M. Gilliam, *Polymer surface treatment and coating technologies*, Handbook of Manufacturing Engineering and Technology, Springer, 99-124 (2015).
  65. W. Yang and C. Wang, *Graphene and the related conductive inks for flexible electronics*, Journal of Materials Chemistry C, **4**, 7193-7207 (2016).
  66. V. Kantola, J. Kulovesi, L. Lahti, R. Lin, M. Zavodchikova and E. Coatan éa, *1.3 Printed Electronics*, Now and Future. Bit Bang 63 (2009).
  67. D. Lupo, W. Clemens, S. Breitung and K. Hecker, *OE-A roadmap for organic and printed electronics*, Applications of Organic and Printed Electronics, Springer, 1-26 (2013).
  68. K. Suganuma, *Introduction to printed electronics*. Springer Science & Business Media, **74** (2014).
  69. W. Wu, *Inorganic nanomaterials for printed electronics: a review*. Nanoscale, **9**, 7342-7372 (2017).
  70. J. Mei, *Formulation and processing of conductive inks for inkjet printing of electrical components*, Doctoral Dissertation, University of Pittsburgh, 15-16 (2005).
  71. A. Kamyshny, J. Steinke and S. Magdassi, *Metal-based inkjet inks for printed electronics*, The Open Applied Physics Journal, **4**, 19-36 (2011).
  72. S. P. Chen, H. L. Chiu, P. H. Wang and Y. C. Liao, *Inkjet printed conductive tracks*

- for printed electronics*, ECS Journal of Solid State Science and Technology, **4**, 3026-3033 (2015).
73. P. J. Yunker, T. Still, M. A. Lohr and A. Yodh, *Suppression of the coffee-ring effect by shape-dependent capillary interactions*, Nature, **476**, 308-311 (2011).
  74. Z. Zhang, X. Zhang, Z. Xin, M. Deng, Y. Wen and Y. Song, *Controlled inkjetting of a conductive pattern of silver nanoparticles based on the coffee-ring effect*, Advanced Materials, **25**, 6714-6718 (2013).
  75. Organic Electronics Association. *OE-A Roadmap for organic and printed electronics*, 3<sup>rd</sup> version, 59 (2009).
  76. A. Russo, B. Y. Ahn, J. J. Adams, E. B. Duoss, J. T. Bernhard and J. A. Lewis, *Pen-on-paper flexible electronics*, Advanced Materials, **23**, 3426-3430 (2011).
  77. S. Walker, *Synthesis and patterning of reactive silver inks*, University of Illinois at Urbana-Champaign (2013).
  78. G. Hu, J. Kang, L. W. T. Ng, X. Zhu, R. C. T. Howe, C. G. Jones, M. C. Hersam and T. Hasan, *Functional inks and printing of two-dimensional materials*, Chemical Society Review., **47**, 3265-3300 (2018).
  79. S. Binder, M. Glatthaar and E. Rädlein, *Analytical investigation of aerosol jet printing*. Aerosol Science and Technology, **48**, 924-929 (2014).
  80. B. Y. Ahn, D. J. Lorang and J. A. Lewis, *Transparent conductive grids via direct writing of silver nanoparticle inks*, Nanoscale, **3**, 2700-2702 (2011).
  81. S. Magdassi, M. Grouchko, O. Berezin and A. Kamyshny, *Triggering the sintering of silver nanoparticles at room temperature*, ACS nano, **4**, 1943-1948 (2010).
  82. M. Grouchko, A. Kamyshny, C. F. Mihailescu, D. F. Anghel and S. Magdassi, *Conductive inks with a "built-in" mechanism that enables sintering at room temperature*, ACS nano, **5**, 3354-3359 (2011).
  83. A. Kosmala, R. Wright, Q. Zhang and P. Kirby, *Synthesis of silver nano particles and fabrication of aqueous Ag inks for inkjet printing*, Materials Chemistry and Physics, **129**, 1075-1080 (2011).
  84. B. T. Anto, S. Sivaramakrishnan, L. L. Chua and P. K. Ho, *Hydrophilic sparse ionic monolayer-protected metal nanoparticles: highly concentrated nano-Au and nano-Ag inks that can be sintered to near-bulk conductivity at 150 °C*. Advanced Functional Materials, **20**, 296-303 (2010).
  85. I. K. Shim, Y. I. Lee, K. J. Lee and J. Joung, *An organometallic route to highly monodispersed silver nanoparticles and their application to ink-jet printing*, Materials Chemistry and Physics, **110**, 316-321 (2008).

86. Z. L. Zhang, X. Y. Zhang, Z. Q. Xin, M. M. Deng, Y. Q. Wen and Y. L. Song, *Synthesis of monodisperse silver nanoparticles for ink-jet printed flexible electronics*, *Nanotechnology*, **22**, 1-8 (2011).
87. M. A. H. Khondoker, S. C. Mun and J. Kim, *Synthesis and characterization of conductive silver ink for electrode printing on cellulose film*. *Applied Physics A*, **112**, 411-418 (2013).
88. S. Jeong, H. C. Song, W. W. Lee, Y. Choi and B. H. Ryu, *Preparation of aqueous Ag Ink with long-term dispersion stability and its inkjet printing for fabricating conductive tracks on a polyimide film*, *Journal of Applied Physics*, **108**, 1-5 (2010).
89. W. F. Shen, X. P. Zhang, Q. J. Huang, Q. S. Xu and W. J. Song, *Preparation of solid silver nanoparticles for inkjet printed flexible electronics with high conductivity*, *Nanoscale*, **6**, 1622-1628 (2014).
90. W. Yang, C. Liu, Z. Zhang, Y. Liu and S. Nie, *Paper-based nanosilver conductive ink*, *Journal of Materials Science: Materials in Electronics*, **24**, 628-634 (2013).
91. J. Mei, M. R. Lovell and M. H. Mickle, *Formulation and processing of novel conductive solution inks in continuous inkjet printing of 3-D electric circuits*, *IEEE transactions on electronics packaging manufacturing*, **28**, 265-273 (2005).
92. A. L. Dearden, P. J. Smith, D. Y. Shin, N. Reis, B. Derby and P. O'Brien, *A low curing temperature silver ink for use in ink-jet printing and subsequent production of conductive tracks*, *Macromolecular Rapid Communications*, **26**, 315-318 (2005).
93. S. F. Jahn, T. Blaudeck, R. R. Baumann, A. Jakob, P. Ecorchard, T. Ruffer, H. Lang and P. Schmidt, *Inkjet printing of conductive silver patterns by using the first aqueous particle-free MOD ink without additional stabilizing ligands*, *Chemistry of Materials*, **22**, 3067-3071 (2010).
94. J. Perelaer, B. J. de Gans and U. S. Schubert, *Ink-jet printing and microwave sintering of conductive silver tracks*, *Advanced materials*, **18**, 2101-2104 (2006).
95. J. J. Valetton, K. Hermans, C. W. Bastiaansen, D. J. Broer, J. Perelaer, U. S. Schubert, G. P. Crawford and P. J. Smith, *Room temperature preparation of conductive silver features using spin-coating and inkjet printing*, *Journal of Materials Chemistry*, **20**, 543-546 (2010).
96. T. Ang, T. Wee and W. Chin, *Three-dimensional self-assembled monolayer (3D SAM) of n-alkanethiols on copper nanoclusters*, *The Journal of Physical Chemistry B*, **108**, 11001-11010 (2004).
97. P. Kanninen, C. Johans, J. Merta and K. Kontturi, *Influence of ligand structure on the stability and oxidation of copper nanoparticles*, *Journal of colloid and interface*

- science, **318**, 88-95 (2008).
98. Y. Kobayashi, S. Ishida, K. Ihara, Y. Yasuda, T. Morita and S. Yamada, *Synthesis of metallic copper nanoparticles coated with polypyrrole*, Colloid and Polymer Science, **287**, 877-880 (2009).
  99. P. Pulkkinen, J. Shan, K. Leppänen, A. Käsäkoski, A. Laiho, M. Järn and H. Tenhu, *Poly (ethylene imine) and tetraethylenepentamine as protecting agents for metallic copper nanoparticles*, ACS Applied Materials & Interfaces, **1**, 519-525 (2009).
  100. W. Yang, C. Liu, Z. Zhang, Y. Liu and S. Nie, *Preparation and conductive mechanism of copper nanoparticles ink*, Journal of Materials Science: Materials in Electronics, **24**, 5175-5182 (2013).
  101. S. Jeong, K. Woo, D. Kim, S. Lim, J. S. Kim, H. Shin, Y. Xia and J. Moon, *Controlling the thickness of the surface oxide layer on Cu nanoparticles for the fabrication of conductive structures by ink-jet printing*, Advanced Functional Materials, **18**, 679-686 (2008).
  102. M. Grouchko, A. Kamyshny and S. Magdassi, *Formation of air-stable copper-silver core-shell nanoparticles for inkjet printing*, Journal of Materials Chemistry, **19**, 3057-3062 (2009).
  103. D. Adner, F. M. Wolf, S. Möckel, J. Perelaer, U. S. Schubert and H. Lang, *Copper (II) ethylene glycol carboxylates as precursors for inkjet printing of conductive copper patterns*, Thin Solid Films, **565**, 143-148 (2014).
  104. D. Y. Deng, T. K. Qi, Y. R. Cheng, Y. X. Jin and F. Xiao, *Copper carboxylate with different carbon chain lengths as metal-organic decomposition ink*, Journal of Materials Science: Materials in Electronics, **25**, 390-397 (2014).
  105. G. G. Rozenberg, E. Bresler, S. P. Speakman, C. Jeynes and J. H. Steinke, *Patterned low temperature copper-rich deposits using inkjet printing*, Applied physics letters, **81**, 5249-5251 (2002).
  106. B. Y. Wang, T. H. Yoo, Y. W. Song, D. S. Lim and Y. J. Oh, *Cu ion ink for a flexible substrate and highly conductive patterning by intensive pulsed light sintering*, ACS Applied Materials & Interfaces, **5**, 4113-4119 (2013).
  107. Y. Farraj, M. Grouchko and S. Magdassi, *Self-reduction of a copper complex MOD ink for inkjet printing conductive patterns on plastics*, Chemical Communications, **51**, 1587-1590 (2015).
  108. W. D. Yang, C. Y. Liu, Z. Y. Zhang, Y. Liu and S. D. Nie, *Copper inks formed using short carbon chain organic Cu-precursors*, RSC Advances, **4**, 60144-60147 (2014).
  109. R. Dharmadasa, M. Jha, D. A. Amos and T. Druffel, *Room temperature synthesis of*

- a copper ink for the intense pulsed light sintering of conductive copper films*. ACS Applied Materials & Interfaces, **5**, 13227-13234 (2013).
110. T. Araki, T. Sugahara, J. Jiu, S. Nagao, M. Nogi, H. Koga, H. Uchida, K. Shinozaki and K. Suganuma, *Cu salt ink formulation for printed electronics using photonic sintering*, Langmuir, **29**, 11192-11197 (2013).
  111. J. Lee, B. Lee, S. Jeong, Y. Kim and M. Lee, *Enhanced surface coverage and conductivity of Cu complex ink-coated films by laser sintering*, Thin Solid Films, **564**, 264-268 (2014).
  112. J. Lee, B. Lee, S. Jeong, Y. Kim and M. Lee, *Microstructure and electrical property of laser-sintered Cu complex ink*, Applied Surface Science, **307**, 42-45 (2014).
  113. S. K. Del, R. Bornemann, A. Bablich, H. Schäfer-Eberwein, J. Li, T. Kowald, M. Östling, P. Haring Bolívar and M. C. Lemme, *Optimizing the optical and electrical properties of graphene ink thin films by laser-annealing*, 2D Materials, **2**, 011003 (2015).
  114. F. Torrisi, T. Hasan, W. Wu, Z. Sun, A. Lombardo, T. S. Kulmala, G. W. Hsieh, S. Jung, F. Bonaccorso and P. J. Paul, *Inkjet-printed graphene electronics*, ACS Nano, **6**, 2992-3006 (2012).
  115. E. B. Secor, P. L. Prabhmirashi, K. Puntambekar, M. L. Geier and M. C. Hersam, *Inkjet printing of high conductivity, flexible graphene patterns*, The Journal of Physical Chemistry Letters, **4**, 1347-1351 (2013).
  116. E. B. Secor, B. Y. Ahn, T. Z. Gao, J. A. Lewis and M. C. Hersam, *Rapid and versatile photonic annealing of graphene inks for flexible printed electronics*, Advanced Materials, **27**, 6683-6688 (2015).
  117. Y. H. Gao, W. Shi, W. C. Wang, Y. P. Leng and Y. P. Zhao, *Inkjet printing patterns of highly conductive pristine graphene on flexible substrates*, Industrial & Engineering Chemistry Research, **53**, 16777-16784 (2014).
  118. C. L. Lee, C. H. Chen and C. W. Chen, *Graphene nanosheets as ink particles for inkjet printing on flexible board*, Chemical Engineering Journal, **230**, 296-302 (2013).
  119. A. Capasso, A. E. Del Rio Castillo, H. Sun, A. Ansaldo, V. Pellegrini and F. Bonaccorso, *Ink-jet printing of graphene for flexible electronics: An environmentally-friendly approach*, Solid State Communications, **224**, 53-63 (2015).
  120. K. Y. Shin, J. Y. Hong and J. Jang, *Micropatterning of graphene sheets by inkjet printing and its wideband dipole-antenna application*, Advanced Materials, **23**,

- 2113-2118 (2011).
121. S. Lim, B. Kang, D. Kwak, W. H. Lee, J. A. Lim and K. Cho, *Inkjet-printed reduced graphene oxide/poly(vinyl alcohol) composite electrodes for flexible transparent organic field-effect transistors*, The Journal of Physical Chemistry C, **116**, 7520-7525 (2012).
  122. S. Porro, R. Giardi and A. Chiolerio, *Real-time monitoring of graphene oxide reduction in acrylic printable composite inks*, Applied Physics A, **117**, 1289-1293 (2014).
  123. Y. Xu, I. Hennig, D. Freyberg, A. James Strudwick, M. Georg Schwab, T. Weitz and K. Chih-Pei Cha, *Inkjet-printed energy storage device using graphene/polyaniline inks*, Journal of Power Sources, **248**, 483-488 (2014).
  124. Z. Liu, K. Parvez, R. Li, R. Dong, X. Feng and K. Mullen, *Transparent conductive electrodes from graphene/PEDOT:PSS hybrid inks for ultrathin organic photodetectors*. Advanced Materials, **27**, 669-675 (2015).
  125. L. H. Li, Y. Z. Guo, X. Y. Zhang and Y. L. Song, *Inkjet-printed highly conductive transparent patterns with water based Ag-doped graphene*, Journal of Materials Chemistry A, **2**, 19095-19101 (2014).
  126. G. Wang, Z. Wang, Z. Liu, J. Xue, G. Xin, Q. Yu, J. Lian and M. Y. Chen, *Annealed graphene sheets decorated with silver nanoparticles for inkjet printing*, Chemical Engineering Journal, **260**, 582-589 (2015).
  127. L. Y. Xu, G. Y. Yang, H. Y. Jing, J. Wei and Y. D. Han, *Ag-graphene hybrid conductive ink for writing electronics*, Nanotechnology, **25**, 055201 (2014).
  128. W. J. Zhang, E. B. Bi, M. Li and L. M. Gao, *Synthesis of Ag/RGO composite as effective conductive ink filler for flexible inkjet printing electronics*, Colloids and Surfaces A: Physicochemical and Engineering Aspects, **490**, 232-240 (2016).
  129. W. Yang, C. Wang, V. Arrighi and F. Vilela, *One step synthesis of a hybrid Ag/rGO conductive ink using a complexation-covalent bonding based approach*. Journal of Materials Science: Materials in Electronics, **28**, 8218-8230 (2017).
  130. A. Cammarano, G. Luca and E. Amendola, *Surface modification and adhesion improvement of polyester films*, Open Chemistry, **11**, 35-45 (2013).
  131. S. Luo and C. Wong, *Improvement of epoxy adhesion to polyimide passivation*, 52<sup>nd</sup> Electronic Components and Technology Conference, IEEE, 1390-1395 (2002).
  132. M. Garg and J. Quamara, *FTIR analysis of high energy heavy ion irradiated kapton-H polyimide*, Indian Journal of Pure and Applied Physics, **45**, 563-568 (2007).

133. L. E. Stephans, A. Myles and R. R. Thomas, *Kinetics of alkaline hydrolysis of a polyimide surface*, *Langmuir*, **16**, 4706-4710 (2000).
134. J. Liu, L. Liu, X. Wu, X. Zhang and T. Li, *Environmentally friendly synthesis of graphene-silver composites with surface-enhanced Raman scattering and antibacterial activity via reduction with l-ascorbic acid/water vapor*, *New Journal of Chemistry*, **39**, 5272-5281 (2015).
135. W. Ma, J. Zhou and X. Lin, *Preparation and characterization of functionalized graphene with ethanolamine*, *Acta Chimica Sinica*, **69**, 1463-1468 (2011).
136. M. M. Alam, W. Ji, H. N. Luitel, Y. Ozaki, T. Watari and K. Nakashima, *Template free synthesis of dendritic silver nanostructures and their application in surface-enhanced Raman scattering*, *RSC Advances*, **4**, 52686-52689 (2014).
137. G. Pike and C. Seager, *Percolation and conductivity: A computer study. I*, *Physical Review B*, **10**, 1421 (1974).
138. L. Fan, B. Su, J. Qu and C. Wong, *Effects of nano-sized particles on electrical and thermal conductivities of polymer composites*, 9<sup>th</sup> International Symposium on Advanced Packaging Materials: Processes, Properties and Interfaces, 193-199 (2004).
139. X. W. Hu, L. H. Li, S. M. Zhao and X. Leng, *Conductive ink and applications in printing antenna of RFID tag*, *Advanced Materials Research*, 577-581 (2011).
140. Q. J. Huang, W. F. Shen and W. J. Song, *Synthesis of colourless silver precursor ink for printing conductive patterns on silicon nitride substrates*. *Applied Surface Science*, **258**, 7384-7388 (2012).
141. K. Black, J. Singh, D. Mehta, S. Sung, C. J. Sutcliffe and P. R. Chalker, *Silver ink formulations for sinter-free printing of conductive films*, *Scientific Reports*, **6**, 1-7 (2016).
142. K. Zope, *Novel synthesis of a solid silver oxalate complex used for printing conductive traces*. Rochester Institute of Technology (2017).
143. J. J. Chen, J. Zhang, Y. Wang, Y. L. Guo and Z. S. Feng, *A particle-free silver precursor ink useful for inkjet printing to fabricate highly conductive patterns*, *Journal of Materials Chemistry C*, **4**, 10494-10499 (2016).
144. J. D. Torrey, T. L. Kirschling and L. F. Greenlee, *Processing and characterization of nanoparticle coatings for quartz crystal microbalance measurements*, *Journal of research of the National Institute of Standards and Technology*, **120**, 1-10 (2015).
145. W. Yang, C. Wang and V. Arrighi, *An organic silver complex conductive ink using both decomposition and self-reduction mechanism in film formation*, *Journal of*



- Materials Science: Materials in Electronics, **29**, 2771-2783 (2018).
146. N. Wu, L. Fu, M. Su, M. Aslam, K. C. Wong and V. P. Dravid, *Interaction of fatty acid monolayers with cobalt nanoparticles*, Nano letters, **4**, 383-386 (2004).
147. Y. Tao, B. Wang, L. Wang and Y. Tai, *A facile approach to a silver conductive ink with high performance for macroelectronics*, Nanoscale Research Letters, **8**, 1-6 (2013).
148. G. Corro, U. Pal, E. Ayala and E. Vidal, *Diesel soot oxidation over silver-loaded SiO<sub>2</sub> catalysts*, Catalysis today, **212**, 63-69 (2013).
149. K. P. Bankura, D. Maity, M. M. R. Mollick, D. Mondal, B. Bhowmick, M. K. Bain, A. Chakraborty, J. Sarkar, K. Acharya and D. Chattopadhyay, *Synthesis, characterization and antimicrobial activity of dextran stabilized silver nanoparticles in aqueous medium*, Carbohydrate Polymers, **89**, 1159-1165 (2012).
150. Y. Dong, X. D. Li, S. H. Liu, Q. Zhu, M. Zhang, J. G. Li and X. D. Sun, *Optimizing formulations of silver organic decomposition ink for producing highly-conductive features on flexible substrates: The case study of amines*, Thin Solid Films, **616**, 635-642 (2016).
151. W. Yang, C. Wang and V. Arrighi, *Preparation and characterization of organic silver precursors for conductive ink*, International Journal of Electronics and Communication Engineering, **12**, 670-677 (2018).
152. N. F. Uvarov, L. P. Burleva, M. B. Mizen, D. R. Whitcomb and C. Zou. *Conductivity of long-chain silver carboxylates and their thermal decomposition products*, Solid State Ionics, **107**, 31-40 (1998).
153. L. Burleva, V. Andreev and V. Boldyrev. *Thermal decompositions of silver carboxylates*, Journal of Thermal Analysis and Calorimetry, **33**, 735-739 (1988).
154. R. Szczyński and E. Szłyk, *Thermal decomposition of some silver (I) carboxylates under nitrogen atmosphere*, Journal of Thermal Analysis and Calorimetry, **111**, 1325-1330 (2013)
155. V. Boldyrev, *Thermal decomposition of silver oxalate*, Thermochemica Acta, **388**, 63-90 (2002).
156. W. Yang, C. Wang and V. Arrighi, *Silver oxalate ink with low sintering temperature and good electrical property*. Journal of Electronic Materials, **47**, 2824-2835 (2018).
157. K. R. Zope, D. Cormier and S. A. Williams, *Reactive silver oxalate ink composition with enhanced curing conditions for flexible substrates*, ACS Appl. Mater. Interfaces, **10**, 3830-3837 (2018).

158. W. Yang, C. Wang and V. Arrighi, *Effects of amine types on the properties of silver oxalate ink and the associated film morphology*, Journal of Materials Science: Materials in Electronics, **29**, 20895-20906 (2018).
159. M. C. Dang, T. M. D. Dang and E. Fribourg-Blanc, *Silver nanoparticles ink synthesis for conductive patterns fabrication using inkjet printing technology*, Advances in Natural Sciences: Nanoscience and Nanotechnology, **6**, 015003 (2015).
160. Y. Dong, Z. J. Lin, X. D. Li, Q. Zhu, J. G. Li and X. D. Sun, *A low temperature and air-sinterable copper-diamine complex-based metal organic decomposition ink for printed electronics*, Journal of Materials Chemistry C, **6**, 6406-6415 (2018).
161. C. Paquet, T. Lacelle, X. Liu, B. Deore, A. J. Kell, S. Lafrenière and P. R. L. Malenfant, *The role of amine ligands in governing film morphology and electrical properties of copper films derived from copper formate-based molecular inks*, Nanoscale, **10**, 6911-6921 (2018).
162. W. Xu and T. Wang, *Synergetic effect of blended alkylamines for copper complex ink to form conductive copper films*, Langmuir, **33**, 82-90 (2017).
163. A. Yabuki and S. Tanaka, *Electrically conductive copper film prepared at low temperature by thermal decomposition of copper amine complexes with various amines*, Materials Research Bulletin, **47**, 4107-4111 (2012).

## Appendices

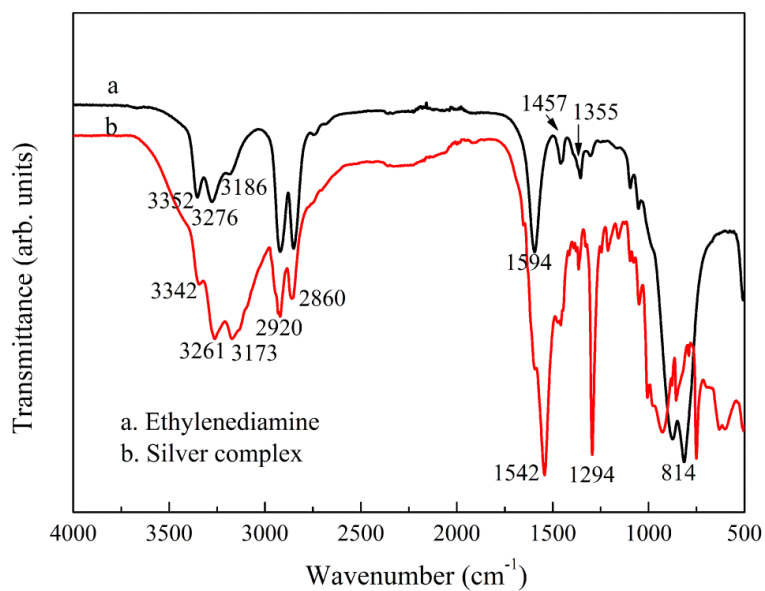


Figure S1 FT-IR spectra of ethylenediamine and the formed silver-amine complex

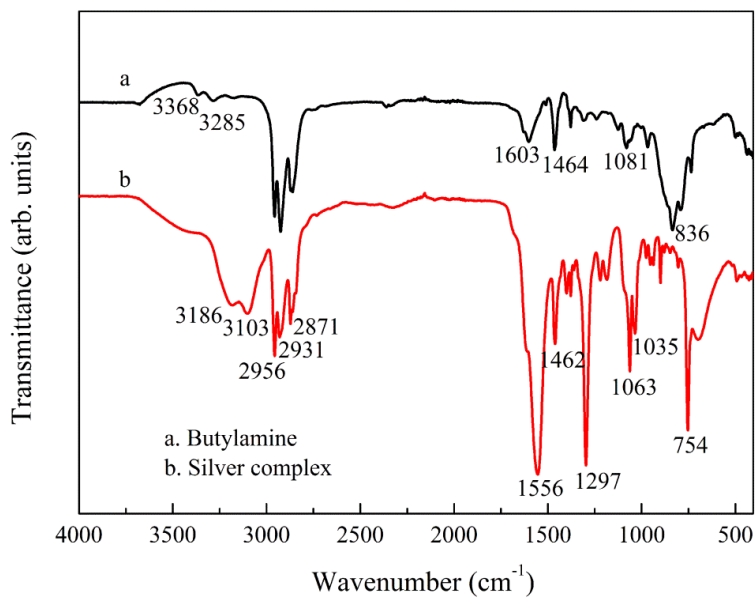


Figure S2 FT-IR spectra of butylamine and the formed silver-amine complex

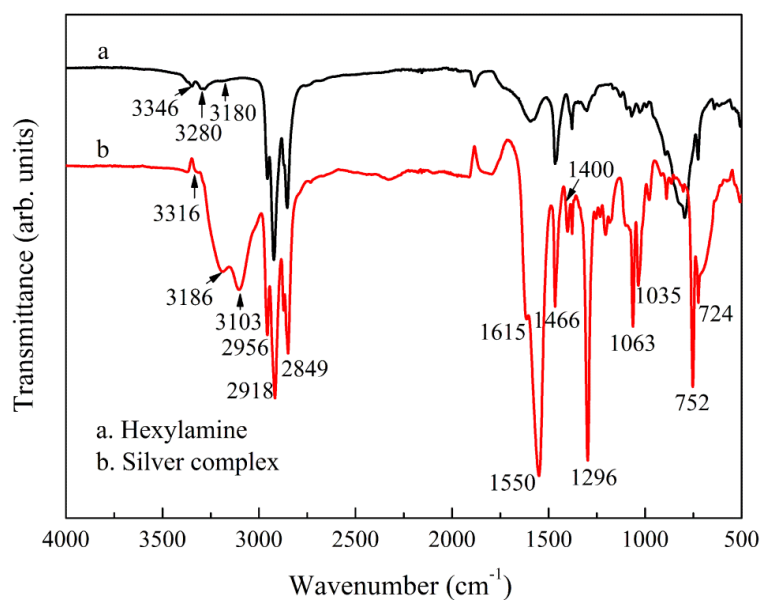


Figure S3 FT-IR spectra of hexylamine and the formed silver-amine complex

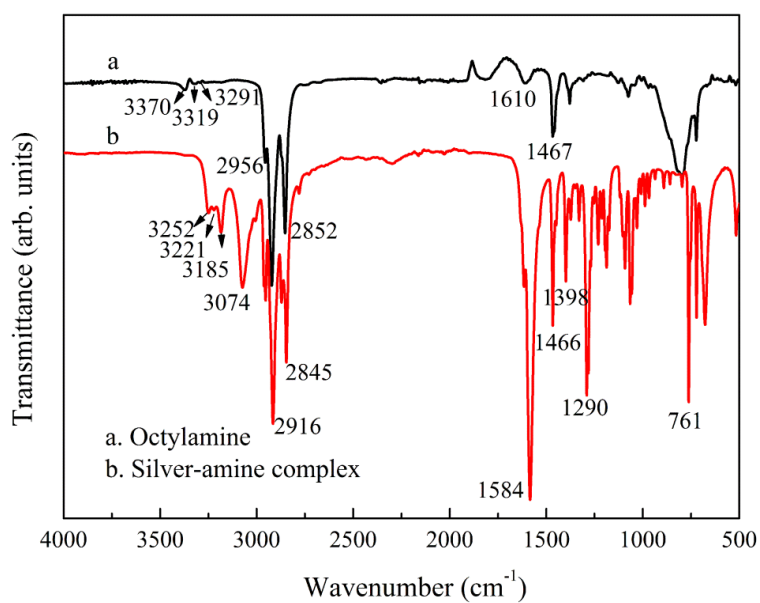


Figure S4 FT-IR spectra of octylamine and the formed silver-amine complex

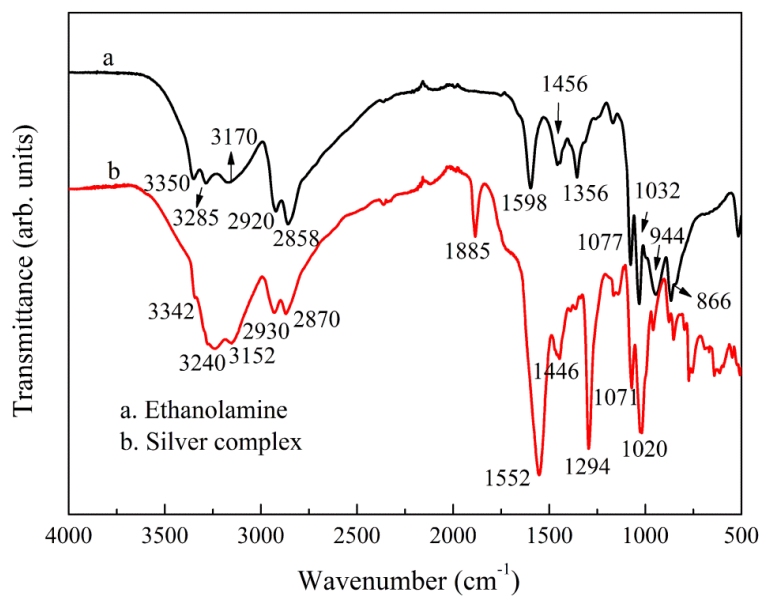


Figure S5 FT-IR spectra of ethanolamine and the formed silver-amine complex